Functional analysis of the EB1-Kinesin-14 complex in chromosome segregation

Inaugural Dissertation
for
the doctoral degree of
Dr. rer. nat.

from the Faculty of Biology
University of Duisburg-Essen
Germany

Submitted by
Nikolay Kornakov
Born in Protvino, Moscow Oblast, Russian Federation

March 2021

The experiments underlying the present work were conducted at the Biology Faculty, Molecular Genetics I Department, Center of Medical Biotechnology (ZMB) at the University of Duisburg-Essen under the supervision of Prof. Stefan Westermann.

1. Examiner:	Prof. Perihan Nalbant
2. Examiner:	Prof. Stefan Westermann
3. Examiner:	57732
Chair of the Board of Examiners:	Prof. Doris Hellerschmied-Jelinek
Date of the oral examination:	02.06.2021

DOI: 10.17185/duepublico/74489
URN: urn:nbn:de:hbz:465-20220713-141413-6

In the context of this doctoral work, the following articles were published:

Kornakov, N., Möllers, B., and Westermann, S. 2020. The EB1–Kinesin-14 complex is required for efficient metaphase spindle assembly and kinetochore bi-orientation. *Journal of Cell Biology*. Dec 7;219(12):e202003072,doi: 10.1083/jcb.202003072.

Dudziak, A., Engelhard, L., Bourque, C., Klink, B.U., Rombaut, P., Kornakov, N., Jänen, K.' Herzog, F., Gatsogiannis, C. and Westermann, S. 2021. Mps1 controlled +TIP interactions trigger Dam1c ring assembly at the outer kinetochore, *under revision*

Kornakov, N. and Westermann, S. 2021. Systematic analysis of EB1-cargo interactions reveals competition for spindle association in budding yeast. *Manuscript in preparation*

Table of content

List of abbreviations

α-factor	alpha factor mating pheromone, WHWLQLKPGQPMY peptide
γ-TuRC	gamma-tubulin ring complex
μg	microgram
μl	microliter
μM	micromolar
μm	micrometer
aa	amino acid
aux	synthetic analog of auxin, 1-Naphthaleneacetic acid (NAA)
ADP	adenosine diphosphate
ATP	adenosine triphosphate
CFU	colony forming units
DNA	deoxyribonucleic acid
dNTP	deoxynucleoside triphosphate
GMCPP	Guanosine-5'-[(α,β)-methyleno]triphosphate
HU	hydroxyurea
M	molar
MTOC	microtubule-organizing center
MTs	microtubules
min	minute
mM	milimolar
mL	milliliter
NA	non applicable
NB	no binding
NLS	nuclear localization signal
NS	non-significant
ng	nanogram
nM	nanomolar
P	phosphate
SD	standard deviation
SEM	standard error of the mean
SEC	size-exclusion chromatography
SLiM	short linear motif
SPB	spindle pole body

s	second
V_{pol}	polymerization speed
V_{depol}	depolymerization speed
WT	wild-type

List of figures

List of tables

Summary

Self-copying is the goal of every organism's life. For some species, like budding yeasts, a single cell constitutes a whole organism. For every cell division the genetic material must be fully duplicated and properly segregated between inheritors. A complex microtubule-based machinery mediates faithful genome inheritance. In this system, microtubule-associated proteins drive the assembly of a supramolecular structure that constitutes the mitotic spindle.

Kinesin-14 molecular motor proteins are known to be required for error-free chromosome segregation in mitosis and meiosis and display an exceptional evolutionary conservation. A variety of functions have been assigned to kinesin-14 family members, but it is unclear how these activities contribute to chromosome segregation. The models for kinesin-14's mode of action fall in the range from support of lateral chromosome transport along microtubules to the regulation of microtubule nucleation at MTOCs. One of the limitations that prevents a deeper characterization of kinesin-14 functions in chromosome segregation is a lack of molecular understanding outside of the well-characterized motor domain. Budding yeasts have a single catalytically active kinesin-14, termed Kar3, which performs mitotic functions in a complex with the kinesin-associated protein Cik1. Using a conditional depletion system and an unbiased mutant screening approach, I have discovered a tripartite binding interface between kinesin-14 and the EB1 homolog Bim1 in budding yeast. The "A-B-C" Bim1-binding motif system is distributed between the Cik1 and Kar3 polypeptide chains and consists of conserved peptide motifs. The resulting Bim1-Cik1-Kar3 complex regulates the assembly of a metaphase spindle of proper length, and promotes microtubule bundle organization and dynamics. Lack of Bim1 binding delays cells in mitosis similar to the absence of Cik1-Kar3 proteins. Artificial plus-end targeting of Cik1-Kar3 bypasses the requirements for Bim1 binding and is sufficient to promote bundle formation in cells. In the absence of Bim1-Cik1-Kar3 cells rely on the conserved microtubule crosslinker Ase1/PRC1 for metaphase spindle assembly and chromosome bi-orientation. Simultaneous loss of plus-end targeted Kar3 and Ase1 is lethal. In summary, I have identified a molecular binding interface between Bim1 and Cik1-Kar3 as a prerequisite for error-free chromosome segregation.

1. Introduction

1.1 History and discovery of Kinesin-14 motor proteins

The first description of a phenotype associated with loss of kinesin-14 functions can be dated back to 1929. Using radiation mutagenesis a mutant was identified that was characterized by abnormal eye color and chromosome missegregation in meiosis and mitosis in *Drosophila* (Sturtevant, 1929; Davis, 1969). This mutant had a deletion of a chromosome fragment with two partially overlapping genes found in that locus (Sequeira et al., 1989, Yamamoto et al., 1989). Defects in *claret* gene lead to dark red eye color and *ncd* (non-claret disjunctional) is responsible for genomic stability. In 1990, the sequence homology between kinesin-1 heavy chain and Ncd was discovered (Endow et al., 1990; McDonald and Goldstein, 1990; Walker et al., 1990; McDonald et al., 1990). Ncd became one the first members of an unusual kinesin-14 family of proteins, having a C-terminal motor homology domain in contrast to all other kinesins. From microtubule gliding experiments it was concluded that Ncd is a minus-end directed motor. However, contrary to *in vitro* motility, Ncd tracked growing microtubules plus ends in cells (Goshima et al., 2005a) (**Figure 1.1**).

In 1990, kinesin-14 Kar3 was identified in *Saccharomyces cerevisiae* (Meluh and Rose, 1990). The name of Kar3 originated from karyogamy – a process of bringing together two nuclei to fuse them after successful cell fusion during mating (Meluh and Rose, 1990; Saunders and Hoyt, 1992). This process depends on minus-end directed gliding of microtubules linked to opposing nuclei (Gibeaux et al., 2013). Kar3 mutants had a reduced rate of diploids formation, exhibited a delay in mitosis and meiotic failure. In 1992, the Kar3 associated protein Cik1 was discovered (chromosome instability and karyogamy) (Page and Snyder, 1992). The cik1 deletion shared phenotypes with Kar3 loss-of-function alleles and localization of Cik1 and Kar3 to microtubules was co-dependent (Page et al., 1994). Cik1-Kar3 presented the first example of heterodimeric kinesin-14 with a single catalytically active kinesin motor domain. From studies of localization of truncated versions of Cik1-Kar3 and dependence on Kar1 for SPB (spindle pole body) binding, it became clear that not a motor domain, but the N-terminal tails target it to specific locations in the cell: microtubule plus ends, microtubule bundles and SPBs (Page et al., 1994; Vallen et al., 1992).

Subsequently, kinesin-14 proteins in other organisms were described by sequence homology with Kar3 and Ncd: KlpA of *Aspergillus nidulans* (O'Connell et al., 1993), HSET (KIFC1), KIFC2 and KIFC3 in *Homo sapiens* and mammals (Ando et al., 1994; Kuriyama et al., 1995; Saito et al., 1997; Yang et al., 1997), XCTK2 of *Xenopus laevis* (Walczak et al., 1997) and Pkl1 and Klp2 in the fission yeast *Schizosaccharomyces pombe* (Pidoux et al., 1996; Troxell et al., 2001). Plant genomes encode a diverse set of kinesin-14 proteins with a variety of molecular structures. For example, *Arabidopsis thaliana* has more than 20 C-terminal kinesins with ATK1, ATK5 and KCBP among best studied of them (Chen et al., 2002; Marcus et al., 2002; Ambrose et al., 2005; Reddy et al., 1996; Song et al., 1997). Some of the plant kinesin-14s can bind to actin by their tail domains in addition to microtubules, therefore crosslinking different cytoskeleton systems (Reddy and Day, 2001).

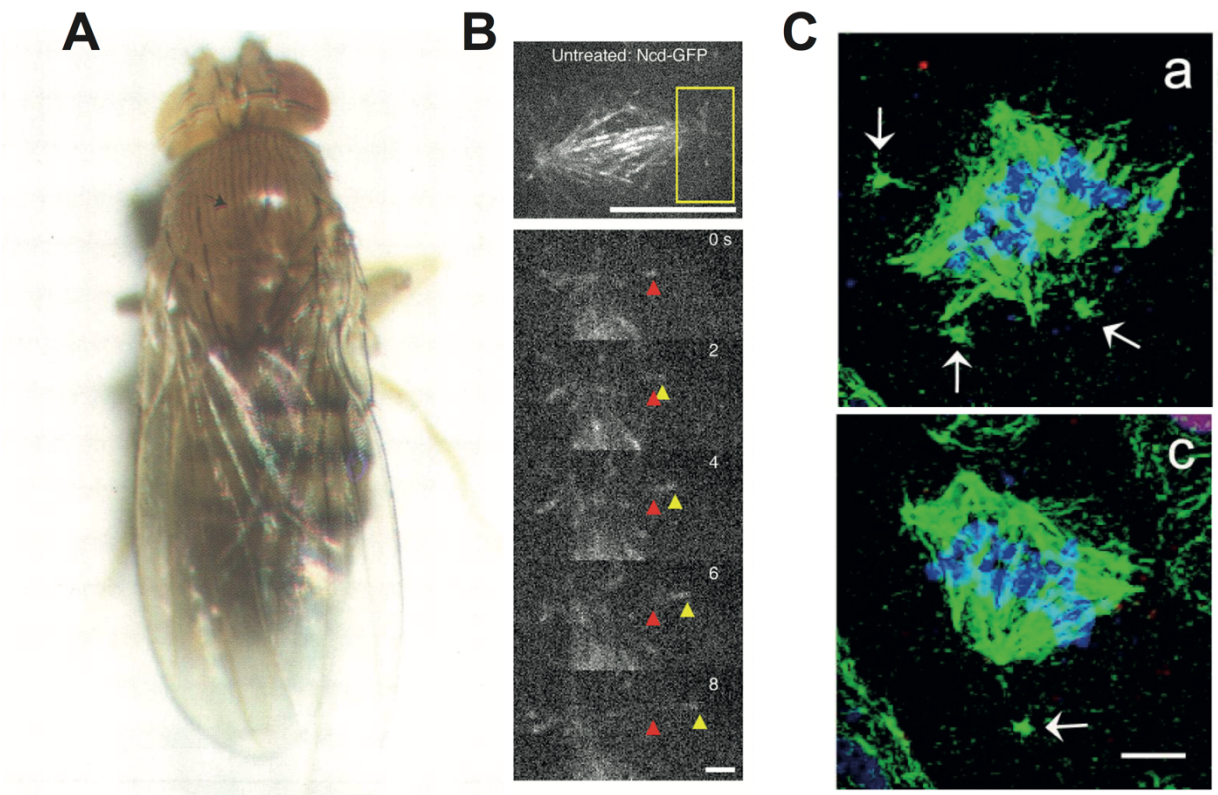

Figure 1.1 Kinesin-14 Ncd is a microtubule motor involved in spindle assembly and chromosome segregation.

A) Mosaic fly aroused after early zygotic chromosome loss. X/X wild-type female tissue on the right side. X/0 yellow and white on the left side. Adapted from (Yamamoto et al., 1989), with changes.
B) Ncd-GFP localization to metaphase spindle. (Bottom) Ncd-GFP tracks polymerizing microtubules plus-ends marked with yellow triangle, initial position labelled with red triangle. Scale bars are 10 μm at top and 1 μm at bottom images. Adapted from (Goshima et al., 2005a), with changes.

C) Ncd-depleted S2 cells (a, c) display multipolar spindles with centrosomes positioned outside of spindles, marked with white arrows. Tubulin is green, DNA is blue, scale bar is 5 μm. Adapted from (Morales-Mulia and Scholey, 2005), with changes.

With a rise in the number of sequenced genomes came the realization, that kinesin-14s are ubiquitous and the most evolutionarily conserved kinesin family in eukaryotes (**Figure 1.2**) (Lawrence et al., 2004; Wickstead et al., 2010). Kinesin-14s are subdivided into two groups – kinesin-14A (Kar3, Ncd, KlpA, HSET) and the less studied kinesin-14B (KIFC2, KIFC3). Some organisms have highly specialized kinesin-14s, like KINDR (kinesin driver), that mediates meiotic drive (Dawe et al., 2018).

Summarizing, virtually every eukaryotic organism has at least one kinesin-14 protein, illuminating conservation and importance of C-terminal motors for faithful genetic information propagation.

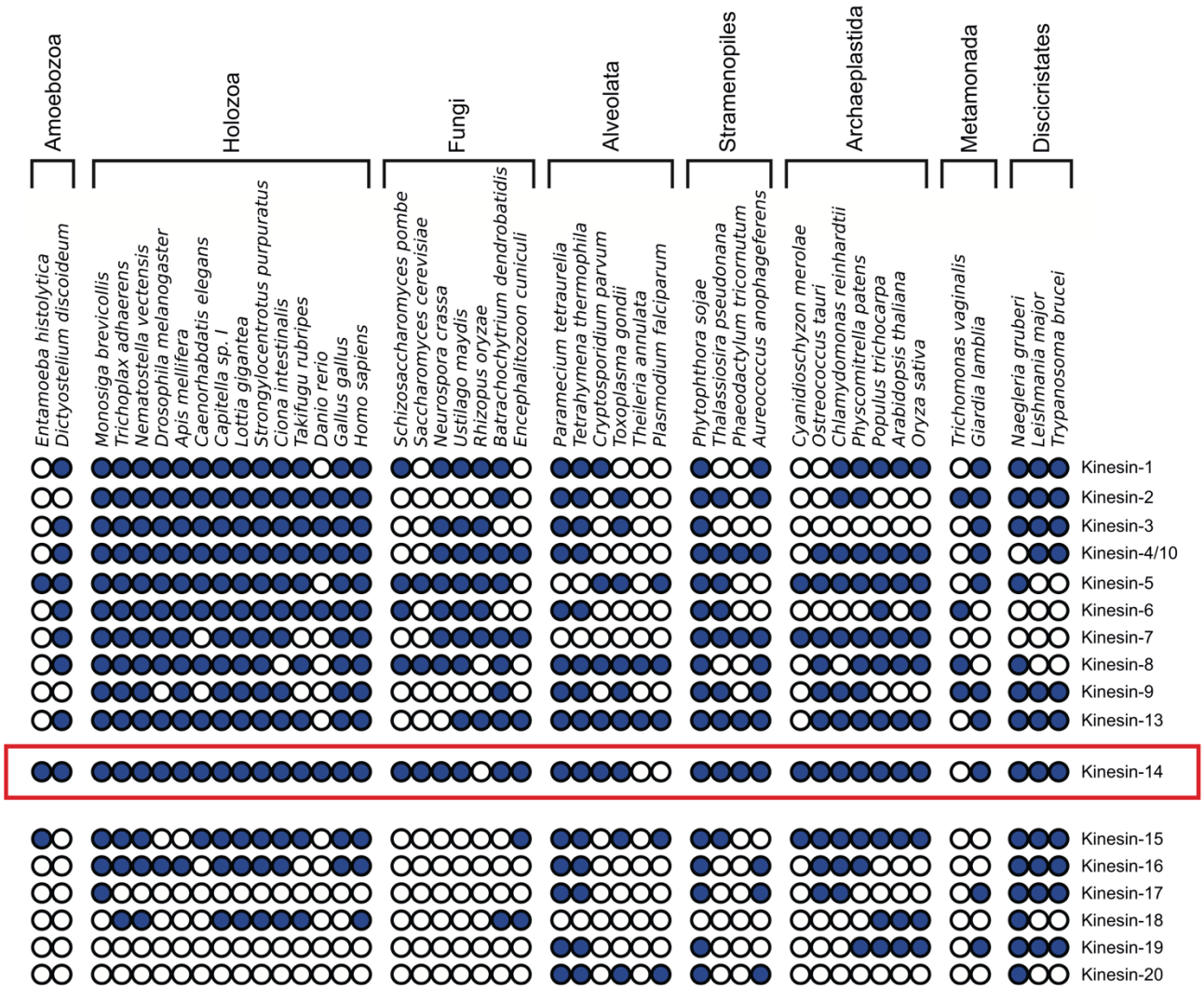

Figure 1.2 Evolution of kinesin family.

Phylogeny of 17 kinesin families. Presence of paralogs marked with filled circles. The Kinesin-14 family highlighted with the red rectangle. Eukaryotic supergroups are signed at the top. Adapted from (Wickstead et al., 2010), with changes.

1.2 Molecular structure of Kinesin-14 motor proteins

Before explaining C-terminal kinesins, I will describe the molecular organization of classical plus-end directed molecules with N-terminal motor domain, using kinesin-1 as an example (**Figure 1.3**).

Kinesin-1 heavy chain has three distinct domains: the N-terminal motor domain, a coiled-coil stalk and a C-terminal tail (Vale et al., 1985; Yang et al., 1989). At the beginning of the coiled-coil a subdomain, called the neck linker is distinguished. The Motor domain is an ATPase, that couples ATP hydrolysis to intramolecular rearrangements that result in directional movement and change in microtubule affinity (Rice et al., 1999). The motor domain is about 340 amino acids in length and has six a-helices surrounding eight beta-sheets. Despite no sequence similarity, the crystal structure of the kinesin motor domain closely resembles the structure of the actin motor myosin. This observation speaks in favor of the common evolutional origin of these proteins (Jon Kull et al., 1996; Kull et al., 1998).

The most conserved part of the motor is a Walker A motif – the Mg-ATP binding pocket with a GxxxxGKT sequence (P-loop) (Walker et al., 1982). Binding and hydrolysis of Mg-ATP alters switch I (SSRSH) and switch II (DLAGSE) regions (Cao et al., 2017). The conformational change is stabilized by interaction of the motor domain with the neck. Neck dimerization synchronizes changes in both motor heads. The motor working cycle can be represented in following steps - in solution kinesin has Mg-ADP docked at the P-loop, binding to microtubule induces nucleotide release and Mg-ATP binding (Hackney, 1988; Nitta et al., 2008). Both nucleotide-free and in complex with ATP states have high microtubule affinity (Crevel et al., 1996). Release of phosphate after ATP hydrolysis finishes the cycle (Milic et al., 2014). Below I will briefly describe the mechanochemistry underlying those transitions. Binding of Mg-ATP to P-loop brings together switch I and switch II and forms a salt bridge between arginine and glutamic acid. Meanwhile, the serines of switch I coordinate Mg^{2+} and the gamma-phosphate of ATP, which also binds to the glycine of switch II. This conformation catalyzes ATP hydrolysis and phosphate release moves switch I and switch II apart. The initial interaction of the motor domain with microtubules during movement involves C-terminal tubulin tails, while a region in proximity of switch II promotes tight binding to negatively charged stretches of helix-12 a-b-tubulin dimers. Docking of the neck to the motor occurs specifically in the ATP-bound state or subsequently to it and is required for force production and directional 8 nm steps

towards the plus-end of the microtubule. In accordance with the hand-over-hand model, the leading head remains tightly bound and the rear head makes a two tubulin dimers wide 16 nm movement toward the plus-end. As a result, the stalk moves by 8 nm for each hydrolyzed molecule of ATP.

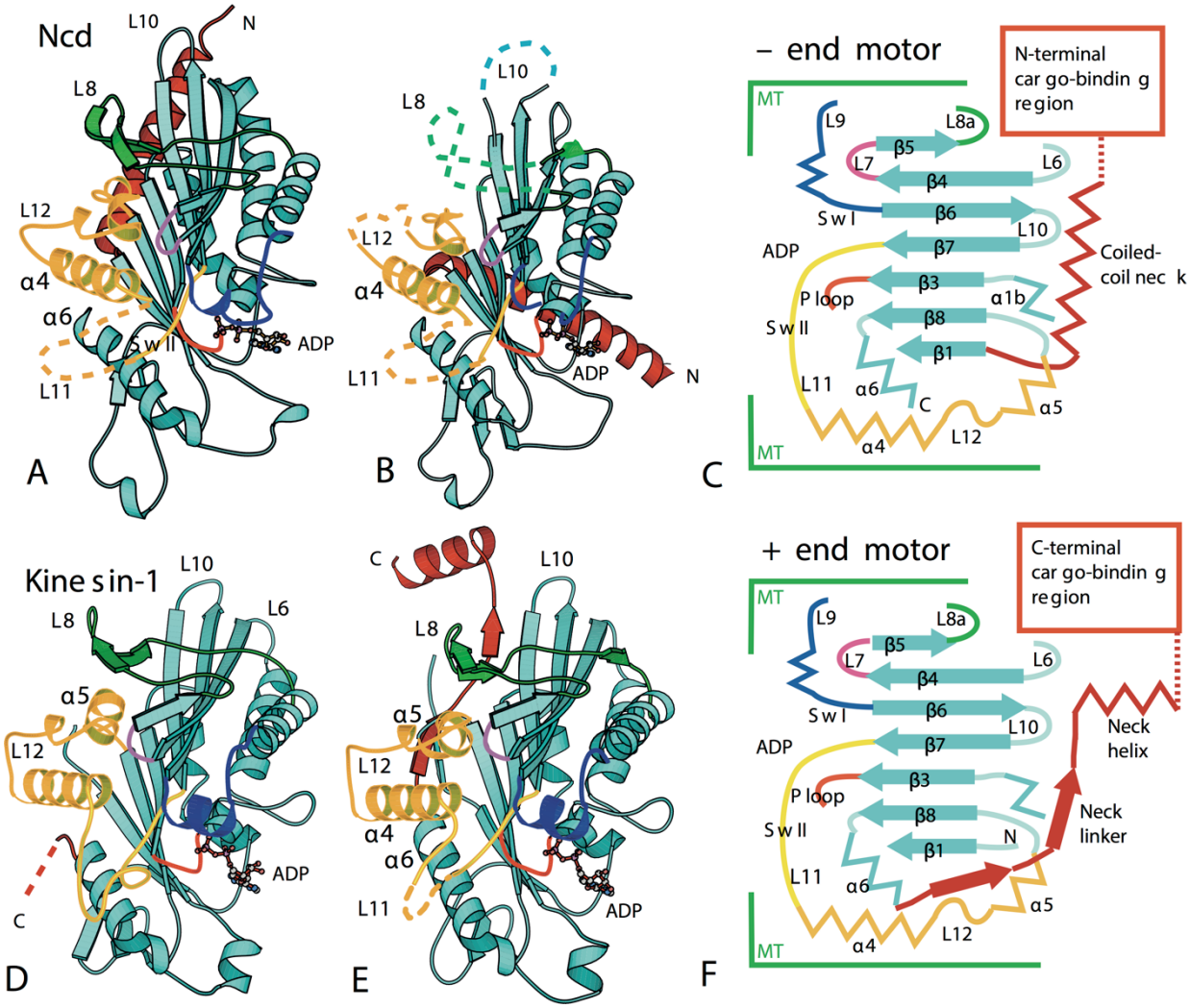

Figure 1.3 Structures of Ncd and Kinesin-1 motor domains.

Crystal structures of Ncd (A, B) and Kinesin-1 (D, E) depicted in a cartoon format. Secondary structure drawn on the right side (C, F), functionally important regions are signed. Microtubule binding interface, adjacent to switch I and switch II regions is marked with green scopes. Proposed changes in neck/neck linker positions are drawn in B and C. The illustration is adapted from (Amos and Hirose, 2007) and is based on crystal structures, PDB codes are 1CZ7, 1N6M, 1BG2, 2KIN.

A short segment of ~40 amino acids containing the neck is sufficient for dimerization and processive movement in vitro (Romberg et al., 1998). However, the kinesin-1 molecule has a long coiled-coil region that has some flexibility and allows the C-terminal tail to fold back to self-inhibit the motor (Dietrich et al., 2008). Kinesin-1

heavy chains bind to a homodimer of light chains with a coiled-coil to coiled-coil interaction. Various cargos are recruited by TPR-repeat domains of the light chains, but some proteins directly interact with the heavy chain coiled-coils and tails. A variety of adaptor proteins bind both heavy and light chains further expanding the cargo repertoire.

Kinesin-14s have a reversed molecular architecture: An N-terminal tail domain, a coiled-coil stalk and a C-terminal motor domain (**Figure 1.3**). The motor structure itself is similar to the kinesin-1 motor, with the main difference between them lying in the neck region. In contrast to kinesin-1, the neck and unbound head rotates towards the microtubule's minus end upon ATP binding. The coiled-coil stalk serves a lever arm, similar to the mode of myosin action on actin filaments, and the length of lever arm determines motor speed (Endres et al., 2006). In fact, a second motor head is not required for directional movement, as it was observed that a single-headed Ncd construct is proficient in microtubule gliding. Other studies contradict these interpretations. It was measured that Ncd requires to hydrolyze 2 ATP molecules to make a single step (Endres et al., 2006). That leads to a model with asymmetry between the Ncd heads, bound to adjacent protofilaments. The model states that one of the heads is in a weak ADP-bound state and ADP is exchanged for ATP soon after microtubule binding. So, one ATP molecule is spent for microtubule binding and conformational change and another one to make a step. The isolated C-terminal motor domain has plus end directionality and the overall movement of the molecule depends on the elements outside of the motor domain (Case et al., 1997) (**Figure 1.4**).

Besides homodimeric molecules, the kinesin-14 family has several examples of heterodimeric proteins. Budding yeast kinesin-14's Cik1-Kar3 and Vik1-Kar3 have heavy chain Kar3 that forms a complex with the non-motor proteins Cik1 or Vik1. The C-terminal part of these proteins is a weak microtubule-binding domain, that helps to keep the molecule on the track after motor domain detachment. How Cik1-Kar3 moves along the microtubule remains unclear. Current models suggest either translocation similar to Ncd or a Brownian ratchet type of movement (Molodtsov et al., 2016). In that case, asymmetry in the potential energy landscape created by the non-motor microtubule binding domain of Cik1 leads to preferential minus-end diffusion (**Figure 1.4**).

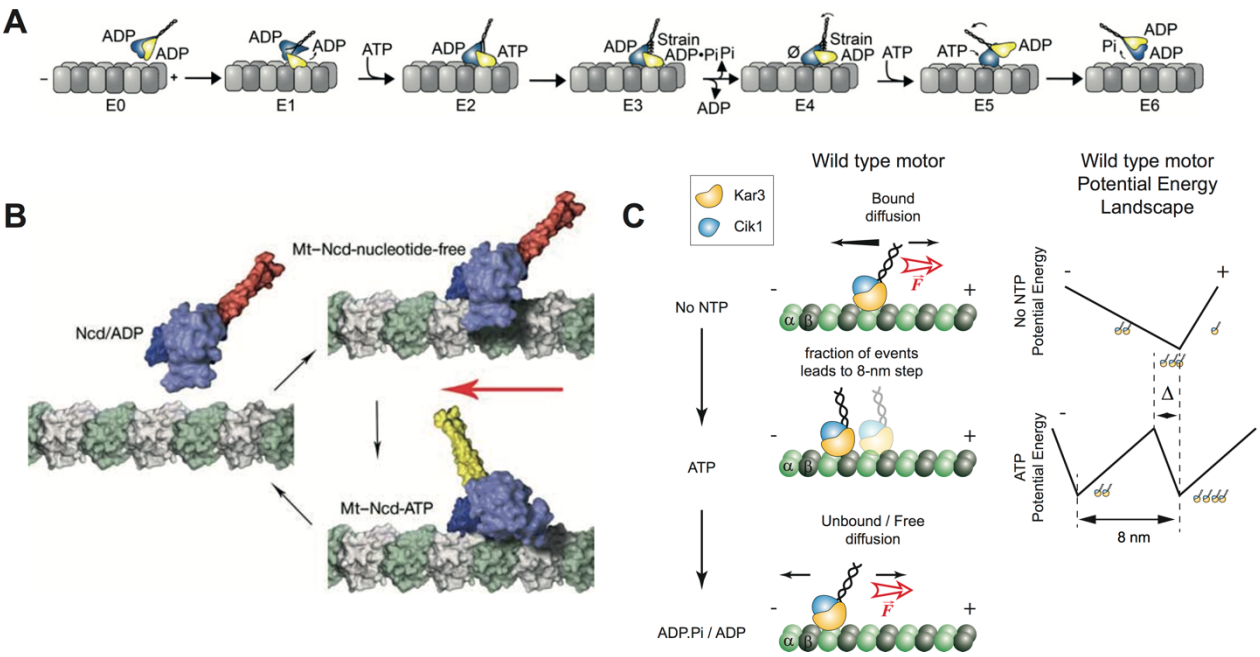

Figure 1.4 Models of kinesin-14s movement.

A) Ncd mechanism of movement, according to (Zhang et al., 2015). Ncd heads are asymmetric and hold ADP with different affinities. Microtubule binding starts with the low ADP affinity head, drawn in yellow color at E0 and E1 steps. Microtubule binding induces ADP release and ATP binding, which promotes association of the other head with adjacent protofilament at E2 step. Energy of ATP hydrolysis by yellow head spent to release ADP from blue head at E3. ATP binding by blue head induces stalk rotation at E4 and E5 states. ATP hydrolysis by blue head finishes the translocation cycle and releases the molecule from microtubule at E6.
B) Ncd mechanism of movement, accordingly to (Endres et al., 2006). Hydrolysis of the single ATP molecule induces stalk rotation towards the minus end, followed by phosphate release and microtubule unbinding. Ncd heads are symmetric and the single head is sufficient for translocation.
C) Hypothetical Cik1-Kar3 Brownian Ratchet-like type of movement. Adapted from (Molodtsov et al., 2016). Without nucleotide Cik1-Kar3 diffuses along the microtubule lattice with higher chance to move towards the minus end. External force (red arrow) can reverse direction of movement. ATP binding does not induce any movement, but changes intramolecular conformation, that alters potential energy landscape, as shown on the right side. ATP hydrolysis/release returns Cik1-Kar3 into the diffusing state.

1.3 Motor properties of Kinesin-14 members

There are a number of parameters describing properties of molecular motors. Directionality, processivity, speed and stall force are among the most studied in vitro. Most of the Kinesin-14s are generally thought to be slow, weak (non)-processive minus end directed motors (She and Yang, 2017).

Several methods have been established to address motor's directionality. In a microtubule-gliding assay, surface-immobilized motors move polarity-marked floating

microtubules, like it was done for kinesin-1 (Vale et al., 1985). In this assay, Ncd, Kar3, KlpA, HSET and other kinesin-14s display minus end directed movement. Another way is to follow free movement of individual motors on microtubules attached to the slide. In this assay kinesin-14 KlpA is a processive plus-end directed motor (Popchock et al., 2017), while Ncd, Kar3 and HSET are weakly (non)-processive minus-end directed motors. Differences between the two assays come from two major reasons: multiple motors are simultaneously involved in microtubule gliding and motor immobilization alters the molecule's conformation. Besides motor neck, additional microtubule-binding domains and coiled-coil region structure determine movement direction. In the case of KlpA that element is a microtubule-binding tail. Deletion of tail or insertion of flexible linker in the middle of coiled-coil converts KlpA into minus end motor (Popchock et al., 2017; Wang et al., 2018) (**Figure 1.5**).

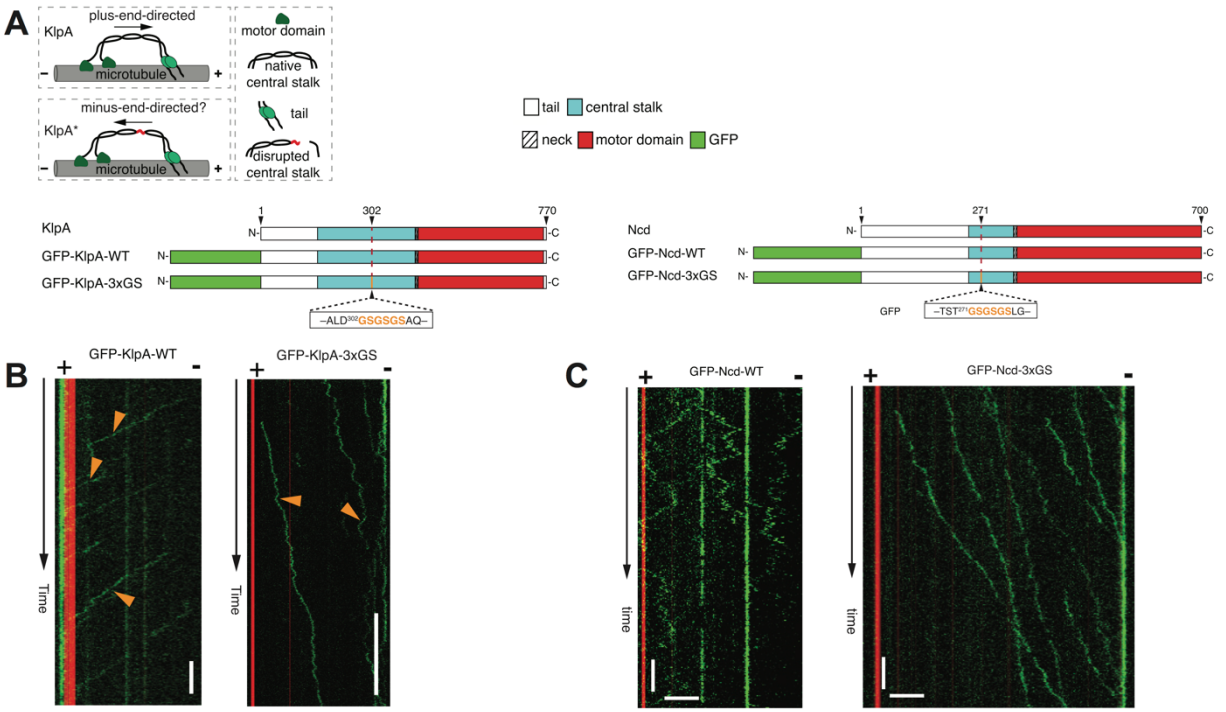

Figure 1.5 Processivity of kinesin-14 motors is defined by elements outside of the motor domain.

A) Processive plus-end directed kinesin-14 KlpA can be converted to the minus-end-directed motor by insertion of a flexible linker in the middle of stalk. Suggested motor movement scheme at the top.
B) Kymograph of GFP-KlpA (left side). Green signal accumulates at plus-end (red) of polarity-marked microtubules. GFP-KlpA-3xGS is a minus-end directed motor (right side). Tracks are shown with arrowheads.
C) Non-processive kinesin-14 Ncd displays bi-directional diffusion with short microtubule residence time (left side). GFP-Ncd-3xGS is a processive minus-end directed motor (right side). Scale bars are 30s on the time axis and 5 μm on the coordinate axis. Adapted from (Wang et al., 2018) with changes.

Processivity is defined as an ability to make many steps without microtubule detachment. There is a big discrepancy in the reported data concerning processivity, speed and microtubule affinity of kinesin-14 motors. A reason might be that that for kinesin-14s these properties are very sensitive to experimental parameters, like ionic strength. In low salt conditions, Ncd displayed a processive movement, dependent on its tail (Furuta and Toyoshima, 2008). Positively charged N-terminal tails of Ncd, HSET and Kar3 may contribute to increased microtubule residence time. They interact with C-terminal tubulin E-hooks and deletion of kinesin-14s tails or partial tubulin digestion reduces or completely abolishes binding of kinesin-14s to microtubules (Reinemann et al., 2018). In addition, Ncd motors can work in ensembles, where multiple motors move processively without microtubule detachment (Furuta et al., 2013). Processive HSET

clusters, that promote microtubule aster formation, are assembled by binding of its tail to soluble tubulin oligomers (Norris et al., 2018) (**Figure 1.6**).

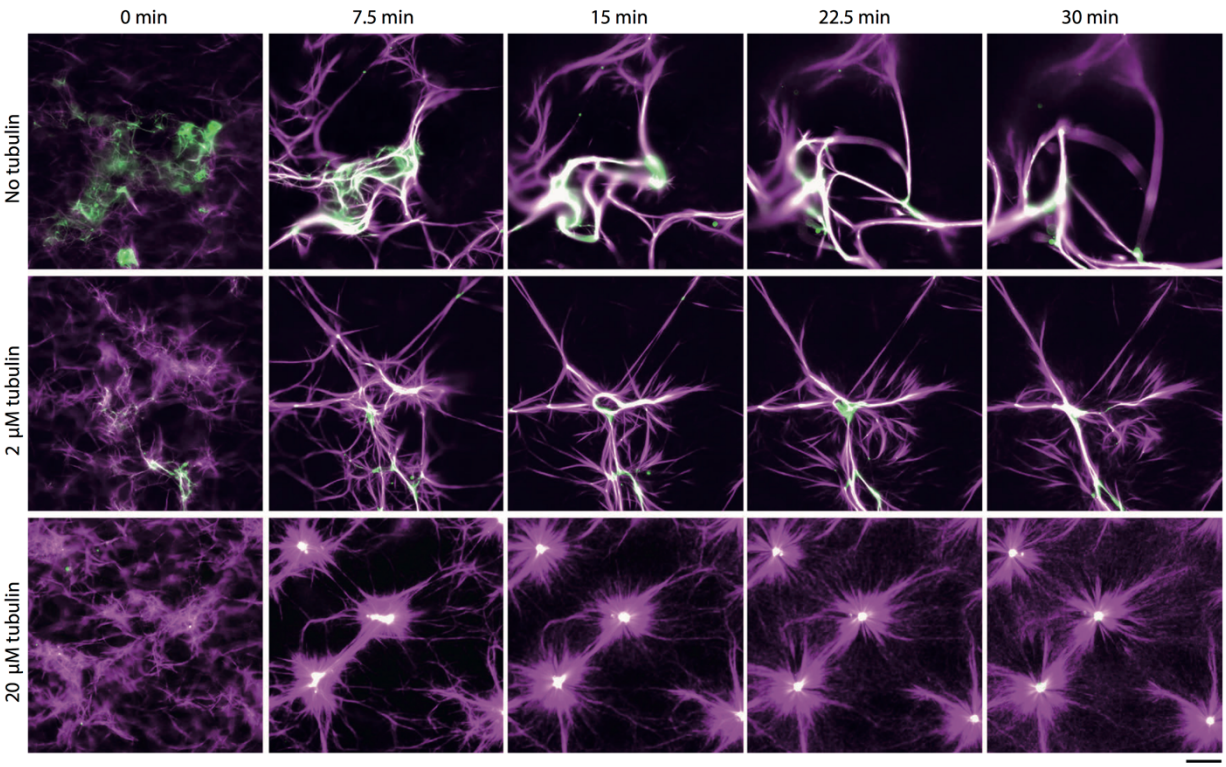

Figure 1.6 HSET clusters bound with soluble tubulin oligomers with tails drive assembly of microtubules into asters.

Reaction contained GMCPP stabilized microtubules (purple), EGFP-HSET (green) and variable concentrations of unlabeled tubulin, incubated for indicated time at 37° C. Scale bar is 50 μm. Adapted from (Norris et al., 2018) with changes.

The reported speeds of kinesin-14s vary greatly between family members. Ncd has a speed of 15 nm/s (Endow, 1998) with very short tracks - about 100 nm, however coupling two or more Ncd molecules together improves track length up to several micrometers (Furuta et al., 2013). Cik1-Kar3 speed is 50 nm/s and average tracks are 500 nm. During movement Ncd, HSET and Cik1-Kar3 frequently make steps in the plus-end direction. For Ncd and Cik1-Kar3 applied force of 0.25 pN stops motors and 0.5 pN changes their direction to opposite (Molodtsov et al., 2016), for HSET stall force is 1 pN (Reinemann et al., 2018). These stall forces are low compared to conventional Kinesin-1. HSET purified from HeLa cells was able to glide microtubules with the speed 5 μm/min (DeLuca et al., 2001). On single microtubules HSET demonstrated diffusional behavior (Braun et al., 2017). In another study, recombinant HSET displayed bi-directional movements up to ~1 μm lengths (Reinemann et al., 2018).

The molecular architecture of kinesin-14s is characterized by a long rigid coiled-coil stalk connecting the motor domain with the tail, containing an additional microtubule binding domain. This configuration prevents interaction of motor and tail with the same microtubule and favors microtubule crosslinking. While wild-type Ncd demonstrated diffusional behavior on single microtubules, insertion of a 3xGS linker into the coiled-coiled increased track lengths to 11 μm and run speed to 207 nm/s (Wang et al., 2018) (**Figure 1.5**).

1.4 Cellular localization and functions of Kinesin-14 motors

In cells kinesin-14s most frequently can be found at microtubule plus ends, microtubule overlapping zones and in the vicinity of MTOCs. Kinesin-14s are in general non-essential proteins, their deletions are viable on the level of organisms. However, they contribute to mitotic and meiotic spindle assembly and are required for microtubule aster formation in the absence of centrosomes. Below, I will describe localization and cellular functions of several kinesin-14 family members.

The first known kinesin-14 Ncd was discovered in fruit flies and its mutations caused a high rate of chromosome missegregation in meiosis and mitosis (Endow et al., 1990). Ncd-deficient flies were viable, but they displayed somatic mosaicism and females were mostly sterile (Sturtevant, 1929, Davis, 1969). In oocytes, Ncd bundles and focuses microtubules to the poles, thus promoting bi-polar spindle formation (Matthies et al., 1996). In early *Drosophila* embryos Ncd is required for establishing the *bcd* mRNA gradient (Fahmy et al., 2014). In mitosis, Ncd works mainly as a microtubule crossllinker. From *in vitro* data, it was hypothesized that Ncd provides inwardly directed force on mitotic spindles by minus-end directed microtubule gliding. However, in opposite to that, Ncd overexpression caused dose-dependent increase in mitotic spindle length (Goshima et al., 2005b). Ncd crosslinks and bundles interpolar microtubules as well as K-fibers and both C-terminal motor domain and N-terminal tail are required for microtubule crosslinking. It was proposed that Ncd promotes static crosslinking of parallel microtubules (Fink et al., 2009). However, Ncd half-recovery time after photobleaching is 2.5 s, indicating high turnover rate on mitotic spindles. Ncd tracks the ends of polymerizing microtubules in EB1-dependent manner and plus-end localization is essential for kinesin-14's cellular functions (Goshima et al., 2005a). Ncd contributes to the formation of a proper spindle structure not only by K-fiber crosslinking but also by focusing microtubules to the poles and their anchoring to

MTOCs. In *Drosophila* S2 cells, Ncd is required to prevent multipolar spindle assembly (Kwon et al., 2008). Ncd is able to slide microtubules against each other within a bundle (Oladipo et al., 2007).

The human HSET motor mainly localizes to spindle microtubules and MTOCs and weakly to kinetochores. *In vitro*, HSET tracks growing microtubule plus-ends in a complex with EB1 (Braun et al., 2013). In wild-type cells HSET depletion in mitosis does not result in severe defects – cells have mildly decreased spindle size and increased spindle width. HSET overexpression leads to increased spindle size that is dependent on motor sliding activity (Cai et al., 2009) **(Figure 1.7)**.

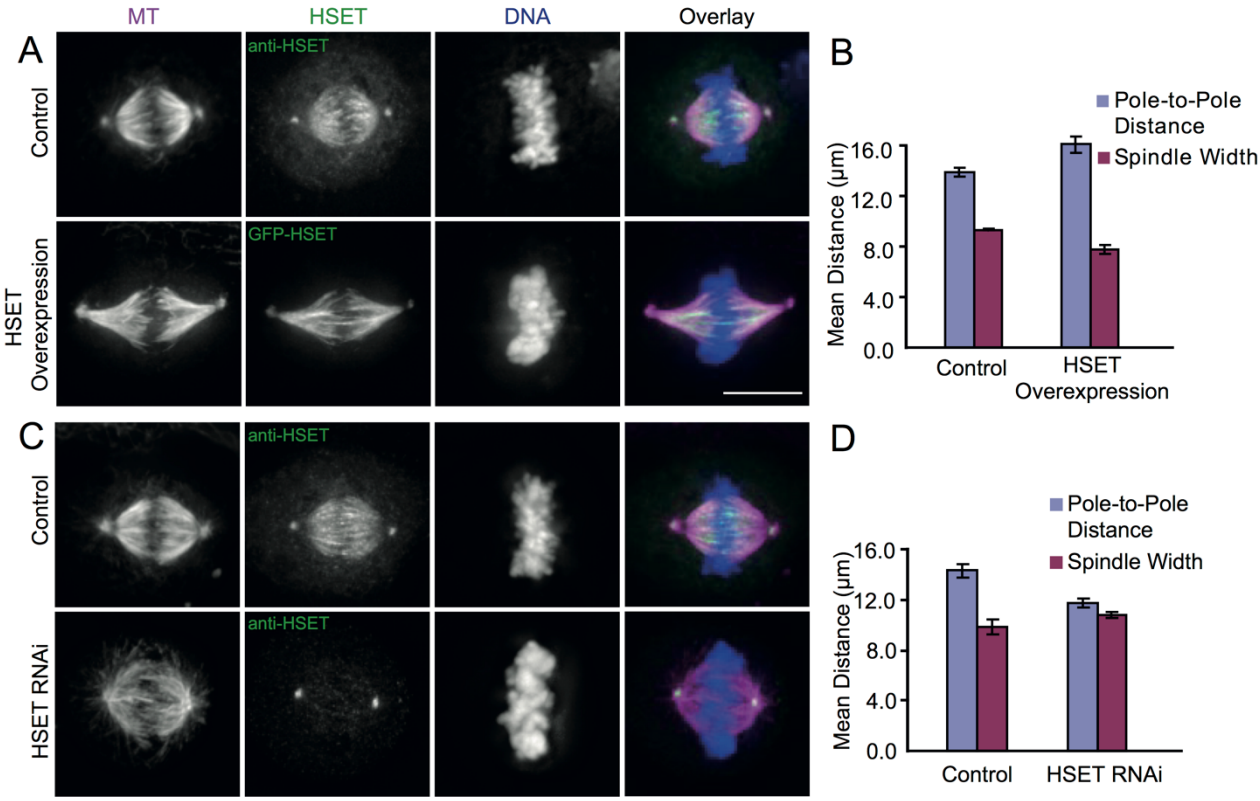

Figure 1.7 HSET affects mitotic spindle structure.

A) Examples of mitotic spindles in control and HSET-overexpression conditions. Merge images have microtubules in purple, HSET in green and DNA in blue colors.
B) HSET overexpression leads to spindle elongation, accompanied with decrease in spindle size.
C) Representative images of control and HSET-depleted cells.
D) HSET depletion leads to decrease in spindle length and increase in spindle width. Centrosomal staining in HSET RNAi is non-specific. Scale bar is 10 μm. Adapted from (Cai et al., 2009) with changes.

Targeting of HSET to the cytoplasm induces microtubule bundling. Kinesin-14 contributes to bipolar spindle assembly by microtubule crosslinking and microtubule focusing. HSET is required for bi-polar spindle formation in cancer cells (Kleylein-Sohn et al., 2012). Loss of HSET functions in microtubule focusing are compensated by centrosome activity in normal cells. HSET overexpression is a common feature of various cancer types that correlates with their aggressiveness. Another study suggests pro-proliferative functions of HSET upstream of HIF1α and Aurora B and a possible interaction of HSET with survivin (Pannu et al., 2015). HSET mediates centrosome clustering thus promoting survival of many extracentrosomal cancer cell lines. This activity requires phosphorylation of HSET by ATM/ATR DNA damage response kinases at S26, which is a part of the EB1-binding SxIP motif (Fan et al., 2021) (**Figure 1.8)**. HSET is an attractive target of anti-cancer therapy since its inhibition can selectively affect cancer, but not normal cells. HSET might also provide a link between Golgi apparatus and microtubules (She et al., 2017).

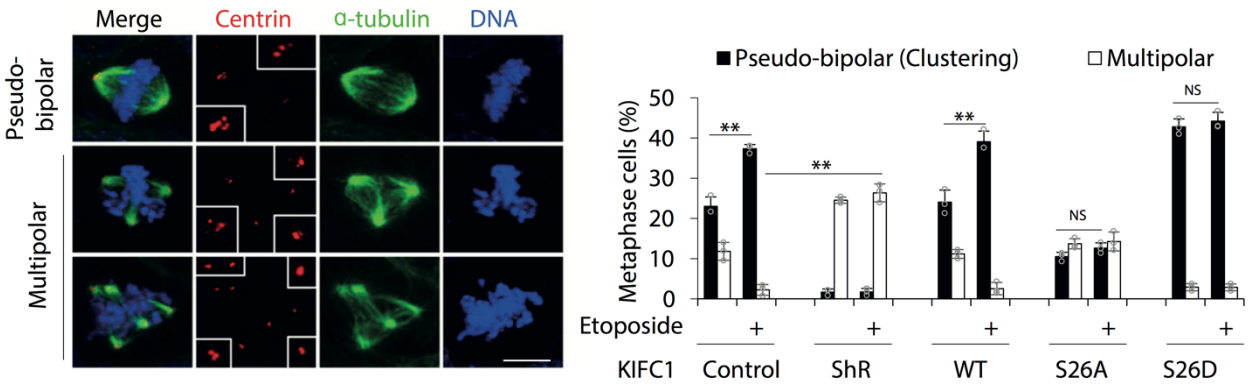

Figure 1.8 HSET (KIFC1) phosphorylation at S26 is required for centrosome clustering.

Images of MDA-MB-231 cells after 15 h of etoposide exposure. Pseudo-bipolar spindles are assembled by HSET-dependent centrosome clustering. Cells were stained with centrin, tubulin and DAPI, as indicated. Scale bar is 10 μm. On the right side is quantification of bi-polar and multipolar metaphase spindles in control, HSET-depleted (ShR) and cells expressing $HSET^{WT}$, $HSET^{S26A}$, $HSET^{S26D}$. ATM/ATR interacts and phosphorylates HSET at S26, stabilizing protein upon DNA damage. Adapted from (Fan et al., 2021) with changes.

The kinesin-14 homolog XCTK2 is required for bi-polar spindle assembly in *Xenopus* cell-free egg extracts (Walczak et al., 1997). Like other kinesin-14s, XCTK2 is a microtubule crosslinker and spindle focusing factor, that is dependent on its N-terminal microtubule-binding tail. Binding of the tail to microtubules is regulated by

interaction of an NLS with α/β-importins. Ran-GTP releases importins and allows XCTK2 to bundle microtubules (Weaver et al., 2015).

Fission yeasts have two kinesin-14 paralogs with distinct cellular localizations and functions – Pkl1 and Klp2. Pkl1 is a nuclear protein that is mainly localized to SPBs and weakly stains spindle microtubules. Pkl1 together with its binding partners Msd1 and Wdr8 anchors spindle microtubules to the poles. Disruption of Pkl1-Msd1-Wdr8 complex leads to pole defocusing and appearance of long protruding microtubule minus-ends curving the nuclear envelope. Pkl1 motor activity is required for its targeting to the SPBs and artificial tethering of a rigor mutant to SPB allows it to fulfill cellular functions (Yukawa et al., 2015). Pkl1 deficiency results in aneuploidy that escapes mitotic checkpoint quality control. Aneuploidy arises after pushing chromosomes segregated in anaphase back to the cytokinesis site, which causes a chromosome cut. Long protruding microtubules minus-ends appear by sliding of antiparallel microtubules with the kinesin-5 Cut7 (Syrovatkina and Tran, 2015) **(Figure 1.9)**. The double mutant *pkl1*Δ *cut7*Δ displays milder phenotypes than each individual mutant. A molecular characterization of kinesin-14 showed that a peptide motif in the Pkl1 tail is responsible for *cut7*Δ suppression. Pkl1 binds to the γ-TuRC, thereby inhibiting microtubule nucleation, while Cut7 competes with Pkl1 for γ-TuRC binding (Olmsted et al., 2013, Olmsted et al., 2014).

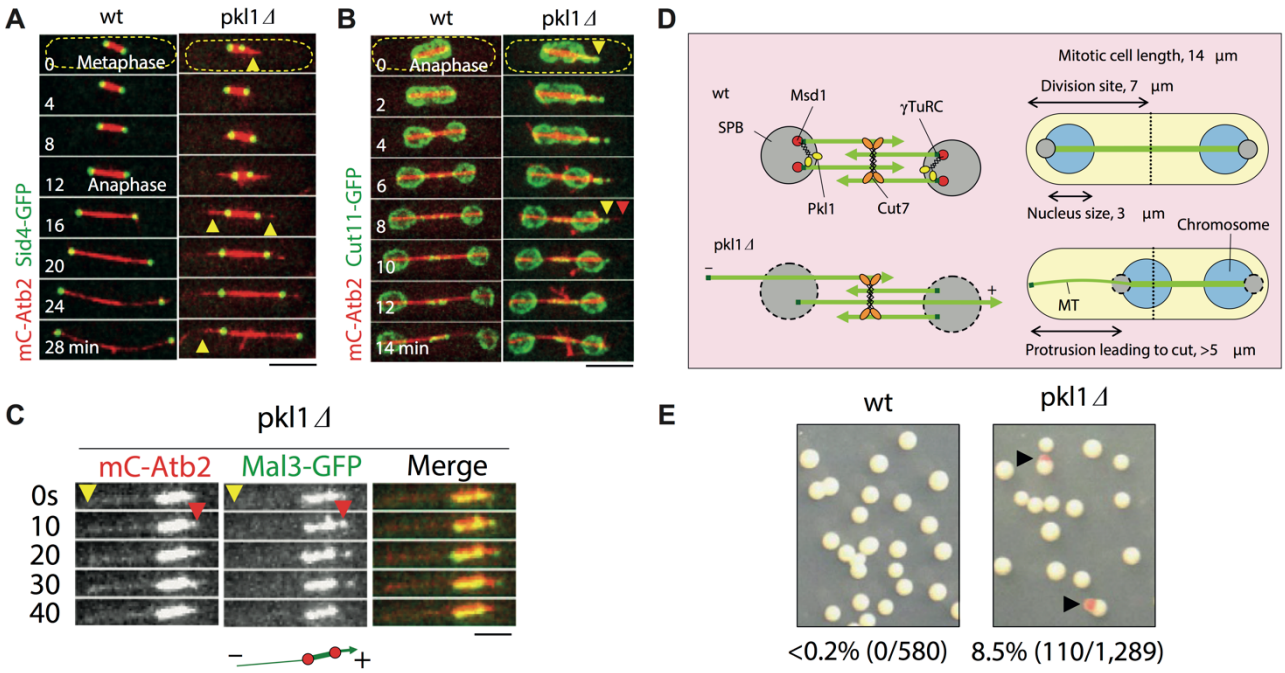

Figure 1.9 Pkl1 anchors microtubule ends at SPBs and prevents chromosome cut.

A) Live-cell microscopy of control and *pkl1*Δ cells. Tubulin is labeled with red color, SPB in green. *pkl1*Δ cells have long microtubule protrusions beyond SPBs, marked with yellow triangles. Scale bar is 5 µm.
B) Time-lapse imaging of control and *pkl1*Δ cells, nuclear membrane is labeled in green. Protruding microtubules are in the nucleus and cause membrane curvature. Protruding microtubules can pierce nuclear envelope, that is marked with red arrowhead.
C) Mal3-GFP was used as a marker of microtubule plus-ends. Long microtubule has no Mal3 signal at the end, labelled with a yellow triangle.
D) Model, describing Pkl1 contribution to microtubule anchoring and chromosome segregation. Protruding microtubules arise after kinesin-5 activity.
E) *pkl1*Δ cells have a high rate of minichromosome loss (pink colonies).
Adapted from (Syrovatkina and Tran, 2015) with changes.

Another fission yeast kinesin-14 Klp2 is a Mal3/EB1-dependent microtubule plus-end tracking protein and microtubule bundler (Mana-Capelli et al., 2012). Klp2 works on both nuclear and cytoplasmic microtubules. Microtubule bundles containing microtubules of both polarities exist in the cytoplasm of interphase fission yeast cells. Klp2 contributes to bundle assembly by transporting newly nucleated microtubules towards the bundle midzone. Klp2 is able to slide only anti-parallel microtubules to this place, where their minus-ends would be fixed in an overlapping zone by Ase1 (Janson et al., 2007) (**Figure 1.10)**. In mitosis, Klp2 localizes along spindle microtubules. It was reported that Klp2 localizes to unattached kinetochores and transports them to the SPB, an activity that depends on the outer kinetochore subunit Dam1c (Gachet et al., 2008).

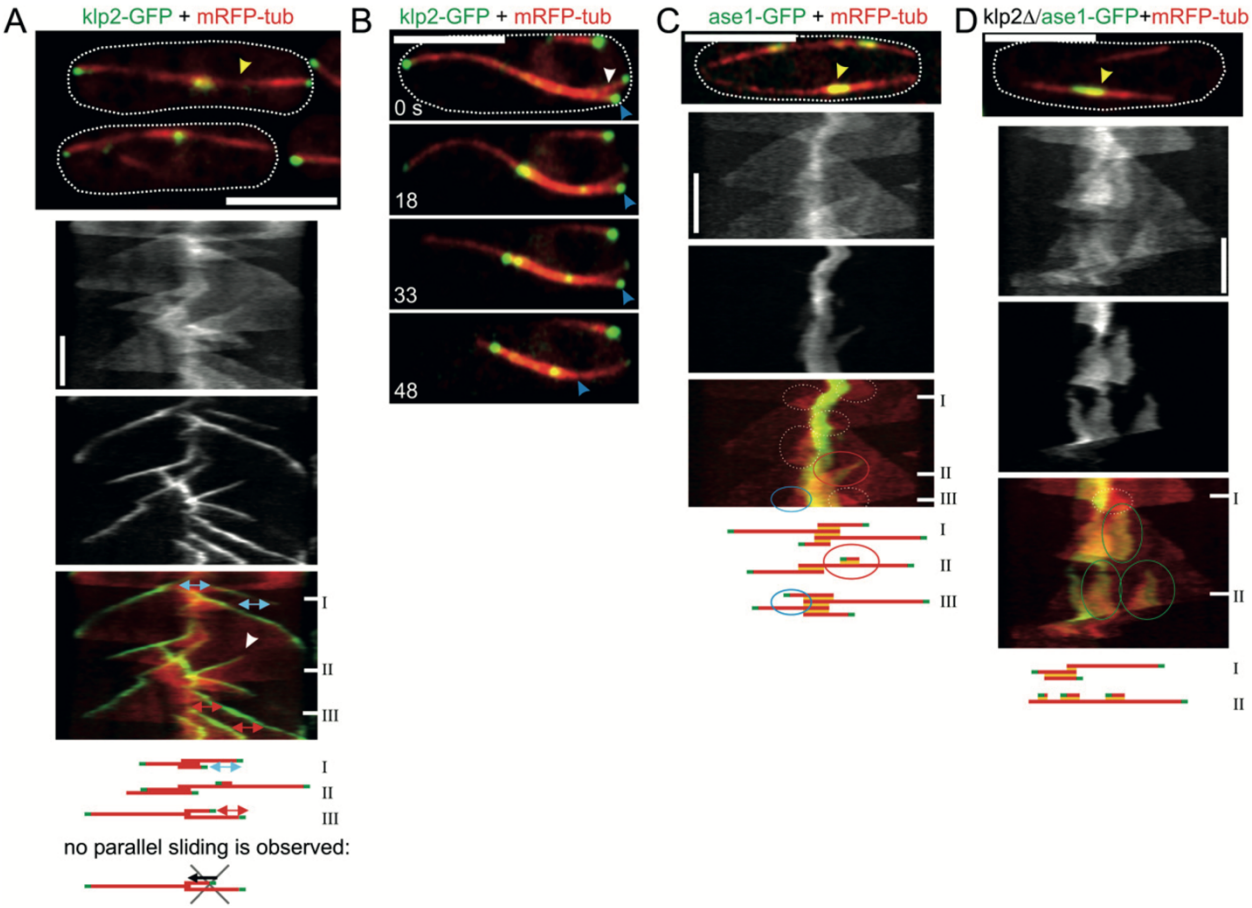

Figure 1.10 Plus-end localized Klp2 slides antiparallel microtubules to bundle midzone.

A) Klp2-GFP is localized to microtubule plus-ends. A newly nucleated microtubule is marked with a white arrowhead. Upper kymograph is for tubulin, middle for Klp2. Klp2 does not slide parallel microtubules, the same distance between plus-ends is shown with blue and red arrows. Scale bars are 5 μm and 2 min.
B) Antiparallel microtubule bundle containing 3 microtubules at 0s. One is growing to the left side, two to the right side. Microtubules are growing and shrinking while midzone remains intact.
C) Microtubule crosslinker Ase1 preferentially localized to anti-parallel overlap zone. Newly nucleated microtubule is labelled with a red oval. Parallel overlapping zone marked with blue oval.
D) Klp2 is required for microtubule sliding. *klp2*Δ causes Ase1 signal spread after bundle disorganization.
Adapted from (Janson et al., 2007) with changes.

Budding yeast kinesin-14 Kar3 exists in two heterodimeric complexes with the kinesin-associated proteins Cik1 or Vik1 (Page and Snyder, 1992, Page et al., 1994, Manning et al., 1999). Cik1-Kar3 has two types of localization, controlled by the expression of different Cik1 isoforms. In cycling cells Cik1-Kar3 displays the behavior

of a typical mitotic protein. It is absent in G1 phase, starts to be expressed when the cell enters S phase and is degraded by the APC/C in anaphase (Benanti et al., 2009). A long Cik1 version is a mitotic isoform that contains an additional 35 N-terminal amino acids with an NLS signal. The short Cik1 isoform binds to cytoplasmic microtubules, is induced by mating pheromone and lacks an NLS. In metaphase, the Cik1-Kar3 signal is detected along the entire spindle with an increased accumulation close to SPBs. As the cell enters anaphase, the signal disappears with rare weak dots in the middle of the spindle remaining. Genetic deletion of Cik1-Kar3 results in accumulation of large-budded cells accompanied by a metaphase delay. The metaphase delay is caused by incorrect tensionless chromosome-microtubule attachments, which are released by Ipl1/Aurora B kinase activity and generate unattached kinetochores that prevent mitotic checkpoint silencing. Loss of Cik1-Kar3 leads to frequent appearance of syntelic attachments that require additional detection mechanisms, like the tension checkpoint component Sgo1 (Jin et al., 2012). Kinesin-14 contributes to microtubule crosslinking and assembly of metaphase spindle of proper length (Hepperla et al., 2014). A *kar3*Δ strain contains an increased cytoplasmic microtubule number and length (Saunders et al., 1997). Further, an *in vitro* study suggests a role of Cik1-Kar3 as a microtubule depolymerase, shortening microtubules at minus-ends (Sproul et al., 2005).

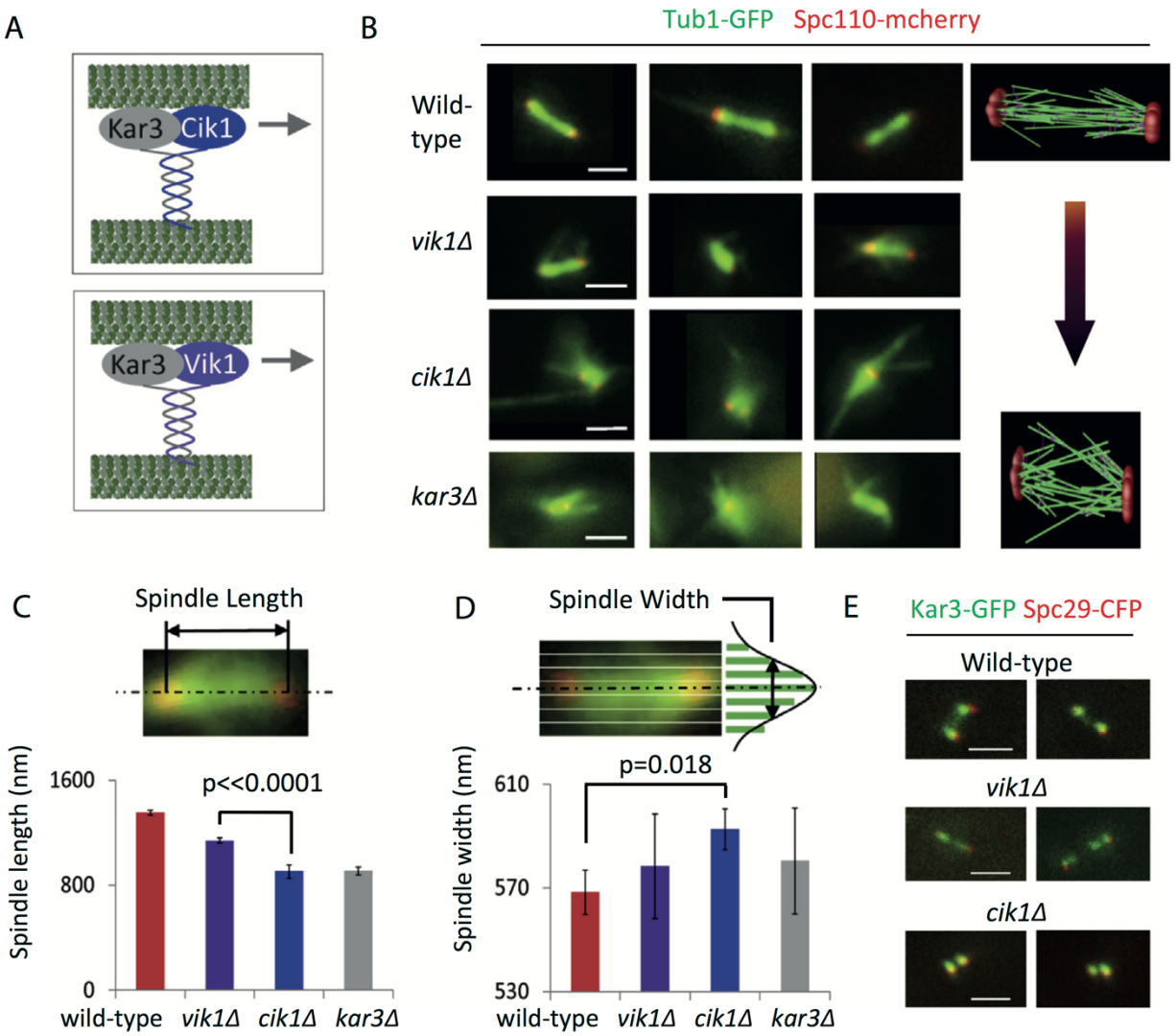

Figure 1.11 Cik1-Kar3 is required for metaphase spindle alignment.

A) Kinesin-14 exists in two functionally distinct complexes in metaphase cells Cik1-Kar3 and Vik1-Kar3
B) Representative images of indicated stains. Scale bar is 1 μm.
C) Quantification of spindle length.
D) Quantification of spindle width.
Adapted from (Hepperla et al., 2014) with changes.

According to the microtubule zippering model, Cik1-Kar3 aligns antiparallel microtubules along the spindle axis. In this model, Cik1-Kar3 tails are attached to misaligned microtubules, while the motor domain moves towards SPB (Hepperla et al., 2014).

Below I will describe the main points of experiments that have reported lateral kinetochore transport by Kar3. That experimental setup has a pGal promoter integrated upstream of the CEN sequence. After cells transfer into the media with galactose as

an energy source, transcription gets activated and displaces kinetochore from centromere. Before that, an essential APC subunit Cdc20 is depleted. Cdc20 depletion results in persistent metaphase arrest with drastic changes in the microtubule cytoskeleton. Normal metaphase cells have 40 nuclear microtubules: 16x2 kinetochore microtubules and 8 interpolar. After 8h of Cdc20 depletion the number of microtubules rose to 56 (O'Toole et al., 1997). Mitotic spindle length increases continuously during the arrest and spindle begins to jump between mother and bud. The nuclear envelope became curved and overextended towards the bud (Witkin et al., 2012). Reactivation of the CEN by transfer cells into glucose-containing media causes an occasional appearance of exceptionally long nuclear microtubules that may by chance interact with de-novo assembled kinetochores. It has been reported that after an interaction with the microtubule's lateral side the kinetochore sometimes undergoes sliding towards the SPB, an activity that depends on Kar3 motor activity (Tanaka et al., 2005, Tanaka et al., 2007).

In α-factor arrested cells Cik1-Kar3 binds to microtubule plus-ends, lattice and SPB. The SPB binding requires Kar1 and is mediated by interaction with the γ-TURC component Spc72 (Vallen et al., 1992, Gibeaux et al., 2013). Loss of Cik1-Kar3 causes a karyogamy defect, as the SPB localized pool of the protein normally captures and slides antiparallel microtubules to bring two nuclei together (Gibeaux et al., 2013). At the shmoo tip Cik1-Kar3 couples depolymerizing plus ends of the microtubule bundle to the membrane (Maddox et al., 2003). By crosslinking plus ends of growing microtubule to pre-existing bundle Cik1-Kar3 promotes microtubule alignment (Molodtsov et al., 2016).

Another kinesin-14 complex in budding yeast is Vik1-Kar3. It is a mitotic protein complex with unclear functions. Vik1-Kar3 is localized to SPBs and may mediate microtubule minus end anchoring to the SPB. Loss of Vik1 results in a relatively mild phenotype with increased tolerance towards the microtubule drug benomyl. Disruption of Cik1 causes a stronger effect than disruption of Kar3, even after taking into account the negative effect of upregulated Vik1-Kar3 in a cik1 deletion. The deletion of both paralogs simultaneously – Cik1 and Vik1 - behaves like the deletion of Kar3 (Manning et al., 1999).

1.5 Molecular interactions of Kinesin-14 motors

1.5.1 Bim1/EB1 binding

Microtubule plus-end tracking is a universal feature of kinesin-14A family members. In most cases that is achieved by interaction with autonomous plus-end tracking proteins of the MAPRE1 gene family (Bim1, Mal3, EB1 and others). EB1 proteins have a specialized CH-domain recognizing a tubulin conformation characteristic to growing microtubule plus-ends. At the same time, the EBH-domain binds to a set of SLiMs (short linear motifs) of cargo proteins. The SxIP and LxxPTPh motifs mediate most of the described EB1-cargo interactions (Honnappa et al., 2009, Kumar et al., 2017). The Ncd interaction with dmEB1 is mediated by SxIP motifs and Ncd-EB1 binding is required for enrichment at plus-ends in living cells (Goshima et al., 2005a, Braun et al., 2013). HSET has two SxIP motifs and elimination of one of them abolishes HSET localization to microtubule plus-ends in vitro (Braun et al., 2013) Phosphorylation of this motif by ATM/ATR promotes survival and drug resistance of cancer cells (Fan et al., 2021). Klp2 interacts with Mal3 via two SxIP motifs in its tail. Mutating both motifs reduces Klp2 loading on microtubules. The Mal3-Klp2 complex formation is inhibited by phosphorylation with the mitotic exit kinase Sid2. Phospho-preventing mutations cause Klp2 mis-localization to anaphase spindles and defects in their elongation (Mana-Capelli et al., 2012). Cik1-Kar3, but not Vik1-Kar3, binds to Bim1 in vitro, and Bim1 is required for localization of Cik1-Kar3 to microtubule plus-ends in cells (Mieck et al., 2015, Molodtsov et al., 2016).

Kinesin-14		Sequence	UniProt Reference
HSET	Human	1-MDPQRSPLLEVKGNIELKRPLIKAPSQLPLSGSRLKRRPDQMEDGLEPEKKRTRGLGATTKITTSHPRVP-70	Q9BW19
Kif1C	Chimpanzee	1-MDPQRSPLLEVKGNIELKRPLIKAPSQLPLSGSRLKRRPDQMEDGLEPEKKRTRGLGATTKITTSHPRVP-70	H2QST6
Kif1C	Gorilla	1-MDPQRSPLLEVKGNIELKRPLIKTPSRLPLSGSRLKRRPDQMEDGLEPEKKRTRGLGATTKITTSHPRVP-70	G3QDE3
Kif1C	Orangatan	1-MD-PKSPLLEVKGNIELKRPLIKAPSRLPLSGSTLKRRPDQMEDGLEPEKKRTRGLGATTRITTSHPRVL-70	H2PIQ1
Kif1C	Gibbon	1-MDLQRSPLLEVKGNIEPKRPLIKAPSRLPLSGSRLKRRPDQMEDGLEPEKKRTRGLGATTKITTSHPRVP-70	G1RA63
KIFC1	Rhesus	1-MDPQRSPLLEVKGNIELKRPRIKAPSRLPLSGSRLKRRPDQMEDGLEPEKKRTRGLGATTKITTSHPRVP-70	I0FRK2
Kif1C	Marmorset	1-MDPQRSPLLELKGNIELKRPLIKAPSRLPLSGSRLKRRPDQMEDGLEPEKKRTRVLGATTKIATSRPRVP-70	F7IR24
KIFC1	Rat	1-MRGRGSRDTGTQSAAFASRPVRTTVDMQAQRAPLMEVKRNLELSTTLVKSSSRLPLPGSRLKRGPDQMED-70	Q5XI63
KIFC1	Mouse	1-MDVQAQRKGREGKRNVELKAALVKSSSRLPLSASSLKRGPDQMEDALEPAKKRTRVMGAVTKVDTSRPRG-70	Q5BJ94
KIFC1	Pig	1-METLRSPLLEVKGNIEVKRPLPKPPSRLPLSGSRLKRGPEQMEEALEPEKKRTRGLGTKIAPSRPRAALL-70	F1RZS7
KIFC1	Cow	1-MEPQRSPLLEVKGNVELKRPLAKAASRLPLSGRRLKRGPDQMEEALEPEKKRTRGLGTRVTTTHPRAAAL-70	A7MBA1
KIFC1	Tasman. devil	1-MEKGSKELKMPSDKASSSRLPVLGLGRKRRLDKENAPEPEKKRIRGTGTTIPMSCLKEATVATIPRAKKQ-70	G3VDU2
KIFC1	Opossum	1-MASCFLQKLSRMEKDNMELKMPPDKASSSQLPVLGLSAKRGLDKENVPEPKKKRARGPGTAATIAISHPR-70	F6XKS9
KIFC1	Chicken	1-MAAVGSGGSVGAAPGMAVVAPLPAPTSRLPVRRAAAKRAASGPQPAAPEQKRARSGTASSQPPGRAPLWA-70	A5HUJ1
KIFC1	Cynops	1-MNVDEKQPVAVMKSVSRLPVPSTLKTKRMRSNENMPVMEKKRLRLSSPDRVAQHRVPASIACTRPKPVAA-70	G4VV28
KIFC1	Octopus	1-MNGQRKVLADTANCSSKLPKLTPKLAKRKNSPNETEQVKKMRFQKPVSKIRTNLAPSSRLVNSQSIAGYN-70	D9D9T7
KIFC1	Crab	1-MSKLPSSASRHLHQPSRLRPPGSAMKRLGSDSAITSPQKKTRHSGDAEDTGAMARSQRLGGPRAAPGLSR-70	D9DBK9
KIFC1	Latimeria	1-MSEKVSSRLPVLKLGKKVLREENQQQRSLKRQCDTSPGHDLPKKKMVVSVVLKQSQAMAPIPRNPRGAGG-70	H3ADW2
KIFC1	Zebrafish	1-MNKENTSRLPVMSGKRAHTNSTDGEQQQPAQKKMRKVEVEPSQRFRPAASVAPPRRPVAVKAPVKPLRPT-70	Q7ZZ74
KLP15	C. elegans	1-MNVARRRSGLFRSTIGATPKITRGRAAAPSTKEANSTTIPRQSAPGGITIGAAARRPPSRLPTPTTPATG-70	P91400
KLP16	C. elegans	1-MNVARRRSGLFRSTIGAPPKATRGRAAAPPIKEADPATIPRQSAPGGITIGAAACRPPSRLPGATISATG-70	Q93366
XCTK2	Xenopus	1-MDSTDKKVQVASRLPVPPKRKYVSNDENQEQMQRKRLRSSLESELPAVRVAASIATSKPRAAPVAALPKP-70	Q5XGK6
Ncd	**Drosophila**	1-MESRLPKPSGLKKPQMPIKTVLPTDRIRAGLGGGAAGAGAFNVNANQTYCGNLLPPLSRDLNNLPQVLER-70	P20480
Klp2	**S. pombe**	1-MEEEGHKSLTSHLPQSSSSLSQSREIAKEFTSNIPPPTIKTNSSSSNILKPRLSLQNEVNQLKPAKFPSK-70	Q9US03
ATK5	**A. thaliana**	1-MPLRNQNRAPLPSPNVKKEALSSIPFDKRRKETQGTGRRQVLSTVNRQDANSDVGSTEECGKVEFTKDEV-70	Q6NQ77

Figure 1.12 N-terminal SxIP motifs are conserved in the kinesin-14 family.

Sequence alignment of 70 amino acids of kinesin-14s in various organisms. SxIP motifs are highlighted. Adapted from (Braun et al., 2013) with changes.

1.5.2 Interaction with γ-TURC components

Kinesin-14s are commonly found localized to MTOCs. Those interactions are mediated by different ways of indirect recruitment to the γ-tubulin ring complex. The role of HSET in centrosome clustering depends on CEP215. CEP215 contains a centrosomin motif 1 that binds to the γ-TURC. Disruption of the CEP215-HSET interaction leads to the formation of multipolar spindles (Chavali et al., 2016). Fission yeast kinesin-14 Pkl1 forms a ternary complex Pkl1-Wdr8-Msd1 and Msd1 binds the γ-TURC protein Alp4/GCP2. Pkl1-Wdr8-Msd1 anchors microtubule ends to SPBs (Yukawa et al., 2015). Pkl1 can also directly interact with the γ-TURC by a short peptide motifs in its tail, and those peptide motifs are conserved in kinesin-14s. Pkl1 blocks microtubule nucleation and the kinesin-5 Cut7 competes with Pkl1 for gamma-TURC binding (Olmsted et al., 2013, Olmsted et al., 2014). Cik1-Kar3 interacts with the gamma-TUSC receptor Spc72 and SPB localized Cik1-Kar3 slides microtubules emanating from opposing nuclei to bring them together (Gibeaux et al., 2013).

1.5.3 NLS signals of Kinesin-14 proteins

One of the intriguing molecular details of kinesin-14s is the presence of NLS signals in their tail domains. While it has an immediate sense for species that have a closed mitosis such as budding or fission yeast, the NLS functions in other organisms are less clear. An interesting observation is that expression of HSET or XCTK2 in the cytoplasm leads to premature microtubule bundle formation that might have a negative effects on mitosis (Cai et al., 2009). Another point is regulation of microtubule crosslinking and sliding by interaction of the NLS with importin. The amino-terminal tails of kinesin-14s contain microtubule-binding domains that can be blocked by importin binding. In this way, local microtubule bundling by kinesin-14s may be regulated by a Ran-GTP gradient (Weaver et al., 2015).

1.5.4 Force balance between Kinesin-5 and Kinesin-14 proteins

A common notion is that minus-end directed kinesin-14s counteract plus-end directed kinesin-5s during spindle formation. However, the nature of this counteraction is poorly defined and unclear, and may vary between different systems.

Kinesin-5 proteins are required for SPB/centrosome separation in many organisms. Typically, a Kinesin-5 deletion, depletion or inhibition leads to a mitotic arrest with an aster-like microtubule structure. An initial genetic observation was made in budding yeast that while the simultaneous deletion of the kinesin-5s Cin8 and Kip1 is lethal, it can be partially rescued by deletion of the kinesin-14 Kar3 (Saunders and Hoyt, 1992). From *in vitro* data it was suggested that those kinesins have an opposite directionality and may produce an opposite force on spindle microtubules. However, the predictions made by this hypothesis contradict, at least in part, the *in vivo* data. For example, according to the initial idea Kar3 provides inwardly directed force and its activity reduces spindle size. But deletion of Kar3 leads to short spindles, similar to deletions of Ncd and HSET, arguing against that. Moreover, genetic studies showed that Cik1-Kar3 works in parallel with Cin8 in promoting microtubule crosslinking. Moreover, deletion of Vik1-Kar3 rescues the viability of *cin8*Δ *kip1*Δ (Manning et al., 1999). Vik1-Kar3 localizes exclusively to SPBs and is not known to contribute to microtubule crosslinking. Recently it was shown that not a motor activity, but a microtubule crosslinking by kinesin-5 drives a bipolar spindle assembly (Leary et al., 2019).

The genetic rescue of a kinesin-5 deletion with a kinesin-14 deletion was also observed in *Aspergilus nidulance*, where KlpA deletion can rescue deletion of kinesin-

5 BimC (O'Connell et al., 1993). However, similar to BimC, KlpA is a processive plus-end directed motor on individual microtubules *in vitro*, although KlpA can slide microtubules towards minus ends. (Popchock et al., 2017).

In human cells centrosome separation can be restored without Eg5 by disruption of kinesin-14 or the CLIP-170-Lis1-dynein-dynactin complex (Tanenbaum et al., 2008). Monopolar spindles formed after Eg5 inhibition are probably caused by an unbalanced inward force provided by minus-end directed motors.

In fission yeast kinesin-14s Pkl1 and to a lesser extent Klp2 counteract kinesin-5 Cut7 in microtubule nucleation. Peptides motifs within the Pkl1 tail bind to γ-tubulin and suppress microtubule nucleation. Cut7 competes with Pkl1 peptides and thus permits microtubule nucleation. In the absence of kinesin-14 kinesin-5 becomes dispensable. Kinesin-14's peptide motifs are conserved from yeast to humans and are able to inhibit growth of mammalian cells (Olmsted et al., 2013, Olmsted et al., 2014). However, deletions of various microtubule-stabilizing proteins also can rescue the *cut7*Δ lethality. Part of them may work in complexes with kinesin-14s, like Pkl1-Wdr8-Msd1 and Mal3-Klp2. Others, like Alp14 and Dis1 are members of XMAP215 family of microtubule polymerases. Destabilization of microtubules with drugs can suppress *cut7*Δ as well (Yukawa et al., 2019). Taken together, these data indicate that the nature of kinesin-14's and kinesin-5's genetic counteraction can be far more complicated than explained by a simple force balance model.

1.6 Specialized kinesin-14s in plants mediate meiotic drive

Meiotic drive is a non-mendelian preferential segregation of selfish genetic elements to inheritors. The phenomenon of meiotic drive has been described in a variety of organisms from plants to mammals. In maize, the kinesin-14s KINDR and TRKIN interact with repetitive DNA sequences on different chromosomes to transport them into oocytes. KINDR and TRKIN are divergent kinesin-14 family members with relatively little sequence similarity to other kinesin-14s outside of the motor domain. KINDR and TRKIN are not homologous to each other and probably represent ancient branches of the kinesin-14's family evolution (Dawe et al., 2018, Swentowsky et al., 2020). However, besides minus-end directed motor activity they have nuclear localization signals, similar to HSET, Ncd and Cik1-Kar3. Interestingly, classical kinesin-14s Cik1-Kar3 and HSET also bind DNA with their tails. Cik1-Kar3 is able to

transport CEN-specific DNA-protein complexes *in vitro* and HSET transports exogenous DNA fragments *in vivo* (Middleton and Carbon, 1994, Farina et al., 2013).

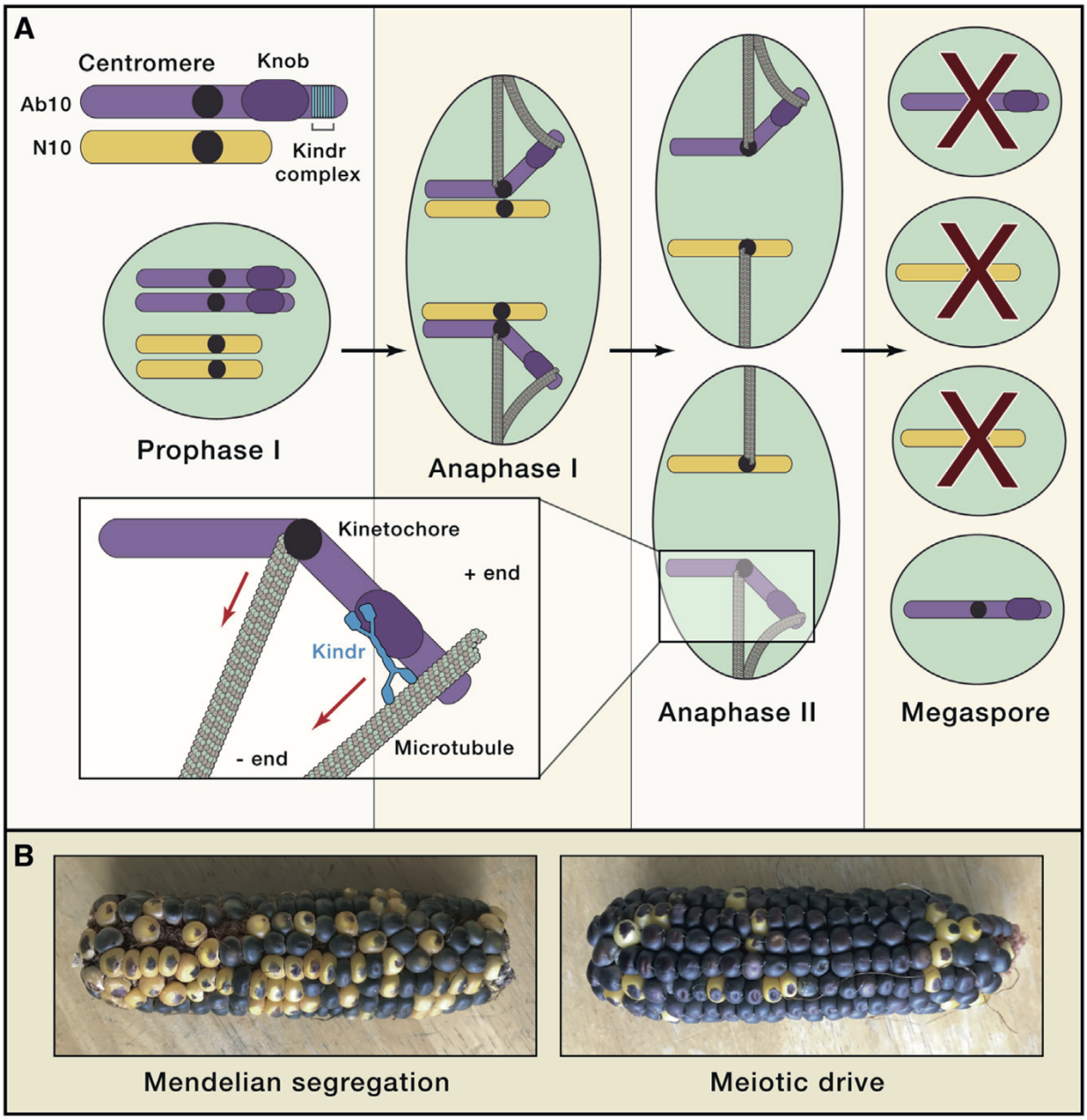

Figure 1.13 The Kinesin-14 KINDR mediates meiotic drive in maize.

A) Ab10 chromosome has a repeat cluster (Knob) with the KINDR gene, cluster is linked to purple kernel marker. Kernels with N10 chromosome are yellow. KINDR induces preferential segregation of Ab10 into megaspore.
B) KINDR drives its own inheritance, more purple than yellow kernels appear.
Figure is adapted from (Schroeder and Malik, 2018).

Aim and questions of the study

Despite the many described roles of Kinesin-14s in different organisms, it has remained unclear which function is most critical for spindle assembly and chromosome segregation. It has also remained unclear, whether Kinesin-14s fulfill their functions autonomously, or whether there are critical partner proteins required for their function.

To study the functions of Kinesin-14s more closely, the aim of the study was to establish a conditional inactivation system for Kinesin-14 in the model system budding yeast, in order to study the consequences of acute loss of Kinesin-14 function. Using genetic complementation, functionally critical motifs in Kinesin-14 should be identified and their role in spindle assembly and chromosome segregation should be studied. Besides genetic experiments, live cell fluorescence microscopy should be used to define Kinesin-14 phenotypes during spindle assembly and chromosome segregation. In addition, biochemical experiments with recombinant motor proteins should be used to define the molecular basis for the observed phenotypes.

2. Materials and methods

2.1 Materials

2.1.1 Media and buffers.

YEP media recipe, dissolve in 900 ml of water:

11 g	Bacto Yeast Extract
22 g	Bacto Peptone
0.05 g	Adenine hemisulfate

Sporulation media recipe, dissolve in 1000 ml of water, add 1:3 dilution of SC complete before use:

10 g	Potassium Acetate
1 g	Bacto Yeast Extract
0.5 g	Glucose

Minimal media recipe, dissolve in 900 ml of water, add SC complete:

8 g	Yeast Nitrogen

200 mL of 100x SC complete mix contains:

0.4 g	Adenine hemisulfate
0.6 g	L-Leucine
0.4 g	L-Tryptophane
0.4 g	Uracil
0.6 g	L-Lysine
0.4 g	L-Histidine

LB media recipe, dissolve in 1000 ml of water:

20 g	LB Broth (Lennox)

For casting plates, 22 g of Bacto Agar is added to 1 L of corresponding media. Sugars are added to final concentration 2% after autoclaving.

MultiBAC plates contained following components:

50 μg/ml	Kanamycin

7 μg/ml	Gentamycin
10 μg/ml	Tetracyclin
40 μg/ml	IPTG
100 μg/ml	X-Gal/Blue Gal

1 L of 10xTE buffer contained:

100 mM	Tris-HCl pH 7.5
10 mM	EDTA pH 8.0

1L of 10xTBS buffer contained:

200 ml	1 M Tris-HCl pH 7.5
300 ml	5 M NaCl
500 ml	water

Table 1. Key materials

REAGENT	SOURCE	IDENTIFIER
Antibodies		
mouse anti-GFP	Roche	Cat# 11814460001
mouse anti-Myc	Covance	9E10, Cat# MMS-150R
mouse anti-PGK	Invitrogen	Cat# 459250
mouse anti-Flag M2-HRP	Sigma	Cat# A 8592
rat anti-tubulin-HRP	Santa Cruz	Cat# sc-53030
anti-mouse-HRP	GE Healthcare	Cat# NA931
Chemicals, Commercial Assays		
Amersham ECL Prime Western Blotting Detection Reagent	Cytiva/GE Healhcare	RPN2232
Cellfectin II Reagent	ThermoFisher Scientific	10362100
Protein Assay Dye Reagent Concentrate	Bio-Rad	5000006
ANTI-FLAG M2 Affinity Agarose Gel	Sigma	A2220
TALON Metal Affinity Resin	Clontech	635503
Spodopan	Pan Biotech	P04-85050
Organisms/Strains		
S. cerevisiae S288C	ATCC	ATTC: 204508
Commercial plasmids		
pLIB/pBig1a		(Weissmann et al., 2016)
pET3a		(Tan, 2001)
pCC508, 509 and 510	Chris Campbell	
pHTN HaloTag	Promega	Cat#G7721

Software		
ImageJ/Fiji	NIH	https://imagej.net/Fiji
SoftWoRx 7	GE Healthcare	
GraphPad Prism 7.0 and 8.0	GraphPad	https://www.graphpad.com
Unipro UGENE	Unipro LLC	http://ugene.net
Adobe Illustrator	Adobe	https://www.adobe.com
Other		

2.2 Methods

2.2.1 DNA technologies

2.2.1.1 PCR protocol

For all basic DNA amplification procedures Q5 hot-start DNA polymerase was used according to manufacturer's recommendations. An example PCR protocol is listed in **Table 2**.

Table 2. Example of PCR protocol

Component	For 25 μl	For 50 μl	For X = μl
H_2O	17.75	34	
5xQ5 buffer	5	10	
20 μM F primer	0.625	1.25	
20 μM R primer	0.625	1.25	
dNTPs	0.5	1	
DMSO	0.75	1.5	
Template DNA	0.1	0.5	
Polymerase, Q5	0.25	0.5	
Annealing temperature	55° C	55° C	

For gene amplifications from plasmids 25 cycles with 30s per 1 kb was routinely used, for genomic DNA as a template, the number of cycles was 32. The extension phase was increased to 1min/kb for difficult templates. PCRs were performed in Biorad thermocycler (C1000 Touch Thermal Cycler).

98° C		2 min	Initial denaturation
25x	98° C	30 s	Denaturation
	55° C	30 s	Primer annealing
	72° C	2 min	Extension phase
72° C		5 min	Final elongation
4° C		∞	Hold

2.2.1.2 Gibson assembly

To prepare constructs for protein co-expression in insect cells the pLIB/pBig1a plasmid system was used (Weissmann et al., 2016). As the first step, protein-coding genes were inserted into the pLIB vector by restriction cloning. After that, genes were amplified by PCRs with cassette primers CASI-CASV. For Kar3 and Cik1 primer pairs αForw/CASI Rev and CASII Forw/ω Rev were used, respectively. PCR products were purified with Invitrogen DNA purification kit. pBig1a vector was linearized by SwaI overnight digestion. 100 ng of pBig1a were mixed with 5x molar excess of inserts in Isothermal reaction (ITR) buffer with Tag ligase, Phusion polymerase and T5 exonuclease **(Table 3)**. The reaction was incubated at 50° C for 1h in the thermocycler and further transformed into XL10 gold competent bacteria cells. Successful integrations were confirmed by SwaI restriction digest.

Table 3. Example of Gibson assembly protocol

Component	**For 20 μl Volume**
5x ITR buffer	4
Taq ligase	2
Pfusion polymerase	0.25
1 to 30 dilution of T5 exolnuclease in 1x ITR buffer	0.25
100 ng of pBig1a vector	
Inserts, 5x molar excess over vector	
H_2O	up to 20 μl

2.2.1.3 Bacmid preparation

pBig1a vectors were transformed into DH10 MultiBac competent cells. 1-2 μg of plasmid were added to 100 μl bacteria cells thawed on ice. The mixture was incubated for 20 min at 4° C and transferred to 42° C for 45 s. Cells were allowed to recover for 5 min at 4° C and then 1mL of SOC was added followed by growth for 3-4 h at 37°. Different amounts of cells were plated on MultiBac plates, which allowed blue-white selection after 1.5-2 days of growth. Bacmids were isolated by alkaline lysis of bacteria followed by isopropanol precipitation.

2.2.1.4 Oligonucleotide synthesis

All DNA oligonucleotides used in the study were synthesized by Eurofins.

2.2.1.5 Whole plasmid amplification

Mutations of several neighboring amino acids to prepare Cik1^{SKAA}, Cik1^{4A} constructs were introduced by whole-plasmid amplification using overlapping primers followed by in-bacteria recombination. For example, the natural SKIP sequence of Cik1 was changed to SKAA using the following pair of primers:

FN185 AACTCCAAAGCAGCGAAACTTTCCTTTCATAGTGATC

RN185 AGGAAAGTTTCGCTGCTTTGGAGTTATTCATGGATCC

Primers partially overlap in the mutation-containing region.

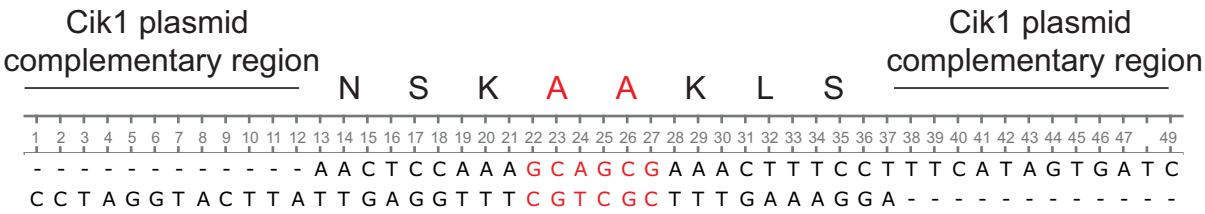

After amplification of mutants, the template was digested by DpnI at 37° for 1h, then the reaction mix was transformed into XL10 gold competent bacteria cells.

2.2.1.6 Restriction digest and ligation

For plasmid restrictions an excess of restriction enzymes (NEB) was used, 3-5 U of enzyme per 1 μg of DNA. Usually, reactions were performed in the CutSmart buffer and incubated for 2 h at 37° C. For DNA ligation 3x-5x molar excess of insert to plasmid was used. Reactions were performed in 20 μl volume at room temperature for 1h or overnight at 16° C. Further, 2-5 μl of ligation mixture (an equivalent of ~ 10-25 ng of ligated vector) were transformed into XL10 bacteria, which typically gave ~ 50-100 colonies.

2.2.1.7 Agarose gel electrophoresis

DNA fragment size and purity was analyzed by electrophoresis in 0.8-1.5% (w/v) SeaKem LE agarose (Lonza) TAE gels, supplemented with peqGREEN (Peqlab) DNA stain. Prior to loading on gels the samples were mixed with 6x loading dye (Thermofisher Scientific). Gels were run at 120 V and visualized with UV illumination (Biorad). For DNA fragments extraction from gel blue light (BLstar 16 Biometra) was used to cut bands that were further purified with gel extraction kit (FastGene NIPPON Genetics).

2.2.1.8 Plasmid DNA purification

Plasmids were purified using a Miniprep kit (Macherey-NAGEL) according to provided instructions.

2.2.2 Recombinant protein work

2.2.2.1 Protein expression and purification in insect cells

Bacmids encoding Cik1-Kar3 complexes were transfected into Sf9 insect cells with Cellfectin II reagent according to the manufacturer's protocol. Cells were grown for 3 days after transfection in 6-well dishes. After that, 2 mL of dish virus-containing media was collected, filtered and added to 100 mL of freshly split Sf9 culture with a cell density of 1-1.2x10^6 cells/ml. Usually, 3 days after infection 80-90% of cells were positive for a GFP reporter construct. For test purification cells were collected by centrifugation and frozen in liquid nitrogen. 100 mL of supernatant was filtered and stored at 4° C for further infections.

For protein purifications, the pellet was thawed on ice and resuspended in lysis buffer by pipetting up and down. Lysis buffer consisted of 25 mM HEPES-KOH pH 7.4, 150 mM NaCl, 1 mM $MgCl_2$, 5% (w/v) glycerol, 0.1% (v/v) Tween-20, 0.5 mM TCEP, 0.5 mM ATP, 0.1 mM PMSF and protease and phosphatase inhibitors (Roche). Cells were lysed by 15-20 strokes in a dounce homogenizer. Lysates were clarified by 30 min centrifugation at 19000 rpm in an SS34 rotor. Cik1-Kar3 complexes were purified by Flag tag on Kar3 using M2-anti-Flag agarose. Beads were washed 3-4 times and proteins were eluted with the lysis buffer supplemented with 2 mg/mL of 3xFlag peptide by incubation for 15 min at room temperature with rotation. Elution fractions were analyzed by SDS-PAGE, frozen in liquid nitrogen and stored at -80°C.

2.2.2.2 Protein expression and purification in bacteria cells

His_6-TEV-Bim1 was cloned into a pET3a vector and transformed into *E.coli* Rosetta cells. A single colony was picked and grown overnight. Next day the overnight culture was diluted to 400 mL and grown to OD_{600}~0.8 at 37° C. Then culture was shifted to 16° C and protein expression was induced by addition of 0.2 mM of IPTG. After 16-24 h cells were pelleted, frozen in liquid nitrogen and stored at -80° C until further usage. The pellet was resuspend in lysis buffer containing 50 mM HEPES-KOH pH 7.4, 300 mM NaCl, 20 mM imidazole, 1 mM $MgCl_2$, 5% (w/v) glycerol, 0.1% (v/v) Tween-20, 0.5 mM TCEP, 0.1 mM PMSF, protease inhibitors (Roche) and lysed by

sonication. His_6-TEV-Bim1 was purified by Ni-NTA affinity chromatography. After purification proteins were desalted, the tag was cleaved off by incubation with TEV-His_6 protease overnight at +4°C. TEV protease was added in ratios of 1:100 or 1:200 to His_6-TEV-Bim1. Bim1 was separated from TEV-His_6 protease by applying the mixture on the Ni-NTA column. Preparative size-exclusion chromatography was used as a final purification step.

2.2.2.3 Size-exclusion chromatography

Analytical size-exclusion chromatography was used to separate protein complexes based on their hydrodynamic radius and address their stability. For Bim1-Cik1-Kar3 complexes SEC buffer contained 25 mM HEPES-KOH pH 7.4, 150 mM NaCl, 1 mM $MgCl_2$, 5% (w/v) glycerol, 0.1% (v/v) Tween-20, 0.5 mM TCEP and Superose 6 3.2/300 or Superdex 200 3.2/300 columns (GE Healthcare) were used. Runs were performed at 4° C. Elution profiles were taken by reading protein UV absorbance at 280 nm. 100 µl fractions were collected in 96 well plates and 5 or 10 µl aliquots were analyzed by SDS-PAGE, gels were stained with Coomassie Brilliant Blue.

2.2.2.4 Quantitative Bim1 pulldowns

To estimate an apparent K'_d of Bim1 binding to Cik1-Kar3 mutants quantitative pulldowns were performed by the following protocol. His_6-Bim1 was immobilized on TALON beads by incubation for 1h at 4° C. Binding buffer contained 25 mM HEPES-KOH pH 7.4, 150 mM NaCl, 10 mM imidazole, 1 mM $MgCl_2$, 5% (w/v) glycerol, 0.1% (v/v) Tween-20, 0.5 mM TCEP and 0.5 mg/ml of BSA. His_6-Bim1 TALON beads were washed 3-4 times and then different amounts of beads were added to Cik1-Kar3 containing tubes. Reaction volumes and Cik1-Kar3 concentrations were the same in all tubes, while the amounts of Bim1 varied. For achieving an equilibrium reactions were incubated for 1h at 4°C with rotation. TALON beads with formed Bim1-Cik1-Kar3 complexes were pelleted by 100 g centrifugation for 5 min at 4° C. Aliquots of the supernatant containing unbound Cik1-Kar3 were analyzed by SDS-PAGE. Gels were stained with Coomassie Brilliant Blue and Kar3 protein band intensities were measured with the gel analysis tool in in ImageJ/Fiji. An apparent K'_d was estimated as an average of three independent experiments from curve fitting in GraphPad Prism. Curve fits were based on a model of one site total binding with specific binding and a linear nonspecific binding component. $Y=B_{max}*X/(K_d+X)+NS*X+Background$, where Y is total

binding, X is ligand, K_d – dissociation constant, NS is slope of unspecific binding and B_{max} is the maximum specific binding.

2.2.3 Yeast methods

2.2.3.1 Yeast strains

Experimental strains were made by modification of DDY1102 (diploid), DDY902 (haploid, Mat a) and DDY904 (haploid, Mat α), taken from laboratory stocks. All used strains had the S288c genetic background.

2.2.3.2 Yeast growth

Yeasts were routinely grown in YEPD media and plates. For AID-experiments glucose was substituted with raffinose and galactose (YEPRG), to induce expression of pGAL-OsTIR. Liquid cultures were grown with 180 rpm shaking at 30°C. Yeast stocks had 25% (v/v) of glycerol and were stored at -80° C.

2.2.3.3 Yeast transformations

Foreign DNA was introduced into yeasts with standard LiAc transformations. Strains from -80° stock collection were restreaked on YEPD plates and grown for one day. Then overnight cultures were installed, starting with OD_{600}~0.2. Next day, overnight cultures were diluted 100x to final volume 50 mL. Cells were grown for 4h at 30° C to OD_{600}~0.8. Cells were collected by centrifugation, washed with water and resuspended on ice in 100 mM LiAc/TE buffer. 50 μl of experimental DNA was mixed with 20 μl of heat-treated salmon-sperm DNA, then 200 μl of yeast were added. As the final step, 1.2 mL of 40% PEG/LiAc/TE was added to the reaction. Final concentrations were ~100 mM LiAc, 1xTE, 32% PEG, ~133 ng/μl of ssDNA. Reaction was rotated for 30 min at room temperature and then 150 μl of DMSO was added with 5 min rotation to mix. Cells were heat-shocked for 12 min at 42° C, pelleted and resuspended in 150 μl of 1xTE. For auxotrophic selection of transformants cells were directly plated on dropout plates. For antibiotic resistance markers cells were put first on YEPD and a day later replica plated on antibiotic-containing plates.

2.2.3.4 Transformants check

Successful DNA integrations were confirmed by PCRs followed by sequencing (Eurofins). In the case of gene tagging with fluorescent proteins, the signal was

examined on a fluorescence microscope. Protein tags were confirmed by western-blotting.

2.2.3.5 Diploid sporulation and dissection

Diploid cells were pelleted from 1 mL of fresh overnight culture, washed with water and resuspend in 4 mL of sporulation medium, supplemented with 1:300 dilution of amino acids. Cells were incubated for 4-7 days with rotation at room temperature. For dissection, 200 μl of sporulation culture was pelleted and resuspend in 37.5 μl of Zymolase. Cells were incubated for 3.5 min at 37° C and put on ice with an addition of 250 μl of potassium-phosphate buffer. Cells were streaked on YEPD plates and tetrads were dissected using a Singer MSM semi-automated dissecting scope. Spores were further allowed to grow for 2.5 days until genotyping.

2.2.3.6 Genotyping of tetrads

Spores genotypes were determined by growth on selection plates. Spores were resuspended in minimal media in 96-well plates and transferred by 48-pin replicator VP407AH (V&P Scientific, Inc). Typically, 12-20 conditions were tested, auxotrophic growth was examined on doHis, doUra, doLys, doAde, doTrp, doLeu plates. For antibiotic resistance G418, ClonNAT and Hygromycin B were tested. Temperature sensitivity was addressed at 25°, 30°, 34° and 37° C. For some situations, HU, Benomyl and YEPRG+auxin plates were used. Mating type testers plates had DDY55 (a) and DDY56 (α) stains. Cells were grown for 1 day.

2.2.3.7 Genomic DNA isolation

Genomic DNA was isolated from freshly growing overnight cultures. An equivalent of OD_{600}~2-3 was pelleted, washed with water and resuspend in 0.5 ml of lysis buffer containing 50 mM Tris-HCl pH 7.5, 20 mM EDTA pH 8.0, 1% SDS. Cell walls were destroyed by bead-beating with glass beads. After 10 min incubation at 75° C, 200 μl of 5 M potassium acetate and 150 μl of 5 M NaCl were added to reaction to precipitate proteins. Mixture was incubated for 10 min on ice. After centrifugation, genomic DNA was pelleted by adding ethanol to final concentration of 66%, washed with 70% ethanol, air-dried and resuspend in 1xTE supplemented with 0.2 mg/ml of RNAse A. After 30 min incubation at room temperature, genomic DNA was stored at - 20° C until further usage.

2.2.3.8 Gene deletion and tagging

Target genes were deleted or tagged using PCR products amplified from plasmid libraries. Deletions were confirmed by PCRs for the absence of wild-type gene and presence of selection marker at correct genomic loci.

2.2.3.9 Plasmid integrations

Plasmids for genome integrations of Cik1 mutants were based on pRS305, and had 5'UTR-Cik1^{mutant}-Flag sequences. Plasmids were linearized by cutting at a single site with AflII, and integrated into the Leu2 locus. Presence of mutations was further confirmed by PCRs from genomic DNA followed by sequencing.

2.2.3.10 Gene replacement

For *Cik1* gene replacements, pRS305-based plasmids contained 3'UTR-5'UTR-Cik1^{mutants}-Flag constructs. Plasmids were linearized by XbaI cut between 3'UTR and 5'UTR.

2.2.3.11 Preparation of Cik1-AID and Kar3-AID strains

The Ubiquitin ligase osTIR1 was integrated into the URA3 locus under the control of a galactose inducible promoter (Nishimura et al., 2009). Cik1 and Kar3 were C-terminally tagged at their genomic loci with AID-9xMyc by integration of a corresponding PCR product. Successful integrations were verified by sequencing. Depletion was achieved by adding 1 mM of auxin (NAA) to the medium/plates.

2.2.3.12 Western blot sample preparation

Yeast cell extracts were prepared using alkaline treatment as described before (Kushnirov, 2000). Briefly, an equivalent of 2 OD_{600} of exponentially growing cells was harvested, washed with H_2O and resuspended in 200 µl of 0.1 M NaOH. After 5 minute incubation at room temperature cells were centrifuged again. The pellet was resuspended in 50 µl 1x SDS sample buffer and boiled for 5 minutes. 8-10 µl of lysate was loaded per gel lane.

2.2.4 Live cell fluorescence microscopy

Live cell fluorescence microscopy protocols are in the annex, taken from:

Kornakov, N., B. Möllers, and S. Westermann. 2020. The EB1–Kinesin-14 complex is required for efficient metaphase spindle assembly and kinetochore bi-orientation. *Journal of Cell Biology*. 219:e202003072. doi:10.1083/jcb.202003072.

2.2.5 Statistical analysis and data presentation

Statistical tests and graphs were made in Graphpad Prism 8. Visual appearance was finally adjusted in Adobe Illustrator. Small points on graphs show values of individual cells, large open circles represent means of biological or technical replicates, as indicated. 95% Confidence Intervals (CI) are usually shown. In the text mean values ±SEM are mentioned. Student's t-test was used to compare continuous data from two strains. Due to small sample size, data distribution was assumed to be normal, but this was not formally tested. Kruscal-Wallis test was applied to datasets with more than two mutants. For discrete data Chi-square test was used.

3. Results

3.1 A conditional depletion system to study Kinesin-14 functions in chromosome segregation

Genetic deletions of kinesin-14 subunits Cik1 and Kar3 lead to severe growth defects. While wild-type cells require 2 days to form visible colonies of 1-2 mm size after dissection, *cik1*Δ and *kar3*Δ strains need 4-5 days. Besides poor growth, loss of kinesin-14 causes increased temperature and hydroxyurea sensitivity. During typical strain construction, cells undergo following steps: diploid dissection, replica plating to testing plates, overnight growth and freezing a glycerol stock into the collection. Cells are growing for ~ 50-70 generations before an experiment, in this time yeasts accumulate suppressor mutations or additional defects. Work with growth-compromised strains is therefore error prone and proper controls are needed on every step. *cik1*Δ cells are known to be aneuploid (Page and Snyder, 1992). Aneuploidy can cause growth defects as well as increased tolerance to stress conditions (Pavelka et al., 2010).

To avoid these potential problems of genetic deletions, I have utilized an auxin-induced conditional depletion system to study the immediate consequences of kinesin-14 loss-of-function. To prevent leaky degradation, the system was designed as a double conditional. The Ubiquitin ligase osTIR1 was integrated into the yeast genome under a GAL promoter, so it was not expressed in a usual growth media with glucose as a sugar source. The Kinesin-14 heavy chain Kar3 and the kinesin-associated protein Cik1 were tagged at C-termini with AID-9xMyc that allowed their immunodetection. Addition of auxin promotes binding of AID by osTIR followed by ubiquitination and proteasome degradation. Cik1 protein expression levels were low in exponentially growing cells, as judged by western blotting, and Kar3 was present in excess of Cik1, consistent with the literature data. Cik1^{short}-Kar3 was overexpressed in a response of mating pheromone exposure **(Fig. 3.1)**. The short, cytoplasmic Cik1 isoform without the 35 N-terminal amino acids arises after transcription from an intragenic promoter. Cik1-Kar3 was efficiently degraded in 30 minutes after auxin exposure. Depletion was ~ 95% efficient, judged by protein band intensity quantification after western blotting.

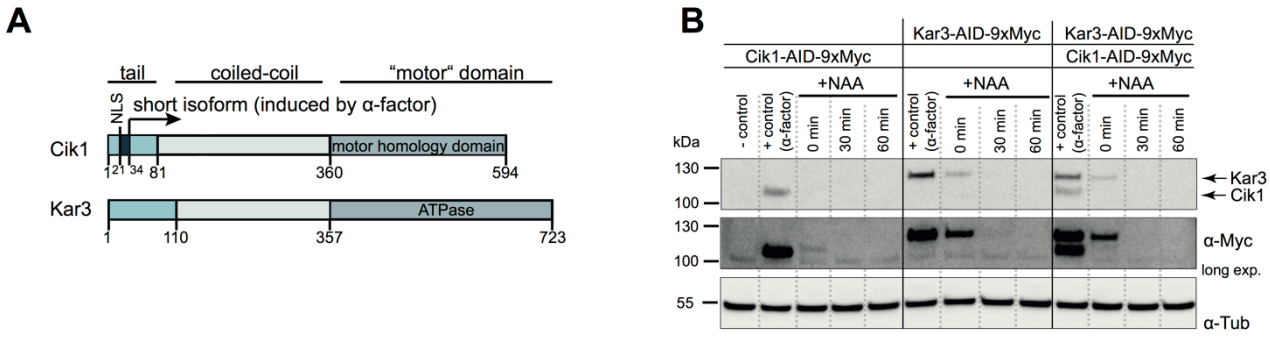

Figure 3.1 Auxin-inducible depletion of Cik1 and Kar3.

A) Scheme shows Cik1 and Kar3 protein structure. Functionally important regions are signed. Protein domains are indicated at the top.
B) Conditional depletion of Cik1-Kar3 AID-tagged proteins. During α-factor arrest Cik1-Kar3 expression rises ~ 20 fold. Two time points (30 min and 60 min) after addition of auxin are shown. AID tagged proteins are indicated at the top. Adapted from (Kornakov et al., 2020) with changes.

To investigate the expression of Cik1-Kar3 during the cell cycle, I have compared it to the expression of the essential APC activator Cdc20. Cdc20 is present at very low levels in G1 cells, accumulated when cells go into mitosis and is degraded at the end of mitosis (Prinz et al., 1998). Using Cdc20 depletion, I have synchronized cells in metaphase. After auxin washout cells quickly resynthesized Cdc20, went into anaphase and further entered the next cell cycle. Cik1-Kar3 expression was low in G1-phase (30-40 min) and accumulated in S-phase (50-60 min). Cik1-Kar3 protein levels peaked ~ 20 min before Cdc20 **(Fig. 3.2)**. Consistent with literature data, Cik1-Kar3 is an early mitotic protein, with proposed roles in spindle assembly and chromosome bi-orientation.

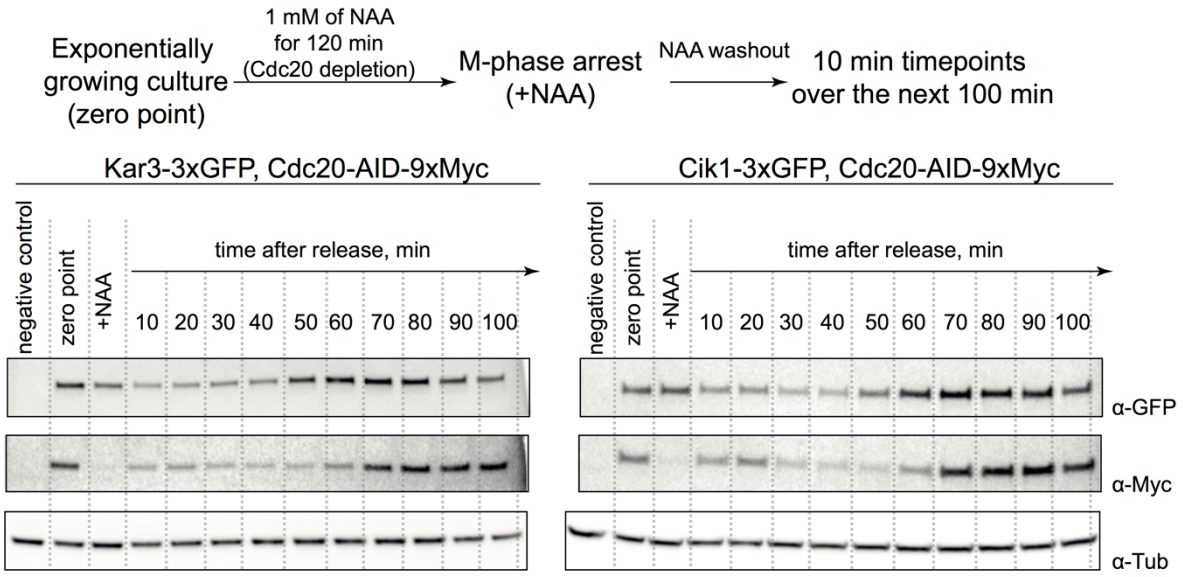

Figure 3.2 Cell cycle analysis of Cik1-Kar3 protein expression.

Experimental scheme at the top, western blots at the bottom. 10 min time-course after release from a metaphase arrest, caused by Cdc20 depletion, is shown. Cik1 or Kar3 were tagged with 3xGFP, Cdc20 was fused to AID-9xMyc. Tubulin was used as a loading control.

To investigate the effect of acute depletion of Cik1-Kar3, I have compared the constructed AID strains to genetic deletions by serial dilution spot assays. The *cik1*Δ deletion displayed a more severe version of *kar3*Δ phenotypes and the double deletion *cik1*Δ *kar3*Δ was similar to *kar3*Δ. In the absence of Cik1, Kar3 more efficiently forms a complex with another kinesin-associated protein Vik1 and elevated Vik1-Kar3 aggravates *cik1*Δ defects (Manning et al., 1999). For example, *cik1*Δ was sensitive to 20 mM of HU, while *kar3*Δ and *cik1*Δ *kar3*Δ were viable under the same conditions. Without addition of auxin, Cik1-AID and Kar3-AID strains showed wild-type growth. Auxin addition caused a growth delay, temperature sensitivity and was lethal in the presence of hydroxyurea. Cik1 and Kar3 depletions had similar, but milder phenotypes to the corresponding genetic deletions **(Fig. 3.3)**. From these results I have concluded that the C-terminally AID-tagged Cik1-Kar3 complex is functional and can be rapidly and almost completely depleted by auxin addition. As a consequence, the AID-system is a suitable tool to study kinesin-14 functions.

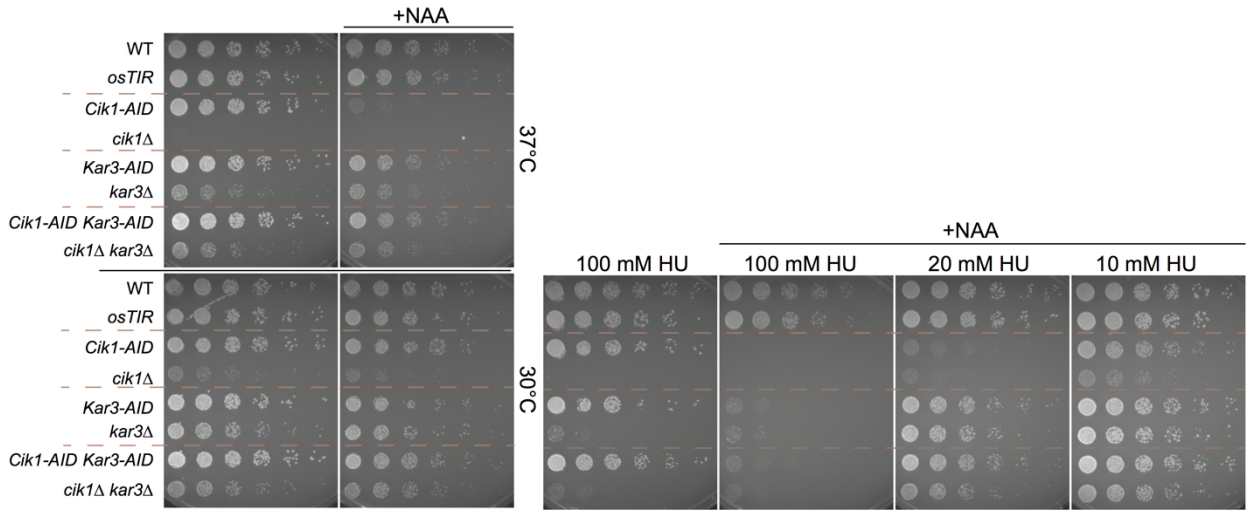

Figure 3.3 Comparison of *cik1*Δ and *kar3*Δ genetic deletions to conditional depletion strains.

1 to 4 serial dilution spot assay, starting OD_{600} =0.4. Plates were incubated for 2.5 days at indicated conditions. Plates marked with +NAA contained 1 mM of NAA. Adapted from (Kornakov et al., 2020) with changes.

The growth delay, observed in the spot assays, may have several reasons. A first possibility is a delay in cell cycle progression in individual cells. Another option is cell death in growing colonies, both variants lead to smaller colonies sizes. Since Cik1-Kar3 depletion did not decrease CFU (colony forming units) number, that excluded the second hypothesis. A cell cycle arrest caused by defects in intracellular processes is typically mediated by a relevant checkpoint system. A G1-S checkpoint controls the beginning of replication as a function of available nutrients, the intra S-phase checkpoint monitors the completion of replication, the mitotic checkpoint delays anaphase entry in response to unattached kinetochores, the spindle positioning checkpoint prevents spindle elongation if it is not positioned correctly on the mother-bud axis. In budding yeast these checkpoints are non-essential, cells efficiently grow, replicate, bi-orient and segregate chromosomes producing viable offspring without checkpoints. However, even if a small defect occurs in any of these processes, cells will rely on a corresponding checkpoint. This situation allows one to use synthetic lethality with an inactivated checkpoint as a powerful and the most sensitive assay to examine a gene's function. Each of 16 budding yeast chromosomes is essential for cell survival therefore the presence of a single unattached kinetochore in a cell without mitotic checkpoint is lethal. Cik1-Kar3 was known to be involved in chromosome segregation in mitosis and meiosis, so I have addressed the question if Cik1-Kar3

depletion would be lethal in the *mad1*Δ background. Indeed, Auxin addition very effectively killed Cik1-AID and Kar3-AID strains even at normal temperature **(Fig. 3.4 A)**. Depletion of kinesin-14 caused accumulation of erroneous chromosome-microtubule attachments corrected during metaphase arrest. If Cik1-Kar3 directly affects chromosome bi-orientation, I would expect to see an increased dependence on kinesin-14 in cells with increased chromosome number. To test this idea, I have prepared diploid strains, in which both Cik1 or Kar3 alleles had AID tags. Indeed, Cik1 depletion was lethal in a diploid strain and Kar3 depletion caused severe growth defects **(Fig. 3.4 B)**.

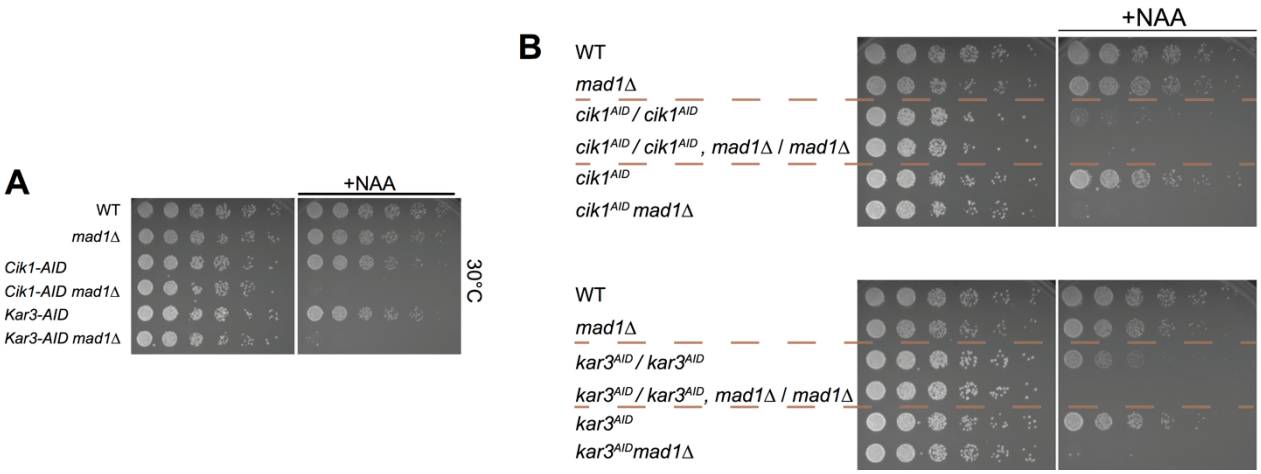

Figure 3.4 Depletion of Cik1-Kar3 is lethal in checkpoint deficient strains and results in severe growth defects in diploids.

A) Spot assays of mitotic checkpoint deficient strains. Depletion of Cik1 or Kar3 is lethal in the *mad1*Δ background.
B) Spot assays of diploid strains with both Cik1 or Kar3 alleles tagged with AID. Adapted from (Kornakov et al., 2020) with changes.

A clear prediction from the observed synthetic lethality of Cik1-Kar3 depletion with *mad1*Δ was a metaphase delay for cells with wild-type checkpoint. Exponentially growing cultures contain ~30% of mitotic cells and only about half of the mitotic cells are in metaphase. To increase the number of cells in mitosis, I have synchronized yeasts by α-factor exposure. In a response to mating signaling cells polarize and arrest in G1-like state. After α-factor washout cell cycle progression was followed by fluorescence microscopy. As markers for the metaphase spindle I have used the SPB component Spc42, labelled with RedStar2 and the microtubule-binding outer kinetochore protein Ndc80, labelled with GFP. SPB separation marks the start of metaphase and the beginning of the process of chromosome bi-orientation. When all

kinetochores become stably attached to microtubules, conditions of mitotic checkpoint are fulfilled and cells progress into anaphase, notable by fast spindle elongation. Cik1 depletion led to a 50% increase in the mean metaphase duration from 29±1 min in wild-type cells to 46±2 min in the auxin-treated cells. Some Cik1-depleted cells displayed an extreme delay of up to 2 h **(Fig. 3.5)**.

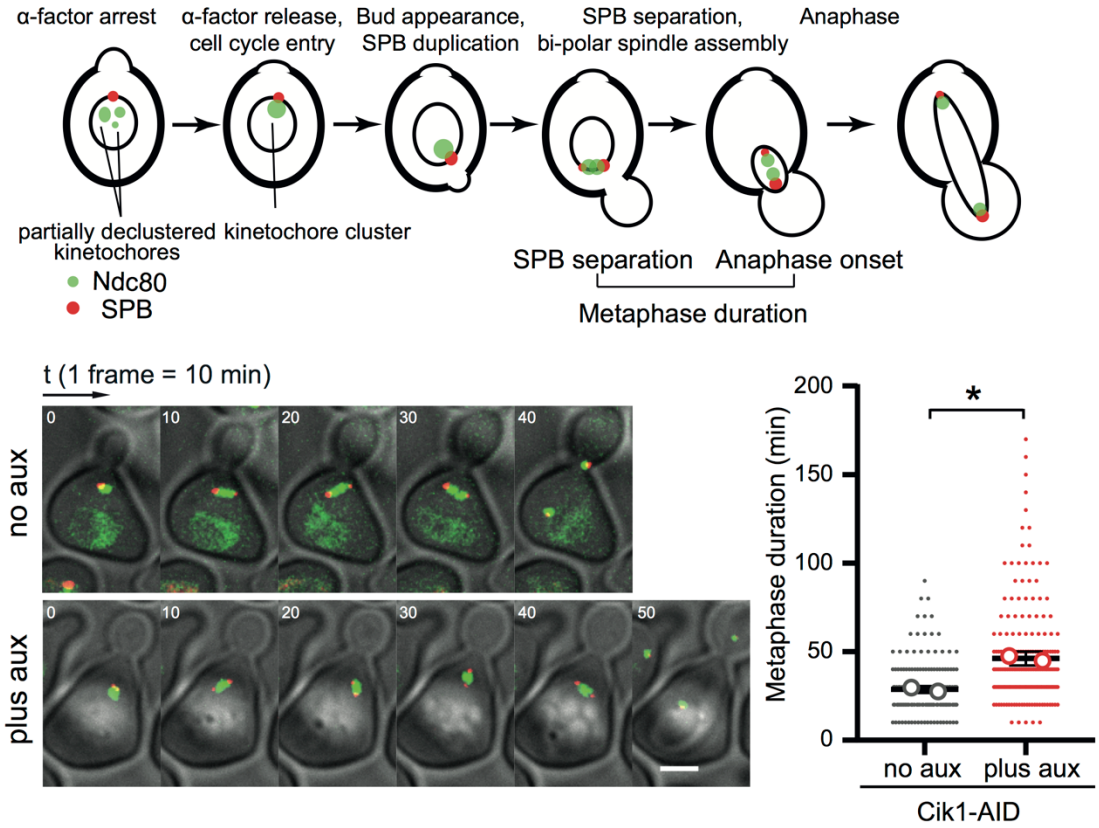

Figure 3.5 Cik1 depletion causes a strong delay in metaphase.

Experimental scheme describing cell cycle after release from α-factor arrest (at the top). Representative merge images of control and Cik1 depleted cells. Scale bar is 2 μm. For measuring duration of metaphase, a total of 200 cells of two biological repeats were analyzed. Individual cells are depicted with small circles and mean values of repeats are marked with big circles. Error bars are mean values with 95% CIs. χ^2 test was applied, $p < 0.0001$. Adapted from (Kornakov et al., 2020) with changes.

Besides the metaphase delay, I have noticed a strong decrease in metaphase spindle length in Cik1-depleted cells. Wild-type cells had about ~1 μm long spindles immediately after bi-polar spindle assembly that gradually grew up to ~2 μm when anaphase started. Cik1-depletion reduced the spindle size by half, preanaphase spindles became only ~1 μm long. The effect was specific to metaphase, since anaphase spindles had similar lengths and maximal elongation speed was the same **(Fig. 3.6)**. A decreased metaphase spindle size was previously described for deletions

of the microtubule-crosslinking proteins Cin8 and Kip1 (kinesin-5s), Ase1/PRC1 and Slk19. If Cik1-Kar3 shares functions with these proteins, it shall also affect microtubule structures.

In summary these experiments show that Cik1 depletion is characterized by a metaphase delay caused by an activated mitotic checkpoint and accompanied by decreased spindle size. From that I have concluded that kinesin-14 organizes the metaphase spindle thus promoting chromosome bi-orientation.

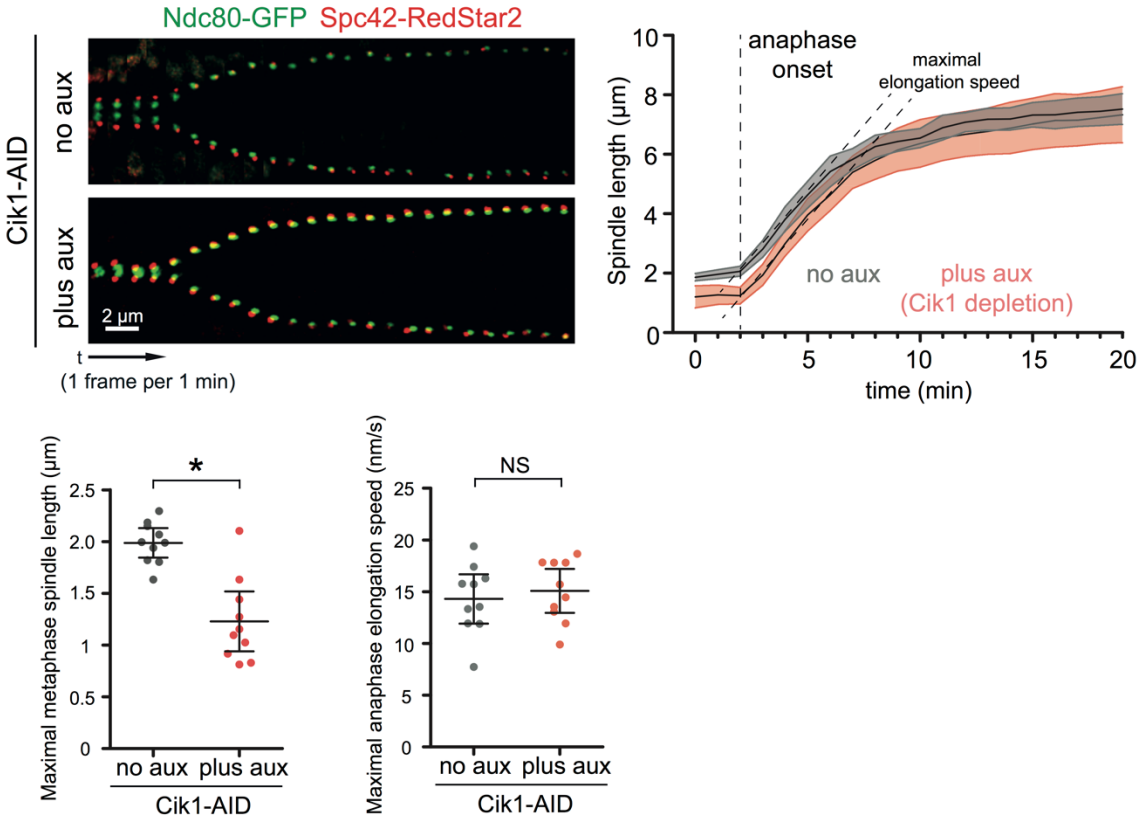

Figure 3.6 Cik1 depletion decreases metaphase spindle size.

Representative images of spindle elongation in control and Cik1-depleted cells (top). Images are aligned to 4 min before anaphase. Quantification of spindle elongation (bottom), N=15. Error bars are mean values with 95% CIs. Student's two-tailed t-test was applied, *p<0.0001, for NS p=0.59. Adapted from (Kornakov et al., 2020) with changes.

3.2 Characterization of the Cik1 depletion phenotype.

To evaluate metaphase spindle structure after Cik1 depletion, I needed to follow the position of microtubules in living cells over the time. However, the introduced label should not affect microtubules structure and organization by itself and cause no synthetic defect in combination with Cik1 depletion. That's why I decided against commonly used markers – C-terminal fusions of GFP with tubulin or with plus-end

tracking protein Bim1/EB1. Tags on these proteins perturb their functions by causing blocking the binding to partner proteins, which can lead to compensatory and secondary mutations. The best fluorescent label I found was Bik1-3xGFP/CLIP-170. Bik1 localization to microtubules is mediated by its own CAP-Gly domain and by interactions with Bim1 and Stu2. Bik1-3xGFP is functional and gives a bright signal, marking nuclear as well as cytoplasmic microtubules at plus-ends and also weakly staining the microtubule lattice. The Stu2-Bik1 complex binds to SPB and kinetochore clusters.

First, I will describe the Bik1-3xGFP distribution in wild-type cells. Quickly after bi-polar spindle assembly Bik1 gained a bar-like localization with stronger accumulation close to SPBs and the signal was confined to a line between the SPBs. The spindle was positioned in proximity of the bud neck with short cytoplasmic microtubules. At least one cytoplasmic microtubule was oriented towards the bud. Cik1 depletion leads to a dispersion of the Bik1 signal with little localization left between the SPBs. Microtubules were directed outside of the spindle axis, displaying strong misalignment **(Fig. 3.7 A)**. During the prolonged metaphase arrest Cik1-depleted cells gradually improved the microtubule alignment. The spindle was sometimes positioned outside of the bud neck with long, curved cytoplasmic microtubules. These results were consistent with the idea of kinesin-14 functioning as a microtubule crosslinker during metaphase spindle assembly, in addition, Cik1-Kar3 may play a role in spindle orientation.

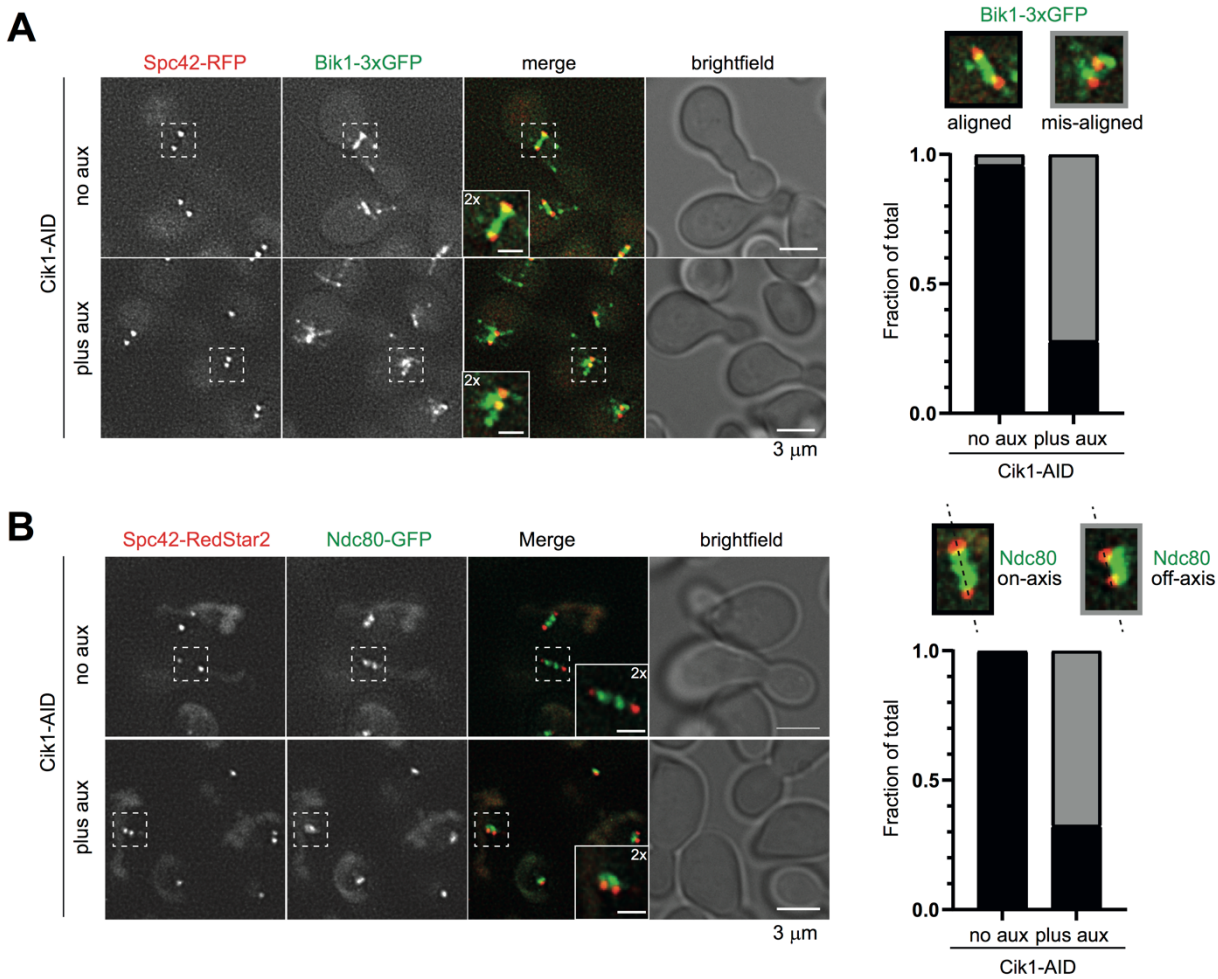

Figure 3.7 Cik1 is required for metaphase spindle alignment and kinetochore clustering.

Representative images of metaphase in control and Cik1-depleted cells. Scale bar is 3 μm. Two times magnifications are shown with scale bar 1 μm. 40 cells were quantified for every condition.
A) Microtubule plus-end marker Bik1-3xGFP.
B) Kinetochore protein Ndc80-GFP.
Adapted from (Kornakov et al., 2020) with changes.

Since, I have observed crosslinking defects after Cik1 depletion, I was interested in the nature of these misaligned microtubules. In metaphase nuclei, haploid budding yeasts have 32 kinetochores and ~8 interpolar microtubules. Kinetochore microtubules are short and have a uniform length distribution with mean ~300 nm (Winey et al., 1995, O'Toole et al., 1997). To follow positions of kinetochores I have used Ndc80-GFP. In S-phase the Ndc80 signal became clustered close to the SPB, as cells progressed through metaphase a visible separation of the Ndc80 clusters appeared. Cik1-depletion resulted in Ndc80 signal mispositioning and declustering. Cik1-depleted cells failed to localize kinetochores to the spindle axis, which happened

early after bipolar spindle assembly in the wild-type situation **(Fig. 3.7 B)**. Similar to Bik1, the Ndc80 signal became more confined after some time, and only after Ndc80 clustering occurred, cells entered anaphase.

3.3 Identification of functionally important elements in Cik1-Kar3 required for error-free chromosome segregation.

After analysis of cellular phenotypes, I have decided to investigate the molecular requirements, underlying kinesin-14 functions in chromosome segregation. The conditional lethality of Cik1-Kar3 depletion in the absence of a mitotic checkpoint provided an excellent tool for this task. The Cik1-Kar3 C-termini are known to be important for microtubule binding/motor activity, so I have focused on the N-terminal part. I have prepared a library of N-terminally truncated Cik1 and Kar3 mutants transformed into Cik1-AID or Kar3-AID *mad1*Δ strains. All Cik1 variants contained a C-terminal SV40 NLS, since natural nuclear localization of Cik1-Kar3 is provided by NLS in Cik1 tail. In the absence of auxin the mutant version of the protein expressed from a CEN plasmid was covered with a functional copy. Addition of auxin depleted Cik1-AID or Kar3-AID and allowed to assay the mutants. To avoid clonal differences and variability of protein expression aroused after multiple integrations, I have used a pool of clones, transformed with centromeric plasmids **(Fig. 3.8)**.

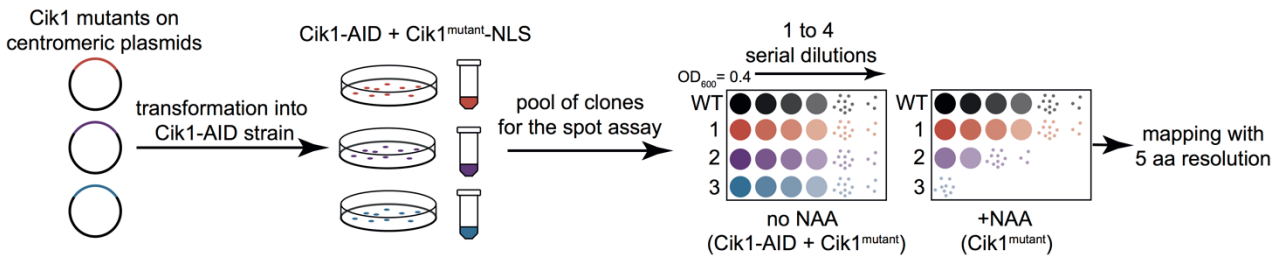

Figure 3.8 Cik1 mutagenesis experimental scheme. Adapted from (Kornakov et al., 2020) with changes.

First, I have mapped functionally important regions with ~20 amino acid resolution in the N-terminal tails. Initial observations indicated that Cik1$^{\Delta 34}$ and Cik1$^{\Delta 54}$ displayed wild-type growth, while Cik1$^{\Delta 74}$ and further truncations were inviable. Precise mapping with higher resolution revealed an “all-or-nothing” transition between Cik1$^{\Delta 69}$ and Cik1$^{\Delta 74}$. This 5 amino acids truncation switched Cik1 from being fully functional to being completely unfunctional, judged in context of *mad1*Δ background lethality **(Fig. 3.9 A)**.

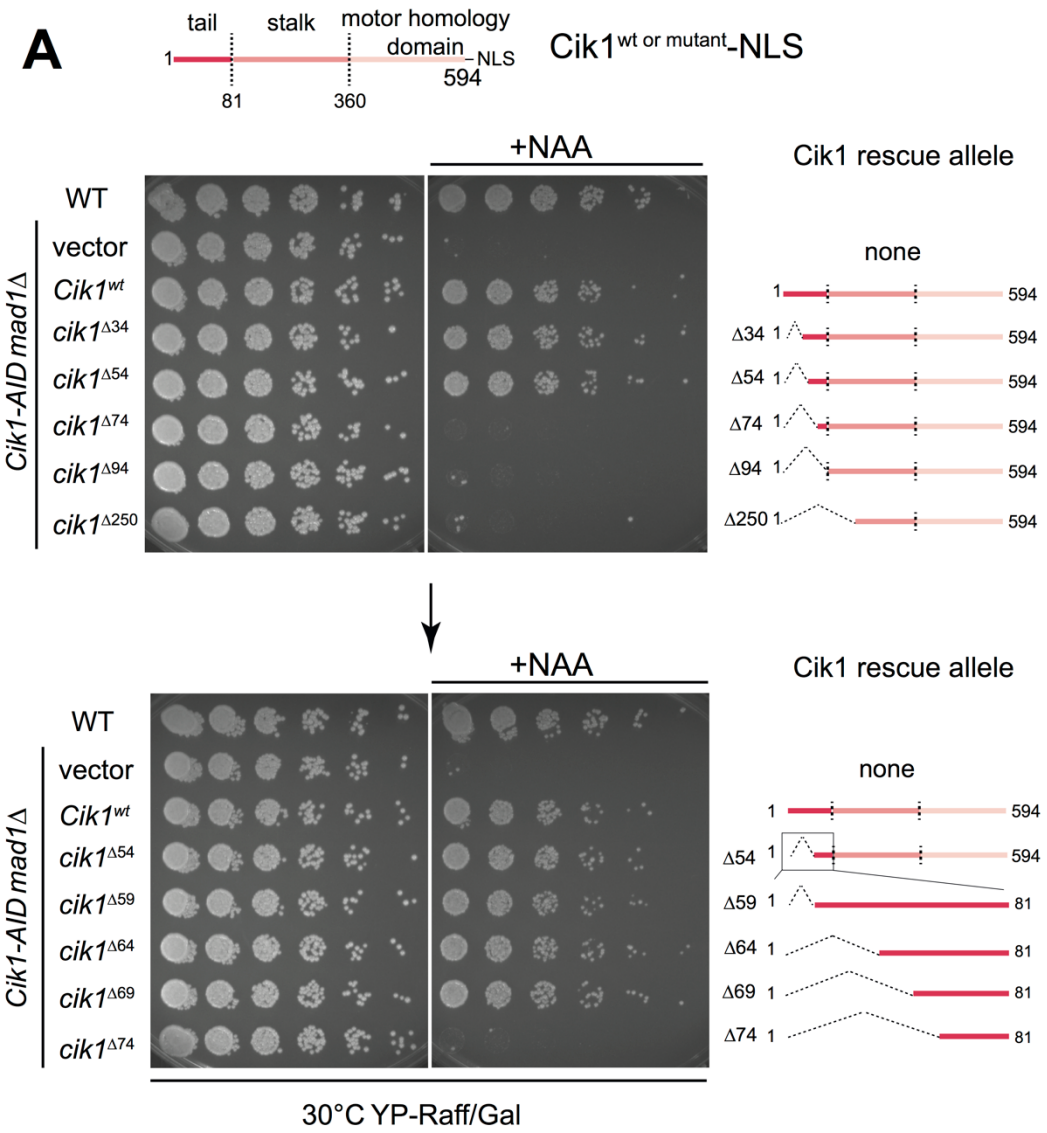

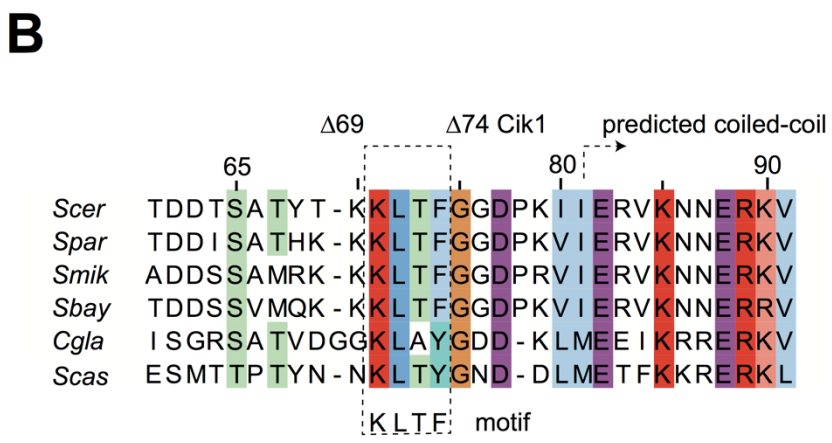

Figure 3.9 Identification of functionally important regions in Cik1 tail.

A) Spot assays of N-terminally truncated Cik1 mutants.
B) Sequence alignment of Cik1 tails from different yeast species. The conserved KLTF motif is marked with a rectangle. Coordinates are given for *Saccharomyces cerevisiae* Cik1.

I expected that the identified region would be evolutionarily conserved, if functions of kinesin-associated proteins Cik1 are also similar in other budding yeasts. Indeed, a multiple sequence alignment showed a conservative KLTF peptide motif, deleted in the Cik1$^{\Delta 74}$ mutant. The KLTF motif was positioned immediately before a predicted coiled-coil region of Cik1, that mediates the dimerization with Kar3 **(Fig. 3.9 B)**. Surprisingly, only a small fraction of the Cik1 tail appeared to be functionally important. This observation raised the question if the Kar3 tail may contain functionally important sequences different from those in Cik1.

N-terminal truncation analysis of Kar3 followed by by a series of internal truncations revealed a key contribution of an evolutionary conserved ELN motif, mapped by deletion of 104-108 amino acids. The ELN motif in Kar3 precedes a predicted coiled-coil domain in a manner similar to the KLTF motif in Cik1 and in the Cik1-Kar3 heterodimer these motifs would be in close physical proximity to each other **(Fig. 3.10)**. The integrity of the first several heptad repeats of the coiled-coil was also important for Kar3 functionality, since Kar3$^{\Delta 108\text{-}129}$ was inviable. That gave me a hint, that KLTF and ELN motifs might share a common function, a hypothesis that will be tested in further experiments. Even more surprisingly, almost all tail of Kar3 could be deleted safely, including all of the described Cdk1 sites, that were previously claimed to be important for Cik1-Kar3 functionality based on *in vitro* data. Also, the Kar3 tail has a high positive charge (pI ~ 11) and was supposed to be involved in microtubule binding. However, my genetic experiments argue against the functional importance of these regions. Even if those Kar3 activities exist, they do not contribute significantly to chromosome segregation.

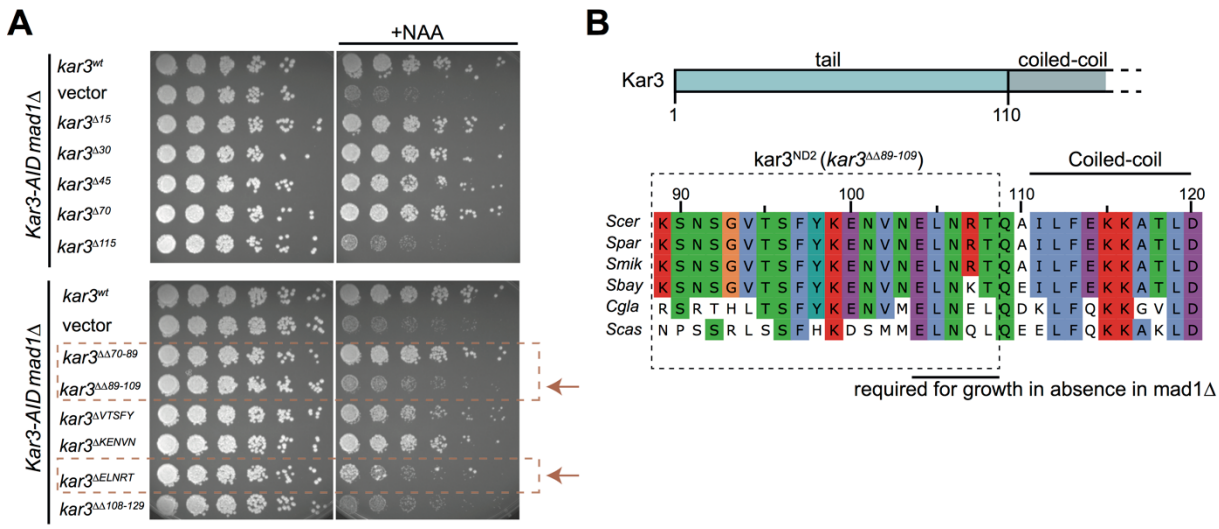

Figure 3.10 Identification of functionally important regions in the Kar3 tail by genetic complementation.

A) Spot assay of N-terminally truncated Kar3 mutants, followed by systematic internal truncations.
B) Sequence alignment of Kar3 tails from different yeast species. The ELN motif within the conserved ND2 region is marked. Coordinates are given for *Saccharomyces cerevisiae* Kar3. Adapted from (Kornakov et al., 2020) with changes.

Budding yeast kinesin-14 heavy chain Kar3 forms two different complexes with the kinesin-associated protein paralogs Cik1 or Vik1. They share only 21% sequence identity, but have a common domain structure. Coiled-coils and motor homology domains are more similar, while the tail regions are highly divergent. I have asked if the discovered KLTF motif is a key molecular determinant of Cik1 functionality, would it convert Vik1 into Cik1 when placed in its tail? To test this hypothesis, I have prepared a series of Cik1-Vik1 chimeras. The Vik1-Cik1-Vik1 (VCV) chimeras VCV1, VCV3 and VCV4 contained the KLTF motif while VCV2 had an entire Cik1 tail without a KLTF motif. Full length Vik1 and VCV2 failed to rescue the Cik1 depletion, while VCV1, VCV3 and VCV4 were viable **(Fig. 3.11)**. Therefore, I conclude that indeed, the KLTF motif inserted into the Vik1 tail allows it to perform the mitotic functions of Cik1.

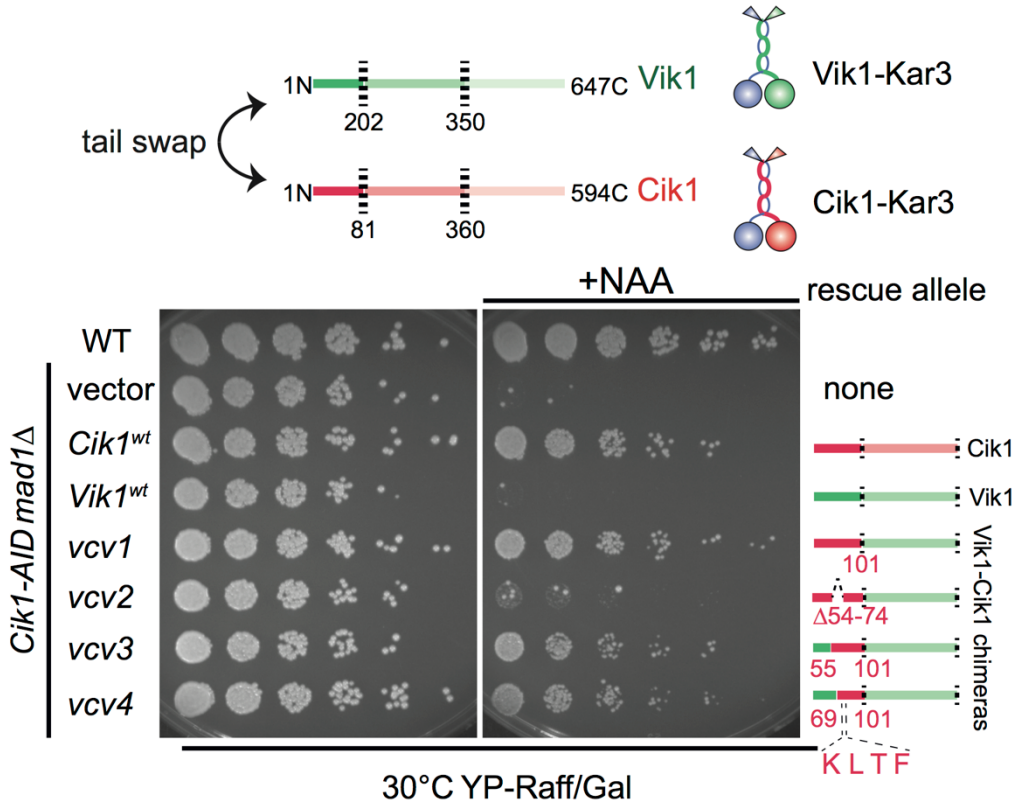

Figure 3.11 KLTF motif is a key molecular determinant of Cik1 functionality and is transferable to Vik1.

Scheme of a tail swap experiment (at top). Spot assays of Vik1-Cik1-Vik1 chimeric mutants. Adapted from (Kornakov et al., 2020) with changes.

3.4 Biochemical characterization of the function of ELN and KLTF peptide motifs.

KLTF and ELN peptide motifs in the tails of Cik1-Kar3 were novel, short linear motifs with unknown binding targets. In all organisms, including budding yeast, common interaction partners of kinesin-14s are microtubule end-binding proteins Bim1/EB1s. My suspicion was that in the functional complementation assay I have identified a binding interface between Cik1-Kar3 and Bim1. To test this idea with biochemical experiments, I have prepared corresponding recombinant proteins, in particular versions that either contained or did not contain the new peptide motifs. Cik1$^{\Delta 69}$-Kar3, Cik1$^{\Delta 74}$-Kar3, and Cik1-Kar3$^{\Delta 89\text{-}109(ND2)}$ were co-expressed in insect cells and Bim1 was expressed in *E.coli*. All kinesin-14 mutants could be purified well, using a Flag tag on the Kar3 subunit, as stoichiometric heterodimers and had identical elution profiles in size-exclusion chromatography (SEC). This confirms that the new peptide

motifs are not involved in heterodimer formation between Cik1 and Kar3. Binding experiments demonstrated that Cik1$^{\Delta 69}$-Kar3 efficiently binds to Bim1 in pulldowns and that the complex was stable during SEC. In contrast, Cik1$^{\Delta 74}$-Kar3 and Cik1-Kar3$^{\Delta 89\text{-}109(ND2)}$ were Bim1-binding deficient **(Fig. 3.12)**. I have interpreted these findings in the following way. The ELN (motif A) and KLTF (motif B) peptides form a common Bim1-binding interface, split between Cik1 and Kar3. Deletion of any single motif disrupts the interaction with Bim1. Motif A and motif B alone are not sufficient for Bim1-binding, since neither Vik1-Kar3 that has motif A, nor Cik1, that has motif B, are alone capable of binding Bim1. Sequence analysis showed that Cik1 has an additional canonical Bim1-binding SxIP motif close to N-terminus (motif C), however, this is not required for high-affinity binding.

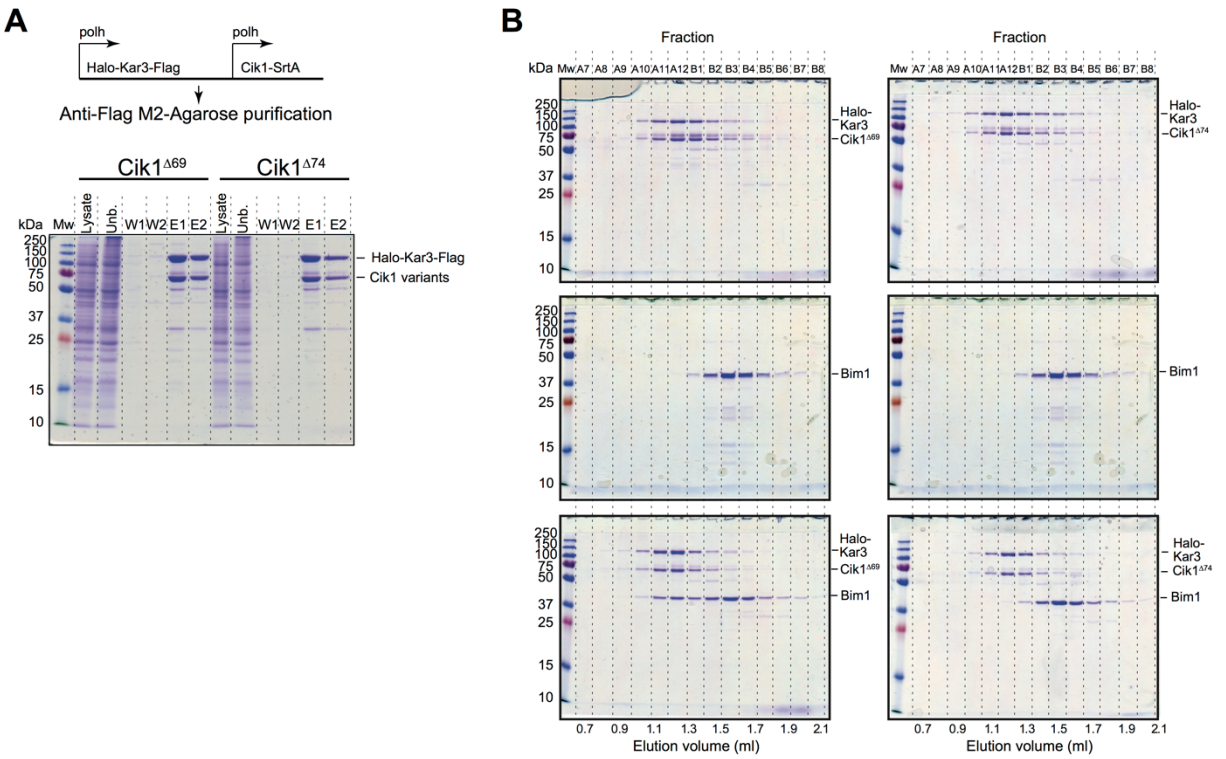

Figure 3.12 KLTF and ELN peptide motifs form a high affinity composite AB Bim1-binding motif.

A) Purifications of Cik1-Kar3 variants expressed in insect cells. Proteins were co-expressed from a single baculovirus. Recombinant proteins were purified via a Flag-tag on Kar3 using M2-anti-Flag Agarose and eluted with 3xFlag peptide.
B) The Bim1-Cik1$^{\Delta 69}$-Kar3 complex is stable in SEC, while Cik1$^{\Delta 74}$-Kar3 does not bind to Bim1. Aliquots of 100 µl SEC fractions were analyzed by SDS-PAGE. Fraction names are indicated at the top, elution volume is indicated at the bottom.
C) Purification and Bim1-pulldown by full-length Cik1-Kar3.
D) Purification and Bim1-pulldown by Cik1-Kar3$^{\Delta 89\text{-}109(ND2)}$
Adapted from (Kornakov et al., 2020) with changes.

To evaluate the affinity of the composite KLTF-ELN motif (AB motif) to Bim1 in a context of Cik1-Kar3 proteins, I have performed a quantitative pull-down experiment. Cik1$^{\Delta69}$-Kar3 was incubated with increasing amounts of Bim1 immobilized on beads. Binding of Cik1$^{\Delta69}$-Kar3 to Bim1 led to depletion of kinesin-14 from the supernatant fraction to the beads. I found that 1h incubation at 4° C might be sufficient for the binding reaction to reach equilibrium. After that the beads were collected at the bottom of the tubes by centrifugation and aliquots of the supernatant were analyzed by SDS-PAGE to quantify the amounts of unbound proteins. An apparent dissociation constant of K'$_d$ ≈ 250 nM was calculated as an average of three independent experiments from fitting the raw data to a one-site binding model (**Figure 3.13**).

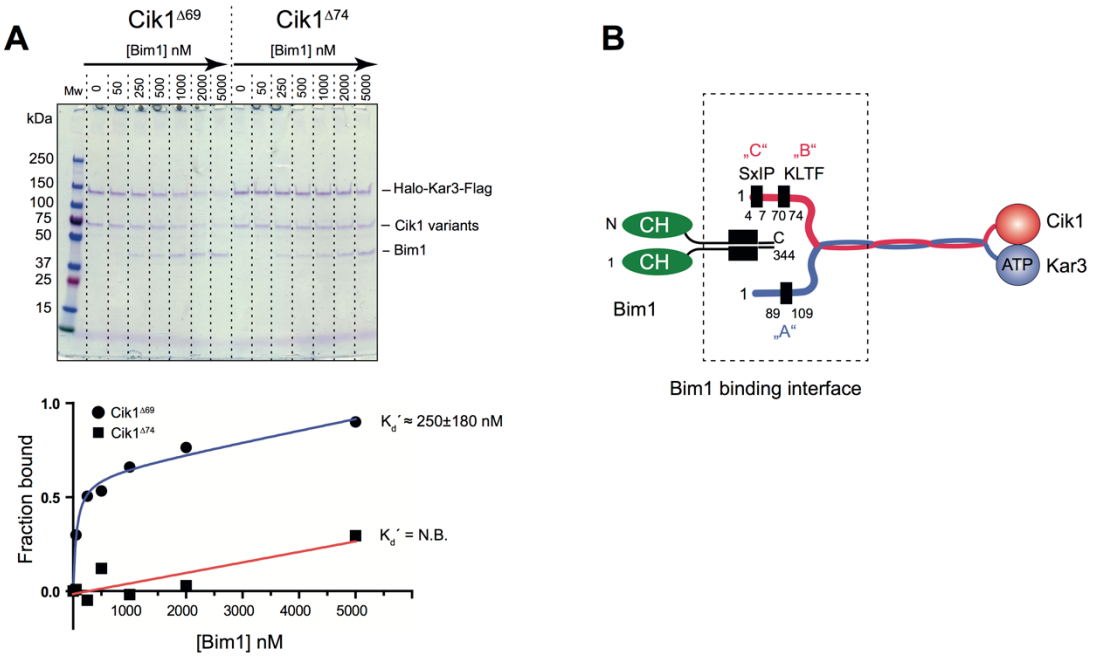

Figure 3.13 Bim1 binds to the KLTF-ELN motif with a has K'$_d$ ≈ 250 nM.

A) Representative gel of quantitative pulldown of Cik1$^{\Delta69}$-Kar3 and Cik1$^{\Delta74}$-Kar3 by His$_6$-Bim1. K'$_d$ was calculated from the one-site total binding model fit, blue curve (R^2=0.99). Cik1$^{\Delta74}$-Kar3 does not bind to Bim1 (red line). K'$_d$ was calculated from three biological replicates. Mean value ±SD is shown, N.B. – no binding.
B) Scheme of Bim1-Cik1-Kar3 binding interface. Adapted from (Kornakov et al., 2020) with changes.

The quantitative pull-down indicated that the AB-motif provided at least an order of magnitude tighter binding than previously reported single EB1-binding motifs, which are typically in the micromolar range. The high affinity of Cik1-Kar3 for Bim1 may not only allow formation of the complex in the cytoplasm, outside of microtubules, but also efficiently outcompete other, ubiquitous SxIP-containing proteins. How can the short

stretch of amino acids provide such tight binding? In contrast to traditional low-affinity SLiMs, the AB-motif is not linear. Motifs on the different polypeptide chains of Cik1 and Kar3 may be positioned to interact with adjacent surfaces of Bim1 EBH-domain.

3.5 Disrupting of Bim1-Cik1-Kar3 binding interface with point mutations.

The best way to assess functions of a particular protein-protein interaction in the cell is to disrupt it with point mutations that keep all other protein activities intact. I have identified the interaction mode between Cik1-Kar3 and Bim1, this has put me in the position to specifically analyze the consequences of disrupting this interaction in cells. My prediction was that full disruption of the Bim1 binding motifs in Cik1-Kar3 would be lethal in *mad1*Δ cells, similar to the Cik1$^{\Delta 74}$ mutant. To test the hypothesis, I have designed three mutants, both as recombinant proteins for biochemical experiments, and as integration constructs in yeast: Cik1^{SKAA} (motif C) impairing the canonical SxIP motif, Cik1^{4A} (motif B), impairing the novel KLTF motif and Cik1$^{SKAA+4A}$ (motifs B and C), impairing both motifs simultaneously. *In vitro* pulldowns showed that Cik1^{SKAA} retained Bim1 binding and Cik1$^{SKAA+4A}$ displayed no binding, while Cik1^{4A} showed reduced, but not fully abolished binding (**Figure 3.14**). Analyzing these alleles in the Cik-AID mad1delta depletion setting showed that mutation in motif C (SxIP) alone caused no growth defect, consistent with the observation that it is not critically required for Bim1 binding. Mutation of motif B (KLTF) produced a growth delay, accompanied with partial loss of viability, but was not as severe as the Cik1delta74 allele, crucially, however, Cik1$^{SKAA+4A}$ (mutation of C and B) was lethal, similar to Cik1$^{\Delta 74}$.

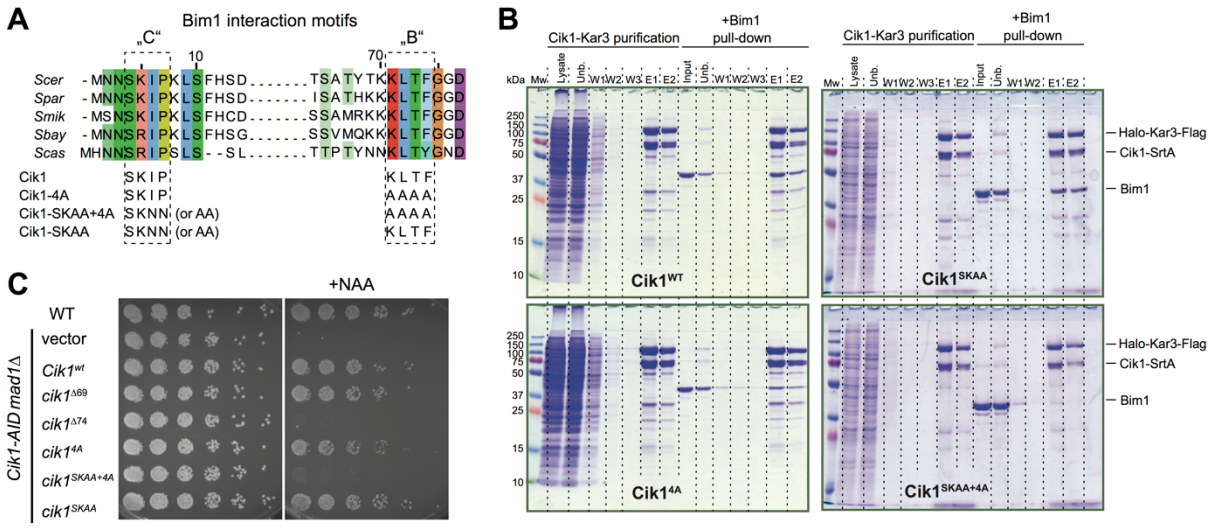

Figure 3.14 Disruption of Bim1-Cik1-Kar3 binding interface with point mutations.

A) Sequence alignment of Cik1 tails shows two conserved regions corresponding to Bim1 binding motifs. Motifs are marked with dashed rectangles and introduced mutations are signed below.
B) Protein purifications and Bim1-pulldowns of indicated Cik1 mutants.
C) Strain viability correlates with Bim1-binding affinity of corresponding Cik1-mutants. Adapted from (Kornakov et al., 2020) with changes.

Further I decided to test my findings using a non-conditional assay with fully integrated mutants, since in the experiments before I relied on the AID system. I prepared diploid strains heterozygous for the respective alleles of two genes. These strains contained *MAD1/mad1*Δ and one of the two Cik1 alleles was replaced by the respective mutant. Diploid dissections showed that Cik1^{4A} spores were growing slowly and in combination with *mad1*Δ , they were lethal. Cik1$^{SKNN+4A}$ spores, on the other hand, displayed severe growth defects or were dead even in the presence of a functional mitotic checkpoint. The Cik1$^{SKNN+4A}$ mutant behaved similar to the *cik1*Δ mutant, indicating that possibly all Cik1-Kar3 mitotic functions rely on Bim1 binding (**Figure 3.15 A**). The pronounced growth defect of the Cik1$^{SKNN+4A}$-containing strain as a single source of Cik1 did not allow further characterization. To circumvent this problem, I have integrated Cik1$^{SKNN+4A}$ into the genome in addition to Cik1-AID. I have analyzed cell cycle progression in this strain by following the budding index of a exponentially growing culture after addition of auxin. While a Cik1^{WT} strain had roughly equal fractions of non-budded (G1), small budded (S) and large budded (M) cells, Cik1$^{SKNN+4A}$ caused a checkpoint-dependent accumulation of large-budded cells after depletion of the covering Cik1-AID protein. The defects of Cik1$^{SKNN+4A}$ were the same as observed in the complete absence of a rescue allele (**Figure 3.15 B**).

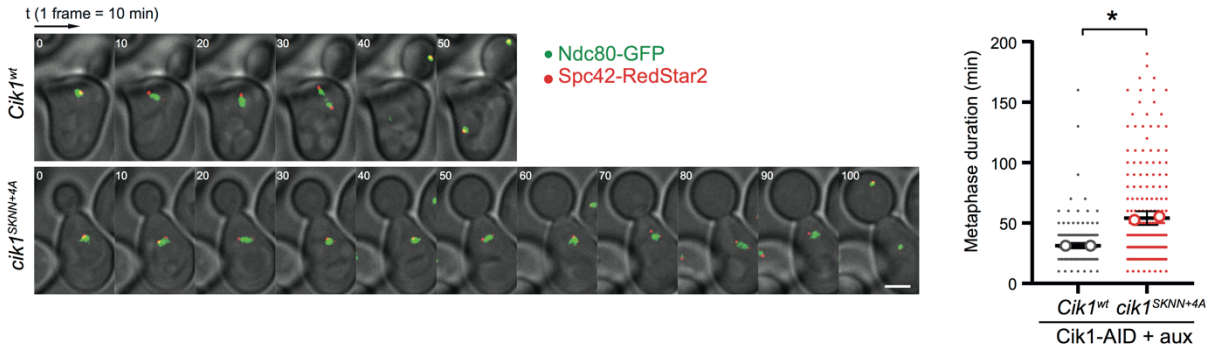

Figure 3.15 Analysis of Cik1-Bim1 interaction mutants

A) Heterozygous diploid dissections. Spores from the same tetrad are in the columns, marked with scopes. Genotypes are indicated with colored circles.
B) Budding index analysis of indicated strains. Exponentially growing cells were exposed to auxin for 3 h. Average values of three experiments are shown. 100 cells were quantified in every repeat. Adapted from (Kornakov et al., 2020) with changes.

Further I have evaluated the effect the Cik1$^{SKNN+4A}$ allele on spindle formation and mitotic progression using live cell imaging. The mean metaphase duration for the Cik1$^{SKNN+4A}$ mutant increased from 31±1 min to 54±3 min. The observed effect again resembled the full Cik1 depletion (**Figure 3.16)**.

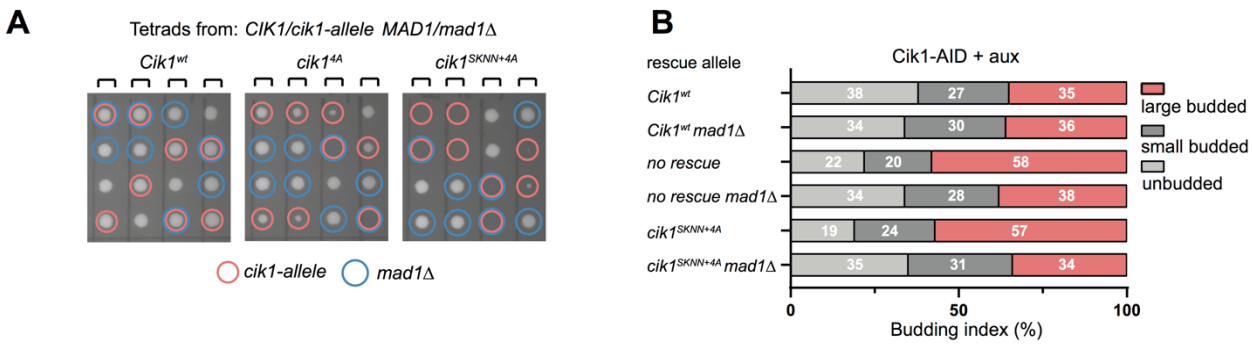

Figure 3.16 Live cell analysis of Cik1-Bim1 interaction mutants

Representative images of *Cik1*^{WT} and *cik1*$^{SKNN+4A}$ metaphase cells. Scale bar is 2 μm. Quantification of metaphase duration in N=200 cells from two technical repeats. Individual cells are depicted with small circles and mean values of repeats are marked with big circles. Error bars are mean values with 95% CIs. χ^2 test was applied, $p < 0.0001$. Adapted from (Kornakov et al., 2020) with changes.

Similar to the depletion of Cik1, the Cik1$^{SKNN+4A}$ allele caused a decrease in metaphase spindle length by half from 2.14±0.07 μm for Cik1^{WT} to 1.16±0.09 μm, while not strongly affecting anaphase spindle elongation (**Figure 3.17)**.

In all assays Cik1$^{SKNN+4A}$ behaved like the Cik1 depletion in the absence of a rescue allele, I have therefore concluded that all kinesin-14 mitotic functions in chromosome segregation are accomplished in a complex with Bim1.

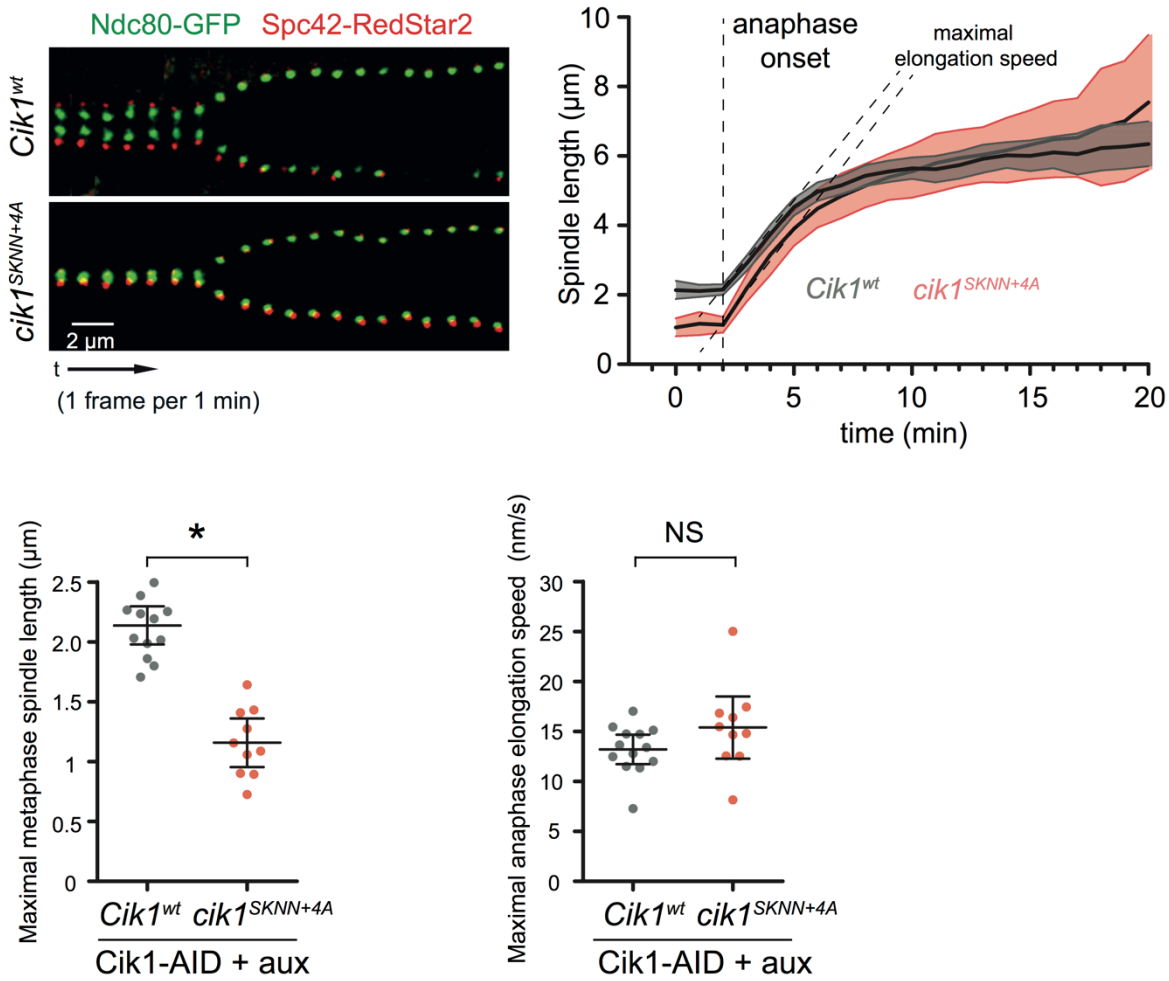

Figure 3.17 Analysis of spindle dynamics in Cik1-Bim1 interaction mutants

Representative images of spindle elongation in *Cik1*^{WT} and *cik1*$^{SKNN+4A}$ cells (at left side). Images are aligned to 7 min before anaphase. Quantification of spindle elongation (middle and right), N=15. Error bars are mean values with 95% CIs. Student's two-tailed t-test was applied, *p<0.0001, for NS p=0.14. Adapted from (Kornakov et al., 2020) with changes.

3.6 Artificial plus-end targeting of Kinesin-14 bypasses the requirements for Bim1 binding.

Which property of Bim1 is required for a functional complex with kinesin-14? Bim1 has a tripartite domain structure. The CH-domain mediates microtubule binding, the EBH domain interacts with Bim1 cargos and the C-terminus binds to the CAP-Gly domain of Bik1. As I have observed that Bim1-Cik1-Kar3 is a microtubule crosslinker *in vivo*, I hypothesized that the CH-domain would be crucial for this function. By fusing the Bim1-binding deficient mutant Cik1$^{\Delta 74}$ to the CH-domains of Bim1 or Ndc80, I have tested whether this fusion bypasses the requirements for Bim1 binding. Indeed, CH-Cik1$^{\Delta 74}$ constructs were able to rescue viability after Cik1 depletion in the mad1delta background, confirming that CH-domains alone are sufficient to provide the properties required for Cik1-Kar3 functions (**Figure 3.18 B**). As a control, I have used a CH-fusion to Kar3. CH-Kar3, however, failed to rescue the Cik1 depletion, indicating that not every CH-fusion is able to rescue lethality and that Cik1 has a functional contribution to the Cik1-Kar3 complex besides plus-end targeting.

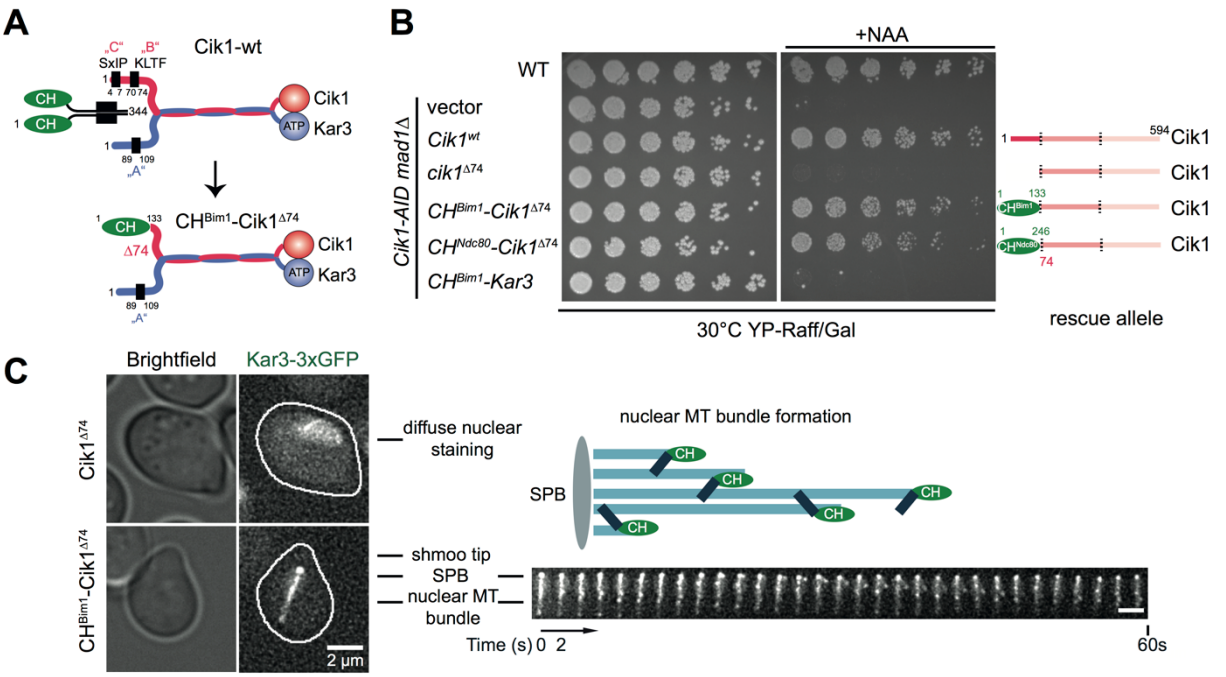

Figure 3.18 Plus-end targeting of Cik1-Kar3 bypasses the requirements for Bim1 binding.

A) Schemes of Bim1-Cik1-Kar3 complex and CH-Cik1$^{\Delta 74}$ mutant.
B) Spot assay shows that CH domain fusions completely rescue viability.
C) Representative images of CH-Cik1$^{\Delta 74}$ and Cik1$^{\Delta 74}$ α-factor arrested cells. Cik1$^{\Delta 74}$ does not localize to microtubules and displays diffuse nuclear staining. the nuclear microtubule bundle in CH-Cik1$^{\Delta 74}$ cells is dynamic. Adapted from (Kornakov et al., 2020) with changes.

Naturally, in α-factor arrested cells Cik1-Kar3 has a cytoplasmic localization, because the short Cik1 isoform lacks an NLS. Expression of Cik1$^{\Delta 74}$-NLS or CH-Cik1$^{\Delta 74}$-NLS promotes nuclear import of Cik1-Kar3. Following the Kar3-3xGFP signal, I noticed that CH-Cik1$^{\Delta 74}$-NLS caused the appearance of a brightly stained nuclear bar-like structure, that was interpreted to be a long microtubule bundle. Individual Kar3-3xGFP dots displayed movement along the bundle, indicating a dynamic behavior of the microtubule bundle. In contrast, Cik1$^{\Delta 74}$-NLS had only diffuse nuclear staining without microtubule localization, with a bit stronger signal at the SPB (**Figure 3.18 C**). This indicates that targeting CH-Cik1$^{\Delta 74}$ to the nucleus is sufficient to induce the formation of a dynamic microtubule bundle in non-mitotic cells.

To characterize bundle formation further, I have used Bik1-3xGFP to visualize microtubule structures. Expression of CH-Cik1$^{\Delta 74}$-NLS in polarized cells induced disorganization and misalignment of cytoplasmic microtubules and formation of a nuclear microtubule bundle. I have concluded that localization of Cik1-Kar3 to microtubules depends on the CH-domain and expression of CH-Cik1$^{\Delta 74}$ is sufficient to induce microtubule bundling.

In cycling cells, expression of CH-Cik1$^{\Delta 74}$-NLS was able to restore metaphase duration back to wild-type upon Cik1 depletion. The observed full restoration of function also implies that the Cik1 tail contains no other elements important for chromosome segregation, besides the Bim1 binding motifs (**Figure 3.19 A** and **B)**.

The third identified Bim1-binding motif A (ELN) is located in the Kar3 tail region termed ND2. I have confirmed that a CH-fusion rescues the viability of Kar3^{ND2}, consistent with the observed role of ELN motif in Bim1 binding (**Figure 3.19 C**).

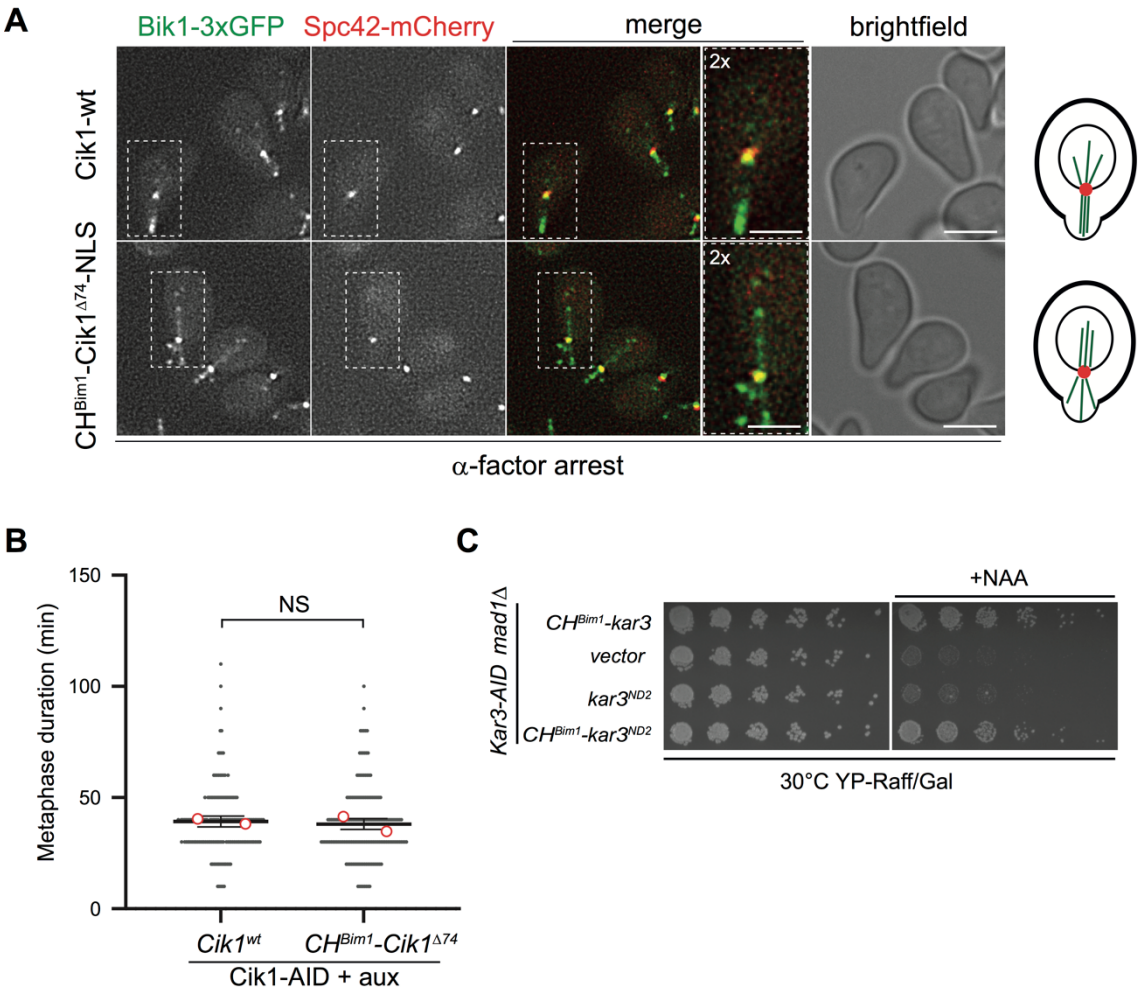

Figure 3.19 The fusion protein CH-Cik1$^{\Delta 74}$ can bundle microtubules and substitute for Cik1^{WT}.

A) Representative images of Cik1^{WT} and CH-Cik1$^{\Delta 74}$-NLS α-factor arrested cells. Scale bar is 3 μm. Two-fold magnifications are shown with scale bar 1 μm.
B) Quantification of metaphase duration in 160 and 170 cells from two technical repeats. Individual cells are depicted with small circles and mean values of repeats are marked with big circles. Error bars are mean values with 95% CIs. χ^2 test was applied, NS means p > 0.9999.
C) Spot assay shows that CH-domain fusion rescues viability of Kar3^{ND2} mutant in the Kar3-AID mad1 delta genetic background. Adapted from (Kornakov et al., 2020) with changes.

3.7 Human kinesin-14 HSET can efficiently substitute for Cik1-Kar3 in chromosome segregation.

Microtubule crosslinking accomplished in a complex with Bim1/EB1 proteins is likely to be a universal function of kinesin-14s. I have decided to test if human kinesin-14 HSET can substitute yeast Bim1-Cik1-Kar3 in chromosome segregation. First, I examined HSET binding to EB1 in vitro. The EB1-HSET complex was not stable in bulk pulldowns, it fell apart during washes. I have estimated HSET affinity for His_6-EB1

using quantitative pulldown, apparent dissociation constant was $K'_d \approx 1400$ nM (**Figure 3.20 A** and **B)**. That low affinity is common for EB1-binding SxIP motifs. However, yeasts have less then 10^3 - 10^4 kinesin molecules per cell, which would correspond to concentrations less than 20-200 nM. In addition, cellular conditions might be more stringent than usual *in vitro* settings, therefore binding constants in micromolar range should be interpreted as no binding in cytoplasm. Consistent with a lack of high-affinity EB1 binding, I observed that HSET was not able to rescue the of Kar3 depletion in the checkpoint deficient strain. I hypothesized that HSET is an inefficient Bim1-binder, and prepared constitutively plus-end targeted CH-HSET instead. Indeed, CH-HSET was capable of rescuing the Kar3 depletion (**Figure 3.20 C**). Despite a different molecular structure and *in vitro* properties plus-end targeted HSET is therefore a functional equivalent of Cik1-Kar3 in chromosome segregation.

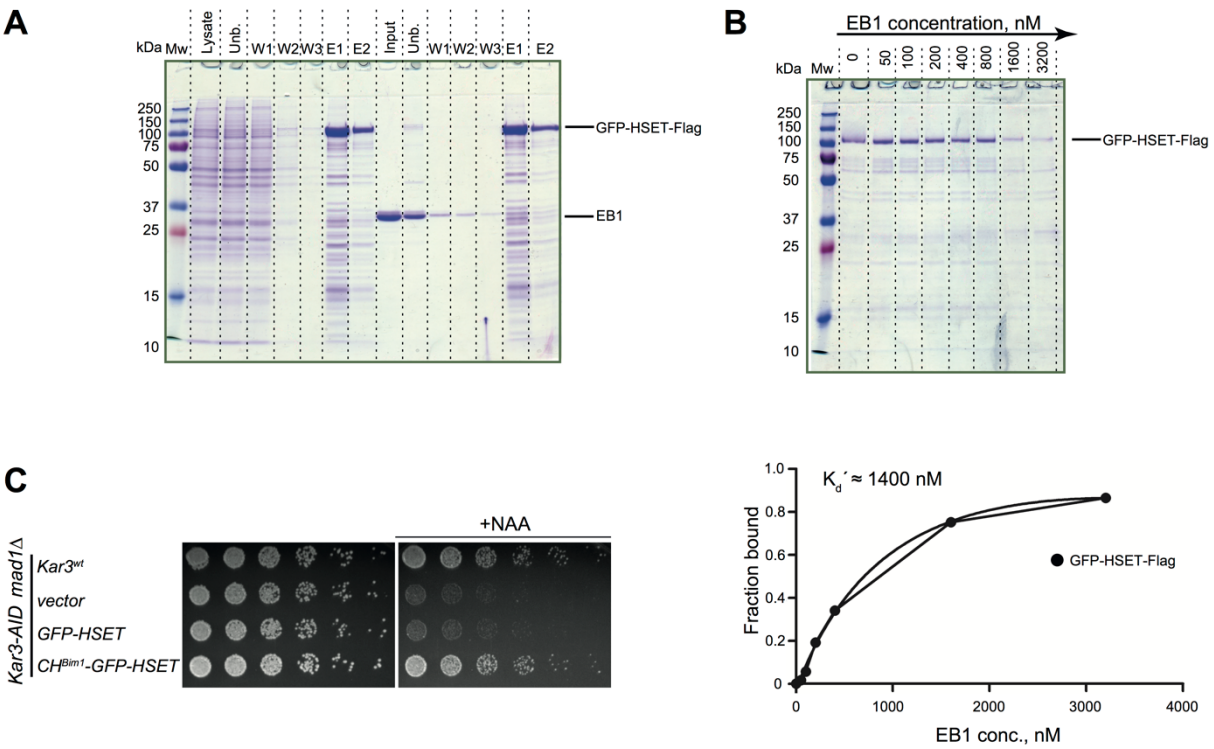

Figure 3.20 Plus-end targeted human kinesin-14 HSET is the functional equivalent of Cik1-Kar3.

A) Purification and Bim1-pulldown by insect cell expressed GFP-HSET-Flag.
B) Quantitative pulldown of HSET by His_6-EB1. K'_d was calculated by fitting to the one-site total binding model.
C) Spot assay shows that CH-HSET rescues Kar3 depletion in *mad1*Δ background. Adapted from (Kornakov et al., 2020) with changes.

3.8 Bim1-Cik1-Kar3 and Ase1 microtubule crosslinkers are partially redundant in metaphase spindle asssemly and chromosome bi-orientation.

As described before, Cik1-depleted cells initially showed strong metaphase alignment defects, but gradually, spindle organization improved and cells were able to progress to anaphase. To understand the basis for this phenomenon, I used a variety of different MAPs tagged with fluorescent proteins as markers and investigated them in the Cik1 depletion setting. I have noticed that Cik1 depletion leads to increased intensities of certain microtubule crosslinkers on the spindle. The most prominent effect was observed for Ase1/PRC1. In wild-type cells Ase1 was absent on nascent bipolar spindles, accumulated during metaphase and peaked in anaphase shortly before spindle disassembly (**Figure 3.21**).

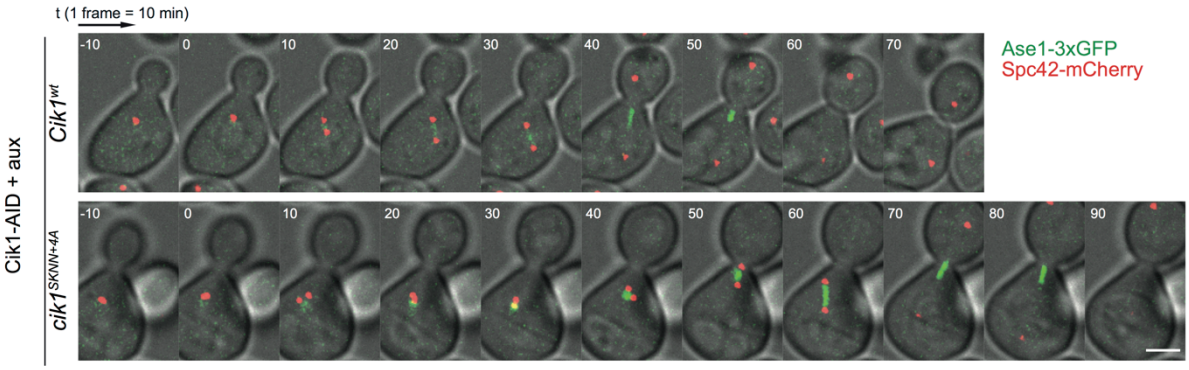

Figure 3.21 Analysis of Ase1 localization in wild-type and Cik1-depleted cells.

Representative images of cell cycle progression in *Cik1*^{WT} and *cik1*$^{SKNN+4A}$ cells after α-factor release. Images are aligned to metaphase start (0 min). 10 min time-lapse is shown. Scale bar is 2 μm. Adapted from (Kornakov et al., 2020) with changes.

After Cik1 depletion (or in a depletion rescued with the Cik1$^{SKNN+4A}$ mutant) the Ase1 signal was visible even before bipolar spindle assembly and accumulated to much higher levels during metaphase. Mean Ase1 intensities on preanaphase spindles of Cik1 depleted and Cik1$^{SKNN+4A}$ cells were 50% higher than in the wild-type situation (445±14, 606±19, 450±14, 648±24 for no auxin, Cik1 depletion, Cik1^{wt} and Cik1$^{SKNN+4A}$ rescues, respectively) (**Figure 3.22**). This observation suggests that in the absence of the Bim1-Cik1-Kar3 complex, Ase1 can take over this important function as a microtubule crosslinker in metaphase.

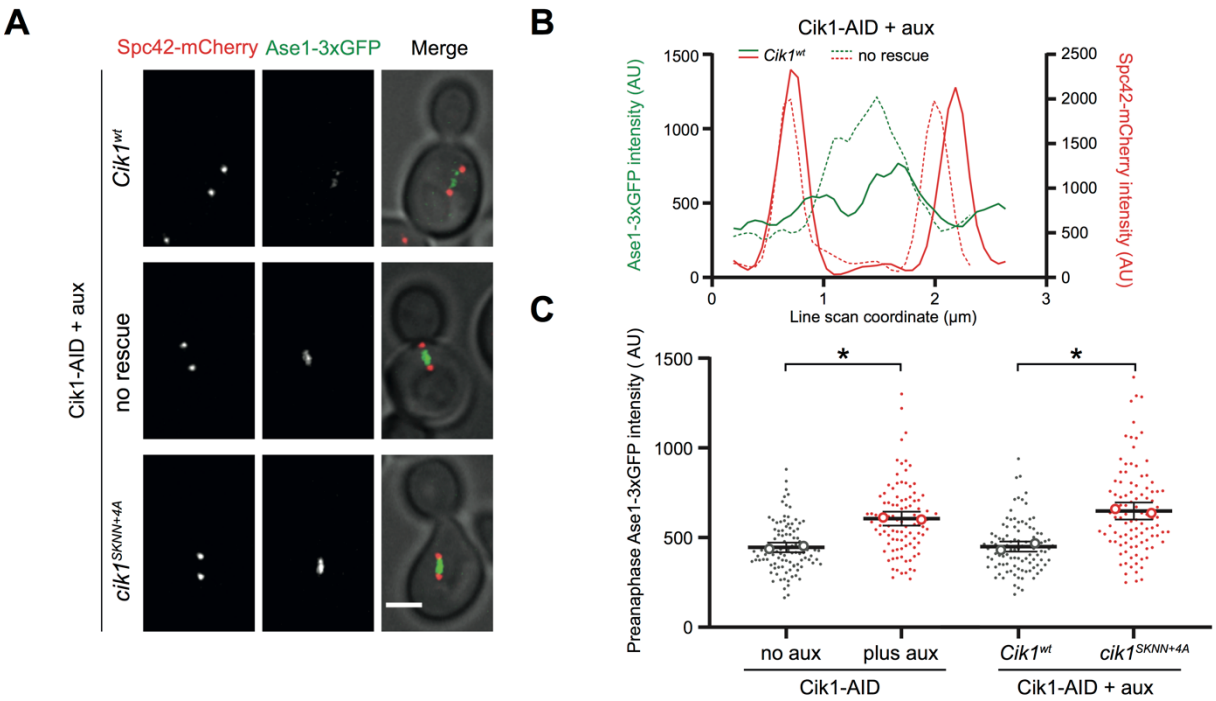

Figure 3.22 Quantification of Ase1 localization

A) Representative images *Cik1*^{WT}, no rescue and *cik1*$^{SKNN+4A}$ preanaphase cells. Scale bar is 3 μm.
B) Line scan profiles across the spindle axis. *Cik1*^{WT} and no rescue spindles of similar size are shown.
C) Quantification of the Ase1-3xGFP signal on preanaphase spindles at indicated conditions. 100 cells from two technical repeats were quantified for every condition. Individual cells are depicted with small circles and mean values of repeats are marked with big circles. Error bars are mean values with 95% CIs. Kruskal-Wallis test was applied, *p<0.0001. Adapted from (Kornakov et al., 2020) with changes.

I speculated that different crosslinkers might compete with each other for binding sites on microtubules of the metaphase spindle, and in the absence of one, the other may bind to microtubules more efficiently, like it was observed for Bim1-Cik1-Kar3 and Ase1. If this was true, I would predict that cell need either Bim1-Cik1-Kar3 or Ase1 for metaphase spindle assembly, and simultaneous loss of both, should be much worse than loss of either one alone. To what degree do their functions overlap? Can increased levels of Ase1 compensate for the lack of Bim1-Cik1-Kar3? To test this idea, I co-depleted Cik1 and Ase1 using the auxin-inducible degradation system. Indeed, this experiment resulted in lethality even in the presence of the mitotic checkpoint. The most likely explanation was that the double depleted cells had strong spindle defects, were unable to bi-orient chromosomes and were therefore permanently arrested in metaphase (**Figure 3.23 A**). As I have observed this situation by live-cell imaging, I have also noticed a strong decrease in spindle size, accompanied with disorganization

of the spindle structure. The measured metaphase spindle lengths in the Cik1-AID Ase1-AID double depletion experiment were 1.65±0.02, 0.97±0.01, 1.26±0.02 and 0.93±0.01 μm for no auxin, plus aux, $Cik1^{wt}$ and $Cik1^{SKNN+4A}$. However, Cik1 and Ase1 co-depletion didn't cause stronger defects in comparison with the single Cik1 depletion. Ase1 depletion alone decreased spindle size, but caused no growth defect or mitotic delay (**Figure 3.23 B**). My interpretation was that only the reduction in spindle size cannot explain the persistent metaphase arrest. Double depleted cells displayed only very little Bik1 signal on the spindle axis, it was instead dispersed and mainly directed outwards (**Figure 3.23 C**), revealing very pronounced spindle organization defects. Similar to Bik1, Ndc80 was also mispositioned outside of the spindle axis. Chromosome bi-orientation is impossible in this configuration, since there has to be a sufficiently large physical separation between the sister chromatids that produces tension.

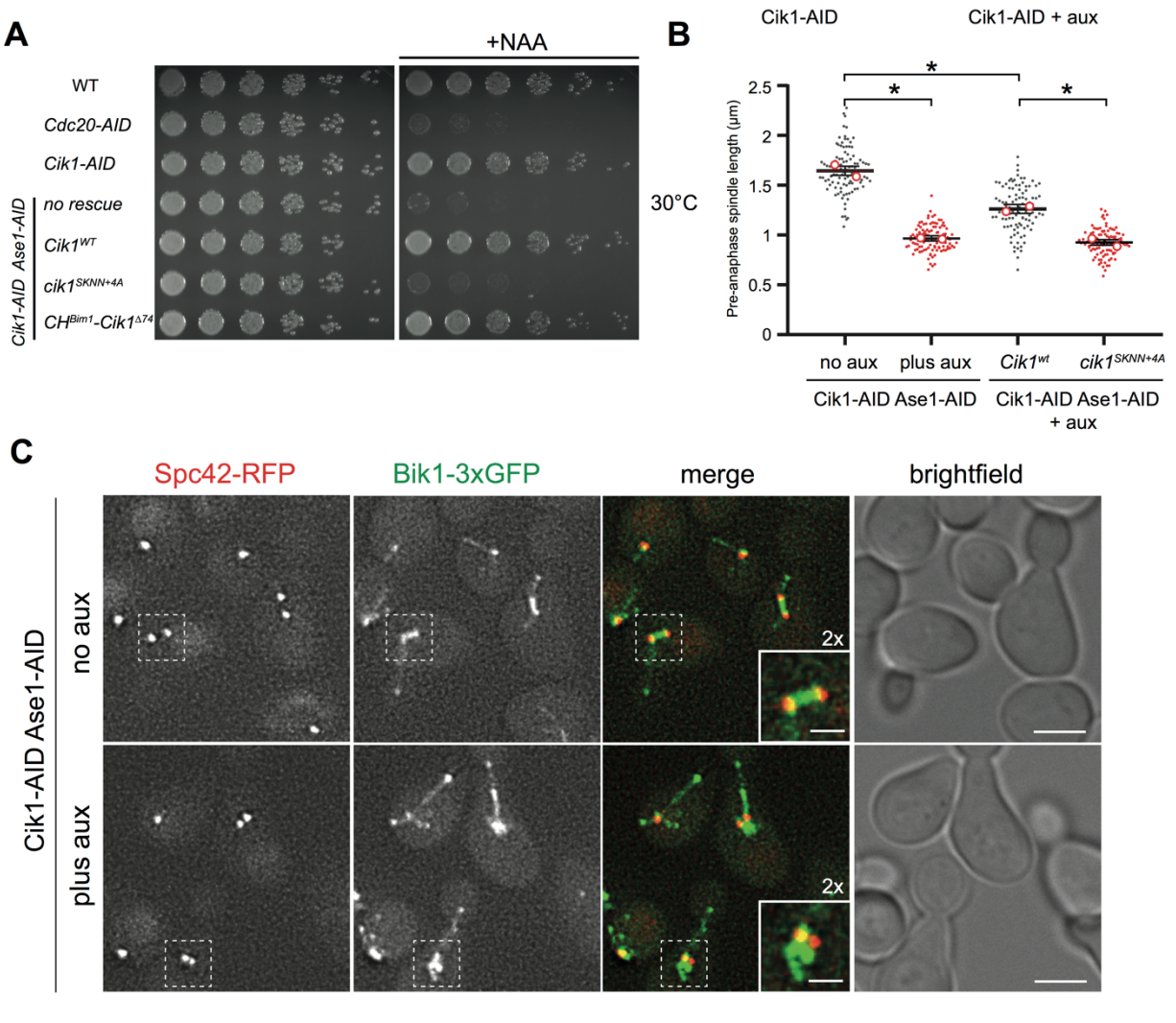

Figure 3.23 Bim1-Cik1-Kar3 and Ase1 have overlapping functions in metaphase spindle assembly and chromosome bi-orientation.

A) Bim1-Cik1-Kar3 and Ase1 are partially redundant for cell viability as judged by the spot assay. Depletion of an essential protein Cdc20 was used as a control.
B) Quantification of preanaphase spindle lengths under the indicated conditions. 100 cells from two technical repeats were quantified for every condition. Individual cells are depicted with small circles and mean values of repeats are marked with big circles. Error bars are mean values with 95% CIs. Kruskal-Wallis test was applied, *p<0.0001.
C) Representative images of control and Cik1 and Ase1 co-depleted metaphase cells. Two-fold magnifications are shown. Scale bars are 3 μm on overview images and 1 μm on magnifications. Adapted from (Kornakov et al., 2020) with changes.

3.9 Kinesin-14 regulates microtubule bundle dynamics at the yeast shmoo tip

In the previously described experiments I have established Bim1-Cik1-Kar3 as an important microtubule crosslinker and bundling factor for the metaphase spindle in mitosis. Does Bim1-Cik1-Kar3 affect parameters of microtubule bundle dynamics? The small size (~1-2 μm) of metaphase spindles in budding yeasts, which contain 40 microtubules, does not allow to directly observe the dynamics of microtubules of the kinetochore clusters. However, budding yeasts provide a different excellent *in vivo* model for observing microtubule bundles. After mating pheromone exposure, cells polarize and assemble a bundle of 3-4 microtubules connecting the SPB with an area of the cytoplasmic membrane (termed the shmoo tip). Microtubule bundle dynamics can be measured from a change in SPB position relative to the shmoo tip (**Figure 3.24 A** and **B**). When a microtubule bundle is growing it pushes SPB away from shmoo tip, when it shrinks, it pulls SPB towards shmoo tip.

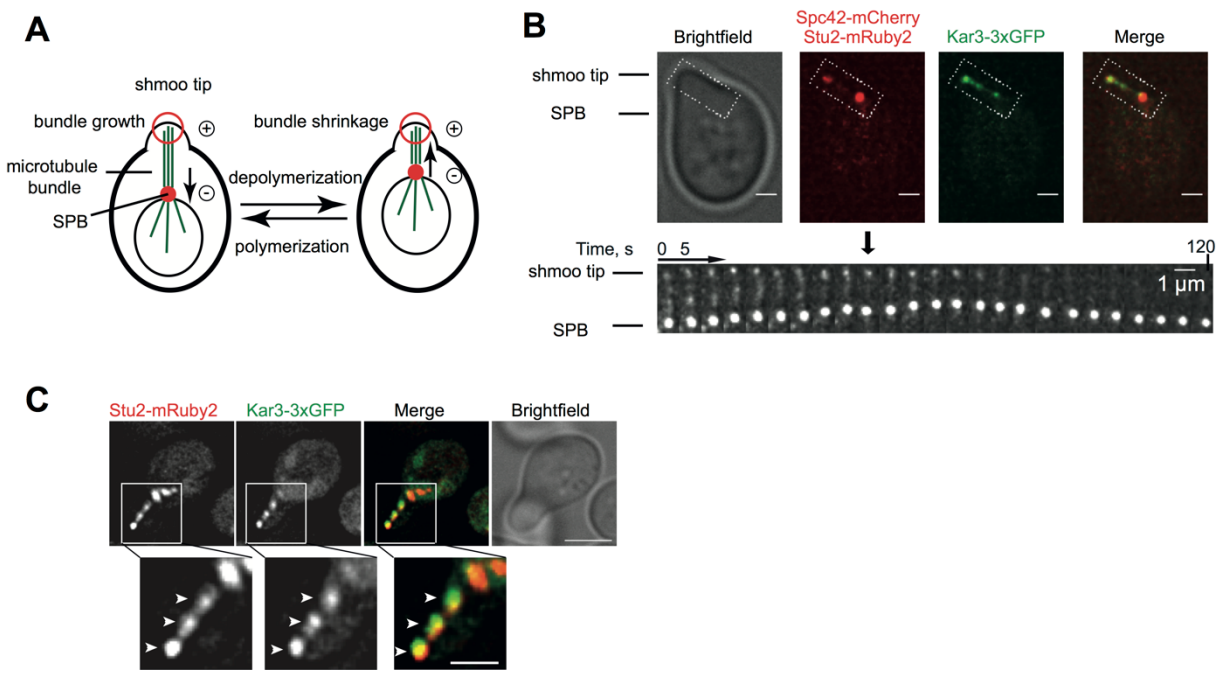

Figure 3.24 Cik1-Kar3 is a plus-end tracking protein on the dynamic shmoo tip microtubule bundle.

A) Scheme of microtubule cytoskeleton in α-factor arrested cells. Switching between bundle polymerization and depolymerization cycles causes a change in the position of the SPB.
B) Representative images of an α-factor arrested cell (top). Time-lapse of indicated area shows changes in microtubule bundle length, accompanied by SPB movements. Scale bars are 1 μm.
C) Kar3-3xGFP signal coincides with the microtubule plus-end marker Stu2-mRuby2. Individual dots are shown with white arrowheads on the magnification. Scale bars are 2 μm on the main image and 1 μm on magnification. Adapted from (Kornakov et al., 2020) with changes.

In α-factor arrested cells kinesin-14 shows a cytoplasmic localization after expression of the short Cik1 isoform that lacks the NLS. Every Kar3-3xGFP fluorescent spot along the bundle overlapped with a Stu2-mRuby2 signal, used as microtubule plus-ends marker (**Figure 3.24 C**). I have evaluated the effect of Kar3 depletion on microtubule bundle behavior using live cell microscopy. In most cases, Kar3 depleted cells had misaligned microtubules, directed outside of shmoo tip (**Figure 3.25**). Kar3 depletion also caused marked increase in microtubule bundle length, but did not affect polymerization and depolymerization speeds. Instead, it caused decrease in dynamicity, as the interval between catastrophes and rescue events increased from 90 s to 130 s (**Figure 3.26 B**).

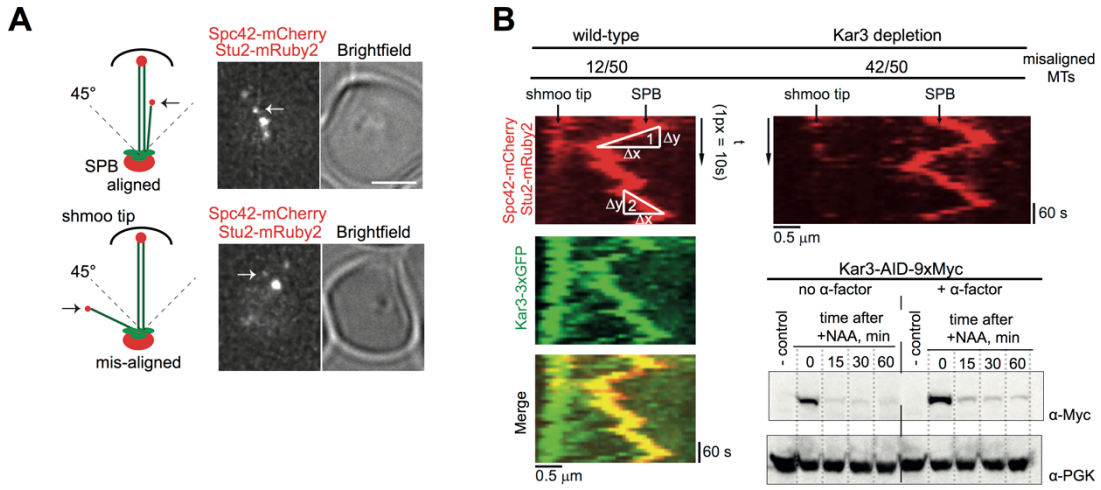

Figure 3.25 Shmoo tip microtubule bundle dynamics are regulated by Kar3

A) Scheme and representative fluorescence microscopy images of aligned and misaligned microtubules. Stu2-mRuby2 signal at microtubules plus-ends is marked with white arrows. Scale bar is 2 μm.
B) Kymographs derived from the line scans along microtubule bundles from shmoo tip to the SPB. White triangles show examples of depolymerization (1) and polymerization (2) cycles. Number of cells with misaligned microtubules during 5 min movies at every condition is shown at the top. Scale bar is 0.5 μm. Western blot shows efficient Kar3-AID depletion in α-factor arrested cell after 1h of auxin addition. Adapted from (Kornakov et al., 2020) with changes.

I have tested if the functions of Cik1-Kar3 in the regulation of microtubule bundle dynamics rely on Bim1 binding. Mutation in the Bim1-binding motif A ($Kar3^{ND2}$) decreased bundle dynamicity. Also, bundle length in $Kar3^{ND2}$ was increased compared

to control cells. **(Figure 3.27)**. Thus, in polarized cells Bim1-Cik1-Kar3 crosslinks microtubules, controls microtubule bundle length and promotes its dynamics, without affecting microtubule polymerization and depolymerization speeds.

To study the bundle dynamics in more detail, I decided to compare the dynamic parameters of individual microtubules to the bundles in α-factor arrested cells. I observed, that nuclear microtubules are partially unbundled, but have preferential growth directions. I have estimated the dynamics of nuclear microtubules using Stu2-GFP as a marker for polymerizing and depolymerizing plus-ends. Individual nuclear microtubules were highly dynamic and had ~2.4 -fold increased polymerization and depolymerization speeds, compared to the shmoo tip bundle. However, in both cases V_{depol}/V_{pol} ratio was ~ 2. (**Figure 3.26**)

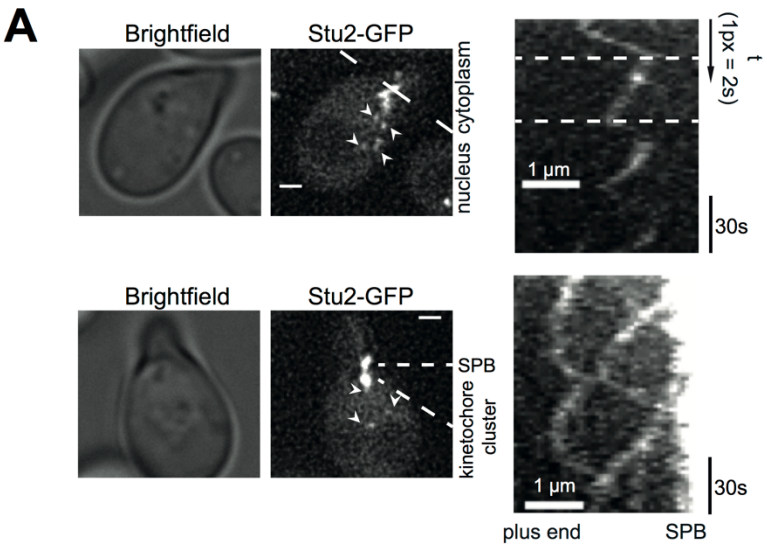

B

		V_{pol}, nm/s	V_{depol}, nm/s	Δt_{cat}, s	Δt_{rescue}, s	pause duration, s	%, paused
individual MT		37.7±8.9	77.7±18.7	N.A.	N.A.	N.A.	N.A.
bundle	wt	15.5±1.7	29.2±4.4	89.4±0.3	89.9±1.1	22.5±0.6	7.6
bundle	no NAA Kar3-AID	15.9±2.3	30.1±5.3	93.9±10.7	91.4±15.1	23.9±5.2	6.5
bundle	+NAA Kar3-AID	17.2±3.3	35.2±5.7	127.2±1.4	133.4±6.5	36.4±5	8.9

Figure 3.26 Comparison between individual microtubule and microtubule bundle dynamics

A) Representative fluorescence microscopy images of two α-factor arrested cells. Microtubule plus-ends in the nucleus are marked with white arrowheads. Scale bar is 1 µm. Kymographs show the dynamic behavior of nuclear microtubules at the right side. Kymographs are derived from line scans from microtubule plus-ends to SPB during 2 min movies. White dashed lines show polymerization phases (upper image). The bottom image shows how different microtubules exchange with each other at the same trajectory.

B) Comparison of individual microtubule dynamics to bundles in the presence of Kar3 and after Kar3 depletion. In red color are parameters that change after Kar3 depletion. Adapted from (Kornakov et al., 2020) with changes.

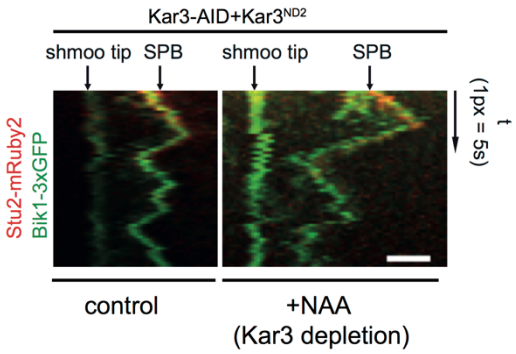

MT bundle dynamics

	V_{pol}, nm/s	V_{depol}, nm/s	Δt_{cat}, s	Δt_{rescue}, s
no NAA	15±4	25±9	80±6	81±7
+NAA	14±3	23±6	138±8	128±6

Figure 3.27 Cik1-Kar3 relies on Bim1 binding in the regulation of microtubule bundle dynamics.

Kymographs show microtubule bundle dynamics in control and Bim1-binding deficient $Kar3^{ND2}$ (motif A) mutant cells. Scale bar is 1 μm. Adapted from (Kornakov et al., 2020) with changes.

How is the dynamic behavior of the microtubule bundle established? Which factor drives the switch between growth and shrinking phases and how may Bim1-Cik1-Kar3 influence that?

To answer these questions, I decided to take a closer look at the switching events. I noticed that Cik1-Kar3 fluorescence intensity at the bundle's plus-end is maximal during the depolymerization to polymerization switches (**Figure 3.28** and **Figure 3.29).** Moreover, the increase in the signal coincided with the arrival of a fluorescent dot at the bundle's end (**Figure 3.29 B**). Given that Bim1-Cik1-Kar3 is a microtubule plus-end tracking protein, I have concluded that bundle polymerization is promoted by an incoming plus-end of a growing microtubule. If that is true, other microtubule plus-end tracking proteins should share similar behavior. Indeed, I have observed that Stu2 (**Figure 3.30 A**) and Bik1 (**Figure 3.30 B**) arrival at the plus-end also coincided with switching to growth. However, it seemed that the number of microtubules in the bundle remained constant over time. After the rescue event, the depolymerizing microtubule detaches from the shmoo tip and continues shortening until it reaches the SPB. (**Figure 3.30)**. In the absence of Bim1-Cik1-Kar3 the microtubule bundle is misaligned and a growing microtubule can hit shmoo tip by chance when microtubule bundle is short. Together, these observations led me to

formulate a “rescue by arrival and microtubule exchange model) (for a description see discussion **Figure 4.2)**.

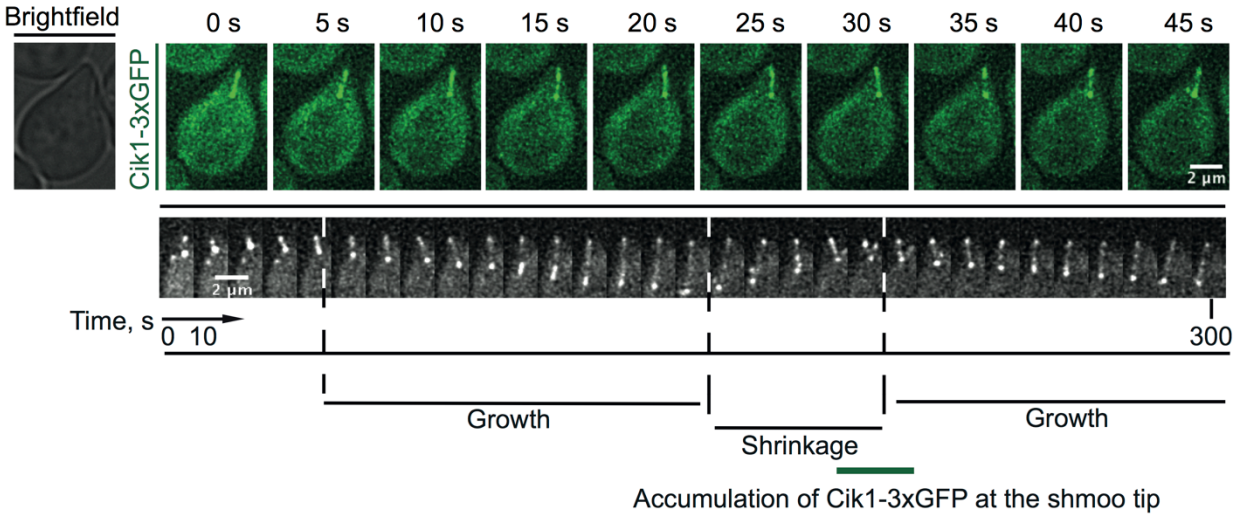

Figure 3.28 Cik1-Kar3 accumulates at the bundle plus-end during shrinkage to growth switches.

Representative time-lapse fluorescence microscopy images of an α-factor arrested cell. Cik1 accumulates during shrinkage to growth switches. Scale bar is 2 µm.

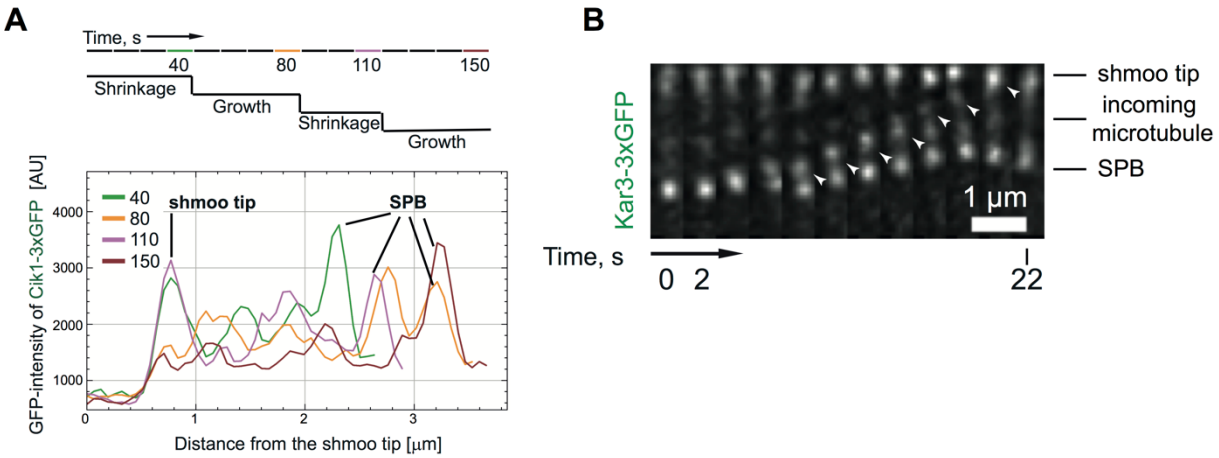

Figure 3.29 Cik1-Kar3 arrives to the shmoo tip at the growing microtubule plus-end.

A) Fluorescence intensity profile scans along shmoo tip microtubule bundle taken at moments of switching. Cik1-3xGFP intensity is maximal during shrinkage to growth switches (40 s and 110 s), green and purple curves.
B) Kymograph shows Kar3-3xGFP signal arrival at the shmoo tip during a rescue event. Microtubule plus-end is marked with white arrowhead. Scale bar is 1 µm.

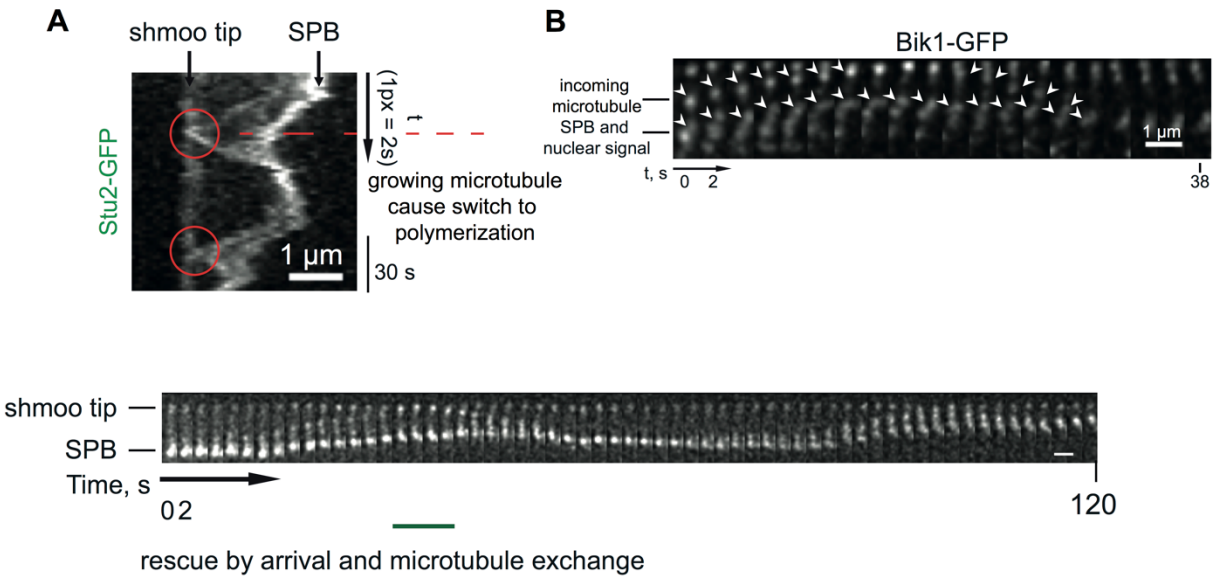

Figure 3.30 Microtubule exchange mechanism

A) Stu2-GFP signal arrives at the shmoo tip at a rescue event and then a depolymerizing microtubule detaches from shmoo tip. With red circles are shown rescue-by-arrival and microtubule exchange events.
B) Time-lapse imaging shows that Bik1-GFP localizes at plus-end of a rescueing microtubule. With white arrowheads microtubule plus-ends (upper) and SPBs (lower) are marked.

4. Discussion

In my work, I have identified the formation of a tight complex between Bim1 with Cik1-Kar3 as a prerequisite for proper metaphase spindle assembly, kinetochore clustering and chromosome bi-orientation. I have dissected the molecular requirements for the formation of this complex, which has allowed me to perform precise genetic manipulations that specifically prevent complex formation in cells. Conversely, I was able analyze constructs in which Cik1-Kar3 is constitutively targeted to microtubule plus-ends via a CH-domain fusion. My experiments have shown that Bim1-Cik1-Kar3 regulates microtubule bundle assembly and dynamics without affecting the microtubule polymerization and depolymerization speeds (Kornakov et al., 2020). Bim1-Cik1-Kar3 works as a microtubule crosslinker that also helps to align growing microtubules along pre-existing bundles. The functions of Bim1-Cik1-Kar3 on metaphase spindles partially overlap with other microtubule crosslinkers, such as Ase1 (**Figure 4.1**). Characterization of the interaction interface between Cik1-Kar3 and Bim1 allowed me to construct specific mutants, deficient in binding. The Cik1$^{SKAA+4A}$ and Kar3^{ND2} alleles behaved like *cik1*Δ and *kar3*Δ in all tested conditions, their application into the conditional system provided a better understanding of kinesin-14 functions without being affected by genetic deletions artefacts. The discovery of the KLTF (motif B) and ELN (motif A) peptide motifs, located on Cik1 and Kar3 polypeptide chains establishes a new type of bi-partite Bim1-binding motif. This AB-motif provides a superior affinity in comparison to classical SxIP motifs. In the future, it would be interesting to understand the structural basis for the tight binding which is unusual for SLiMs.

4.1 My study in a context of previous works.

In the following I will discuss my findings in the context of existing data and previously suggested models for Kinesin-14 function and extend it with hypothetical interpretations.

In a recent work Mieck et al., 2015 proposed that Cik1-Kar3 is a processive motor in contrast to other kinesin-14 family members. The conclusions originated from an *in vitro* reconstitution system. Recombinant insect-cell expressed Cik1-Kar3 displayed many micron long movements along pig-brain tubulin microtubules. Moreover, based on co-localization and coordinated movements of fluorescently labelled Cik1-Kar3 and Ndc80 it was claimed that Ndc80 can be transported by kinesin-14 and that this

transport may have physiological importance. However, the suggested model contradicts other previously published data. The only known clear example of Cik1-Kar3 motor activity *in vivo* is the promotion of microtubule gliding during nuclear congression. This process is driven by multiple Cik1-Kar3 molecules immobilized at the SPB by binding to gamma-tubulin. Cik1-Kar3 localization to microtubule structures is mediated by elements outside of the motor domain. Cik1-Kar3 localizes to the plus-ends of microtubules in cells and motor-dependent minus-end directed movement has never been observed *in vivo*. Cik1-Kar3 is overexpressed in the cytoplasm of α-factor arrested cells and is not co-localized with Ndc80. Mieck's model gives several testable predictions. A first prediction is that Cik1-Kar3 binding to Ndc80 should be mediated by functionally important sequence-specific elements in the tail of either Cik1 or Kar3. Second, Cik1-Kar3 shall display robust microtubule binding by itself and accumulate at minus-ends in cells, since microtubule binding is a prerequisite for processive movement.

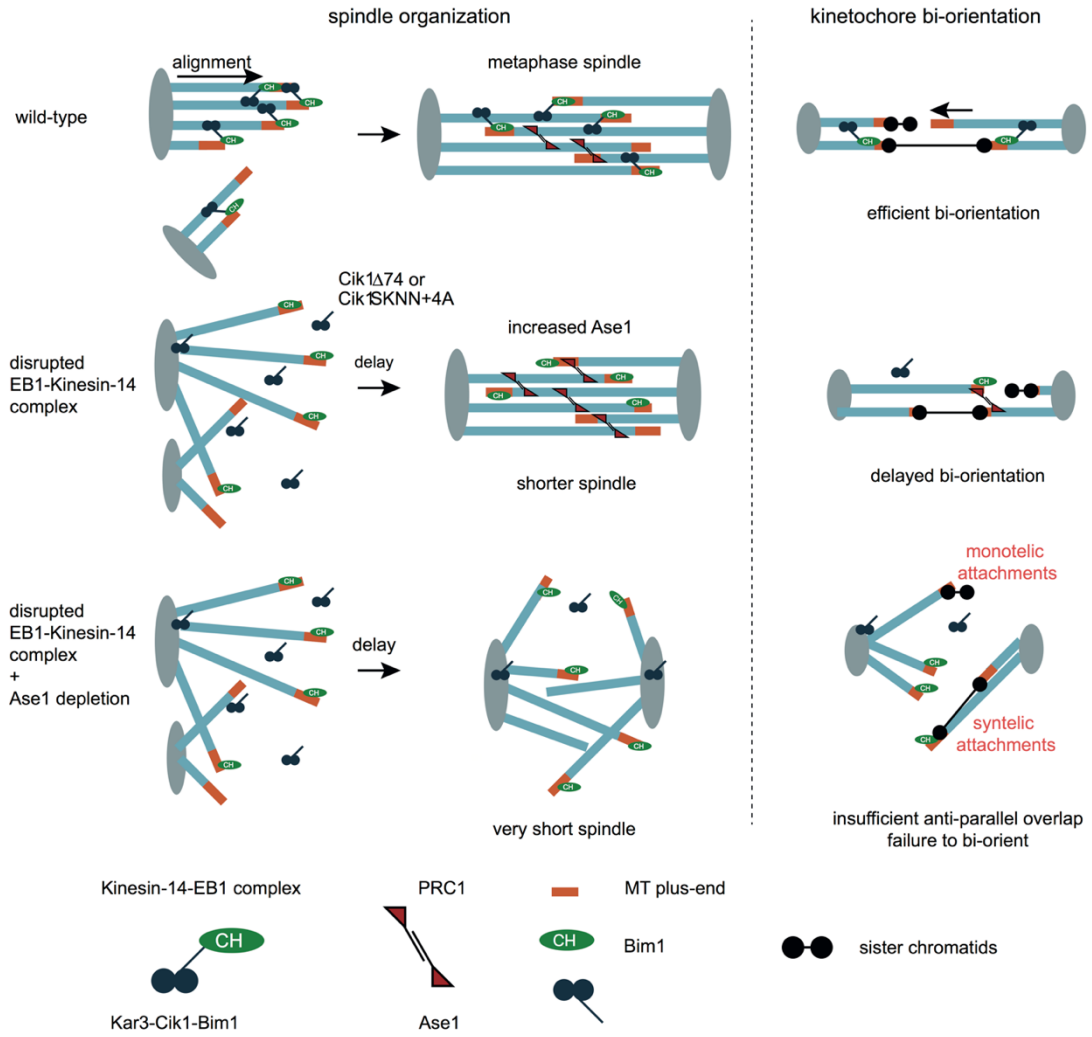

Figure 4.1 Proposed model of Bim1-Cik1-Kar3 action in chromosome segregation.

Adapted from (Kornakov et al., 2020) with changes.

My study shows that Bim1-Cik1-Kar3 is a microtubule bundler and that this function of Cik1-Kar3 relies strictly on Bim1 (Kornakov et al., 2020). Using a comprehensive mutant screen, I have not found any other functionally important, non-redundant, elements besides the Bim1-binding motifs. Moreover, CH-domain fusions can rescue the functionality of tailless Cik1-Kar3 constructs in chromosome segregation. Bim1-binding deficient mutants have diminished microtubule binding, indicating that Cik1-Kar3 recruitment to microtubules depends on Bim1 in cells. Human homodimeric kinesin-14 HSET can replace heterodimeric Cik1-Kar3 in budding yeast, when being targeted to the plus-ends. All these data argue that the observation of autonomous, processive motility along individual microtubules made by Mieck et al., does not substantially contribute to Kar3 function in cells. Moreover, I have shown that Bim1-Cik1-Kar3 is partially redundant with another antiparallel microtubule crosslinker Ase1/PRC1 in metaphase spindle assembly and chromosome bi-orientation (Kornakov et al., 2020). My conclusions are in line with models of other kinesin-14s action, and I propose that the molecule's structure is optimized to produce microtubule crosslinking in the bundles and to avoid motor binding to individual microtubules.

Another widely cited model regarding Kinesin-14 in budding yeast, is based on Tanaka's findings (Tanaka et al., 2005, Tanaka et al., 2007) and proposes that Kar3 mediates the transport of laterally attached chromosomes towards the SPB. The genetic model system used to analyze the role of Kinesin-14 is described in the introduction, and here I will therefore focus on alternative interpretations and potential outcomes. While the motor activity is required for chromosome transport in the setting described by Tanaka, it is unclear which Kar3 complex is responsible for that. If the process has physiological importance for chromosome segregation, it should be Cik1-Kar3. My work demonstrates that Cik1-Kar3 functions in chromosome segregation rely on Bim1. I would expect that Bim1-Cik1-Kar3 binds to microtubule plus-ends, where it can crosslink microtubules. Localization of Kar3 to an unattached CEN, as observed by Tanaka, means either that microtubule's plus-end exists in the vicinity of CEN or that Cik1-Kar3 has other binding partners among kinetochore proteins. The second option is unlikely, since it assumes that HSET is also capable of binding yeast kinetochores. The first variant is favorable. Stu2-dependent microtubule nucleation by unattached kinetochores was observed in the same model system (Kitamura et al., 2010). Therefore, my interpretation would be that chromosome transport is likely to be

driven by Bim1-Cik1-Kar3 through sliding of short kinetochore-originated microtubules towards the SPB.

My findings are consistent with the previously detected evolutionary conservation of EB1-Kinesin-14 interactions. Moreover, using specific point mutants, I found that all mitotic functions of Cik1-Kar3 rely on its recruitment to microtubule plus-ends by the CH-domain of Bim1. One of the previous models for Kar3 function during spindle assembly has proposed antiparallel microtubule zippering, based on minus-end directed motor activity of Kar3 as a way to align microtubules (Hepperla et al., 2014). However, I have observed that mutants lacking Bim1 binding ($Cik1^{\Delta 74}$, $Cik1^{SKAA+4A}$, $Kar3^{ND2}$) do not localize to microtubules. That challenges a zippering model or at least assumes that its own Cik1-Kar3 motor activity is subsequent to Bim1 binding. More likely, crosslinking of parallel and anti-parallel microtubules by Bim1-Cik1-Kar3 mediates kinetochore positioning on the spindle axis and promotes the assembly of a metaphase spindle of proper length.

Bim1 binding recruits Cik1-Kar3 to microtubules, similar to fission yeast Klp2 being recruited to microtubules by an interaction with Mal3. These complexes also share a similar reduction in localization on microtubules in anaphase. In fission yeast, the Mal3-Klp2 complex formation is inhibited by Sid2 phosphorylation when the cell finishes mitosis (Mana-Capelli et al., 2012). It would be intriguing to test if the Bim1-Cik1-Kar3 complex is regulated by mitotic exit kinases in addition to degradation by the APC/C. If Bim1-Cik1-Kar3 is a functional analog of Mal3-Klp2, then maybe Vik1-Kar3 is an analog of the second Kinesin-14 protein Pkl1? Pkl1's role in the organization of MTOCs and in the regulation of microtubule nucleation is well established, while Vik1-Kar3 functions are largely unknown. In this regard some interesting questions are: does Vik1-Kar3 directly bind to γ-tubulin and what is the basis of functional counteraction between Cik1-Kar3 and Vik1-Kar3.

The centromeres of all 16 budding yeast chromosomes are located in physical proximity to each other. Chromosomes are thought to be glued together by chromatin crosslinkers. Fluorescently labelled pericentromeric regions on different chromosomes display coordinated movements (Stephens et al., 2013). Those movements are produced by synchronized changes in microtubules length within a bundle. These observations lead to a hypothesis that budding yeast centromeres are organized into larger complexes connected to multiple microtubules, resembling kinetochore organization in higher eukaryotes. But which factors are responsible for regulation of microtubule bundle assembly and dynamics are not clear. I have proposed that Bim1-

Cik1-Kar3 aligns and crosslinks kinetochore microtubule bundles. In that scenario, chromosome bi-orientation in budding yeasts is a cooperative process as a single bi-oriented chromosome causes an increased chance to form a correct attachment for the next incoming microtubule. In this way, chromatin and microtubule crosslinkers can work together in building a cooperative chromosome bi-orientation machinery.

The Bim1-Cik1-Kar3 complex may promote kinetochore microtubule bundle dynamics and controls its length according to a rescue-by-arrival and microtubule exchange mechanism, similar to the shmoo tip microtubule bundle. Since kinetochore microtubules have a median length of ~300 nm, newly nucleated microtubules will reach the bundle's end in ~ 7.5 s and an opposite kinetochore cluster in ~ 25-40 s. That would lead to high-frequency low-amplitude oscillations of the kinetochore bundle around a constant length. In the absence of Bim1-Cik1-Kar3 kinetochore microtubule dynamics is suppressed and growing microtubules have a poor chance to hit an opposing kinetochore cluster. Microtubule dynamics is important for chromosome bi-orientation and tension generation between sister chromatids, which was previously observed with β-tubulin mutants (Huang and Huffaker, 2006). In this way, Bim1-Cik1-Kar3 may cooperate with Ipl1/Aurora B kinase, which resolves tensionless attachments.

After cell cycle entry, rising Cdk1 activity allows genome replication and prevents the degradation of microtubule crosslinkers, which are absent in G1 cells. The protein levels of kinesin-5, kinesin-14 and Ase1 gradually rise, which also can be visually observed by their recruitment to spindle structures. It was shown before that microtubule crosslinking by kinesin-5 is sufficient for SPB separation (Leary et al., 2019). However, I have shown that Bim1-Cik1-Kar3 is needed for proper metaphase spindle alignment and length even when kinesin-5 is present. The functions of Ase1 were mostly studied in anaphase, where it is required for spindle elongation, microtubule crosslinking by Ase1 in metaphase is inhibited by Cdk1 phosphorylation. However, I found that in the absence of Bim1-Cik1-Kar3 cells rely on Ase1 for chromosome bi-orientation.

Parallel microtubule bundles dynamics has been the focus of interest of many studies for the last 30 years. The most interesting examples of such bundles are kinetochore microtubules and microtubule arrays in polarized cells. Bundles ends are typically not free, they are anchored to MTOCs and chromosomes or to cytoplasmic membrane areas. Switching between bundle shrinkage and growth produces pulling and pushing forces on associated structures. Mechanistic *in vitro* studies performed

by Liedewij Laan and colleagues (Laan et al., 2008) demonstrated a cooperative behavior of individual microtubules within a bundle. In accordance with their ideas, under a small applied force the bundle will oscillate around a constant length. Switches to bundle polymerization would be coupled to the arrival of new polymerizing microtubule to the bundle's end. Importantly, their model system lacked any microtubule-associated proteins, but still resembled features of in vivo microtubule bundles. My observations of shmoo tip bundle behavior and rescue-by-arrival and microtubule exchange model is in agreement with their model (**Figure 4.2**). However, I have assumed that the number of microtubules in the bundle stays constant over time. A growing microtubule replaces one of the old ones and switches the bundle to polymerization. The shmoo tip bundle is 1-2 μm in length and contains only 2-3 full-sized microtubules. From in vitro simulations of Laan et al., I would expect that this would correspond to less than 1-2 pN of constant applied force. Would such a force be sufficient to move a nucleus? Probably yes, as cytoplasmic viscosity is estimated in the 0.9 pN s/μm ^{2} range (900 times higher than water). But how can Bim1-Cik1-Kar3 affect the bundle length and the frequency of switches? Liedewij Laan's work allows me to suggest an explanation, alternative to my own. If Bim1-Cik1-Kar3 suppresses microtubule nucleation when localized to the SPB, then without it the number of microtubules in the bundle might increase. Force production by microtubule bundles scales linearly with the number of microtubules within the bundle. So, one additional microtubule in the shmoo tip bundle will increase force production by 33-50%, and also increase average length and increase time periods between catastrophes. The observed changes in the bundle dynamics after Kar3 depletion fall within that range.

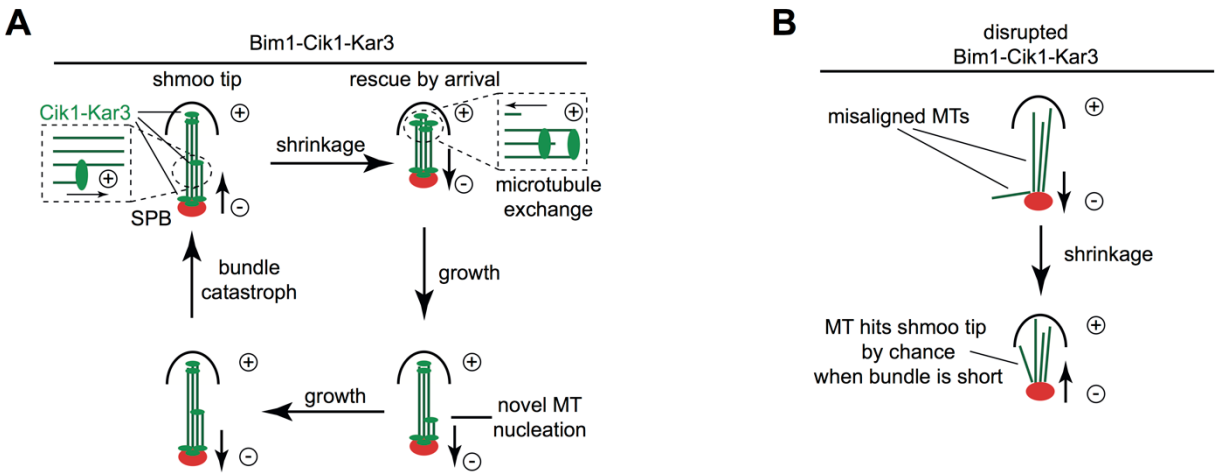

Figure 4.2 Rescue-by-arrival and microtubule exchange mechanism to maintain microtubule bundle length dynamically.

A) Wild-type situation. A growing microtubule is aligned along the bundle and causes switch to polymerization upon arrival at shmoo tip. Incoming microtubule replaces one of the old microtubules which detaches and depolymerizes. Microtubule alignment and nucleation modulate the frequency of switches.
B) In the absence of Bim1-Cik1-Kar3 microtubule bundle dynamics is suppressed. After microtubule misalignment less microtubules can reach the bundle plus-end leading to fewer rescue events. By chance misaligned microtubules only reach the shmoo tip when the bundle is short.

4.2 Potential future directions of my research.

The identification of Bim1/EB1 binding motifs and the search for determinants of localization at microtubules is in the focus of interest in many fields, from medicine-associated studies of cancer treatment to fundamental science. So far three types of Bim1/EB1-binding motifs were described - SxIP, LxxPTPh and the bi-partite KLTF-ELN. However, available data suggests that many more plus-end targeting sequences remain uncharacterized. In budding yeast more than 50 different proteins were found associated with Bim1 by IP-MS. Among them there are proteins involved in cellular growth signaling and morphogenesis (Tor, Bck1, Gin4 and Kin4), vesicular transport (Eis1, Sbe22) and chromosome segregation. In most cases Bim1-binding modes are still unclear and the absence of specific mutants disrupting interactions limits the understanding of physiological functions.

The discovery of the Bim1-Cik1-Kar3 binding interface enables me to use the Bim1-binding deficient mutants of Cik1-Kar3 as a tool to examine potential plus-end targeting sequences. Restoring plus-end localization of a Kinesin-14 will rescue its associated phenotypes. Assayed DNA sequences could be fused with Bim1-binding deficient Cik1 mutants. For example, assay could score an ability of extragenic Cik1 versions to rescue colony growth after Cik1-AID depletion in checkpoint-deficient strain. The screening could be based on a library constructed from sequences of previously identified IP-MS hits or be genome-wide. In addition, a common pattern in three known Bim1-binding motifs allows to make a synthetic hydrophobic core motif surrounded by variable amino acids. An alternative approach is to construct homodimeric and heterodimeric plus-end targeting motif libraries by expression as GST-VN fusions or as artificial coiled-coils (synzips). Positive clones for VC-Bim1 binding could be selected with FACS. Genome-wide mapping of Bim1-binding motifs might be accompanied by microscopy study of localization of potential hits.

References

Ambrose, J.C., W. Li, A. Marcus, H. Ma, and R. Cyr. 2005. A Minus-End–directed Kinesin with Plus-End Tracking Protein Activity Is Involved in Spindle Morphogenesis. *Mol. Biol. Cell*. 16:1584–1592. doi:10.1091/mbc.e04-10-0935.

Amos, L.A., and K. Hirose. 2007. A cool look at the structural changes in kinesin motor domains. *J. Cell Sci.* 120:3919–3927. doi:10.1242/jcs.016931.

Ando, A., Y. Kikuti, H. Kawata, N. Okamoto, T. Imai, T. Eki, K. Yokoyama, E. Soeda, T. Ikemura, K. Abe, and H. Inoko. 1994. Cloning of a new kinesin-related gene located at the centromeric end of the human MHC region. *Immunogenetics*. 39. doi:10.1007/BF00241260.

Benanti, J.A., M.E. Matyskiela, D.O. Morgan, and D.P. Toczyski. 2009. Functionally Distinct Isoforms of Cik1 Are Differentially Regulated by APC/C-Mediated Proteolysis. *Mol. Cell*. 33:581–590. doi:10.1016/j.molcel.2009.01.032.

Braun, M., Z. Lansky, S. Bajer, G. Fink, A.A. Kasprzak, and S. Diez. 2013. The human kinesin-14 HSET tracks the tips of growing microtubules in vitro: HSET Microtubule Tip-tracking. *Cytoskeleton*. 70:515–521. doi:10.1002/cm.21133.

Braun, M., Z. Lansky, A. Szuba, F.W. Schwarz, A. Mitra, M. Gao, A. Lüdecke, P.R. Ten Wolde, and S. Diez. 2017. Changes in microtubule overlap length regulate kinesin-14-driven microtubule sliding. *Nat. Chem. Biol.* 13:1245–1252. doi:10.1038/nchembio.2495.

Cai, S., L.N. Weaver, S.C. Ems-McClung, and C.E. Walczak. 2009. Kinesin-14 Family Proteins HSET/XCTK2 Control Spindle Length by Cross-Linking and Sliding Microtubules. *Mol. Biol. Cell*. 20:1348–1359. doi:10.1091/mbc.e08-09-0971.

Cao, L., S. Cantos-Fernandes, and B. Gigant. 2017. The structural switch of nucleotide-free kinesin. *Sci. Rep.* 7:42558. doi:10.1038/srep42558.

Case, R.B., D.W. Pierce, N. Hom-Booher, C.L. Hart, and R.D. Vale. 1997. The Directional Preference of Kinesin Motors Is Specified by an Element outside of the Motor Catalytic Domain. *Cell*. 90:959–966. doi:10.1016/S0092-8674(00)80360-8.

Chavali, P.L., G. Chandrasekaran, A.R. Barr, P. Tátrai, C. Taylor, E.K. Papachristou, C.G. Woods, S. Chavali, and F. Gergely. 2016. A CEP215–HSET complex links centrosomes with spindle poles and drives centrosome clustering in cancer. *Nat. Commun.* 7:11005. doi:10.1038/ncomms11005.

Chen, C., A. Marcus, W. Li, Y. Hu, J.-P.V. Calzada, U. Grossniklaus, R.J. Cyr, and H. Ma. 2002. The Arabidopsis ATK1 gene is required for spindle morphogenesis in male meiosis. *Dev. Camb. Engl.* 129:2401–2409.

Crevel, I.M., A. Lockhart, and R.A. Cross. 1996. Weak and strong states of kinesin and ncd. *J. Mol. Biol.* 257:66–76. doi:10.1006/jmbi.1996.0147.

Davis, D.G. 1969. Chromosome Behavior under the Influence of Claret-Nondisjunctional in DROSOPHILA MELANOGASTER. *Genetics*. 61:577–594.

Dawe, R.K., E.G. Lowry, J.I. Gent, M.C. Stitzer, K.W. Swentowsky, D.M. Higgins, J. Ross-Ibarra, J.G. Wallace, L.B. Kanizay, M. Alabady, W. Qiu, K.-F. Tseng, N. Wang, Z. Gao, J.A. Birchler, A.E. Harkess, A.L. Hodges, and E.N. Hiatt. 2018. A Kinesin-14 Motor Activates Neocentromeres to Promote Meiotic Drive in Maize. *Cell*. 173:839-850.e18. doi:10.1016/j.cell.2018.03.009.

DeLuca, J.G., C.N. Newton, R.H. Himes, M.A. Jordan, and L. Wilson. 2001. Purification and Characterization of Native Conventional Kinesin, HSET, and CENP-E from Mitotic HeLa Cells. *J. Biol. Chem.* 276:28014–28021. doi:10.1074/jbc.M102801200.

Dietrich, K.A., C.V. Sindelar, P.D. Brewer, K.H. Downing, C.R. Cremo, and S.E. Rice. 2008. The kinesin-1 motor protein is regulated by a direct interaction of its head and tail. *Proc. Natl. Acad. Sci.* 105:8938–8943. doi:10.1073/pnas.0803575105.

Endow, S.A. 1998. Determinants of Kinesin Motor Polarity. *Science*. 281:1200–1202. doi:10.1126/science.281.5380.1200.

Endow, S.A., S. Henikoff, and L. Soler-Niedziela. 1990. Mediation of meiotic and early mitotic chromosome segregation in Drosophila by a protein related to kinesin. *Nature*. 345:81–83. doi:10.1038/345081a0.

Endres, N.F., C. Yoshioka, R.A. Milligan, and R.D. Vale. 2006. A lever-arm rotation drives motility of the minus-end-directed kinesin Ncd. *Nature*. 439:875–878. doi:10.1038/nature04320.

Fahmy, K., M. Akber, X. Cai, A. Koul, A. Hayder, and S. Baumgartner. 2014. αTubulin 67C and Ncd Are Essential for Establishing a Cortical Microtubular Network and Formation of the Bicoid mRNA Gradient in Drosophila. *PLoS ONE*. 9:e112053. doi:10.1371/journal.pone.0112053.

Fan, G., L. Sun, L. Meng, C. Hu, X. Wang, Z. Shi, C. Hu, Y. Han, Q. Yang, L. Cao, X. Zhang, Y. Zhang, X. Song, S. Xia, B. He, S. Zhang, and C. Wang. 2021. The ATM and ATR kinases regulate centrosome clustering and tumor recurrence by targeting KIFC1 phosphorylation. *Nat. Commun.* 12:20. doi:10.1038/s41467-020-20208-x.

Farina, F., P. Pierobon, C. Delevoye, J. Monnet, F. Dingli, D. Loew, M. Quanz, M. Dutreix, and G. Cappello. 2013. Kinesin KIFC1 actively transports bare double-stranded DNA. *Nucleic Acids Res.* 41:4926–4937. doi:10.1093/nar/gkt204.

Fink, G., L. Hajdo, K.J. Skowronek, C. Reuther, A.A. Kasprzak, and S. Diez. 2009. The mitotic kinesin-14 Ncd drives directional microtubule–microtubule sliding. *Nat. Cell Biol.* 11:717–723. doi:10.1038/ncb1877.

Furuta, K., A. Furuta, Y.Y. Toyoshima, M. Amino, K. Oiwa, and H. Kojima. 2013. Measuring collective transport by defined numbers of processive and nonprocessive kinesin motors. *Proc. Natl. Acad. Sci.* 110:501–506. doi:10.1073/pnas.1201390110.

Furuta, K., and Y.Y. Toyoshima. 2008. Minus-End-Directed Motor Ncd Exhibits Processive Movement that Is Enhanced by Microtubule Bundling In Vitro. *Curr. Biol.* 18:152–157. doi:10.1016/j.cub.2007.12.056.

Gachet, Y., C. Reyes, T. Courthéoux, S. Goldstone, G. Gay, C. Serrurier, and S. Tournier. 2008. Sister Kinetochore Recapture in Fission Yeast Occurs by Two Distinct Mechanisms, Both Requiring Dam1 and Klp2. *Mol. Biol. Cell*. 19:1646–1662. doi:10.1091/mbc.e07-09-0910.

Gibeaux, R., A.Z. Politi, F. Nedelec, C. Antony, and M. Knop. 2013. Spindle pole body-anchored Kar3 drives the nucleus along microtubules from another nucleus in preparation for nuclear fusion during yeast karyogamy. *Genes Dev.* 27:335–349. doi:10.1101/gad.206318.112.

Goshima, G., F. Nédélec, and R.D. Vale. 2005a. Mechanisms for focusing mitotic spindle poles by minus end–directed motor proteins. *J. Cell Biol.* 171:229–240. doi:10.1083/jcb.200505107.

Goshima, G., R. Wollman, N. Stuurman, J.M. Scholey, and R.D. Vale. 2005b. Length Control of the Metaphase Spindle. *Curr. Biol.* 15:1979–1988. doi:10.1016/j.cub.2005.09.054.

Hackney, D.D. 1988. Kinesin ATPase: rate-limiting ADP release. *Proc. Natl. Acad. Sci. U. S. A.* 85:6314–6318. doi:10.1073/pnas.85.17.6314.

Hepperla, A.J., P.T. Willey, C.E. Coombes, B.M. Schuster, M. Gerami-Nejad, M. McClellan, S. Mukherjee, J. Fox, M. Winey, D.J. Odde, E. O'Toole, and M.K. Gardner. 2014. Minus-End-Directed Kinesin-14 Motors Align Antiparallel Microtubules to Control Metaphase Spindle Length. *Dev. Cell*. 31:61–72. doi:10.1016/j.devcel.2014.07.023.

Honnappa, S., S.M. Gouveia, A. Weisbrich, F.F. Damberger, N.S. Bhavesh, H. Jawhari, I. Grigoriev, F.J.A. van Rijssel, R.M. Buey, A. Lawera, I. Jelesarov, F.K. Winkler, K. Wüthrich, A. Akhmanova, and M.O. Steinmetz. 2009. An EB1-Binding Motif Acts as a Microtubule Tip Localization Signal. *Cell*. 138:366–376. doi:10.1016/j.cell.2009.04.065.

Huang, B., and T.C. Huffaker. 2006. Dynamic microtubules are essential for efficient chromosome capture and biorientation in S. cerevisiae. *J. Cell Biol.* 175:17–23. doi:10.1083/jcb.200606021.

Janson, M.E., R. Loughlin, I. Loïodice, C. Fu, D. Brunner, F.J. Nédélec, and P.T. Tran. 2007. Crosslinkers and Motors Organize Dynamic Microtubules to Form Stable Bipolar Arrays in Fission Yeast. *Cell*. 128:357–368. doi:10.1016/j.cell.2006.12.030.

Jin, F., H. Liu, P. Li, H.-G. Yu, and Y. Wang. 2012. Loss of Function of the Cik1/Kar3 Motor Complex Results in Chromosomes with Syntelic Attachment That Are Sensed by the Tension Checkpoint. *PLoS Genet.* 8:e1002492. doi:10.1371/journal.pgen.1002492.

Jon Kull, F., E.P. Sablin, R. Lau, R.J. Fletterick, and R.D. Vale. 1996. Crystal structure of the kinesin motor domain reveals a structural similarity to myosin. *Nature*. 380:550–555. doi:10.1038/380550a0.

Kitamura, E., K. Tanaka, S. Komoto, Y. Kitamura, C. Antony, and T.U. Tanaka. 2010. Kinetochores Generate Microtubules with Distal Plus Ends: Their Roles and Limited Lifetime in Mitosis. *Dev. Cell*. 18:248–259. doi:10.1016/j.devcel.2009.12.018.

Kleylein-Sohn, J., B. Pöllinger, M. Ohmer, F. Hofmann, E.A. Nigg, B.A. Hemmings, and M. Wartmann. 2012. Acentrosomal spindle organization renders cancer cells dependent on the kinesin HSET. *J. Cell Sci.* 125:5391–5402. doi:10.1242/jcs.107474.

Kornakov, N., B. Möllers, and S. Westermann. 2020. The EB1–Kinesin-14 complex is required for efficient metaphase spindle assembly and kinetochore bi-orientation. *J. Cell Biol.* 219:e202003072. doi:10.1083/jcb.202003072.

Kull, F.J., R.D. Vale, and R.J. Fletterick. 1998. The case for a common ancestor: kinesin and myosin motor proteins and G proteins. *J. Muscle Res. Cell Motil.* 19:877–886. doi:10.1023/a:1005489907021.

Kumar, A., C. Manatschal, A. Rai, I. Grigoriev, M.S. Degen, R. Jaussi, I. Kretzschmar, A.E. Prota, R. Volkmer, R.A. Kammerer, A. Akhmanova, and M.O. Steinmetz. 2017. Short Linear Sequence Motif LxxPTPh Targets Diverse Proteins to Growing Microtubule Ends. *Structure*. 25:924-932.e4. doi:10.1016/j.str.2017.04.010.

Kuriyama, R., M. Kofron, R. Essner, T. Kato, S. Dragas-Granoic, C.K. Omoto, and A. Khodjakov. 1995. Characterization of a minus end-directed kinesin-like motor protein from cultured mammalian cells. *J. Cell Biol.* 129:1049–1059. doi:10.1083/jcb.129.4.1049.

Kushnirov, V.V. 2000. Rapid and reliable protein extraction from yeast. *Yeast Chichester Engl.* 16:857–860. doi:10.1002/1097-0061(20000630)16:9<857::AID-YEA561>3.0.CO;2-B.

Kwon, M., S.A. Godinho, N.S. Chandhok, N.J. Ganem, A. Azioune, M. Thery, and D. Pellman. 2008. Mechanisms to suppress multipolar divisions in cancer cells with extra centrosomes. *Genes Dev.* 22:2189–2203. doi:10.1101/gad.1700908.

Laan, L., J. Husson, E.L. Munteanu, J.W.J. Kerssemakers, and M. Dogterom. 2008. Force-generation and dynamic instability of microtubule bundles. *Proc. Natl. Acad. Sci.* 105:8920–8925. doi:10.1073/pnas.0710311105.

Lawrence, C.J., R.K. Dawe, K.R. Christie, D.W. Cleveland, S.C. Dawson, S.A. Endow, L.S.B. Goldstein, H.V. Goodson, N. Hirokawa, J. Howard, R.L. Malmberg, J.R. McIntosh, H. Miki, T.J. Mitchison, Y. Okada, A.S.N. Reddy, W.M. Saxton, M. Schliwa, J.M. Scholey, R.D. Vale, C.E. Walczak, and L. Wordeman. 2004. A standardized kinesin nomenclature. *J. Cell Biol.* 167:19–22. doi:10.1083/jcb.200408113.

Leary, A., S. Sim, E. Nazarova, K. Shulist, R. Genthial, S.K. Yang, K.H. Bui, P. Francois, and J. Vogel. 2019. Successive Kinesin-5 Microtubule Crosslinking and Sliding Promote Fast, Irreversible Formation of a Stereotyped Bipolar Spindle. *Curr. Biol.* 29:3825-3837.e3. doi:10.1016/j.cub.2019.09.030.

Maddox, P.S., J.K. Stemple, L. Satterwhite, E.D. Salmon, and K. Bloom. 2003. The Minus End-Directed Motor Kar3 Is Required for Coupling Dynamic Microtubule Plus Ends to the Cortical Shmoo Tip in Budding Yeast. *Curr. Biol.* 13:1423–1428. doi:10.1016/S0960-9822(03)00547-5.

Mana-Capelli, S., J.R. McLean, C.-T. Chen, K.L. Gould, and D. McCollum. 2012. The kinesin-14 Klp2 is negatively regulated by the SIN for proper spindle elongation and telophase nuclear positioning. *Mol. Biol. Cell*. 23:4592–4600. doi:10.1091/mbc.e12-07-0532.

Manning, B.D., J.G. Barrett, J.A. Wallace, H. Granok, and M. Snyder. 1999. Differential Regulation of the Kar3p Kinesin-related Protein by Two Associated Proteins, Cik1p and Vik1p. *J. Cell Biol.* 144:1219–1233. doi:10.1083/jcb.144.6.1219.

Marcus, A.I., J.C. Ambrose, L. Blickley, W.O. Hancock, and R.J. Cyr. 2002. Arabidopsis thaliana protein, ATK1, is a minus-end directed kinesin that exhibits non-processive movement. *Cell Motil. Cytoskeleton*. 52:144–150. doi:10.1002/cm.10045.

Matthies, H.J., H.B. McDonald, L.S. Goldstein, and W.E. Theurkauf. 1996. Anastral meiotic spindle morphogenesis: role of the non-claret disjunctional kinesin-like protein. *J. Cell Biol.* 134:455–464. doi:10.1083/jcb.134.2.455.

McDonald, H.B., and L.S.B. Goldstein. 1990. Identification and characterization of a gene encoding a kinesin-like protein in Drosophila. *Cell*. 61:991–1000. doi:10.1016/0092-8674(90)90064-L.

McDonald, H.B., R.J. Stewart, and L.S.B. Goldstein. 1990. The kinesin-like ncd protein of Drosophila is a minus end-directed microtubule motor. *Cell*. 63:1159–1165. doi:10.1016/0092-8674(90)90412-8.

Meluh, P. 1990. KAR3, a kinesin-related gene required for yeast nuclear fusion. *Cell*. 60:1029–1041. doi:10.1016/0092-8674(90)90351-E.

Middleton, K., and J. Carbon. 1994. KAR3-encoded kinesin is a minus-end-directed motor that functions with centromere binding proteins (CBF3) on an in vitro yeast kinetochore. *Proc. Natl. Acad. Sci.* 91:7212–7216. doi:10.1073/pnas.91.15.7212.

Mieck, C., M.I. Molodtsov, K. Drzewicka, B. van der Vaart, G. Litos, G. Schmauss, A. Vaziri, and S. Westermann. 2015. Non-catalytic motor domains enable processive movement and functional diversification of the kinesin-14 Kar3. *eLife*. 4:e04489. doi:10.7554/eLife.04489.

Milic, B., J.O.L. Andreasson, W.O. Hancock, and S.M. Block. 2014. Kinesin processivity is gated by phosphate release. *Proc. Natl. Acad. Sci. U. S. A.* 111:14136–14140. doi:10.1073/pnas.1410943111.

Molodtsov, M.I., C. Mieck, J. Dobbelaere, A. Dammermann, S. Westermann, and A. Vaziri. 2016. A Force-Induced Directional Switch of a Molecular Motor Enables Parallel Microtubule Bundle Formation. *Cell*. 167:539-552.e14. doi:10.1016/j.cell.2016.09.029.

Morales-Mulia, S., and J.M. Scholey. 2005. Spindle Pole Organization in *Drosophila* S2 Cells by Dynein, *Abnormal Spindle* Protein (Asp), and KLP10A. *Mol. Biol. Cell*. 16:3176–3186. doi:10.1091/mbc.e04-12-1110.

Nishimura, K., T. Fukagawa, H. Takisawa, T. Kakimoto, and M. Kanemaki. 2009. An auxin-based degron system for the rapid depletion of proteins in nonplant cells. *Nat. Methods*. 6:917–922. doi:10.1038/nmeth.1401.

Nitta, R., Y. Okada, and N. Hirokawa. 2008. Structural model for strain-dependent microtubule activation of Mg-ADP release from kinesin. *Nat. Struct. Mol. Biol.* 15:1067–1075. doi:10.1038/nsmb.1487.

Norris, S.R., S. Jung, P. Singh, C.E. Strothman, A.L. Erwin, M.D. Ohi, M. Zanic, and R. Ohi. 2018. Microtubule minus-end aster organization is driven by processive HSET-tubulin clusters. *Nat. Commun.* 9:2659. doi:10.1038/s41467-018-04991-2.

O'Connell, M.J., P.B. Meluh, M.D. Rose, and N.R. Morris. 1993. Suppression of the bimC4 mitotic spindle defect by deletion of klpA, a gene encoding a KAR3-related kinesin-like protein in Aspergillus nidulans. *J. Cell Biol.* 120:153–162. doi:10.1083/jcb.120.1.153.

Oladipo, A., A. Cowan, and V. Rodionov. 2007. Microtubule Motor Ncd Induces Sliding of Microtubules In Vivo. *Mol. Biol. Cell*. 18:3601–3606. doi:10.1091/mbc.e06-12-1085.

Olmsted, Z.T., A.G. Colliver, T.D. Riehlman, and J.L. Paluh. 2014. Kinesin-14 and kinesin-5 antagonistically regulate microtubule nucleation by γ-TuRC in yeast and human cells. *Nat. Commun.* 5:5339. doi:10.1038/ncomms6339.

Olmsted, Z.T., T.D. Riehlman, C.N. Branca, A.G. Colliver, L.O. Cruz, and J.L. Paluh. 2013. Kinesin-14 Pkl1 targets γ-tubulin for release from the γ-tubulin ring complex (γ-TuRC) . *Cell Cycle*. 12:842–848. doi:10.4161/cc.23822.

O'Toole, E.T., D.N. Mastronarde, T.H. Giddings, M. Winey, D.J. Burke, and J.R. McIntosh. 1997. Three-dimensional analysis and ultrastructural design of mitotic spindles from the cdc20 mutant of Saccharomyces cerevisiae. *Mol. Biol. Cell*. 8:1–11. doi:10.1091/mbc.8.1.1.

Page, B., L. Satterwhite, M. Rose, and M. Snyder. 1994. Localization of the Kar3 kinesin heavy chain-related protein requires the Cik1 interacting protein. *J. Cell Biol.* 124:507–519. doi:10.1083/jcb.124.4.507.

Page, B.D., and M. Snyder. 1992. CIK1: a developmentally regulated spindle pole body-associated protein important for microtubule functions in Saccharomyces cerevisiae. *Genes Dev.* 6:1414–1429. doi:10.1101/gad.6.8.1414.

Pannu, V., P.C.G. Rida, A. Ogden, R.C. Turaga, S. Donthamsetty, N.J. Bowen, K. Rudd, M.V. Gupta, M.D. Reid, G. Cantuaria, C.E. Walczak, and R. Aneja. 2015. HSET overexpression fuels tumor progression via centrosome clustering-independent mechanisms in breast cancer patients. *Oncotarget*. 6:6076–6091. doi:10.18632/oncotarget.3475.

Pavelka, N., G. Rancati, J. Zhu, W.D. Bradford, A. Saraf, L. Florens, B.W. Sanderson, G.L. Hattem, and R. Li. 2010. Aneuploidy confers quantitative proteome changes and phenotypic variation in budding yeast. *Nature*. 468:321–325. doi:10.1038/nature09529.

Pidoux, A.L., M. LeDizet, and W.Z. Cande. 1996. Fission yeast pkl1 is a kinesin-related protein involved in mitotic spindle function. *Mol. Biol. Cell*. 7:1639–1655. doi:10.1091/mbc.7.10.1639.

Popchock, A.R., K.-F. Tseng, P. Wang, P.A. Karplus, X. Xiang, and W. Qiu. 2017. The mitotic kinesin-14 KlpA contains a context-dependent directionality switch. *Nat. Commun.* 8:13999. doi:10.1038/ncomms13999.

Prinz, S., E.S. Hwang, R. Visintin, and A. Amon. 1998. The regulation of Cdc20 proteolysis reveals a role for the APC components Cdc23 and Cdc27 during S phase and early mitosis. *Curr. Biol.* 8:750–760. doi:10.1016/S0960-9822(98)70298-2.

Reddy, A.S., and I.S. Day. 2001. Kinesins in the Arabidopsis genome: A comparative analysis among eukaryotes. *BMC Genomics*. 2:2. doi:10.1186/1471-2164-2-2.

Reddy, A.S.N., F. Safadi, S.B. Narasimhulu, M. Golovkin, and X. Hu. 1996. A Novel Plant Calmodulin-binding Protein with a Kinesin Heavy Chain Motor Domain. *J. Biol. Chem.* 271:7052–7060. doi:10.1074/jbc.271.12.7052.

Reinemann, D.N., S.R. Norris, R. Ohi, and M.J. Lang. 2018. Processive Kinesin-14 HSET Exhibits Directional Flexibility Depending on Motor Traffic. *Curr. Biol.* 28:2356-2362.e5. doi:10.1016/j.cub.2018.06.055.

Rice, S., A.W. Lin, D. Safer, C.L. Hart, N. Naber, B.O. Carragher, S.M. Cain, E. Pechatnikova, E.M. Wilson-Kubalek, M. Whittaker, E. Pate, R. Cooke, E.W. Taylor, R.A. Milligan, and R.D. Vale. 1999. A structural change in the kinesin motor protein that drives motility. *Nature*. 402:778–784. doi:10.1038/45483.

Romberg, L., D.W. Pierce, and R.D. Vale. 1998. Role of the Kinesin Neck Region in Processive Microtubule-based Motility. *J. Cell Biol.* 140:1407–1416. doi:10.1083/jcb.140.6.1407.

Saito, N., Y. Okada, Y. Noda, Y. Kinoshita, S. Kondo, and N. Hirokawa. 1997. KIFC2 Is a Novel Neuron-Specific C-Terminal Type Kinesin Superfamily Motor for Dendritic Transport of Multivesicular Body-Like Organelles. *Neuron*. 18:425–438. doi:10.1016/S0896-6273(00)81243-X.

Saunders, W., D. Hornack, V. Lengyel, and C. Deng. 1997. The Saccharomyces cerevisiae Kinesin-related Motor Kar3p Acts at Preanaphase Spindle Poles to Limit the Number and Length of Cytoplasmic Microtubules. *J. Cell Biol.* 137:417–431. doi:10.1083/jcb.137.2.417.

Saunders, W.S., and M.A. Hoyt. 1992. Kinesin-related proteins required for structural integrity of the mitotic spindle. *Cell*. 70:451–458. doi:10.1016/0092-8674(92)90169-D.

Schroeder, C.M., and H.S. Malik. 2018. Kindr Motors Drive in Meiosis. *Cell*. 173:813–815. doi:10.1016/j.cell.2018.04.021.

Sequeira, W., C.R. Nelson, and P. Szauter. 1989. Genetic analysis of the claret locus of Drosophila melanogaster. *Genetics*. 123:511–524.

She, Z.-Y., M.-Y. Pan, F.-Q. Tan, and W.-X. Yang. 2017. Minus end-directed kinesin-14 KIFC1 regulates the positioning and architecture of the Golgi apparatus. *Oncotarget*. 8:36469–36483. doi:10.18632/oncotarget.16863.

She, Z.-Y., and W.-X. Yang. 2017. Molecular mechanisms of kinesin-14 motors in spindle assembly and chromosome segregation. *J. Cell Sci.* 130:2097–2110. doi:10.1242/jcs.200261.

Song, H., M. Golovkin, A.S.N. Reddy, and S.A. Endow. 1997. In vitro motility of AtKCBP, a calmodulin-binding kinesin protein of Arabidopsis. *Proc. Natl. Acad. Sci.* 94:322–327. doi:10.1073/pnas.94.1.322.

Sproul, L.R., D.J. Anderson, A.T. Mackey, W.S. Saunders, and S.P. Gilbert. 2005. Cik1 Targets the Minus-End Kinesin Depolymerase Kar3 to Microtubule Plus Ends. *Curr. Biol.* 15:1420–1427. doi:10.1016/j.cub.2005.06.066.

Stephens, A.D., C.E. Snider, J. Haase, R.A. Haggerty, P.A. Vasquez, M.G. Forest, and K. Bloom. 2013. Individual pericentromeres display coordinated motion and stretching in the yeast spindle. *J. Cell Biol.* 203:407–416. doi:10.1083/jcb.201307104.

Sturtevant, A.H. 1929. The claret mutant type of Drosophila simulans: a study of chromosome elimination and cell lineage. *Z. Wiss. Zool.* 135:325–326.

Swentowsky, K.W., J.I. Gent, E.G. Lowry, V. Schubert, X. Ran, K.-F. Tseng, A.E. Harkess, W. Qiu, and R.K. Dawe. 2020. Distinct kinesin motors drive two types of maize neocentromeres. *Genes Dev.* 34:1239–1251. doi:10.1101/gad.340679.120.

Syrovatkina, V., and P.T. Tran. 2015. Loss of kinesin-14 results in aneuploidy via kinesin-5-dependent microtubule protrusions leading to chromosome cut. *Nat. Commun.* 6:7322. doi:10.1038/ncomms8322.

Tan, S. 2001. A Modular Polycistronic Expression System for Overexpressing Protein Complexes in Escherichia coli. *Protein Expr. Purif.* 21:224–234. doi:10.1006/prep.2000.1363.

Tanaka, K., E. Kitamura, Y. Kitamura, and T.U. Tanaka. 2007. Molecular mechanisms of microtubule-dependent kinetochore transport toward spindle poles. *J. Cell Biol.* 178:269–281. doi:10.1083/jcb.200702141.

Tanaka, K., N. Mukae, H. Dewar, M. van Breugel, E.K. James, A.R. Prescott, C. Antony, and T.U. Tanaka. 2005. Molecular mechanisms of kinetochore capture by spindle microtubules. *Nature*. 434:987–994. doi:10.1038/nature03483.

Tanenbaum, M.E., L. Macůrek, N. Galjart, and R.H. Medema. 2008. Dynein, Lis1 and CLIP-170 counteract Eg5-dependent centrosome separation during bipolar spindle assembly. *EMBO J.* 27:3235–3245. doi:10.1038/emboj.2008.242.

Troxell, C.L., M.A. Sweezy, R.R. West, K.D. Reed, B.D. Carson, A.L. Pidoux, W.Z. Cande, and J.R. McIntosh. 2001. *pkl1* $^{+}$ and *klp2* $^{+}$: Two Kinesins of the Kar3 Subfamily in Fission Yeast Perform Different Functions in Both Mitosis and Meiosis. *Mol. Biol. Cell*. 12:3476–3488. doi:10.1091/mbc.12.11.3476.

Vale, R., T. Reese, and M. Sheetz. 1985. Identification of a novel force-generating protein, kinesin, involved in microtubule-based motility. *Cell*. 42:39–50. doi:10.1016/S0092-8674(85)80099-4.

Vallen, E., M. Hiller, T. Scherson, and M. Rose. 1992. Separate domains of KAR1 mediate distinct functions in mitosis and nuclear fusion. *J. Cell Biol.* 117:1277–1287. doi:10.1083/jcb.117.6.1277.

Walczak, C.E., S. Verma, and T.J. Mitchison. 1997. XCTK2: A Kinesin-related Protein That Promotes Mitotic Spindle Assembly in Xenopus laevis Egg Extracts. *J. Cell Biol.* 136:859–870. doi:10.1083/jcb.136.4.859.

Walker, J.E., M. Saraste, M.J. Runswick, and N.J. Gay. 1982. Distantly related sequences in the alpha- and beta-subunits of ATP synthase, myosin, kinases and other ATP-requiring enzymes and a common nucleotide binding fold. *EMBO J.* 1:945–951.

Walker, R.A., E.D. Salmon, and S.A. Endow. 1990. The Drosophila claret segregation protein is a minus-end directed motor molecule. *Nature*. 347:780–782. doi:10.1038/347780a0.

Wang, P., K.-F. Tseng, Y. Gao, M. Cianfrocco, L. Guo, and W. Qiu. 2018. The Central Stalk Determines the Motility of Mitotic Kinesin-14 Homodimers. *Curr. Biol.* 28:2302-2308.e3. doi:10.1016/j.cub.2018.05.026.

Weaver, L.N., S.C. Ems-McClung, S.-H.R. Chen, G. Yang, S.L. Shaw, and C.E. Walczak. 2015. The Ran-GTP Gradient Spatially Regulates XCTK2 in the Spindle. *Curr. Biol.* 25:1509–1514. doi:10.1016/j.cub.2015.04.015.

Weissmann, F., G. Petzold, R. VanderLinden, P.J. Huis in 't Veld, N.G. Brown, F. Lampert, S. Westermann, H. Stark, B.A. Schulman, and J.-M. Peters. 2016. biGBac enables rapid gene assembly for the expression of large multisubunit protein complexes. *Proc. Natl. Acad. Sci.* 113:E2564–E2569. doi:10.1073/pnas.1604935113.

Wickstead, B., K. Gull, and T.A. Richards. 2010. Patterns of kinesin evolution reveal a complex ancestral eukaryote with a multifunctional cytoskeleton. *BMC Evol. Biol.* 10:110. doi:10.1186/1471-2148-10-110.

Winey, M., C.L. Mamay, E.T. O'Toole, D.N. Mastronarde, T.H. Giddings, K.L. McDonald, and J.R. McIntosh. 1995. Three-dimensional ultrastructural analysis of the Saccharomyces cerevisiae mitotic spindle. *J. Cell Biol.* 129:1601–1615. doi:10.1083/jcb.129.6.1601.

Witkin, K.L., Y. Chong, S. Shao, M.T. Webster, S. Lahiri, A.D. Walters, B. Lee, J.L.Y. Koh, W.A. Prinz, B.J. Andrews, and O. Cohen-Fix. 2012. The Budding Yeast Nuclear Envelope Adjacent to the Nucleolus Serves as a Membrane Sink during Mitotic Delay. *Curr. Biol.* 22:1128–1133. doi:10.1016/j.cub.2012.04.022.

Yamamoto, A.H., D.J. Komma, C.D. Shaffer, V. Pirrotta, and S.A. Endow. 1989. The claret locus in Drosophila encodes products required for eyecolor and for meiotic chromosome segregation. *EMBO J.* 8:3543–3552.

Yang, J.T., R.A. Laymon, and L.S.B. Goldstein. 1989. A three-domain structure of kinesin heavy chain revealed by DNA sequence and microtubule binding analyses. *Cell*. 56:879–889. doi:10.1016/0092-8674(89)90692-2.

Yang, Z., D.W. Hanlon, J.R. Marszalek, and L.S.B. Goldstein. 1997. Identification, Partial Characterization, and Genetic Mapping of Kinesin-like Protein Genes in Mouse. *Genomics*. 45:123–131. doi:10.1006/geno.1997.4901.

Yukawa, M., C. Ikebe, and T. Toda. 2015. The Msd1–Wdr8–Pkl1 complex anchors microtubule minus ends to fission yeast spindle pole bodies. *J. Cell Biol.* 209:549–562. doi:10.1083/jcb.201412111.

Yukawa, M., Y. Yamada, and T. Toda. 2019. Suppressor Analysis Uncovers That MAPs and Microtubule Dynamics Balance with the Cut7/Kinesin-5 Motor for Mitotic Spindle Assembly in *Schizosaccharomyces pombe*. *G3amp58 GenesGenomesGenetics*. 9:269–280. doi:10.1534/g3.118.200896.

Zhang, P., W. Dai, J. Hahn, and S.P. Gilbert. 2015. *Drosophila* Ncd reveals an evolutionarily conserved powerstroke mechanism for homodimeric and heterodimeric kinesin-14s. *Proc. Natl. Acad. Sci.* 112:6359–6364. doi:10.1073/pnas.1505531112.

Publications

Kornakov, N., B. Möllers, and S. Westermann. 2020. The EB1–Kinesin-14 complex is required for efficient metaphase spindle assembly and kinetochore bi-orientation. *Journal of Cell Biology*. 219:e202003072. doi:10.1083/jcb.202003072.

All experiments were planned, executed and analyzed by Nikolay Kornakov.

Experiments corresponding to **Figure 3.23, Figure 3.24** and **Figure 3.25** were performed together with Bastian Möllers.

Acknowledgements

I would like to thank my supervisor, professor Stefan Westermann for my PhD project, scientific discussions that improved the quality and understandability of my work, his support and patience over these years. I want to thank prof. Dominik Boos and prof. Hemmo Meyer and their labs members for sharing reagents and equipment, advice and general help.

I thank all current and former members of Molecular Genetics I department for the friendly and productive atmosphere (and Kerstin Killinger for tasty birthday cakes). I want to express my gratitude to Miriam Böhm for help with translations from german and support in fighting bureaucracy. My special regards to Alexander Dudziak and Bastian Möllers for scientific collaboration and positive attitude to the difficult and sometimes disappointing research process. I thank Florian Schmitzberger for helping during the initial stages of my project in design of the protein conditional depletion and sharing his experience. My thanks to Ivana Primorac, as we worked together on establishing insect cell culture in the lab. I am grateful to Pedro Fereira for participation in discussions and interesting questions during my progress reports.

Last but not least, I would like to express my gratitude to my dear friends Vadim Kotov and Elena Kotova, my parents and my brother for their endless support and optimism. That was not an easy time for me and I am glad that it has finally reached its logical end.

CURRICULUM VITAE

The curriculum vitae is not included in the online version for data protection reasons

Declarations required for the submission of the thesis

Declaration:

In accordance with § 6 (para. 2, clause g) of the Regulations Governing the Doctoral Proceedings of the Faculty of Biology for awarding the doctoral degree Dr. rer. nat., I hereby declare that I represent the field to which the topic "**Functional analysis of the EB1-Kinesin-14 complex in chromosome segregation***"* is assigned in research and teaching and that I support the application of **Nikolay Kornakov**.

Essen, date: _____ _____ _____

Name of the scientific supervisor | Signature of the supervisor

Declaration:

In accordance with § 7 (para. 2, clause d and f) of the Regulations Governing the Doctoral Proceedings of the Faculty of Biology for awarding the doctoral degree Dr. rer. nat., I hereby declare that I have written the herewith submitted dissertation independently using only the materials listed, and have cited all sources taken over verbatim or in content as such.

Essen, date: _____ _____

Signature of the doctoral candidate

Declaration:

In accordance with § 7 (para. 2, clause e and g) of the Regulations Governing the Doctoral Proceedings of the Faculty of Biology for awarding the doctoral degree Dr. rer. nat., I hereby declare that I have undertaken no previous attempts to attain a doctoral degree, that the current work has not been rejected by any other faculty, and that I am submitting the dissertation only in this procedure.

Essen, date: _____ _____

Signature of the doctoral candidate

JCB Journal of Cell Biology

ARTICLE

The EB1–Kinesin-14 complex is required for efficient metaphase spindle assembly and kinetochore bi-orientation

Nikolay Kornakov, Bastian Möllers, and Stefan Westermann

Kinesin-14s are conserved molecular motors required for high-fidelity chromosome segregation, but their specific contributions to spindle function have not been fully defined. Here, we show that key functions of budding yeast Kinesin-14 Cik1-Kar3 are accomplished in a complex with Bim1 (yeast EB1). Genetic complementation of mitotic phenotypes identifies a novel KLTF peptide motif in the Cik1 N-terminus. We show that this motif is one element of a tripartite binding interface required to form a high-affinity Bim1–Cik1-Kar3 complex. Lack of Bim1-binding by Cik1-Kar3 delays cells in mitosis and impairs microtubule bundle organization and dynamics. Conversely, constitutive targeting of Cik1-Kar3 to microtubule plus ends induces the formation of nuclear microtubule bundles. Cells lacking the Bim1–Cik1-Kar3 complex rely on the conserved microtubule bundler Ase1/PRC1 for metaphase spindle organization, and simultaneous loss of plus-end targeted Kar3 and Ase1 is lethal. Our results reveal the contributions of an EB1–Kinesin-14 complex for spindle formation as a prerequisite for efficient kinetochore clustering and bi-orientation.

Introduction

Microtubules are dynamic polymers responsible for chromosome segregation, cell polarity, and intracellular transport in eukaryotes. They are inherently polar structures with a minus end that is usually anchored at a microtubule organizing center (in yeast, the spindle pole body [SPB]) and a dynamic plus end. A number of microtubule-associated proteins regulate microtubule nucleation and dynamic instability properties and promote assembly and organization of individual microtubules into supramolecular structures (Wieczorek et al., 2015; Akhmanova and Steinmetz, 2015).

Kinesin-14s are evolutionarily conserved minus end–directed microtubule motors required for error-free mitosis and meiosis (McDonald and Goldstein, 1990; Walczak et al., 1997; Meluh and Rose, 1990; Cai et al., 2010; Wickstead et al., 2010). Based on in vitro characterization and cellular analysis, different activities of Kinesin-14 motors have been described: they produce minus end–directed motility using an ATP-dependent rotation of the stalk (Endres et al., 2006). With this activity, they can slide microtubules relative to each other in vitro and thus can provide a balancing force against oppositely directed Kinesin-5 motors (Saunders et al., 1997). An extension of this activity is the ATP-dependent sorting of microtubules into parallel bundles (Braun et al., 2009) or the zippering of antiparallel microtubules during spindle assembly (Hepperla et al., 2014). In addition, yeast Kar3 has been proposed to act as a microtubule depolymerase (Sproul et al., 2005). The motor has been found to copurify with reconstituted centromeric DNA on beads (Middleton and Carbon, 1994), and it has been implicated in lateral kinetochore transport, an intermediate step in sister-chromatid bi-orientation (Tanaka et al., 2007). However, it is unclear which of these proposed activities is critical for mitosis and how it would facilitate chromosome segregation.

Budding yeasts have a single catalytically active Kinesin-14 Kar3 that forms heterodimers with the kinesin-associated protein Cik1 (Fig. 1 A) or Vik1 (Page and Snyder, 1992; Manning et al., 1999; Allingham et al., 2007; Chu et al., 2005). Cik1-Kar3 is required for efficient resolution of syntelic kinetochore-microtubule attachments by an unknown mechanism (Jin et al., 2012). Loss of Cik1-Kar3 function also leads to a delay in cell cycle progression and hypersensitivity to stress agents such as hydroxyurea and elevated temperature (Manning et al., 1999; Liu et al., 2011). We recently reported a novel biochemical activity of Kinesin-14 motors common to several members, including Cik1-Kar3: these molecules have the ability to align a

Department of Molecular Genetics, Faculty of Biology, Center of Medical Biotechnology, University of Duisburg-Essen, Essen, Germany.

Correspondence to Stefan Westermann: Stefan.Westermann@uni-due.de.

growing microtubule along an existing one and thereby promote the formation of parallel microtubule bundles from a common microtubule organizing center (Molodtsov et al., 2016). This microtubule "guiding" activity involves an interaction between the motor and the growing plus ends of microtubules via the autonomous plus-end tracker EB1. During this process, the Kinesin-14 motor remains associated with growing plus ends and acts as a compliant cross-linker that promotes the organization of microtubules into bundles. To which extent this activity—and the interaction between Kinesin-14 motors and EB1 in general—is relevant in vivo and how it may contribute to mitotic spindle function in cells has not been tested, partly because separation-of-function mutants that specifically interfere with this activity but leave other aspects of motor function unchanged have not been available.

Here, taking an unbiased approach to defining new molecular elements required for Kinesin-14 function in budding yeast, we show that the mitotic function of Cik1-Kar3 critically requires an interaction with the autonomous plus-end tracker Bim1, and we define the molecular organization of the relevant binding interface. Our results show that the EB1–Kinesin-14 system contributes to key aspects of microtubule organization during metaphase spindle assembly and is therefore a prerequisite for kinetochore bi-orientation and timely progression through mitosis.

Results

Acute depletion of Cik1-Kar3 delays yeast cells in metaphase

To study Kar3 function in yeast cells, we used a conditional depletion system that circumvents the pitfalls of genetic deletions such as adaptations or secondary mutations. To this end, we integrated auxin-inducible degron (AID) tags (Nishimura et al., 2009) at the chromosomal locations of Kar3 and Cik1 and characterized the cellular phenotypes after conditionally depleting the proteins by addition of auxin. Western blotting confirmed that both Cik1 and Kar3 were efficiently depleted within 30 min after auxin addition (Fig. 1 B). Compared with α-factor–arrested cells, which express a short Cik1 isoform lacking the first 35 amino acids, the level of mitotic Cik1 was very low, as described previously (Page and Snyder, 1992; Benanti et al., 2009). In serial dilution assays, the depletion strains displayed similar phenotypes compared with the respective gene deletions (Fig. 1 C). In particular, conditional depletion of Cik1 conferred temperature sensitivity at 37°C, which was partially suppressed by codepleting Kar3. This is consistent with the notion that the phenotypes of Cik1 depletion can partially be attributed to the inappropriate formation of Vik1–Kar3 complexes (Manning et al., 1999). Slow growth may be a consequence of different defects. As Kinesin-14s are involved in chromosome segregation, we suspected that errors in mitosis would be prevented by prolonged activation of the spindle assembly checkpoint, which delays anaphase onset until all chromosomes have bi-oriented. Indeed, conditional depletion of both Cik1 and Kar3 was lethal at 30°C in the absence of the mitotic checkpoint (Fig. 1 D), indicating that these proteins perform important functions before anaphase onset.

To characterize cellular phenotypes after Cik1 depletion, we synchronized cells in a G1-like state by pheromone treatment and released them into a medium containing auxin. We then filmed Cik1-depleted and control cells simultaneously using live-cell fluorescence microscopy to determine the duration of metaphase in individual cells, defined as the time between SPB separation and anaphase onset (Fig. 1 E). We found that the mean metaphase duration of Cik1-depleted cells (46 ± 2 min) was significantly increased compared with control cells (29 ± 1 min).

Closer inspection of spindle length (pole-to-pole distance) and dynamics (change of pole-to-pole distance over time) revealed that Cik1-depleted cells initiated anaphase from a significantly shorter metaphase spindle than control cells (Fig. 1 F). During anaphase, the fast increase in pole-to-pole distance (Phase I) occurred with similar velocity, although Cik1-depleted cells displayed an overall greater variance in anaphase elongation dynamics. We conclude that Cik1 depletion delays anaphase onset and is characterized by a short metaphase spindle, while anaphase phenotypes are relatively mild in comparison.

Cik1 depletion impairs microtubule alignment and kinetochore clustering during metaphase spindle assembly

To define the underlying causes for the shortened metaphase spindle in Cik1-depleted cells, we observed microtubule plus-end markers (Bik1–3xGFP/CLIP-170) and kinetochore markers (Ndc80-GFP) by live-cell microscopy in synchronized cells. Following SPB separation, nuclear Bik1 signals in control cells were typically confined between the two spindle poles. In addition, cytoplasmic Bik1 signals were targeted toward the bud during nuclear migration (Fig. 2 A and Video 1). By contrast, about two thirds of Cik1-depleted cells displayed Bik1 signals that projected away from the spindle axis, indicating severe misalignment of microtubules during spindle assembly. Prior to anaphase onset, Bik1 localization eventually became more confined to the spindle axis also in Cik1-depleted cells (Video 2).

In addition, Ndc80-GFP was followed to determine kinetochore position and bi-orientation in Cik1-AID cells (Fig. 2 B). When control cells were released from α-factor, the Ndc80-GFP signal formed a tight cluster in the vicinity of the SPB. That cluster persisted throughout metaphase and became well separated immediately before anaphase onset, as cells achieved bi-orientation. Throughout the entire process, the Ndc80-GFP signal remained on axis between the two SPBs (0/40 cells with off-axis kinetochores). By contrast, depletion of Cik1 resulted in less tightly clustered Ndc80 immediately after α-factor release. As these cells progressed into mitosis, they separated their spindle poles, but the Ndc80-GFP signal was frequently mispositioned off axis relative to the SPBs (27/40 cells with off-axis kinetochores). Eventually, Cik1-depleted cells also managed to cluster and position Ndc80 on axis between the SPBs, and only after this had occurred were they able to progress into anaphase.

Cik1 depletion impairs microtubule bundle dynamics at the shmoo tip

The small size of the yeast nucleus makes it difficult to assess the dynamics of individual microtubules or organized groups of

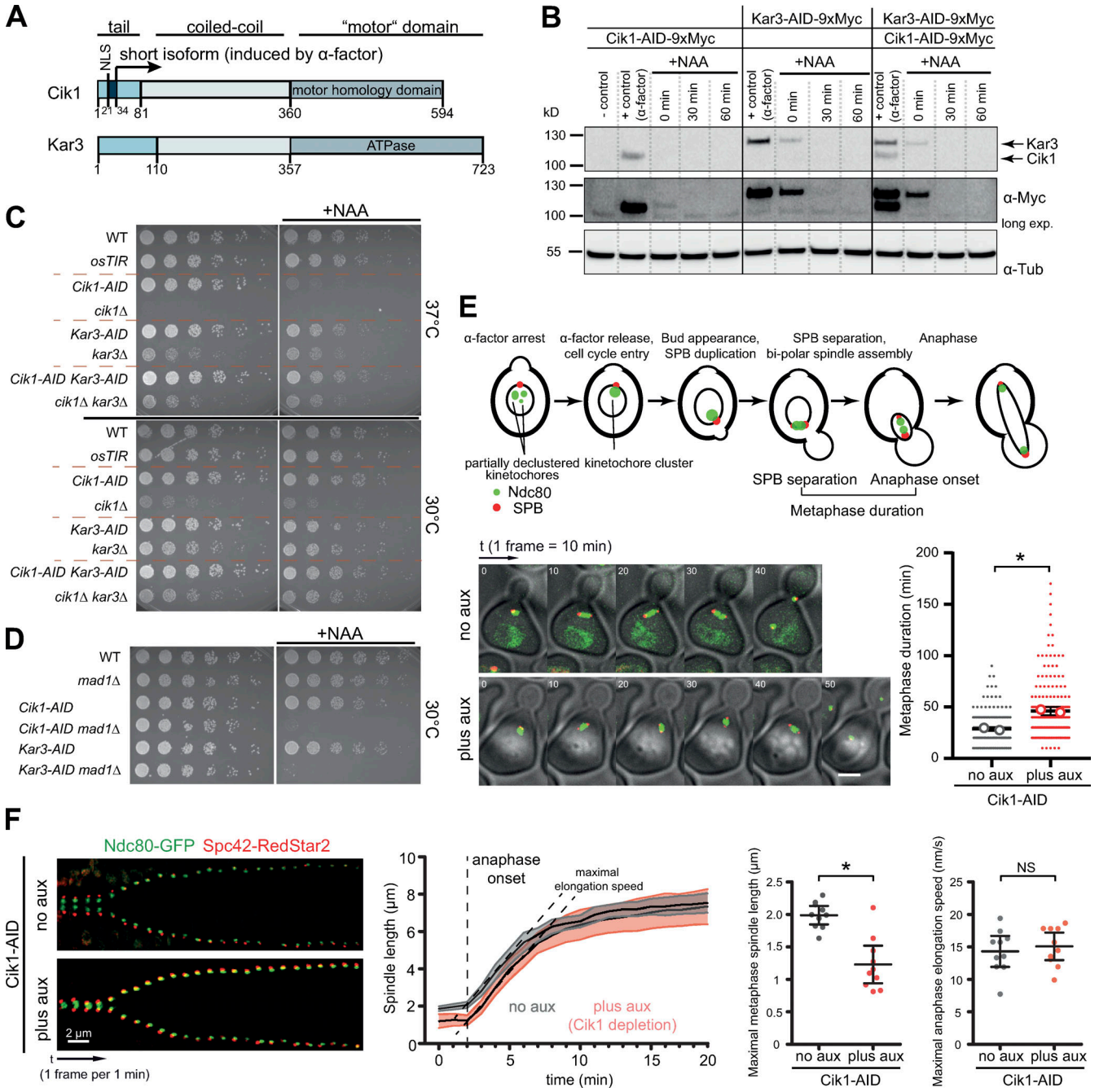

Figure 1. **Depletion of Cik1-Kar3 leads to chromosome mis-segregation and has phenotypes similar to those of knockouts. (A)** Schematic overview of Cik1-Kar3 protein structure. Functionally important regions are highlighted and assigned accordingly. **(B)** Western blot analysis of Cik1-AID and Kar3-AID upon addition of NAA. Kar3 is present in excess over Cik1 in mitotic cells. α-Factor–arrested cells have increased amounts of a shorter Cik1 isoform. Long exp., ong exposure; α-Tub, anti-Tubulin blot. **(C)** Serial dilution spot assays compare *cik1* and *kar3* genetic deletions with the respective conditional depletion alleles. Temperature sensitivity was assayed at 37°C. Plates marked +NAA contained 1 mM of NAA. Plates were incubated for 2.5 d at the stated temperature. **(D)** Analysis of Cik1 or Kar3 depletion in a checkpoint-deficient strain. Plates were incubated for 2.5 d at 30°C. **(E)** Schematic representation of mitotic timing. Metaphase duration is defined as the time between SPB separation and anaphase onset. Gallery of consecutive frames from live-cell imaging of Cik1-AID strains. aux, auxin. The SPB was labeled with Spc42-RedStar2, kinetochores with Ndc80-GFP. Scale bar is 2 µm. Movies are aligned with the separation of SPBs displayed in the first frame. Quantification of metaphase duration in individual Cik1-AID cells. A total of 200 cells from two biological replicates were analyzed. Open circles represent mean duration from each individual experiment; error bars show 95% CI. χ^2 test was applied; *, P < 0.0001. **(F)** Analysis of spindle size and dynamics in Cik1-depleted cells. Left panel: Gallery of consecutive frames from live-cell imaging. Middle and right panels: Quantification of spindle elongation for *n* = 15 cells. Error bars are means with 95% CIs. Student's two-tailed *t* tests were made (*, P < 0.0001; NS, P = 0.59).

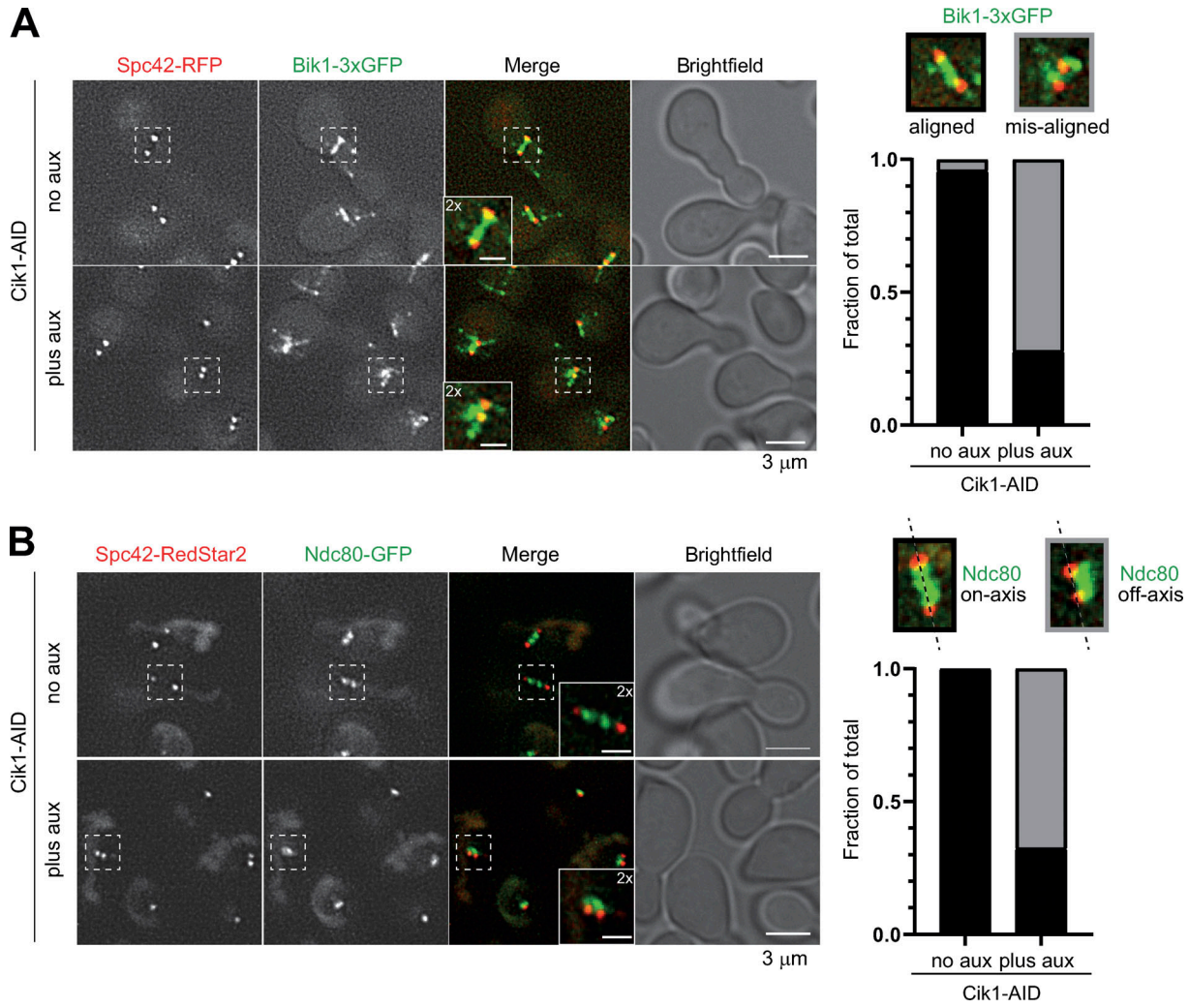

Figure 2. **Cik1 depletion impairs microtubule alignment and kinetochore clustering in metaphase spindles. (A)** Cik1-AID cells expressing the microtubule plus-end marker Bik1-3xGFP and the SPB marker Spc42-RFP were imaged in the presence and absence of auxin. Scale bar is 3 µm. Micrograph inserts show 2× magnification of marked spindle. Scale bar is 1 µm. Metaphase spindle morphology in 40 cells was categorized into aligned and misaligned spindles. **(B)** Analysis of kinetochore position in Cik1-depleted cells. Representative fluorescence images of cells expressing the kinetochore marker Ndc80-GFP and the SPB marker Spc42-RedStar2 are shown. Scale bars are 3 µm. Inserts show 2× magnification of a kinetochore cluster together with the SPBs marked by Spc42-RedStar2. Scale bars in the insets are 3 µm. Kinetochore organization in 40 metaphase spindles was categorized into on-axis and off-axis Ndc80 signals relative to the SPBs.

microtubules. We therefore turned to polarized yeast cells, generated by exposure to the mating pheromone α-factor, in which microtubule bundle dynamics can be readily observed by following the movement of the SPB associated with the nuclear membrane. When the microtubule bundle is polymerizing, it pushes the nucleus away from the shmoo tip. Conversely, when the bundle is depolymerizing, it pulls the nucleus toward the shmoo tip (Fig. S1 A). As reported before, Kar3-3xGFP was present as individual dots along the shmoo tip bundle (Molodtsov et al., 2016; Gibeaux et al., 2013), colocalizing with the plus-end marker Stu2 (Fig. S1, B and C). By analyzing kymographs of SPB displacement (tagged with Spc42-mCherry) relative to the shmoo tip over time, we quantified microtubule bundle dynamics parameters, as well as microtubule alignment, in the presence and in the absence of Kar3 (Fig. S1, D and E). We also compared overall bundle dynamics with individual nuclear microtubules or cytoplasmic microtubules outside the shmoo tip bundle (Fig. S1 F). Interestingly, Kar3 depletion in α-factor–arrested cells affected neither net polymerization nor depolymerization velocity of the bundle (Fig. S1 G) but instead caused microtubule bundle disorganization, with 42/50 examined cells displaying microtubules that failed to align along the SPB-shmoo tip axis. Moreover, the switches between bundle polymerization and depolymerization occurred less frequently in Kar3-depleted cells, causing a 50% increase in time between catastrophes or rescues from 90 s in control to 135 s in Kar3-depleted cells (Δt catastrophe/rescue; Fig. S1 G).

The overall dynamics of microtubule bundles were drastically different from those of individual microtubules, as analyzed by following Stu2-GFP signals, which labeled both polymerizing and depolymerizing plus ends. By obtaining movies with high time resolution, we found that individual

nuclear microtubules had polymerization and depolymerization speeds ~2.4 times faster than those of the microtubule bundle (Fig. S1 F). These observations in α-factor–arrested cells show that Cik1-Kar3 is required to align microtubules into a parallel bundle and to promote frequent switches between overall polymerization and depolymerization of the bundle.

Identification of novel sequence elements required for Cik1-Kar3 function in vivo

We took advantage of the lethality of Cik1 depletion in a *mad1Δ* strain to screen for novel molecular elements required for the mitotic function of Cik1. To this end, Cik1-AID strains were transformed with Cik1 wild type or mutants encoded on centromeric plasmids. To ensure targeting into the nucleus, all constructs contained an SV40 NLS. Viability in the absence of the mitotic checkpoint was scored on plates as a readout for the ability to support error-free chromosome segregation (Fig. 3 A). Since it was previously shown that the C-terminal motor homology domain of Cik1 is required for proper Cik1-Kar3 function (Liu et al., 2011; Mieck et al., 2015), we focused on the contribution of the N-terminal tail. Amino-terminal truncations of increasing size, followed by fine mapping with a resolution of five amino acids, revealed a striking difference between Cik1 variants lacking N-terminal 69 versus 74 residues (Fig. 3 B). While Cik1$^{\Delta 69}$ supported viability upon Cik1 depletion indistinguishable from that of wild-type Cik1, the Cik1$^{\Delta 74}$ mutant was inviable. Multiple sequence alignments of various yeasts revealed that the difference between these Cik1 versions is the presence of a conserved KLTF peptide motif, which is located just N-terminal of a predicted coiled-coil domain in the Cik1 tail (Fig. 3 C).

Since the KLTF peptide motif was specific to Cik1, we asked if placing it into the paralog Vik1 would allow the transfer of critical mitotic Cik1 functions. Overall, Cik1 and Vik1 share a similar organization but display only 20% sequence identity. We generated chimeric constructs in which parts of the Cik1 tail were fused to Vik1 (Fig. 3 D). While full-length Vik1 was unable to rescue the lethality of a Cik1 depletion, chimeric Vik1 constructs containing the Cik1 tail supported viability, but only if these constructs contained the KLTF motif (Vik1-Cik1-Vik1 chimeras VCV1, VCV3, and VCV4). Thus, the key functional difference between the paralogs Cik1 and Vik1 lies in the presence of the KLTF motif, and transferring it to Vik1 allows Vik1 to perform the key mitotic functions otherwise only provided by Cik1 (Fig. 3 D).

We performed a similar complementation analysis for Kar3-AID, focusing on the contribution of the Kar3 N-terminus to mitotic function. This analysis revealed that an internal deletion of residues 89–109 (hereafter termed the ND2 domain) and, within this region more specifically, the deletion of residues 104–108, phenocopied the lack of a rescue allele (Fig. S2, A and B). Interestingly, the identified Kar3 region preceded a predicted coiled-coil domain similar to the corresponding KLTF motif in Cik1, suggesting they might perform a common function.

The Cik1 KLTF motif is a key part of the Bim1-binding interface of Cik1-Kar3

To delineate the molecular function of the KLTF motif in Cik1, we compared the biochemical properties of recombinant Kinesin-14 motors produced in Sf9 insect cells that contained either the Cik1$^{\Delta 69}$ or the Cik1$^{\Delta 74}$ version. Both Cik1 variants were able to form heterodimers with Kar3 (Fig. 4 A) and supported ATP-dependent microtubule motility in vitro (not shown). Since the budding yeast EB1 homologue Bim1 is the only biochemically described binding partner (Mieck et al., 2015), we compared the ability to bind Bim1 in vitro. Strikingly, while Bim1 coeluted with Cik1$^{\Delta 69}$-Kar3 during size exclusion chromatography (SEC), Bim1 binding was abolished for the Cik1$^{\Delta 74}$ variant (Fig. 4 B). We confirmed this result in quantitative pull-down assays, binding soluble motors to increasing amounts of immobilized Bim1 on beads. By quantifying the protein depletion from the supernatant, we estimated an apparent dissociation constant of $K_d \approx 250$ nM for the Cik1$^{\Delta 69}$-Kar3 complex with Bim1, while Cik$^{\Delta 74}$-Kar3 did not display any appreciable affinity (Fig. 4 C). With a dissociation constant in the nanomolar range, the KLTF sequence as part of a novel Bim1-binding motif provides much tighter binding than single EB1-interacting motifs, which have been reported to be in the above micromolar range (Honnappa et al., 2009; Kumar et al., 2017).

A similar biochemical analysis confirmed that the ND2 region in Kar3 also contributes to Bim1 binding in vitro (Fig. S3, A and B). Taken together, our results allow the definition of a composite binding interface between Cik1-Kar3 and Bim1 (Fig. 4 D). This interface is split between Cik1 and Kar3 and consists of two critical parts: first, the ND2 region of Kar3 (motif A), which is necessary but not sufficient to bind Bim1, since it is shared between Vik1–Kar3 and Cik1–Kar3 complexes and Vik1–Kar3 is unable to bind Bim1 (Mieck et al., 2015); and second, the newly identified KLTF peptide motif in Cik1 (motif B), which constitutes the key difference between the Cik1 and Vik1 paralogs. An intact AB-motif is required for high-affinity Bim1 binding. In addition, there is a third, canonical Bim1-binding SxIP motif (Honnappa et al., 2009) at the extreme N-terminus of Cik1 (motif C). This organization is fully consistent with a previously obtained proximity map derived from chemical cross-linking mass spectrometry (XL-MS) experiments (Molodtsov et al., 2016). In particular, Cik1 Lys71 of the "KLTF" motif was found to cross-link to Bim1 Lys223 in the cargo-binding domain. In addition, several cross-links of residues just C-terminal of the KLTF motif with residues in the Bim1 linker- and cargo-binding domain and also to Kar3 ND2 are consistent with the proposed organization (Fig. S4).

Bim1-binding–deficient Cik1 mutants display severe mitotic phenotypes

The definition of the Bim1-binding interface allowed us to construct novel Cik1 mutants defective in the Bim1–Cik1-Kar3 interaction and use these to probe the specific functional contribution of this complex in cells. In particular, we constructed Cik1 mutants in which the Bim1-binding motifs C (SxIP) and B (KLTF) were either mutated individually (to SKNN(AA) or 4A, respectively) or in combination (SKNN(AA)+4A; Fig. 5 A). Using conditional depletion of Cik1-AID in *mad1Δ* cells, we found that the Cik1-SKAA mutant was fully viable, while Cik1-4A displayed slow growth. Combining both mutations in the Cik1-SKAA+4A mutant, however, caused lethality upon Cik1 depletion,

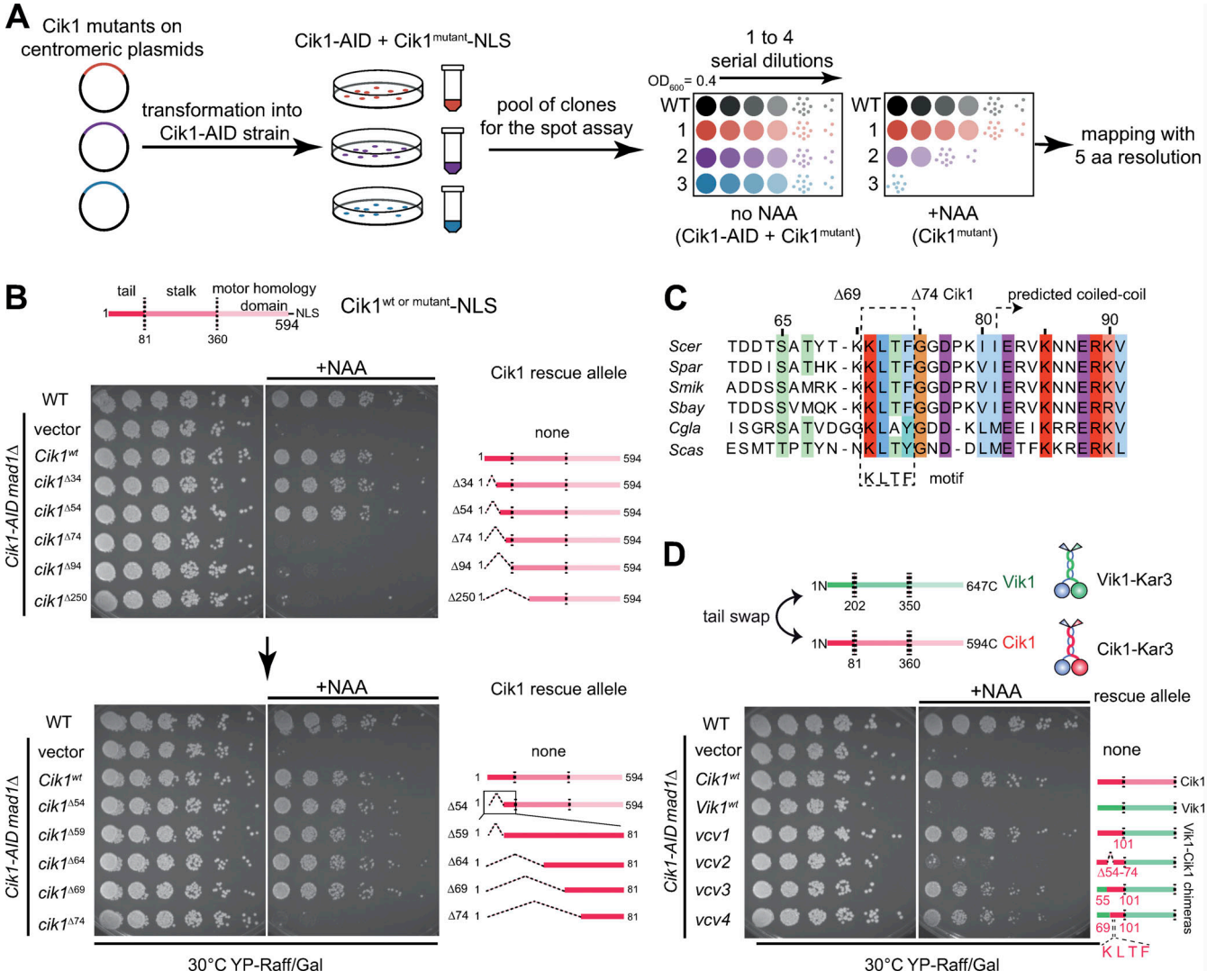

Figure 3. **Molecular dissection of the Cik1 N-terminus reveals a conserved KLTF motif. (A)** Scheme of Cik1 mutagenesis screen. Cik1 mutants were encoded on centromeric plasmids and targeted to the nucleus by an SV40 NLS. After addition of auxin, the only remaining version of Cik1 in the cell was an assayed mutant. **(B)** Subsequent N-terminal truncations of Cik1 allowed to identify a novel functionally important region in the N-terminus. Second panel shows the precise mapping of a region between 54 and 74 aa of Cik1. **(C)** Sequence alignment of Cik1 tail regions from six budding yeast species illustrates a conserved KLTF peptide motif as the difference between Cik1$^{\Delta 69}$ and Cik1$^{\Delta 74}$. Residues were labeled with the ClustalW coloring scheme in Jalview. **(D)** The KLTF peptide motif defines the key difference between the two kinesin-associated proteins Cik1 and Vik1. Construction of Cik1-Vik1-Cik1 chimeras is shown schematically. Transplantation of the 69–101 aa region, including KLTF, of Cik1 to Vik1 allows the VCV4 (Vik1-Cik1-Vik1) chimera to fulfill Kinesin-14 mitotic functions.

similar to the Cik1$^{\Delta 74}$ mutant (Fig. 5 B). Using gene replacements in diploid cells, which also contained a heterozygous deletion of the checkpoint gene *MAD1*, we found that Cik1-4A spores grew poorly, and we failed to recover Cik1-4A spores that also lacked *MAD1* (Fig. 5 C). The Cik1$^{SKNN+4A}$ mutant displayed an even more severe phenotype. The respective spores rarely grew in a wild-type background and were never recovered in a mitotic checkpoint-deficient strain. Analysis of Kar3-3xGFP localization in different cell cycle stages revealed that both Cik1-4A and Cik1$^{SKNN+4A}$ mutants eliminate Kar3 localization to plus ends between the SPBs in both metaphase and anaphase spindles (Fig. S5 A). We confirmed the expression of the different Cik1 alleles by Western blotting (Fig. S5 B). The Cik1-4A mutation also strongly reduced the level of Kar3-3xGFP on the shmoo tip bundle (Fig. S5 C), although some residual colocalization with Stu2 was still visible (Fig. S5 D).

In biochemical experiments, the Cik1-4A mutant eliminated Bim1 interaction during SEC (Fig. S5 E), while it retained some affinity in solid-phase pull-downs. The Cik1–SKAA+4A mutant did not display any affinity for Bim1, even in the pull-down assay, consistent with the most severe phenotypes of this mutant (Fig. S5 F). We used the conditional Cik1-AID system to further characterize the phenotypes of Bim1-binding–deficient Cik1 mutants. Expression of Cik1$^{SKNN+4A}$ led to a checkpoint-dependent accumulation of large-budded cells, similar to those lacking a Cik1 rescue allele (Fig. 5 D). Live-cell imaging further confirmed that expression of wild-type Cik1 rescued the metaphase delay that occurred upon depletion of endogenous Cik1. By

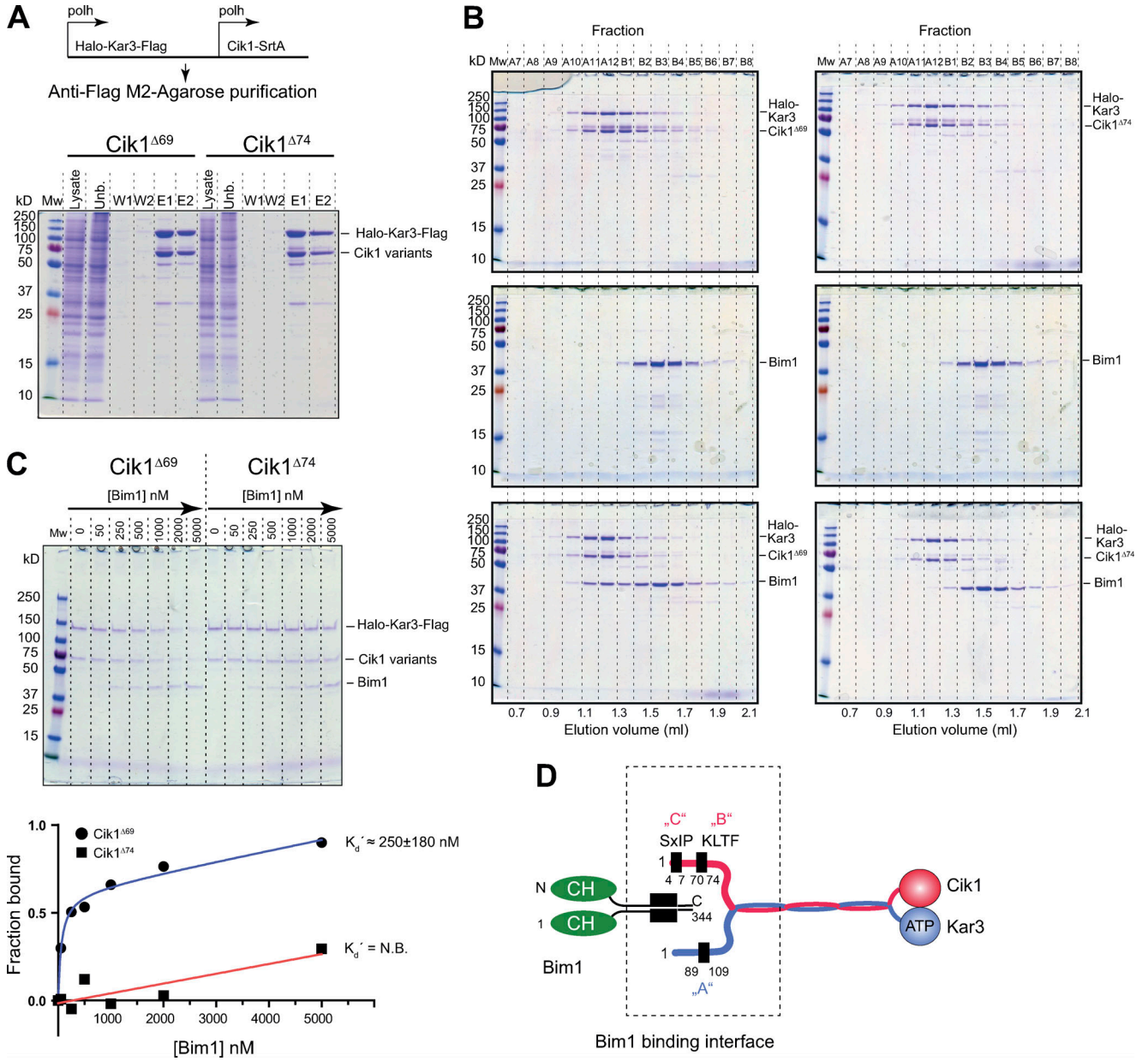

Figure 4. **The novel KLTF peptide motif is responsible for high-affinity Bim1 binding by Cik1-Kar3. (A)** Purification of Cik1$^{\Delta69}$-Kar3 and Cik1$^{\Delta74}$-Kar3. Proteins were eluted from M2-agarose beads with 3xFlag peptide. Gel lanes show Sf9 lysate, unbound fraction (Unb.), wash 1, and wash 2 followed by the two elution fractions E1 and E2. polh, polyhedrin promoter; Mw, molecular weight marker. **(B)** Analysis of Bim1 binding to Cik1$^{\Delta69}$-Kar3 and Cik1$^{\Delta74}$-Kar3 in a SEC experiment. Sample fractions from Superose 6 column were resolved on SDS-PAGE and visualized by Coomassie staining. For comparison, the identical Bim1 gel is shown side by side in the middle panel. Input concentration of proteins was 5 µM for the respective Halo–Kar3–Cik1 complex and 10 µM for Bim1. **(C)** Analysis of Bim1 binding in a quantitative pull-down experiment. Representative gel of supernatant fractions from pull-down experiment using Bim1 immobilized on beads incubated with Cik1$^{\Delta69}$-Kar3 and Cik1$^{\Delta74}$-Kar3 in solution. Binding is well approximated with the one-site total binding model (smooth line), R^2 = 0.99. Bim1 does not bind to Cik1$^{\Delta74}$-Kar3 under the given conditions. Experiments were performed at +4°C. Dissociation constant represents mean value of three biological repeats ± SD. N.B., no binding. **(D)** Schematic representation of the binding interface between Cik1-Kar3 and Bim1; the discovered elements of the binding interface are highlighted.

contrast, the Bim1-binding–deficient Cik1$^{SKNN+4A}$ caused an increase in the mean metaphase duration from 31 ± 1 min to 54 ± 3 min (Fig. 5 E). Analysis of spindle dynamics additionally showed that Cik1$^{SKNN+4A}$ cells initiated anaphase from a significantly shorter metaphase spindle (length means ± SEM were 2.14 ± 0.07 µm for Cik1^{WT} and 1.16 ± 0.09 µm for Cik1$^{SKNN+4A}$), while overall anaphase dynamics did not differ strongly from that of wild-type cells (Fig. 5 G). We conclude that Bim1-binding–deficient Cik1 mutants phenocopy Cik1 depletion, showing that the functionally relevant form of Cik1-Kar3 in yeast cells is its complex with Bim1.

To analyze the impact of the Bim1–Cik1-Kar3 complex on microtubule bundle dynamics in α-factor–arrested cells, we used the Kar3^{ND2} allele, as the Cik1-4A mutant maintained some

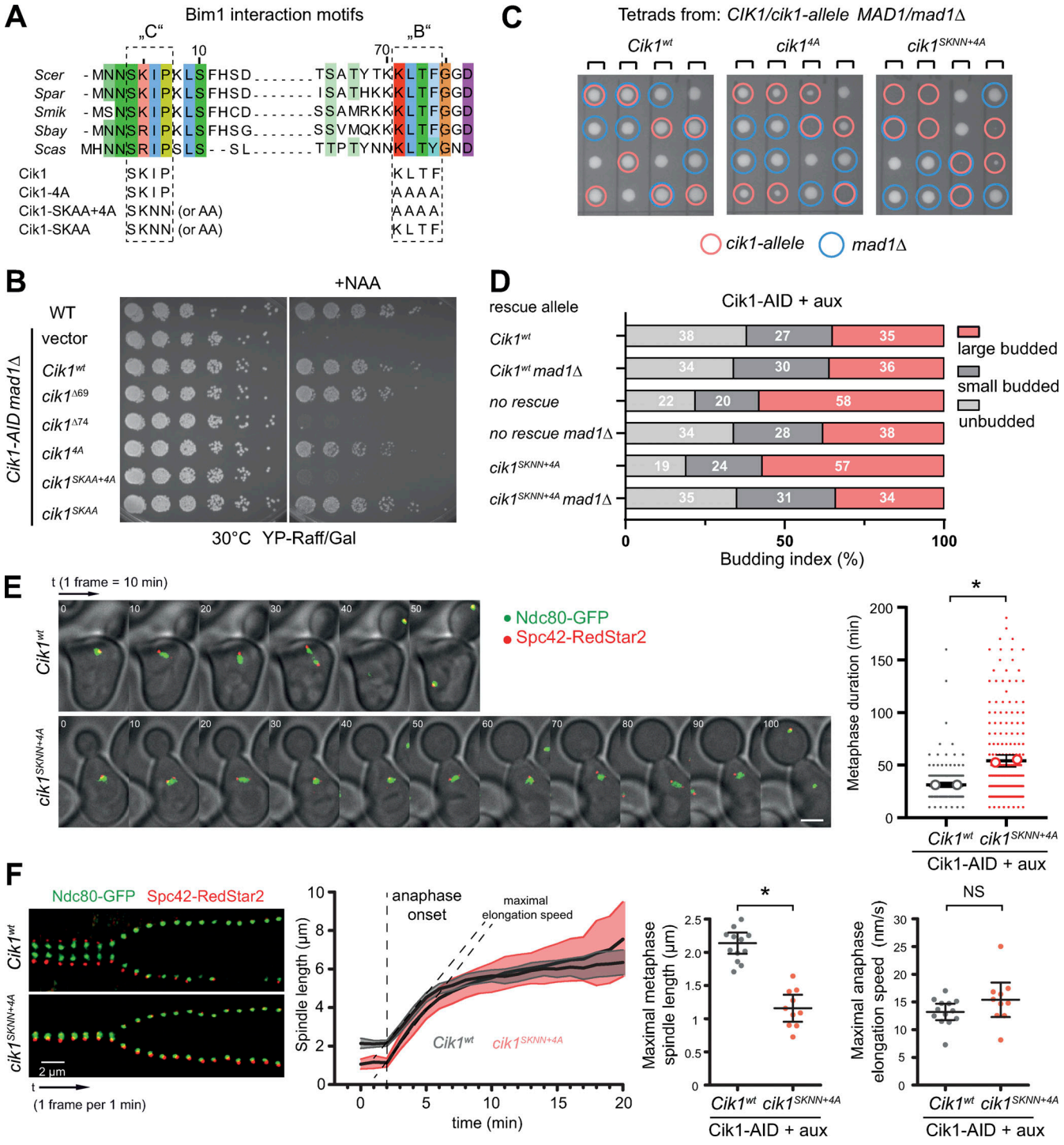

Figure 5. **Bim1–Cik1 interaction mutants display severe mitotic phenotypes. (A)** Scheme of the constructed Bim1–Cik1 interface mutants. Multiple sequence alignment reveals the presence of a conserved canonical EB1 binding motif (SxIP) and the novel KLTF motif. The constructed Cik1 mutants are shown below the alignment. **(B)** Serial dilution assay testing viability of different Cik1 mutants in the Cik1-AID *mad1Δ* background. **(C)** Heterozygous diploid dissection of different Cik1 alleles in a *mad1Δ* background. The four spores from an individual tetrad are shown in the respective columns; the indicated gentoypes are marked by circles. Combined mutations in SKIP and KLTF motifs result in a severe growth defect. **(D)** Budding index assay of Cik1-depleted strains expressing the indicated rescue constructs. Log-phase cells were treated with auxin for 3 h. The percentage of the respective cell cycle stage is indicated in white on the graph. Average means of three independent experiments are shown. **(E)** Live-cell microscopy analysis of metaphase duration in Cik1-AID strains expressing a wild-type Cik1 or the Cik1$^{SKNN+4A}$ allele. Galleries show consecutive frames from live-cell imaging, aligned at the time of SPB separation. Scale bar is 2 µm. Quantification of metaphase duration is from 200 individual cells (two technical repeats). Open circles represent mean duration from each individual experiment. Bars show mean values and 95% CI. χ^2 test was applied; *, P < 0.0001. **(F)** Analysis of spindle size and dynamics in Cik1-depleted cells expressing either Cik1 wild-type or Cik1$^{SKNN+4A}$. Left panel: Gallery of consecutive frames from live-cell imaging. Middle and right panels: Quantification of spindle elongation for *n* = 15 cells. Error bars are means with 95% CIs. Student's two-tailed *t* tests were made (*, P < 0.0001; NS, P = 0.14).

plus-end localization of Kar3 (see above). The mutant Kar3, unable to bind Bim1, failed to rescue the decreased frequency between polymerization and depolymerization phases of the shmoo tip bundle, which occurs upon depleting Kar3 (see Fig. S1, C and D), and also caused misalignment of shmoo tip microtubules (Fig. S5 G). We conclude that Cik1-Kar3 function both in mitosis and in α-factor–arrested cells critically requires complex formation with Bim1, which leads to plus-end targeting.

Constitutive plus-end targeting of Cik1-Kar3 restores viability by promoting the alignment of nuclear microtubules

If Bim1 was the only critical interaction partner for Cik1-Kar3, we would predict that constitutive targeting to the microtubule plus end should bypass the molecular requirements for Bim1 binding and restore the mitotic function of the motor. We tested this idea by fusing the N-terminal CH domain of Bim1 (residues 1–133) or of Ndc80 (residues 1–246) directly to the Bim1-binding–deficient Cik1$^{\Delta 74}$ mutant (Fig. 6 A). Strikingly, the constructed CH-Cik1 chimeras were capable of supporting viability of *mad1Δ* cells after Cik1 depletion (Fig. 6 B). A corresponding CH-domain fusion to Kar3 failed to rescue the Cik1 depletion, consistent with the notion that Cik1 also contributes to Kar3 function via its motor homology domain (Mieck et al., 2015).

We investigated the effect of the CH-Cik1 chimera on the microtubule cytoskeleton of yeast cells in more detail, specifically by comparing cells that either expressed Bim1-binding–deficient Cik1$^{\Delta 74}$-NLS or the fusion protein CH^{Bim1}-Cik1$^{\Delta 74}$-NLS. Upon expression of Cik1$^{\Delta 74}$-NLS in α-factor–arrested cells, the shmoo tip bundle localization of Kar3 was abolished and Kar3-3xGFP was visible as a diffuse nuclear background signal, which failed to localize to microtubule structures and only showed slight enrichment proximal to the SPB (Fig. 6 C). This confirms that Kar3 localization to the nucleus depends on an NLS normally only present in the mitotic isoform of Cik1 (Benanti et al., 2009). Upon expression of CH-Cik1$^{\Delta 74}$–NLS, however, Kar3-3xGFP strongly localized to microtubules emanating as a bundle from the SPB. The nuclear bundle was dynamic, with Kar3-3xGFP appearing as motile spots along the length of the bundle.

We used Bik1-3xGFP to investigate the distribution of plus ends in α-factor–arrested cells. In Cik1 wild-type cells, Bik1 localized prominently to a tightly aligned shmoo tip bundle and displayed weak localization to individual nuclear plus ends (Fig. 6 D). Upon expression of CH-Cik1$^{\Delta 74}$–NLS, however, Bik1-3xGFP strongly localized to a nuclear bundle in which individual plus ends were aligned along a common axis. In contrast to this, the shmoo tip bundle in these cells displayed organization defects (Fig. 6 D). Analysis of metaphase duration in individual cells showed that there was no significant difference between Cik1^{WT} and CH-Cik1$^{\Delta 74}$–NLS (39 ± 2 min versus 38 ± 2 min, respectively), showing that the fusion protein fully rescued the mitotic timing of Cik1-depleted cells (Fig. 6 E). Just like Cik1$^{\Delta 74}$, the Bim1-binding–deficient Kar3^{ND2} mutant could also be rescued by a CH-domain fusion (Fig. 6 F). Microtubule cross-linking and bundle formation via plus-end targeted Kinesin-14s is likely a universal function of these proteins. In line with this notion, we found that the human Kinesin-14 HSET, when fused with the CH-domain of Bim1 to its tail, was able to complement the depletion of Kar3 in a checkpoint-deficient strain (Fig. 6 G).

Cik1 mutants rely on the microtubule cross-linking protein Ase1/PRC1 for metaphase spindle assembly

While Bim1–Cik1 interaction mutants initially displayed severe microtubule alignment defects, spindle organization eventually improved, and cells were able to enter anaphase with a delay (see Fig. 1 E and Fig. 5 E). To ask how Cik1 mutant cells accomplished spindle assembly, we visualized several other microtubule-binding proteins involved in this process. While we did not detect strong effects on the recruitment of the Kinesin-5 motor Cin8 or the Kinesin-8 Kip3 (data not shown), we noticed that the conserved microtubule bundling protein Ase1/PRC1, which localized only faintly to wild-type metaphase spindles, was significantly enriched on Cik1-depleted or Cik1 mutant spindles (Fig. 7, A and B). Crucially, at the time of anaphase onset, Cik1 mutant spindles contained ∼50% more Ase1 than wild-type spindles, as judged by fluorescence microscopy (mean ± SEM). Ase1-3xGFP intensities were 445 ± 14, 606 ± 19, 450 ± 14, and 648 ± 24 a.u. for no auxin, Cik1 depletion, Cik1^{wt}, and Cik1$^{SKNN+4A}$ rescues, respectively (Fig. 7, C and D). If Ase1 recruitment were important for metaphase spindle organization in this context, we would expect synthetic defects between Cik1 and Ase1 mutants. Indeed, codepletion of Cik1 and Ase1 was lethal, even in checkpoint-proficient yeast cells, and viability could be rescued by expression of wild-type Cik1 but not of Bim1-binding–deficient Cik1$^{SKNN+4A}$ (Fig. 7 E). Consistent with the key role for plus-end targeting of Kar3, the CH-Cik1$^{\Delta 74}$ fusion was able to rescue the lethality of the Cik1/Ase1 codepletion.

We furthermore investigated the phenotypes of Cik1/Ase1–codepleted cells by live cell microscopy: after addition of auxin, codepleted cells were characterized by a very short spindle, whose length was decreased relative to that of Cik1-depleted cells or of Cik1/Ase1–codepleted cells rescued by a Cik1 wild-type construct (representing the effect of the individual Ase1 depletion; Fig. 7 F; means ± SEM spindle lengths were 1.65 ± 0.02, 0.97 ± 0.01, 1.26 ± 0.02, and 0.93 ± 0.01 µm for no auxin, plus aux, Cik1^{wt}, and Cik1$^{SKNN+4A}$, respectively). Visualizing microtubule plus ends with Bik1-3xGFP in this strain revealed that codepleted cells had a highly abnormal spindle morphology characterized by severe microtubule alignment defects, with most of the nuclear Bik1 fluorescence localized away from the pole-to-pole axis (Fig. 7 G). We conclude that lack of Kar3 plus-end targeting and simultaneous depletion of Ase1 prevent the assembly of a functional metaphase spindle.

Discussion

Here, we define the molecular basis for the formation of a complex between EB1 and Kinesin-14 in budding yeast and analyze the contribution of this complex to spindle organization and function. The definition of the binding interface allowed us to construct highly specific point mutants that avoid complications that arise from interpreting phenotypes of deletion mutants. A Cik1 deletion mutant, for example, will not only prevent the formation of Cik1–Kar3 complexes but will also change the

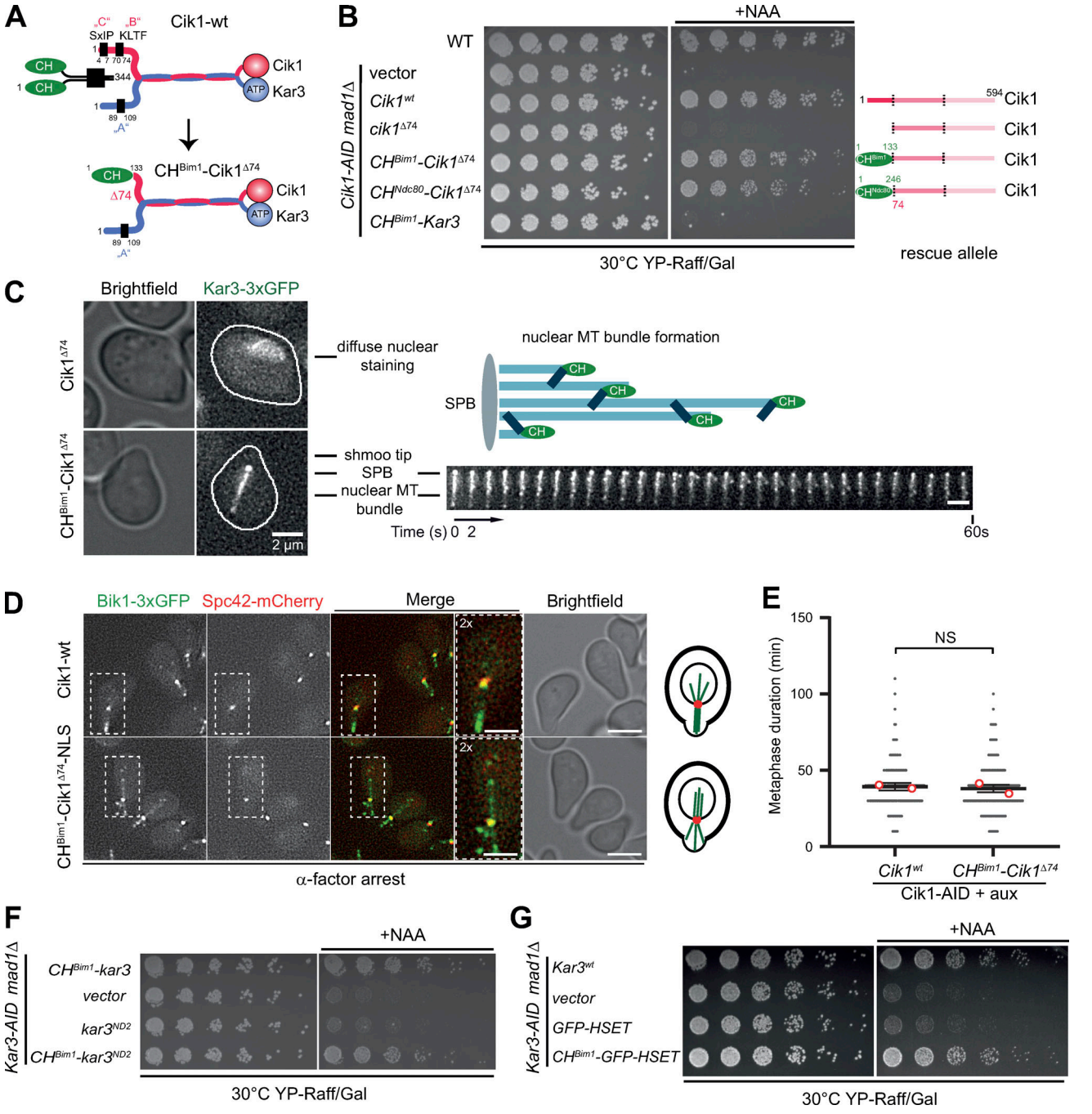

Figure 6. **Artificial targeting of Cik1-Kar3 to the plus end is sufficient to induce nuclear bundle formation and restore viability in the absence of a checkpoint. (A)** Cartoon describing the construction of the CH^{Bim1}-$Cik1^{\Delta74}$ construct. The CH domain of Bim1 (residues 1–133) was fused to a Cik1 mutant that lacks Bim1 binding. **(B)** Serial dilution assay of different Cik1 alleles in the Cik1-AID *mad1Δ* strain background. **(C)** Analysis of Kar3 localization in Bim1-binding–deficient $Cik1^{\Delta74}$ or CH^{Bim1}-$Cik1^{\Delta74}$ cells during an α-factor arrest. Scale bar is 2 µm. Montage on the right side shows 30 consecutive frames with 2-s time interval of the nuclear microtubule bundle in the CH^{Bim1}-$Cik1^{\Delta74}$ strain. Scale bar is 2 µm. **(D)** Fluorescence micrographs of α-factor–arrested Cik1 wild-type or CH^{Bim1}-$Cik1^{\Delta74}$-NLS cells expressing the plus-end marker Bik1-3xGFP and Spc42 mCherry. Scale bar is 4 µm. Insert shows 2× magnification of the indicated area. Scale bar is 2 µm. Cartoon on the right depicts organization of the microtubule cytoskeleton. **(E)** Quantification of metaphase duration in Cik1-AID cells treated with auxin and expressing either Cik1 wild-type (39 ± 2 min) or CH^{Bim1}-$Cik1^{\Delta74}$-NLS (38 ± 2 min). 160 and 170 cells, respectively, were quantified from two technical repeats. Open circles represent mean duration from each individual experiment. Bars denote 95% CIs. χ^2 test was applied; NS, $P > 0.9999$. **(F)** A CH-domain fusion rescues the growth defect of the Bim1-binding–deficient $Kar3^{ND2}$ mutant. Serial dilution assay of the indicated strains in a Kar3-AID *mad1Δ* strain background. **(G)** A CH-domain fusion to human Kinesin-14 HSET can rescue the lethality of the Kar3 depletion in a checkpoint-deficient strain.

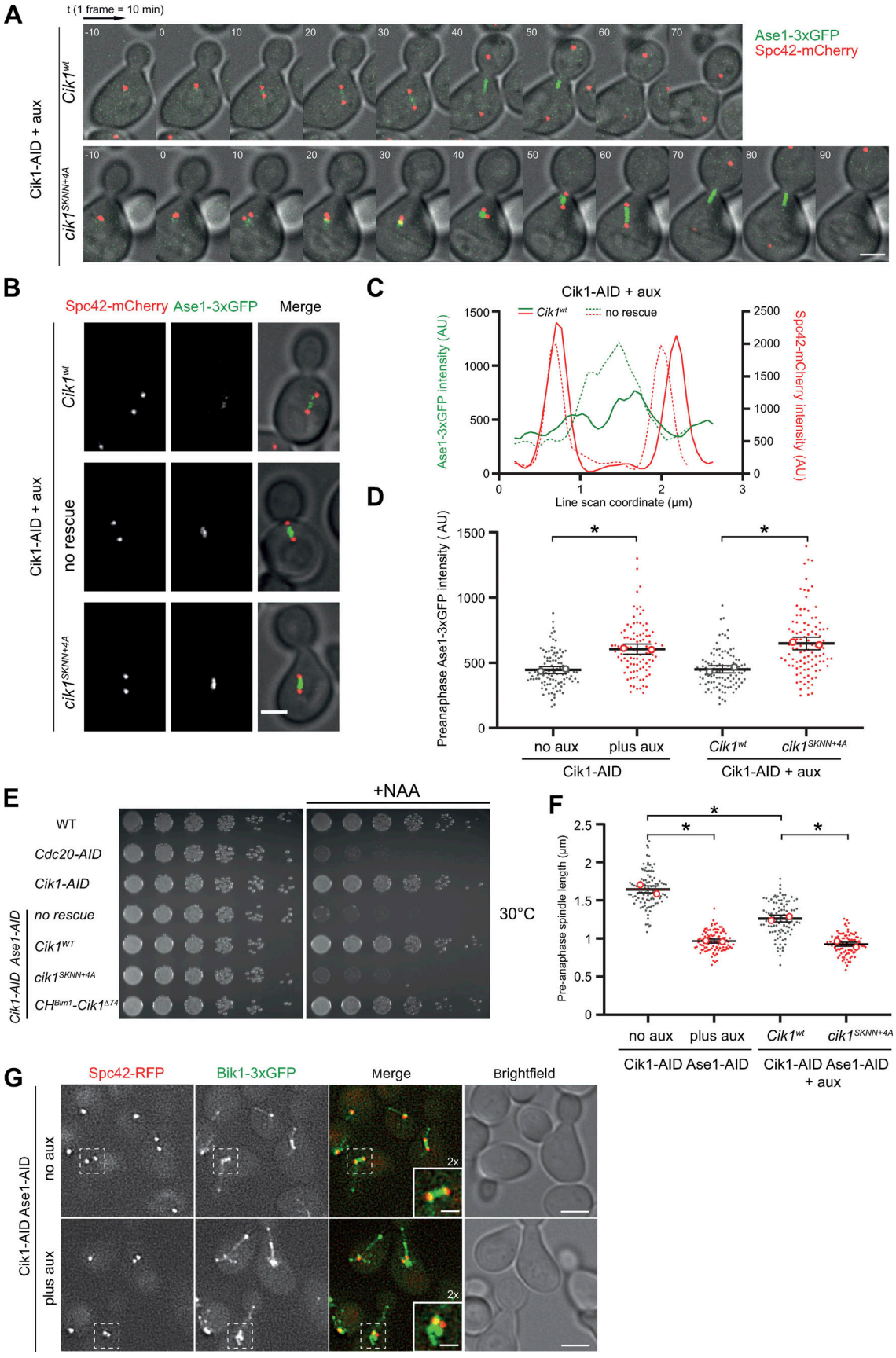

Figure 7. **Bim1–Cik1 interaction mutants rely on the conserved microtubule cross-linker Ase1/PRC1 for metaphase spindle assembly. (A)** Live-cell imaging of Ase1 recruitment to Cik1 wild-type or Cik1$^{SKNN+4A}$ mutant cells. Consecutive frames from live-cell movies are displayed, aligned to the time of SPB

separation. Scale bar is 2 µm. **(B)** Fluorescence micrographs showing Ase1 recruitment to metaphase spindles. Equally intensity-scaled fluorescence micrographs are shown. Scale bar is 3 µm. **(C)** Line scan profile quantifying Ase1-3xGFP on metaphase spindles in Cik1-AID cells treated with auxin and containing either Cik1 wild-type or no rescue allele. **(D)** Quantification of Ase1-3xGFP intensity on pre-anaphase spindles under the indicated conditions. 100 cells were analyzed for each condition from two technical repeats. Open circles represent mean intensity from each individual experiment. Bars denote 95% CI. Kruskal-Wallis test was done; *, $P < 0.0001$. **(E)** Simultaneous depletion of Cik1 and Ase1 is analyzed by a serial dilution assay of the indicated strains on YP-Raff/Gal at 30°C in the absence and presence of auxin. Cdc20-AID is included as a control for the depletion of an essential protein. **(F)** Quantification of pre-anaphase spindle length in the indicated strains. 100 cells were analyzed for each condition from two technical repeats. Bars denote 95% CI. Kruskal-Wallis test was done; *, $P < 0.0001$. Difference between plus aux and Cik1$^{SKNN+4A}$ was not significant. **(G)** Fluorescence microscopy of Cik1-AID Ase1-AID codepleted cells expressing the microtubule plus-end marker Bik1-3xGFP. Scale bar is 3 µm. Inserts are 2× magnifications of the indicated areas. Scale bar is 1 µm.

amount of Vik1–Kar3 complexes in the cell (our unpublished data). In addition, the N-terminal domains of Cik1 and Kar3 encode a number of other functionalities, such as nuclear localization signals or degron sequences (Benanti et al., 2009). The discovery of the KLTF motif in Cik1 is another example of short binding motifs that are present in addition to—or instead of—the well-documented SxIP motifs in EB1 cargos (Kumar et al., 2017). It will be interesting to see whether different binding modes reflect different functionalities of EB1–cargo complexes. In some cases, the EB1 interaction may simply be used for local enrichment of the cargo at the microtubule plus end; in other cases, however, the EB1–cargo complex may perform a joint biochemical function, requiring a high-affinity interaction. The EB1–Kinesin-14 complex seems to be an example for the latter mode of action.

We show that a key biochemical activity of the EB1–Kinesin-14 complex is its ability to convert highly dynamic individual microtubules into bundles, while at the same time promoting the overall ability of the bundle to switch between polymerization and depolymerization. Our results show that microtubule alignment by the Bim1–Cik1-Kar3 complex contributes to building a dynamic metaphase spindle on which sister chromatid bi-orientation can occur efficiently. We propose that the EB1–Kinesin-14 complex contributes to this process via multiple different mechanisms (Fig. 8):

First, bundle formation contributes to early spindle assembly and microtubule alignment, consistent with previously reported phenotypes for a *cik1Δ* strain (Hepperla et al., 2014). The reduced size of the metaphase spindle and the mispositioned kinetochores that we observed upon Cik1 depletion or in the Bim1-interaction mutants are consistent with this interpretation. Our results show, however, that these functions of Cik1-Kar3 are accomplished as a complex with Bim1 at the microtubule plus end, suggesting that the type of antiparallel zippering proposed by Gardner and colleagues (Hepperla et al., 2014), which would include Bim1-independent translocation along microtubules, may provide only a secondary contribution. We rather favor the idea that parallel bundles generated by Bim1–Cik1-Kar3 from both SPBs serve as optimized binding sites with sufficient overlap for Kinesin-5 motors whose role in early spindle formation was described recently (Leary et al., 2019).

Second, bundle formation contributes to the spatial organization of yeast kinetochores into SPB-proximal clusters (Jin et al., 2000). This type of organization may facilitate the bi-orientation process, and there is evidence for coordinated movements between different pericentromeres, suggesting that they behave as a single unit (Stephens et al., 2013). In this way, Bim1–Cik1-Kar3 can contribute to the organization of a half-spindle as a kinetochore fiber that links to 16 individual kinetochores, thus resembling the organization of bundle attachments to a single kinetochore in higher eukaryotes (Nixon et al., 2015; Vukušić et al., 2017). In higher eukaryotes, plus end–directed motors such as CENP-E make important contributions to kinetochore congression during prometaphase (Kapoor et al., 2006), while microtubule bundle organization also requires nucleation of new microtubules via the Augmin complex (Petry et al., 2013; David et al., 2019), which is absent in yeast. These distinct functional requirements may reflect differences in dimension and organization between different types of mitotic spindles.

Third, the high density of microtubules in the spindle provided by tight bundling through Bim1–Cik1-Kar3 allows the generation of a sufficient number of accessible binding surfaces for kinetochores to effectively switch between lateral and end-on attachments during the error correction process (Kalantzaki et al., 2015). In addition, the Bim1–Cik1-Kar3 complex promotes frequent transitions of the microtubule bundle between polymerization and depolymerization, thus ensuring that it is dynamic. This activity is best exemplified at the shmoo tip bundle, where depletion of Cik1-Kar3 makes the bundle less dynamic without affecting the speed of polymerization or depolymerization. The frequent switches are important for the quality control of kinetochore–microtubule interactions, as the error correction process requires repeated attempts to generate tension across the kinetochore structure (Suzuki et al., 2016; Tanaka et al., 2002). Consequently, tubulin mutants that display reduced dynamics also delay bi-orientation (Huang and Huffaker, 2006). By promoting microtubule bundle dynamics, Bim1–Cik1-Kar3 supports Ipl1 kinase (Aurora B) in the resolution of syntelic attachments (Tanaka et al., 2002). More direct roles for Kar3 in lateral kinetochore transport, as suggested from experiments using a CEN-reactivation system (Tanaka et al., 2007), are probably not making a substantial contribution to bi-orientation during regular mitosis, or at least our genetic analysis argues that they could only be secondary to the Bim1-provided plus-end function of the complex.

We further show that Cik1 mutant cells rely on the conserved microtubule–cross-linker Ase1 for successful metaphase spindle assembly. Given the pronounced defects in microtubule alignment and overlap in Bim1–Cik1 interaction mutants, it was surprising that Ase1 nevertheless accumulated on these misorganized spindles. We envision at least two possible explanations for this effect. First, the prolonged metaphase arrest may simply give Ase1 more time to associate with metaphase spindles.

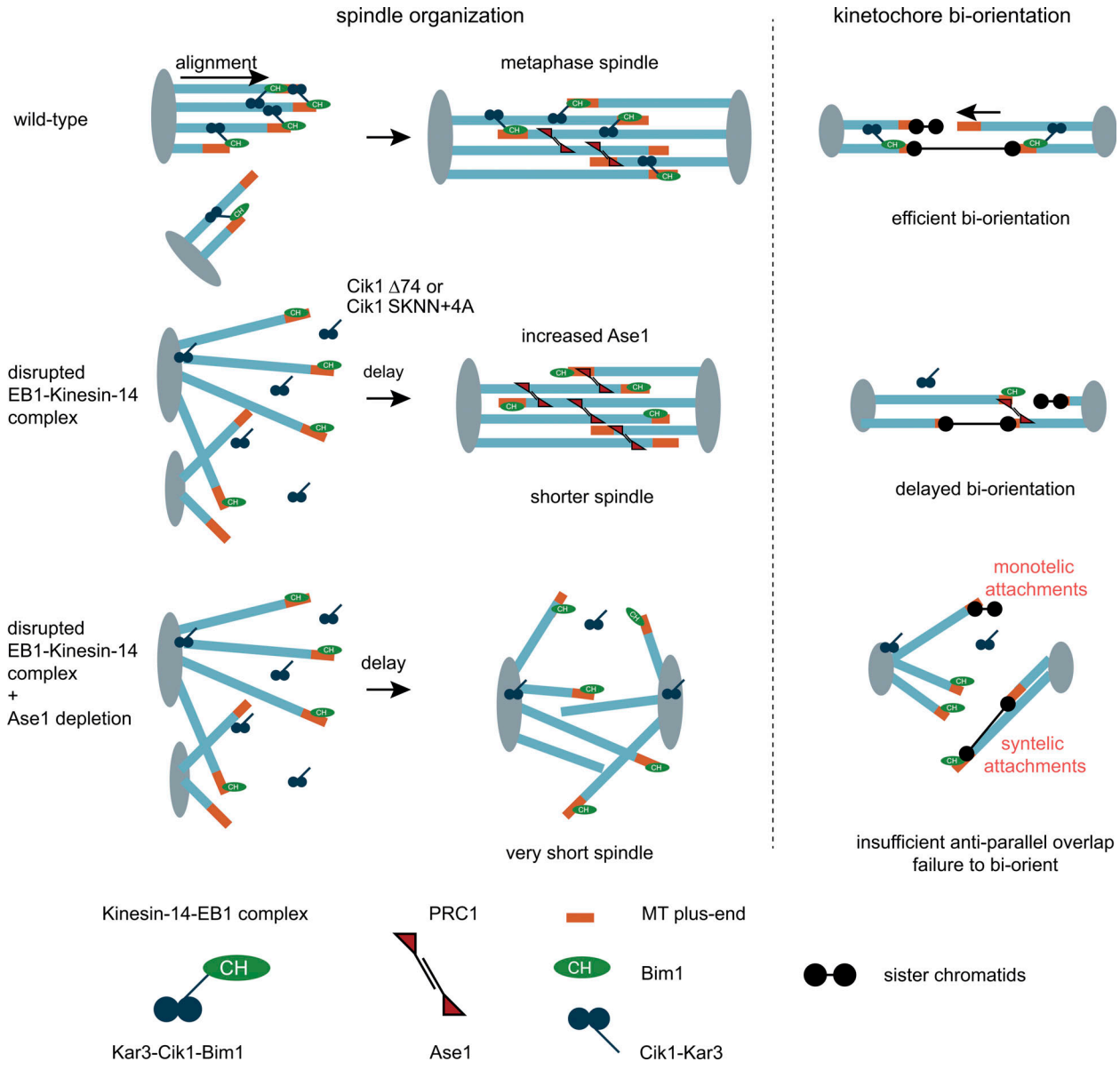

Figure 8. **Model for the role of the EB1–Kinesin-14 complex during spindle function.** Schematic description of spindle assembly and kinetochore bi-orientation in wild-type cells (top row), cells with a disrupted EB1–Kinesin 14 complex (middle row), and simultaneous loss of EB1–Kinesin-14 and Ase1/PRC1 (bottom row). Left side depicts effects on spindle microtubule organization. Right side describes consequences for sister chromatid bi-orientation. Please see Discussion for details.

Alternatively, the lack of plus end–targeted Kar3 may liberate binding sites on the metaphase spindle previously inaccessible to Ase1. Wild-type cells limit the accumulation of Ase1 on the spindle via phosphorylation in order to prevent premature sliding of interpolar MTs in metaphase (Khmelinskii et al., 2009). In the Cik1 mutant situation, however, Ase1 recruitment appears to be beneficial, and simultaneous loss of plus end–targeted Kar3 and Ase1 yields spindles that manage to separate SPBs but cannot generate sufficient microtubule alignment and anti-parallel overlap to allow kinetochore bi-orientation (Fig. 8). This is consistent with recent studies demonstrating that the initial step in the monopolar-to-bipolar transition is driven by Kinesin-5–based cross-linking (Leary et al., 2019). Our results indicate, however, that despite the presence of Kinesin-5, plus-end targeted Kinesin-14 and Ase1 are critically required for the maturation of the nascent metaphase spindle into a properly organized scaffold for kinetochores to bi-orient. Previously, Ase1 phenotypes have mostly been described affecting anaphase spindle elongation (Khmelinskii et al., 2007). Synthetic defects observed with a conditional Cin8 depletion, however, are consistent with the idea that Ase1 also makes important contributions to metaphase spindle assembly (Kotwaliwale et al., 2007). In the same context, fission yeast Ase1 is required for spindle assembly in the absence of opposing Kinesin-5 and -14 motors (Rincon et al., 2017), and it collaborates with Kinesin-14 for the generation of bipolar microtubule bundles in the cytoplasm (Janson et al., 2007).

Overall, our study identifies microtubule organization by the EB1–Kinesin-14 complex as an important prerequisite for efficient chromosome bi-orientation. Future research will have to address how the successive action of multiple motors, bundlers, and plus-end trackers is coordinated and how bundle dynamics within the spindle are regulated on a molecular level.

Materials and methods

Yeast genetics

All used strains were derived by modification of the wild-type strains DDY1102, DDY902, and DDY904 (S288c background; Table S1). Genetic modifications were performed by standard LiAc transformation using homologous recombination (Janke et al., 2004; Longtine et al., 1998). Yeasts were generally maintained in YPD medium. For protein depletion experiments, yeasts were grown in YEP medium/plates with raffinose and galactose (YP-Raff/Gal) as a sugar source at 30°C unless otherwise stated.

Preparation of Cik1-AID and Kar3-AID strains

The Ubiquitin ligase osTIR1 was integrated into the URA3 locus under the control of a galactose-inducible promoter (Nishimura et al., 2009). Cik1 and Kar3 were C-terminally tagged at their genomic loci with AID-9xMyc by integration of a corresponding PCR product. Successful integrations were verified by sequencing. Depletion was achieved by adding 1 mM auxin (NAA) to the medium/plates.

Gene deletion and tagging

Target genes were deleted or tagged using PCR products amplified from plasmid libraries. Deletions were confirmed by PCRs for the absence of the wild-type gene and the presence of a selection marker at the correct genomic loci.

Western blot sample preparation

Yeast cell extracts were prepared using alkaline treatment as described before (Kushnirov, 2000). Briefly, the equivalent of 2 OD_{600} of exponentially growing cells was harvested, washed with H_2O, and resuspended in 200 µl 0.1 M NaOH. After 5-min incubation at room temperature, cells were centrifuged again. The pellet was resuspended in 50 µl 1× SDS sample buffer and boiled for 5 min. 8–10 µl lysate was loaded per gel lane.

Used antibodies and visualization

Antibodies used were α-GFP (Roche; from mouse, catalog no. 11814460001) 1:1,000; α-myc (Covance; 9E10 from mouse, catalog no. MMS-150R) 1:1,000; α-PGK 1:10,000 (Invitrogen; from mouse, catalog no. 459250); α-Flag M2-HRP (Sigma; from mouse, catalog no. A 8592) 1:10,000; α-tubulin-HRP 1:1,000 (Santa Cruz; from rat, catalog no. sc-53030); and HRP-coupled α-mouse (GE Healthcare; catalog no. NA931) 1:10,000. All antibodies were diluted in 5% (wt/vol) milk in Tris-buffered saline containing 0.01% (vol/vol) Tween-20.

For visualization Amersham ECL Prime Western Blotting Detection Reagent (GE Healthcare) was used. Images were acquired by Amersham Imager 600 (GE Healthcare).

Plasmid construction

All plasmids generated and used are listed in Table S2. For generation of protein–protein fusions overlapping, PCR was routinely used. Mutations were usually introduced by whole-plasmid amplification using overlapping primers followed by in-bacteria recombination, similar to what was described (Xia et al., 2015). Constructs for insect cell expression were cloned into pLIB and pBig1a plasmids using Gibson assembly as described before (Weissmann and Peters, 2018).

Recombinant protein expression and purification

Cik1–Kar3 complexes and HSET constructs were expressed from recombinant baculoviruses in Sf9 insect cells, cultivated in Spodopan (Pan Biotech) media for 3 d after infection. At that time point, 80–90% of cells were positive for a GFP reporter construct. Cells were collected by centrifugation, and the pellet was frozen in liquid nitrogen and stored at −80°C until further use. Proteins were purified as described before (Molodtsov et al., 2016). Briefly, cells were lysed using a Dounce homogenizer, and proteins were purified using M2-anti-Flag agarose. Lysis buffer contained 25 mM Hepes-KOH, pH 7.4, 150 mM NaCl, 1 mM $MgCl_2$, 5% (wt/vol) glycerol, 0.1% (vol/vol) Tween-20, 0.5 mM Tris(2-carboxyethyl)phosphin (TCEP), 0.5 mM ATP, 0.1 mM PMSF, and protease and phosphatase inhibitors (Roche). After washing, proteins were eluted with 2 mg/ml of 3xFlag peptide dissolved in 25 mM Hepes-KOH pH, 7.4, 150 mM NaCl, 1 mM $MgCl_2$, 5% (wt/vol) glycerol, 0.1% (vol/vol) Tween-20, and 0.5 mM TCEP buffer and stored at −80°C.

Bim1 and EB1 were expressed in *Escherichia coli* Rosetta cells and purified by Ni-NTA affinity chromatography via a His_6-tag in Lysis buffer containing 300 mM NaCl. After purification, proteins were desalted, and the tag was cleaved off by incubation with Tobacco Etch Virus protease overnight at +4°C. Proteins were loaded onto a Superdex 200 column as a second purification step.

SEC

Analytical SEC runs were performed at 4°C in buffer containing 25 mM Hepes-KOH, pH 7.4, 150 mM NaCl, 1 mM $MgCl_2$, 5% (wt/vol) glycerol, 0.1% (vol/vol) Tween-20, and 0.5 mM TCEP. Superose 6 3.2/300 or Superdex 200 3.2/300 columns were used. Protein complexes were used at 5-µM input concentration for the motor complexes and 10-µM input concentration for Bim1. 100-µl fractions were collected in 96-well plates, and aliquots were analyzed by SDS-PAGE.

Quantitative Bim1 pull-downs

His_6-Bim1 was coupled to prewashed TALON beads in SEC buffer supplemented with 10 mM imidazole and 0.5 mg/ml of BSA at 4°C for 1 h. Beads were washed four times and resuspended in a desired volume. The suspension was added to recombinant Cik1-Kar3, and to allow binding, the mixture was incubated at 4°C for 1 h with rotation. Afterward, beads were collected by centrifugation, and aliquots of the supernatant were analyzed by SDS-PAGE. Coomassie-stained protein bands were quantified in ImageJ/Fiji. Curve fit assumes one-site total binding, which includes specific binding and a linear nonspecific binding

component: $Y = B_{max} * X/(K_d + X) + NS * X + Background$, where Y is total binding, X is ligand, K_d is dissociation constant, NS is the slope of unspecific binding, and B_{max} is the maximum specific binding.

Live-cell fluorescence microscopy

Quantification of mitotic timing and spindle phenotypes

For protein depletion experiments, cells were grown for 18–20 h in YEPRG (2% of raffinose and 0.2% of galactose, vol/vol) and diluted to 0.1–0.2 OD_{600} in YEPRG. Cells were allowed to achieve exponential growth for 3 h at 30°C. Then, 0.01 mg/ml of α-factor was added for 2 h to arrest cells in a G1-like state.

Synchronized cells were collected by centrifugation, and α-factor was washed away with prewarmed media three times. The second wash contained pronase. For protein depletion, the third wash contained 1 mM NAA. After the last wash, cells were resuspended in drop-out tryptophan minimal media with Raff/Gal as a sugar source. For protein depletion experiments, 1 mM NAA was kept in all media during all steps. Cells were immobilized on Concanavalin A–coated ibidi Glass Bottom 4 Well µ-Slide 1.5H and proceeded for imaging. Live-cell microscopy was performed at 30°C using the DeltaVison Elite wide-field microscope system (GE Healthcare) equipped with a scientific CMOS camera. A 100× objective (Olympus; NA = 1.40) and immersion oil with a refractive index of $n = 1.518$ were used. Images were acquired by optical axis integration (OAI) scans over 3-µm width. Usually, images were taken every 10 min. Kinetochore clustering was evaluated by connecting the SPBs with a line of 10-pixel width and quantifying off-axis (mispositioned) versus on-axis (correctly positioned) KTsubunit–GFP signal.

Quantification of microtubule dynamics

Individual dynamics of nuclear microtubules were measured in α-factor–arrested cells by following the Stu2-GFP signal. OAI scans were taken every 2 s. To quantify shmoo tip bundle dynamics, short (2-min) and long (5-min) movies were recorded. In the short movies, a z-stack was recorded every 5 s, whereas the time between two z-stacks in the longer movies was 10 s. z-Stacks had 3-µm width, with 0.3-µm spacing between imaging planes.

Image processing

All images were deconvolved using SoftWoRx 7 (options: enhanced ratio, aggressive); image analysis was performed using ImageJ/Fiji software.

Statistical analysis

Statistical tests and graphs were prepared using Graphpad Prism 8. Small points on graphs show values of individual cells, and large open circles represent means of biological or technical replicates, as indicated. 95% confidence intervals (CIs) are usually shown. In the text, mean values ± SEM are mentioned. Student's *t* test was used to compare continuous data from two strains. Due to small sample size, data distribution was assumed to be normal, but this was not formally tested. The Kruskal-Wallis test was applied to datasets with more than two mutants. For discrete data, the χ^2 test was used.

Online supplemental material

Fig. S1 shows characterization of the Kar3 depletion phenotype on microtubule bundle dynamics in α-factor–arrested yeast cells, related to Fig. 1. Fig. S2 shows genetic identification of key molecular elements in Kar3, related to the corresponding Cik1 analysis in Fig. 3. Fig. S3 shows biochemical analysis of the $Kar3^{ND2}$ mutant. Fig. S4 displays chemical cross-linking data illustrating the organization of the Bim1–Cik1-Kar3 interface. Fig. S5 shows additional characterization of Bim1-binding–deficient Cik1 mutants, as well as characterization of the $Kar3^{ND2}$ mutant. Video 1 shows microtubule plus ends labeled with Bik1-3xGFP (green) and SPBs labeled with Spc42-RFP (red) in Cik1-AID cells over the course of a synchronized cell cycle under control conditions. Video 2 shows Bik1-3xGFP and Spc42-RFP upon depletion of Cik1-AID. Note misorganization of microtubule plus ends on the nascent metaphase spindle at t = 10 min. Table S1 lists yeast strains used in this study. Table S2 lists the relevant plasmids used in this study.

Acknowledgments

The authors acknowledge Kerstin Killinger, Alexander Dudziak, and Miriam Böhm for critical reading of the manuscript and all members of the Westermann laboratory for discussions. The authors thank Chris Campbell (University of Vienna, Vienna, Austria) for providing plasmids. We acknowledge the use of the imaging equipment and the support in microscope usage and image analysis by the "Imaging Center Campus Essen" (ICCE), Center of Medical Biotechnology (ZMB), University of Duisburg-Essen.

N. Kornakov and S. Westermann acknowledge support from the Collaborative Research Center CRC1093 Supramolecular Chemistry on Proteins.

The authors declare no competing financial interests.

Author contributions: Conceptualization: S. Westermann and N. Kornakov. Formal Analysis: N. Kornakov. Investigation: N. Kornakov and B. Möllers. Funding acquisition: S. Westermann. Project administration and supervision: S. Westermann. Visualization: N. Kornakov and S. Westermann. Writing: N. Kornakov and S. Westermann.

Submitted: 12 March 2020
Revised: 28 July 2020
Accepted: 10 September 2020

References

Akhmanova, A., and M.O. Steinmetz. 2015. Control of microtubule organization and dynamics: two ends in the limelight. *Nat. Rev. Mol. Cell Biol.* 16:711–726. https://doi.org/10.1038/nrm4084

Allingham, J.S., L.R. Sproul, I. Rayment, and S.P. Gilbert. 2007. Vik1 modulates microtubule-Kar3 interactions through a motor domain that lacks an active site. *Cell.* 128:1161–1172. https://doi.org/10.1016/j.cell.2006.12.046

Benanti, J.A., M.E. Matyskiela, D.O. Morgan, and D.P. Toczyski. 2009. Functionally distinct isoforms of Cik1 are differentially regulated by APC/C-mediated proteolysis. *Mol. Cell.* 33:581–590. https://doi.org/10.1016/j.molcel.2009.01.032

Braun, M., D.R. Drummond, R.A. Cross, and A.D. McAinsh. 2009. The kinesin-14 Klp2 organizes microtubules into parallel bundles by an

ATP-dependent sorting mechanism. *Nat. Cell Biol.* 11:724–730. https://doi.org/10.1038/ncb1878

Cai, S., L.N. Weaver, S.C. Ems-McClung, and C.E. Walczak. 2010. Proper organization of microtubule minus ends is needed for midzone stability and cytokinesis. *Curr. Biol.* 20:880–885. https://doi.org/10.1016/j.cub.2010.03.067

Chu, H.M.A., M. Yun, D.E. Anderson, H. Sage, H.-W. Park, and S.A. Endow. 2005. Kar3 interaction with Cik1 alters motor structure and function. *EMBO J.* 24:3214–3223. https://doi.org/10.1038/sj.emboj.7600790

David, A.F., P. Roudot, W.R. Legant, E. Betzig, G. Danuser, and D.W. Gerlich. 2019. Augmin accumulation on long-lived microtubules drives amplification and kinetochore-directed growth. *J. Cell Biol.* 218:2150–2168. https://doi.org/10.1083/jcb.201805044

Endres, N.F., C. Yoshioka, R.A. Milligan, and R.D. Vale. 2006. A lever-arm rotation drives motility of the minus-end-directed kinesin Ncd. *Nature.* 439:875–878. https://doi.org/10.1038/nature04320

Gibeaux, R., A.Z. Politi, F. Nédélec, C. Antony, and M. Knop. 2013. Spindle pole body-anchored Kar3 drives the nucleus along microtubules from another nucleus in preparation for nuclear fusion during yeast karyogamy. *Genes Dev.* 27:335–349. https://doi.org/10.1101/gad.206318.112

Hepperla, A.J., P.T. Willey, C.E. Coombes, B.M. Schuster, M. Gerami-Nejad, M. McClellan, S. Mukherjee, J. Fox, M. Winey, D.J. Odde, et al. 2014. Minus-end-directed Kinesin-14 motors align antiparallel microtubules to control metaphase spindle length. *Dev. Cell.* 31:61–72. https://doi.org/10.1016/j.devcel.2014.07.023

Honnappa, S., S.M. Gouveia, A. Weisbrich, F.F. Damberger, N.S. Bhavesh, H. Jawhari, I. Grigoriev, F.J.A. van Rijssel, R.M. Buey, A. Lawera, et al. 2009. An EB1-binding motif acts as a microtubule tip localization signal. *Cell.* 138:366–376. https://doi.org/10.1016/j.cell.2009.04.065

Huang, B., and T.C. Huffaker. 2006. Dynamic microtubules are essential for efficient chromosome capture and biorientation in S. cerevisiae. *J. Cell Biol.* 175:17–23. https://doi.org/10.1083/jcb.200606021

Janke, C., M.M. Magiera, N. Rathfelder, C. Taxis, S. Reber, H. Maekawa, A. Moreno-Borchart, G. Doenges, E. Schwob, E. Schiebel, et al. 2004. A versatile toolbox for PCR-based tagging of yeast genes: new fluorescent proteins, more markers and promoter substitution cassettes. *Yeast.* 21:947–962. https://doi.org/10.1002/yea.1142

Janson, M.E., R. Loughlin, I. Loïodice, C. Fu, D. Brunner, F.J. Nédélec, and P.T. Tran. 2007. Crosslinkers and motors organize dynamic microtubules to form stable bipolar arrays in fission yeast. *Cell.* 128:357–368. https://doi.org/10.1016/j.cell.2006.12.030

Jin, Q.W., J. Fuchs, and J. Loidl. 2000. Centromere clustering is a major determinant of yeast interphase nuclear organization. *J. Cell Sci.* 113:1903–1912.

Jin, F., H. Liu, P. Li, H.-G. Yu, and Y. Wang. 2012. Loss of function of the Cik1/Kar3 motor complex results in chromosomes with syntelic attachment that are sensed by the tension checkpoint. *PLoS Genet.* 8. e1002492. https://doi.org/10.1371/journal.pgen.1002492

Kalantzaki, M., E. Kitamura, T. Zhang, A. Mino, B. Novák, and T.U. Tanaka. 2015. Kinetochore-microtubule error correction is driven by differentially regulated interaction modes. *Nat. Cell Biol.* 17:421–433. https://doi.org/10.1038/ncb3128

Kapoor, T.M., M.A. Lampson, P. Hergert, L. Cameron, D. Cimini, E.D. Salmon, B.F. McEwen, and A. Khodjakov. 2006. Chromosomes can congress to the metaphase plate before biorientation. *Science.* 311:388–391. https://doi.org/10.1126/science.1122142

Khmelinskii, A., C. Lawrence, J. Roostalu, and E. Schiebel. 2007. Cdc14-regulated midzone assembly controls anaphase B. *J. Cell Biol.* 177:981–993. https://doi.org/10.1083/jcb.200702145

Khmelinskii, A., J. Roostalu, H. Roque, C. Antony, and E. Schiebel. 2009. Phosphorylation-dependent protein interactions at the spindle midzone mediate cell cycle regulation of spindle elongation. *Dev. Cell.* 17:244–256. https://doi.org/10.1016/j.devcel.2009.06.011

Kotwaliwale, C.V., S.B. Frei, B.M. Stern, and S. Biggins. 2007. A pathway containing the Ipl1/aurora protein kinase and the spindle midzone protein Ase1 regulates yeast spindle assembly. *Dev. Cell.* 13:433–445. https://doi.org/10.1016/j.devcel.2007.07.003

Kumar, A., C. Manatschal, A. Rai, I. Grigoriev, M.S. Degen, R. Jaussi, I. Kretzschmar, A.E. Prota, R. Volkmer, R.A. Kammerer, et al. 2017. Short Linear Sequence Motif LxxPTPh Targets Diverse Proteins to Growing Microtubule Ends. *Structure.* 25:924–932.E4. https://doi.org/10.1016/j.str.2017.04.010

Kushnirov, V.V. 2000. Rapid and reliable protein extraction from yeast. *Yeast.* 16:857–860. https://doi.org/10.1002/1097-0061(20000630)16:9<857::AID-YEA561>3.0.CO;2-B

Leary, A., S. Sim, E. Nazarova, K. Shulist, R. Genthial, S.K. Yang, K.H. Bui, P. Francois, and J. Vogel. 2019. Successive Kinesin-5 Microtubule Cross-linking and Sliding Promote Fast, Irreversible Formation of a Stereotyped Bipolar Spindle. *Curr. Biol.* 29:3825–3837.E3. https://doi.org/10.1016/j.cub.2019.09.030

Liu, H., F. Jin, F. Liang, X. Tian, and Y. Wang. 2011. The Cik1/Kar3 motor complex is required for the proper kinetochore-microtubule interaction after stressful DNA replication. *Genetics.* 187:397–407. https://doi.org/10.1534/genetics.110.125468

Longtine, M.S., A. McKenzie, III, D.J. Demarini, N.G. Shah, A. Wach, A. Brachat, P. Philippsen, and J.R. Pringle. 1998. Additional modules for versatile and economical PCR-based gene deletion and modification in Saccharomyces cerevisiae. *Yeast.* 14:953–961. https://doi.org/10.1002/(SICI)1097-0061(199807)14:10<953::AID-YEA293>3.0.CO;2-U

Manning, B.D., J.G. Barrett, J.A. Wallace, H. Granok, and M. Snyder. 1999. Differential regulation of the Kar3p kinesin-related protein by two associated proteins, Cik1p and Vik1p. *J. Cell Biol.* 144:1219–1233. https://doi.org/10.1083/jcb.144.6.1219

McDonald, H.B., and L.S.B. Goldstein. 1990. Identification and characterization of a gene encoding a kinesin-like protein in Drosophila. *Cell.* 61:991–1000. https://doi.org/10.1016/0092-8674(90)90064-L

Meluh, P.B., and M.D. Rose. 1990. KAR3, a kinesin-related gene required for yeast nuclear fusion. *Cell.* 60:1029–1041. https://doi.org/10.1016/0092-8674(90)90351-E

Middleton, K., and J. Carbon. 1994. KAR3-encoded kinesin is a minus-end-directed motor that functions with centromere binding proteins (CBF3) on an in vitro yeast kinetochore. *Proc. Natl. Acad. Sci. USA.* 91:7212–7216. https://doi.org/10.1073/pnas.91.15.7212

Mieck, C., M.I. Molodtsov, K. Drzewicka, B. van der Vaart, G. Litos, G. Schmauss, A. Vaziri, and S. Westermann. 2015. Non-catalytic motor domains enable processive movement and functional diversification of the kinesin-14 Kar3. *eLife.* 4. e04489. https://doi.org/10.7554/eLife.04489

Molodtsov, M.I., C. Mieck, J. Dobbelaere, A. Dammermann, S. Westermann, and A. Vaziri. 2016. A Force-Induced Directional Switch of a Molecular Motor Enables Parallel Microtubule Bundle Formation. *Cell.* 167:539–552.E14. https://doi.org/10.1016/j.cell.2016.09.029

Nishimura, K., T. Fukagawa, H. Takisawa, T. Kakimoto, and M. Kanemaki. 2009. An auxin-based degron system for the rapid depletion of proteins in nonplant cells. *Nat. Methods.* 6:917–922. https://doi.org/10.1038/nmeth.1401

Nixon, F.M., C. Gutiérrez-Caballero, F.E. Hood, D.G. Booth, I.A. Prior, and S.J. Royle. 2015. The mesh is a network of microtubule connectors that stabilizes individual kinetochore fibers of the mitotic spindle. *eLife.* 4. e07635. https://doi.org/10.7554/eLife.07635

Page, B.D., and M. Snyder. 1992. CIK1: a developmentally regulated spindle pole body-associated protein important for microtubule functions in Saccharomyces cerevisiae. *Genes Dev.* 6:1414–1429. https://doi.org/10.1101/gad.6.8.1414

Petry, S., A.C. Groen, K. Ishihara, T.J. Mitchison, and R.D. Vale. 2013. Branching microtubule nucleation in Xenopus egg extracts mediated by augmin and TPX2. *Cell.* 152:768–777. https://doi.org/10.1016/j.cell.2012.12.044

Rincon, S.A., A. Lamson, R. Blackwell, V. Syrovatkina, V. Fraisier, A. Paoletti, M.D. Betterton, and P.T. Tran. 2017. Kinesin-5-independent mitotic spindle assembly requires the antiparallel microtubule crosslinker Ase1 in fission yeast. *Nat. Commun.* 8:15286. https://doi.org/10.1038/ncomms15286

Saunders, W., V. Lengyel, and M.A. Hoyt. 1997. Mitotic spindle function in Saccharomyces cerevisiae requires a balance between different types of kinesin-related motors. *Mol. Biol. Cell.* 8:1025–1033. https://doi.org/10.1091/mbc.8.6.1025

Sproul, L.R., D.J. Anderson, A.T. Mackey, W.S. Saunders, and S.P. Gilbert. 2005. Cik1 targets the minus-end kinesin depolymerase kar3 to microtubule plus ends. *Curr. Biol.* 15:1420–1427. https://doi.org/10.1016/j.cub.2005.06.066

Stephens, A.D., C.E. Snider, J. Haase, R.A. Haggerty, P.A. Vasquez, M.G. Forest, and K. Bloom. 2013. Individual pericentromeres display coordinated motion and stretching in the yeast spindle. *J. Cell Biol.* 203:407–416. https://doi.org/10.1083/jcb.201307104

Suzuki, A., B.L. Badger, J. Haase, T. Ohashi, H.P. Erickson, E.D. Salmon, and K. Bloom. 2016. How the kinetochore couples microtubule force and centromere stretch to move chromosomes. *Nat. Cell Biol.* 18:382–392. https://doi.org/10.1038/ncb3323

Tanaka, T.U., N. Rachidi, C. Janke, G. Pereira, M. Galova, E. Schiebel, M.J.R. Stark, and K. Nasmyth. 2002. Evidence that the Ipl1-Sli15 (Aurora

kinase-INCENP) complex promotes chromosome bi-orientation by altering kinetochore-spindle pole connections. *Cell*. 108:317–329. https://doi.org/10.1016/S0092-8674(02)00633-5

Tanaka, K., E. Kitamura, Y. Kitamura, and T.U. Tanaka. 2007. Molecular mechanisms of microtubule-dependent kinetochore transport toward spindle poles. *J. Cell Biol.* 178:269–281. https://doi.org/10.1083/jcb.200702141

Vukušić, K., R. Buđa, A. Bosilj, A. Milas, N. Pavin, and I.M. Tolić. 2017. Microtubule Sliding within the Bridging Fiber Pushes Kinetochore Fibers Apart to Segregate Chromosomes. *Dev. Cell*. 43:11–23.E6. https://doi.org/10.1016/j.devcel.2017.09.010

Walczak, C.E., S. Verma, and T.J. Mitchison. 1997. XCTK2: a kinesin-related protein that promotes mitotic spindle assembly in Xenopus laevis egg extracts. *J. Cell Biol.* 136:859–870. https://doi.org/10.1083/jcb.136.4.859

Weissmann, F., and J.-M. Peters. 2018. Expressing Multi-subunit Complexes Using biGBac. *Methods Mol. Biol.* 1764:329–343. https://doi.org/10.1007/978-1-4939-7759-8_21

Wickstead, B., K. Gull, and T.A. Richards. 2010. Patterns of kinesin evolution reveal a complex ancestral eukaryote with a multifunctional cytoskeleton. *BMC Evol. Biol.* 10:110. https://doi.org/10.1186/1471-2148-10-110

Wieczorek, M., S. Bechstedt, S. Chaaban, and G.J. Brouhard. 2015. Microtubule-associated proteins control the kinetics of microtubule nucleation. *Nat. Cell Biol.* 17:907–916. https://doi.org/10.1038/ncb3188

Xia, Y., W. Chu, Q. Qi, and L. Xun. 2015. New insights into the QuikChange™ process guide the use of Phusion DNA polymerase for site-directed mutagenesis. *Nucleic Acids Res.* 43. e12. https://doi.org/10.1093/nar/gku1189

JCB

Supplemental material

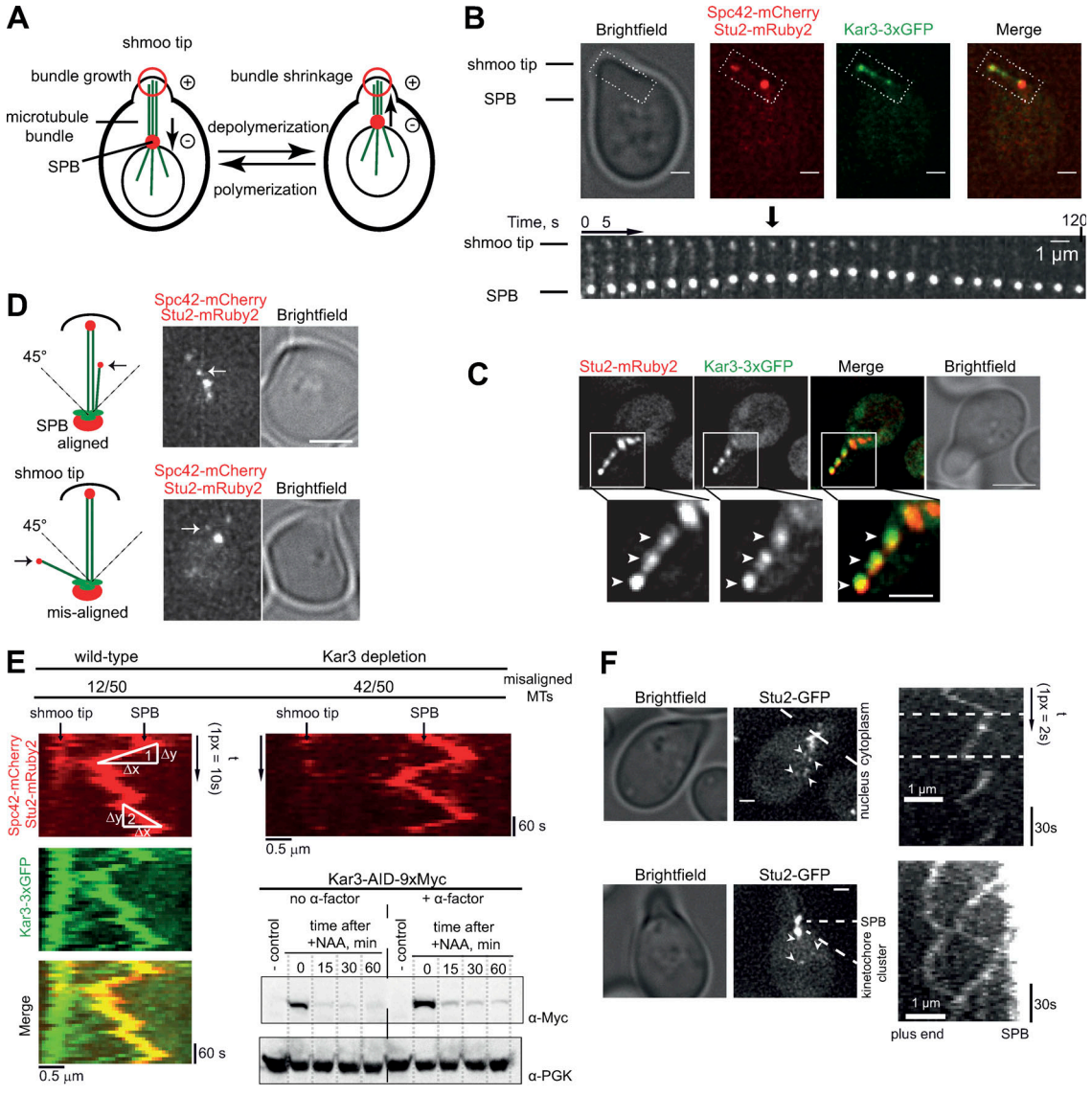

		V_{pol}, nm/s	V_{depol}, nm/s	Δt_{cat}, s	Δt_{rescue}, s	pause duration, s	%, paused
individual MT		37.7±8.9	77.7±18.7	N.A.	N.A.	N.A.	N.A.
bundle	wt	15.5±1.7	29.2±4.4	89.4±0.3	89.9±1.1	22.5±0.6	7.6
bundle	no NAA Kar3-AID	15.9±2.3	30.1±5.3	93.9±10.7	91.4±15.1	23.9±5.2	6.5
bundle	+NAA Kar3-AID	17.2±3.3	35.2±5.7	127.2±1.4	133.4±6.5	36.4±5	8.9

Figure S1. **Cik1-Kar3 promotes shmoo tip microtubule bundle dynamics without affecting polymerization and depolymerization speed. (A)** Diagram describing microtubule bundle dynamics in an α-factor–arrested cell. Cycles of bundle shrinkage and growth cause pulling and pushing of the nucleus toward and away from the shmoo tip. **(B)** Representative image of a polarized cell. The dotted white rectangle includes the microtubule bundle between the shmoo tip and the SPB. Below, a montage of the area is shown; 25 consecutive frames with 5-s time intervals. Scale bar is 1 µm. **(C)** Fluorescence micrographs showing colocalization of Kar3 and Stu2 to individual plus ends (depicted by arrowheads) in the shmoo tip bundle. Scale bar is 2 µm; in magnified inset, scale bar is 1 µm. **(D)** Examples for scoring for shmoo tip alignment defects. Bundle was scored as misaligned when growing Stu2-mRuby2 comets deviated >45° from the SPB to the shmoo tip axis. Arrows point to aligned versus misaligned microtubules. Scale bar is 2 µm. **(E)** Kymographs from a 5-min-long movie of a wild-type and Kar3-AID + NAA cell are shown. The triangles show Δx and Δy as an example for how bundle dynamics values were acquired (1 = depolymerization; 2 = polymerization). Number of cases when at least one microtubule was misaligned during movie acquisition is shown above the kymographs. Scale bars are 0.5 µm. Immunoblotting shows time course and efficiency of Kar3-AID depletion after addition of 1 mM NAA in exponentially growing and α-factor–arrested cells. α-PGK, anti-Phospho-glycerol kinase blot as loading control. **(F)** Individual nuclear microtubules are highly dynamic. α-Factor–arrested cells expressing Stu2-GFP were followed by live-cell microscopy. Arrowheads point to individual microtubule plus ends. Kymographs from 2-min high time-resolution movies of Stu2-GFP. Upper panel shows a single individual microtubule; bottom panel has several microtubules replacing each other. Dashed lines show one polymerization cycle. Scale bar is 1 µm. **(G)** Parameters of dynamics of individual microtubules (top row) and MT bundles (three bottom rows) are listed in the table. pol, polymerization; depol, depolymerization; cat, catastrophe. Parameters that differ from others are highlighted in red. Experiments were repeated at least three times, and means ± SD are shown. N.A., nonapplicable.

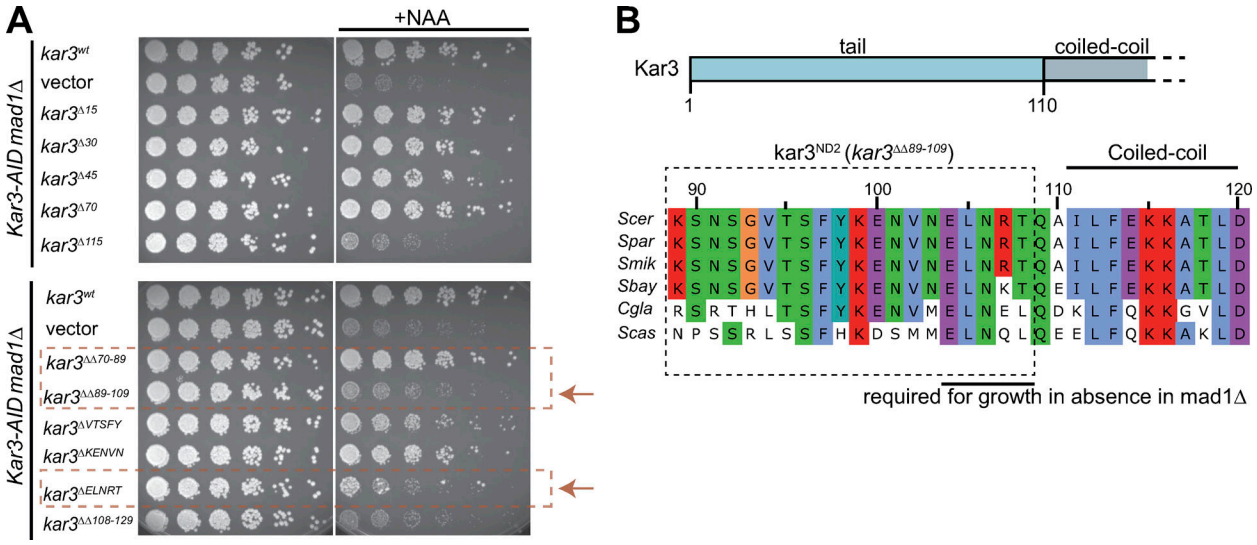

Figure S2. **Identification of key molecular elements in the Kar3 N-terminus. (A)** Kar3 mutagenesis screen. Different Kar3 rescue constructs were transformed into the Kar3-AID *mad1Δ* strain and tested for viability after depletion of endogenous Kar3 by the addition of auxin. Panels show N-terminal truncations (top) and finer mapping of critical regions close to a predicted coiled-coil as functionally important (bottom). Important mutants are highlighted with arrows and dashed rectangles. **(B)** Sequence alignment of the identified Kar3 sequence from six budding yeast species.

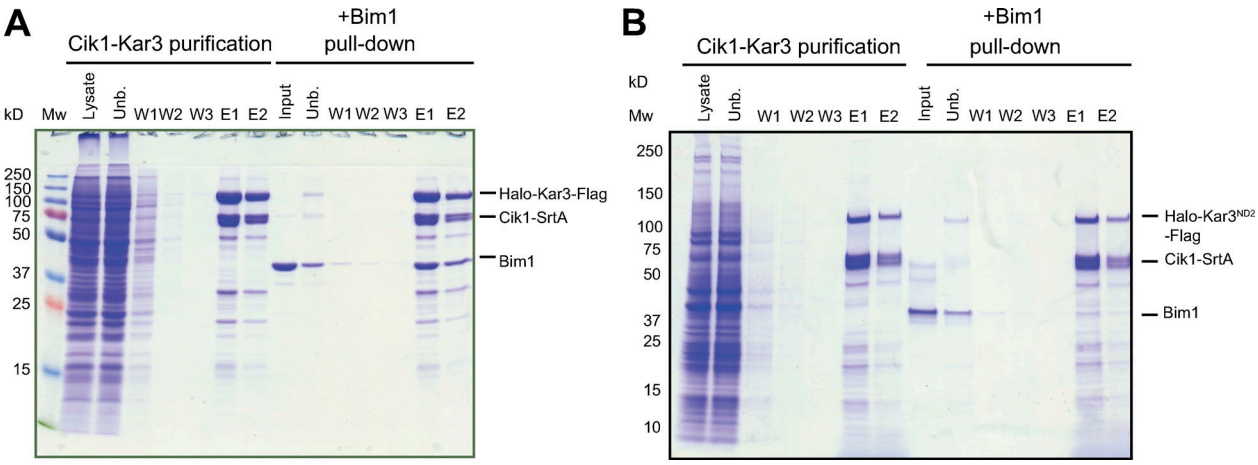

Figure S3. **Kar3^{ND2} mutants are defective in Bim1 binding. (A and B)** Purification and subsequent Bim1 pull-down experiment with Cik1-Kar3 wild-type (A) or Cik1–Kar3^{ND2} complex. Unb., unbound fraction. **(B)** Cik1–Kar3 complexes were purified from Sf9 extracts, bound to M2 agarose beads, incubated with Bim1, washed, and subsequently released from beads with 3× Flag peptide. Bim1 fails to copurify with the Kar3^{ND2} mutant.

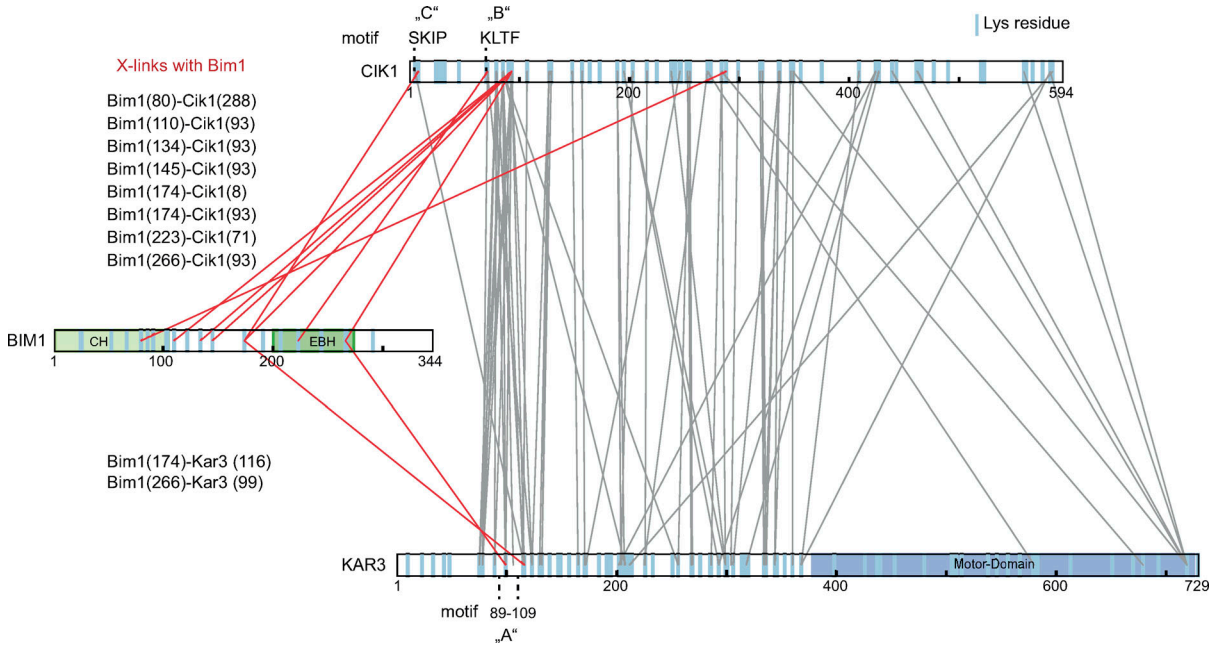

Figure S4. **Relation between the identified binding motifs and the subunit topology of the Bim1–Cik1-Kar3 complex.** Display of chemical cross-linking data from (Molodtsov et al., 2016). Each line represents an individual Lys-Lys cross-link. Cross-links to Bim1 are highlighted in red and listed on the left. Numbers in parenthesis indicate the cross-linked lysine residue. The positions of Bim1-binding motifs A, B, and C are indicated; blue lines in the protein schemes denote all available lysine residues in the primary sequence.

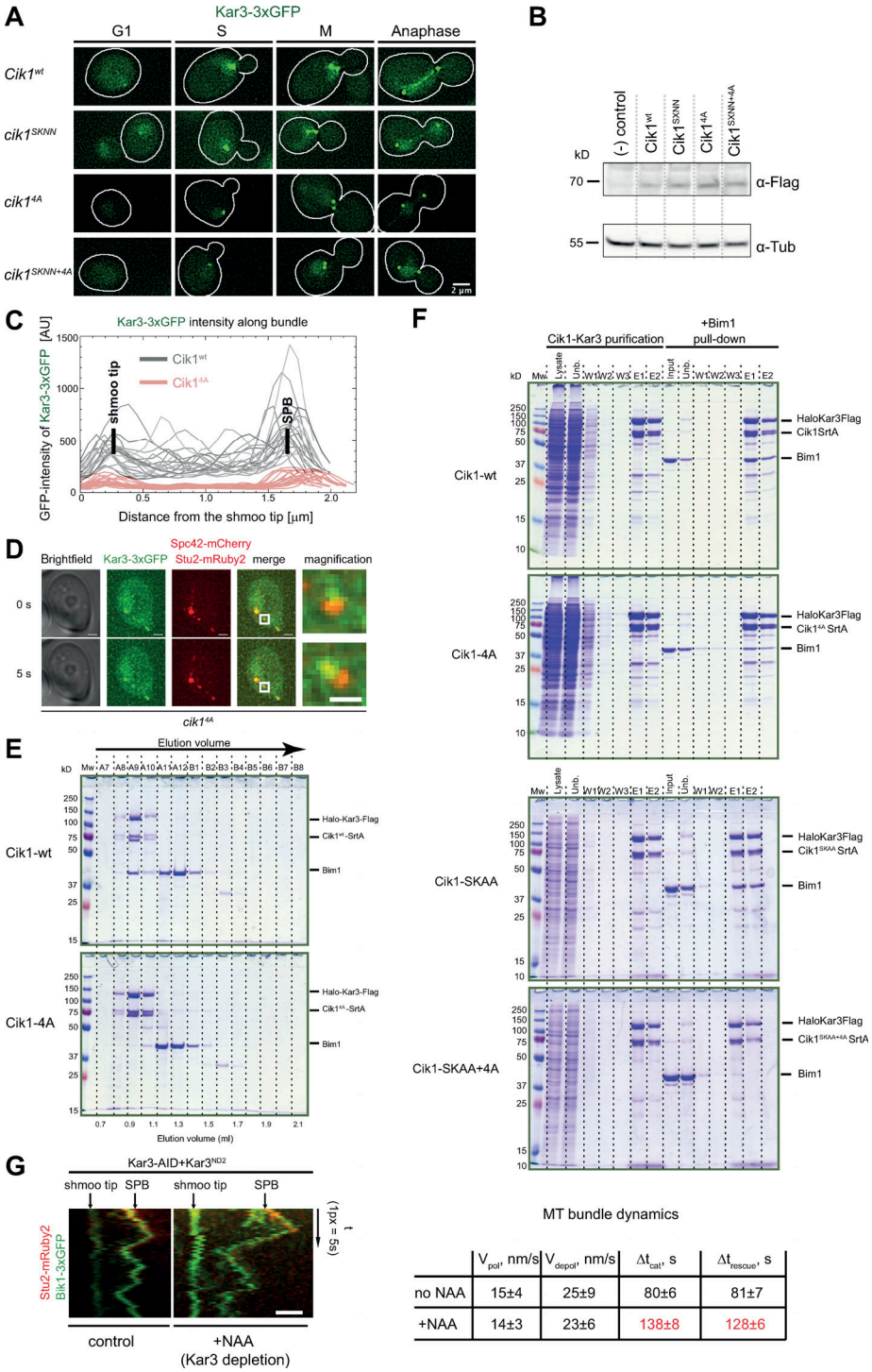

	V_{pol}, nm/s	V_{depol}, nm/s	Δt_{cat}, s	Δt_{rescue}, s
no NAA	15±4	25±9	80±6	81±7
+NAA	14±3	23±6	138±8	128±6

Figure S5. **Additional characterization of Cik1 mutants. (A)** Bim1 binding is required for an efficient association of Cik1-Kar3 with microtubule plus ends. Representative images show Kar3-3xGFP signals over different cell cycle stages in indicated Cik1 mutants. Cik1^{SKNN}-Kar3 was still able to follow microtubule plus ends and bind to the metaphase spindle. The KLTF motif mutation abrogated plus-end localization. Scale bar is 2 µm. **(B)** Western blot analysis of Flag-tagged Cik1 rescue alleles. **(C)** Overlay of 15 line scans along the shmoo tip microtubule bundle of Kar3-3xGFP in Cik1^{wt} and cik1^{4A} genetic backgrounds. The KLTF motif mutation leads to a fourfold decrease in recruitment to the microtubule bundle. **(D)** Residual colocalization between Kar3-3xGFP and Stu2-mRuby2 in the Cik1-4A mutant. Microscopy images of two consecutive frames of α-factor–arrested cells are shown. Scale bar in panels 1–4 are 1 µm; scale bar for magnification is 0.5 µm. **(E)** Analytical SEC experiment showing that the Cik1-4A mutation in the KLTF motif prevents stable association between Cik1-Kar3 and Bim1. **(F)** Purification and subsequent Bim1 pull-down experiment with Cik1–Kar3 complexes containing either Cik1 wild type, Cik1-4A mutant, Cik1-SKAA mutant, or Cik1-SKAA+4A mutant. Note that only Cik1-SKAA+4A fully eliminates Bim1 binding in the pull-down assay. **(G)** Analysis of shmoo tip bundle dynamics in Kar3^{ND2} cells. Kar3-AID cells expressing the Kar3^{ND2} mutant and the plus-end markers Bik1-3xGFP and Stu2-mRuby2 were imaged in α-factor–arrested cells in the absence (control) and presence of auxin. Parameters of MT bundle dynamics are shown on the right; deviations from wild-type parameters are highlighted in red.

Video 1. **Time-lapse epifluorescence microscopy of yeast cells expressing the microtubule-binding protein Bik1-3xGFP (green) and the SPB marker Spc42-RFP (red) in Cik1-AID cells.** OAI scans were taken every 10 min following synchronization of the cells with α-factor. Video shows cells under control conditions (no auxin added), corresponding to Fig. 2 A, upper panel (no aux). Video is displayed at 4 frames per second; scale bar is 2 µm. Fluorescence channels are merged with the corresponding bright-field images.

Video 2. **Time-lapse epifluorescence microscopy of yeast cells expressing Bik1-3xGFP (green) and Spc42-RFP (red) upon depletion of Cik1-AID with auxin, corresponding to Fig. 2 A, bottom panel (plus aux).** OAI scans were taken every 10 min following synchronization of the cells with α-factor. Video is displayed at 4 frames per second; scale bar is 2 µm. Fluorescence channels are merged with the corresponding bright-field images. Note misorganization of microtubules on the nascent metaphase spindle at t = 10 min and 20 min, which eventually improves at t = 30 min.

Provided online are two tables. Table S1 lists yeast strains used in this study. Table S2 lists the relevant plasmids used in this study.

Table S1. Yeast strains used

Relevant genotypes are as follows: Strains are modifications of DDY902, DDY904, DDY1102.

NKY1	*MAT a, ura3::pGAL-osTIR::URA3*	*Fig. 1b,c*
NKY2-1	*MAT a, ura3::pGAL-osTIR::URA3, Kar3-AID-9xMyc::KanMX*	*Fig. 1b,c*
NKY5-1	*MAT a, ura3::pGAL-osTIR::URA3, Cik1-AID-9xMyc::KanMX*	*Fig. 1b,c*
NKY7-1	*MAT a, ura3::pGAL-osTIR::URA3, Kar3-AID-9xMyc::KanMX, mad1Δ::HIS3*	*Fig.1c*
NKY8-1	*MAT a, ura3::pGAL-osTIR::URA3, Cik1-AID-9xMyc::KanMX, mad1Δ::HIS3*	*Fig.1c*
NKY24	*$Cik1^{wt}$ pRS315 (LEU) in NKY8-1*	*Fig.3b*
NKY25	*$Cik1^{\Delta 34}$ pRS315 (LEU) in NKY8-1*	*Fig.3b*
NKY26	*$Cik1^{\Delta 54}$ pRS315 (LEU) in NKY8-1*	*Fig.3b*
NKY27	*$Cik1^{\Delta 74}$ pRS315 (LEU) in NKY8-1*	*Fig.3b*
NKY28	*$Cik1^{\Delta 94}$ pRS315 (LEU) in NKY8-1*	*Fig.3b*
NKY29	*$Cik1^{\Delta 250}$ pRS315 (LEU) in NKY8-1*	*Fig.3b*
NKY37	*$Cik1^{\Delta 59}$ pRS315 (LEU) in NKY8-1*	*Fig.3b*
NKY38	*$Cik1^{\Delta 64}$ pRS315 (LEU) in NKY8-1*	*Fig.3b*
NKY39	*$Cik1^{\Delta 69}$ pRS315 (LEU) in NKY8-1*	*Fig.3b*
NKY45	*VCV1 (Vik1-Cik1-Vik1) pRS315 (LEU) in NKY8-1*	*Fig.3d*
NKY46	*VCV2 pRS315 (LEU) in NKY8-1*	*Fig.3d*
NKY47	*VCV3 pRS315 (LEU) in NKY8-1*	*Fig.3d*
NKY48	*VCV4 pRS315 (LEU) in NKY8-1*	*Fig.3d*
NKY58	*Vik1 pRS315 (LEU) in NKY8-1*	*Fig.3d*
NKY63	*$Kar3^{wt}$ pRS315 (LEU) in NKY7-1*	*Supp Fig. 2A*
NKY64	*$Kar3^{\Delta 30}$ pRS315 (LEU) in NKY7-1*	*Supp Fig. 2A*
NKY71	*$Kar3^{\Delta 15}$ pRS315 (LEU) in NKY7-1*	*Supp Fig. 2A*
NKY72	*$Kar3^{\Delta 45}$ pRS315 (LEU) in NKY7-1*	*Supp Fig. 2A*
NKY73	*$Kar3^{\Delta 70}$ pRS315 (LEU) in NKY7-1*	*Supp Fig. 2A*
NKY74	*$Kar3^{\Delta 115}$ pRS315 (LEU) in NKY7-1*	*Supp Fig. 2A*
NKY127	*MAT a, ura3::pGAL-osTIR::URA3, Cik1-AID-9xMyc::KanMX, Ndc80-GFP::HIS3, Spc42-RedStar2:: natMX4*	*Fig.1e,f; Fig.2b*
NKY137	*$Cik1^{4A}$ pRS315 (LEU) in NKY8-1*	*Fig. 5b*
NKY159	*$Cik1^{SKAA+4A}$ pRS315 (LEU) in NKY8-1*	*Fig. 5b*
NKY237	*$Kar3^{\Delta\Delta 89-109}$ pRS315 (LEU) in NKY7-1*	*Supp Fig. 2A, Fig. 6f*
NKY238	*$Kar3^{\Delta\Delta 108-129}$ pRS315 (LEU) in NKY7-1*	*Supp Fig. 2A*
NKY335	*CH^{Bim1}-$Cik1^{\Delta 74}$ pRS315 (LEU) in NKY8-1*	*Fig.6b*
NKY337	*CH^{Ndc80}-$Cik1^{\Delta 74}$ pRS315 (LEU) in NKY8-1*	*Fig.6b*

NKY341	*CH^{Bim1}-Kar3 pRS315 (LEU) in NKY7-1*	*Fig.6f*
NKY343	*CH^{Bim1}-Kar3^{ND2} pRS315 (LEU) in NKY7-1*	*Fig.6f*
NKY345	*CH^{Bim1}-Kar3^{ND3} pRS315 (LEU) in NKY7-1*	*Fig.6f*
NKY381	*MAT a, ura3::pGAL-osTIR::URA3, Kar3-AID-9xMyc::KanMX, Cik1-AID-9xMyc:: natMX4*	*Fig. 1c*
NKY428-1	*cik1::Cik1$^{SKNN+4A}$::LEU2 in BMY4*	*Supp. Fig. 5a*
NKY429-1	*cik1::Cik1$^{\Delta 74}$-NLS::LEU2 in BMY4*	*Fig. 6c*
NKY430-1	*cik1::CH^{Bim1}-Cik1$^{\Delta 74}$-NLS::LEU2 in BMY4*	*Fig. 6c*
NKY435	*Cik1^{4A} pRS315 (LEU) in NKY8-1*	*Fig.5b*
NKY437	*Cik1$^{SKAA+4A}$ pRS315 (LEU) in NKY8-1*	*Fig.5b*
NKY439	*Cik1^{SKAA} pRS315 (LEU) in NKY8-1*	*Fig.5b*
NKY482	*CH^{Bim1}-Kar3-NLS pRS315 (LEU) in NKY8-1*	*Fig. 6b*
NKY526	*CH^{Bim1}-GFP-HSET pRS315 (LEU) in NKY7-1*	*Fig.6g*
NKY892	*MAT a, ura3::pGAL-osTIR::URA3, Kar3-AID-9xMyc::KanMX, Stu2-mRuby2::KanMX, mad1Δ::HIS3, Bik1-3xGFP:: natMX4*	*Supp. Fig. 3c*
NKY947	*MAT a, ura3::pGAL-osTIR::URA3, Cik1-AID-9xMyc::KanMX, Ase1-3xGFP::natMX4 Spc42-mCherry::HIS3*	*Fig.7b,c,d,f*
NKY950-1	*MAT a, ura3::pGAL-osTIR::URA3, Cik1-AID-9xMyc::KanMX, Ase1-3xGFP::natMX4 Spc42-mCherry::HIS3, leu2::Cik1^{wt}::LEU2*	*Fig.7a,b,c,d*
NKY951-1	*MAT a, ura3::pGAL-osTIR::URA3, Cik1-AID-9xMyc::KanMX, Ase1-3xGFP::natMX4 Spc42-mCherry::HIS3, leu2:: Cik1$^{SXNN+4A}$::LEU2*	*Fig.7a,b,d*
NKY953-1	*MAT a, ura3::pGAL-osTIR::URA3, Cik1-AID-9xMyc::KanMX, Spc42-mCherry::HIS3, Bik1-3xGFP:: natMX4*	*Fig. 2a*
NKY955-1	*MAT a, ura3::pGAL-osTIR::URA3, Cik1-AID-9xMyc::KanMX, Ase1-AID-9xMyc:: hphMX4, Spc42-mCherry::HIS3*	*Fig.7e,f*
NKY963	*MAT a, ura3::pGAL-osTIR::URA3, Cik1-AID-9xMyc::KanMX, Ase1-AID-9xMyc:: hphMX4, Spc42-mCherry::HIS3, leu2::Cik1^{wt}::LEU2*	*Fig.7e*
NKY964	*MAT a, ura3::pGAL-osTIR::URA3, Cik1-AID-9xMyc::KanMX, Ase1-AID-9xMyc:: hphMX4, Spc42-mCherry::HIS3, leu2::Cik1$^{SXNN+4A}$::LEU2*	*Fig.7e*
NKY965	*MAT a, ura3::pGAL-osTIR::URA3, Cik1-AID-9xMyc::KanMX, Ase1-AID-9xMyc:: hphMX4, Spc42-mCherry::HIS3, leu2::CH^{Bim1}-Cik1$^{\Delta 74}$-NLS::LEU2*	*Fig.7e*

NKY986	*MAT a, ura3::pGAL-osTIR::URA3, Cik1-AID-9xMyc::KanMX, Ase1-AID-9xMyc:: hphMX4, Spc42-mCherry::HIS3, Bik1-3xGFP:: natMX4*	*Fig.7g*
BMY4	*MAT a, ura3::pGAL-osTIR::URA3, Kar3-3xGFP:: natMX4, Stu2-mRuby2::KanMX, Spc42-mCherry::HIS3*	*Supp. Fig.1*

Table S2: Plasmids used in this study

pNK32	*Cik1^{wt} pRS315*
pNK33	*Cik1$^{\Delta 34}$ pRS315*
pNK34	*Cik1$^{\Delta 54}$ pRS315*
pNK35	*Cik1$^{\Delta 74}$ pRS315*
pNK36	*Cik1$^{\Delta 94}$ pRS315*
pNK37	*Cik1$^{\Delta 250}$ pRS315*
pNK38	*Vik1 pRS315*
pNK39	*Cik1$^{\Delta 59}$ pRS315*
pNK40	*Cik1$^{\Delta 64}$ pRS315*
pNK41	*Cik1$^{\Delta 69}$ pRS315*
pNK43	*VCV1 pRS315*
pNK44	*VCV2 pRS315*
pNK45	*VCV3 pRS315*
pNK46	*VCV4 pRS315*
pNK55	*Cik1^{SKAA} pRS315*
pNK56	*Cik1^{4A} pRS315*
pNK57	*Cik1$^{SKAA+4A}$ pRS315*
pNK60	*Kar3^{wt} pRS315*
pNK61	*Kar3$^{\Delta 30}$ pRS315*
pNK62	*Kar3$^{\Delta 15}$ pRS315*
pNK63	*Kar3$^{\Delta 45}$ pRS315*

pNK64	*Kar3$^{\Delta 70}$ pRS315*
pNK65	*Kar3$^{\Delta 115}$ pRS315*
pNK116	*CH^{Bim1}-Cik1$^{\Delta 74}$ pRS315*
pNK150	*Cik1^{wt} pRS305*
pNK151	*Cik1^{SKAA} pRS305*
pNK152	*Cik1^{4A} pRS305*
pNK153	*Cik1$^{SKAA+4A}$ pRS305*
pNK154	*Cik1$^{\Delta 74}$ pRS305*
pNK155	*CH^{Bim1}-Cik1$^{\Delta 74}$ pRS305*
pNK202	*Kar3$^{\Delta\Delta 89-109}$ pRS315*
pNK203	*Kar3$^{\Delta\Delta 108-129}$ pRS315*
pNK251	*CH^{Bim1}-Kar3 pRS315*
pNK252	*CH^{Bim1}-Kar3^{ND2} pRS315*
pNK253	*CH^{Bim1}-Kar3^{ND3} pRS315*
pNK301	*Kar3^{wt} pRS305*
pNK304	*Kar3^{ND2} pRS305*
pNK401	*Bim1 pET3aTr*
pNK402	*EB1 pET3aTr*
pNK505	*Cik1^{SKAA} pLIB*
pNK506	*Cik1^{4A} pLIB*
pNK507	*Cik1$^{SKAA+4A}$ pLIB*
pNK508	*Cik1$^{\Delta 74}$ pLIB*
pNK551	*Kar3 pLIB*
pNK552	*Kar3^{ND2} pLIB*

Additional Plasmids that were used in this study:

AID-tagging	pCC508 (KanMX)
Fluorescent labelling	pFA6a-link-yomRuby2-Kan was obtained from Addgene (Addgene plasmid # 44953; http://n2t.net/addgene:44953; RRID: Addgene_44953)
Halo-tag	Promega
HSET and EB1 CDS	Provided by Maxim Molodtsov
Primers and plasmids	Christine Mieck